# UNIVERSITY OF CALIFORNIA, SAN DIEGO

Characterization of the Short-term Oxygen Sensor Signal Response

A dissertation submitted in partial satisfaction of the requirements for the degree of

Doctor of Philosophy

in

Bioengineering

by

Shayda Moshirvaziri

Committee in charge:

Professor David Gough, Chair
Professor David Benson
Professor Jeff Hasty
Professor Orville Kolterman
Professor Kenneth Kreutz-Delgado
Professor Geert Schmid-Schönbein

2010

The dissertation of Shayda Moshirvaziri is approved, and it is acceptable in quality and form for publication on microfilm and electronically:

_____

_____

_____

_____

_____

_____
Chair

University of California, San Diego

2010

# TABLE OF CONTENTS

# LIST OF FIGURES

# LIST OF TABLES

# VITA

## Studies:

- B.S., Electrical Engineering, University of California, Los Angeles 2003.
- M.S., Bioengineering, University of California, San Diego 2007.
- Ph.D., Bioengineering, University of California, San Diego 2010.

## Teaching:

Teaching Assistant, Bioengineering, 2004-2006.

# ABSTRACT OF THE DISSERTATION

Characterization of the Short-term Oxygen Sensor Signal Response

by

Shayda Moshirvaziri

Doctor of Philosophy in Bioengineering

University of California, San Diego, 2010

Professor David Gough, Chair

Recent advances in biosensor technology resulted in the development of biosensors that can be implanted in living tissue for prolonged periods of time to monitor concentration of oxygen, glucose, and other metabolites. The implanted sensors function by electrochemical consumption of the metabolite producing continuous current signal that is proportional to blood metabolite concentration. Despite these advances, precise correlation of the sensor signal to the metabolite concentration still remains to be a challenge. Tissue signals are often contaminated by local fluctuations in metabolite concentration and no efficient algorithm that allows for characterization and removal of the signal noise has been developed.

Characterization of the different types of variations observed in the in vivo tissue signals would be of tremendous value not only for implanted sensors, but also to stem cell implants, b-cell islet constructs and for various other tissue engineered cellular devices. The objective of this project was to design an algorithm that correlates the *in vivo* short-term oxygen sensor signal response to the blood oxygen levels. *In vivo* oxygen signals were pre-acquired from sensors implanted in hamster and pig animal models. Using these signals, we first identified and classified various fluctuations observed within the oxygen signals. The signal variations were classified as biological or non-biological based on a review of the physiological ranges of oxygen fluctuation within tissue. Next, a filtering algorithm was designed to specifically remove the non-biological signal features from the oxygen signal to prevent the signal analysis from being distorted and contaminated by the these unwanted features. Finally, digital and statistical signal processing, and time series analysis methods were used to characterize the filtered oxygen signal. The power spectrums of the filtered oxygen signals were estimated, and interestingly, an oscillatory pattern was identified that supports a fundamental frequency of 10 ± 5 mHz for arteriolar vasomotion within the tissue. Correlation analysis revealed periodic cycles of regional tissue oxygen perfusion ranging from 0.29 to 2.1 mHz. The signals were also analyzed using continuous wavelet transforms, and the short-term oxygen signals were determined to be both stationary and non-stationary. These results strengthen the hypothesis that the short-term oxygen signals are composites of many different types of biological variations which occur at different time intervals within the tissue. Significantly, probability distribution analysis showed that the oxygen signals

collected from the same sensor array share the same non-Gaussian probability distribution properties. Using these characterizations, the effect of the local heterogeneous tissue environment can be removed from the short-term *in vivo* oxygen signals creating an oxygen signal representative of the global blood oxygen environment. Therefore, the design of an algorithm to characterize the tissue sensor signal variations is extremely valuable and will ultimately lead to design of highly accurate implantable metabolite tissue sensors.

# Chapter I: Background

## I.A Background and Motivation

The field of sensors and continuous *in vivo* monitoring of metabolites is rapidly growing in development. In particular, there is great interest in the development of a sensor that can monitor *in vivo* metabolites continuously and over a long-term time period of weeks to years. One category of such sensors is the enzyme electrode sensors that can be implanted in subcutaneous tissue for the long-term continuous monitoring of oxygen, glucose, lactate, pyruvate, and other key metabolites. Ideally, the implanted sensor would continuously monitor the dynamics of the metabolite blood concentration, and subsequently provide timely and accurate indication of any metabolite imbalances. The development of such a long-term continuous sensor would be highly beneficial for a variety of clinical applications including glucose monitoring for diabetes, lactate monitoring in cardiac therapy and extreme exertion, and oxygen monitoring for feedback control of variable-rate pacemakers, to name a few [1].

The enzyme electrode sensor is a potentiostatic sensor that works by electrochemical reaction of oxygen at a membrane-covered, polarized, noble metal electrode. The membrane contains immobilized enzymes that couple the electrochemical reaction of oxygen with the electrochemical consumption of the metabolite of interest to produce a continuous current signal that is proportional to metabolite's concentration in tissue blood. The purpose of the sensor is to correlate

the collected signal, a measurement of the local metabolite's tissue blood concentration, to the respective systemic blood concentration of the metabolite. However, correlation of the local tissue concentration of the metabolite to the systemic blood concentration of the metabolite is extremely complicated. Heterogeneous tissue effects, such as heterogeneous microvasculature and spatial distribution of metabolites or endogenous mechanisms of metabolite regulation are believed to play a significant role on the collected sensor electrode signal response [2, 3]. In addition, transient changes in local or systemic metabolite blood concentration are expected to have a significant effect on the signal response. Examples of transient changes would include variations in regional or local metabolite perfusion and lags due to metabolite diffusion from nearby microvessels to the sensor. Consequently, the sensor signal response is highly dynamic with many different types of variations observed within the signal. Characterization of the different types of signal variances would be tremendously valuable to the development of long-term implantable tissue sensors, and also to stem cell implants, b-cell islet constructs and other various tissue engineered cellular devices.

As the implantable and continuous enzyme electrode sensors are based on electrochemical sensing of oxygen, the oxygen sensor will serve as the model for the study of the sensor signal characteristics.

The goal of this project is to analyze the collected signals from implantable oxygen electrode tissue sensors, and to characterize the signal variations. The major obstacle in the sensor signal analysis is that the signals are confounded by the combined effect of the inherent variances from the tissue system, and also by

electronic noise. Characterization of these inherent system variances and noise, and the design of an efficient algorithm that allows for their analysis would be beneficial to the field of implantable sensors and other tissue engineered devices.

## I.B Enzyme Electrode Sensor Theory

The implantable oxygen sensor is a potentiostatic platinum electrode covered by a semipermeable membrane that selectively allows oxygen passage to the electrode surface. The resulting electrochemical reactions occur at the electrode surface and produce a continuous current. The theory for the sensor is discussed in detail by Gough, et al. [4, 5, 6, 7, 8]. The following is a brief theoretical summary of the mass-transfer reaction boundary equations and conditions for the sensor electrode signals.

Figure 1 presents the electrode disc covered by a homogenous membrane of thickness $\delta_m$. The disc radius R is large compared to the diffusion boundary layer so the edge effects can be neglected and only variations of substrate concentration in the Z-direction need to be considered.

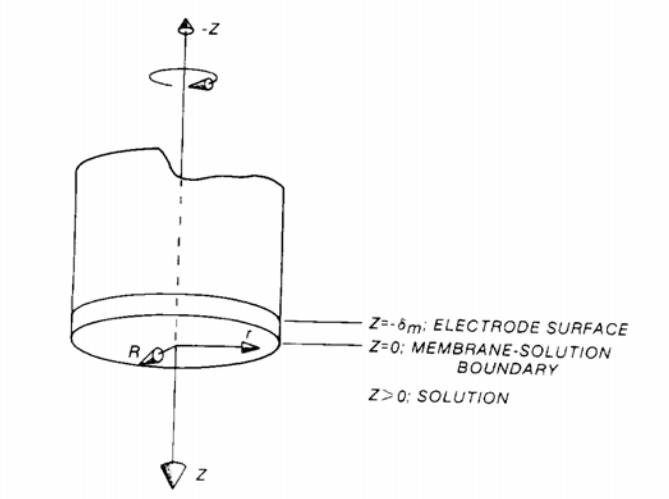


**Figure I-1. The coordinate system for the membrane covered platinum electrode [6].**

At Z = 0, the membrane-solution boundary is set with Z positive and increasing in the downward direction. Also, it is assumed that there is no convective flow within the membrane. Therefore, the diffusion equation is

$$\frac{d^2C_m}{dZ^2} = 0 \qquad -\delta_m \le Z \le 0, \qquad \text{(I-1)}$$

where $C_m$ is the substrate concentration in the membrane. In the solution for Z > 0, the convective diffusion equation is stated as

$$v_z(Z)\frac{dC}{dZ} = D\frac{d^2C}{dZ^2} \quad 0 \le Z \le \infty, \qquad \text{(I-2)}$$

where C is the substrate concentration, D is the diffusion coefficient in the solution, and $v_z(Z)$ is the fluid velocity in the Z-direction. Far away from the electrode disc as $Z \rightarrow \infty$ , the concentration of the reacting substrate equals the bulk substrate concentration $C_B$.

$$C = C_B \text{ as } Z \rightarrow \infty \qquad \text{(I-3)}$$

And when there is complete diffusion control, the substrate concentration at the electrode surface is zero

$$C = 0 \quad Z = -\delta_m \qquad \text{(I-4)}$$

At the membrane-solution interface of Z = 0, the conservation of mass states that

$$D_m \frac{dC_m}{dZ} = D\frac{dC}{dZ} \qquad Z = 0 \qquad \text{(I-5)}$$

where $D_m$ is the diffusion coefficient within the membrane. The last boundary condition involves the partition coefficient $\alpha$, that defines the equilibrium ratio of the substrate concentration in the membrane to the solution at the Z = 0 membrane-solution interface.

$$\frac{C_m}{C} = \alpha \qquad Z = 0 \qquad \text{(I-6)}$$

Integration of equations 1 and 2 with the evaluation of the boundary conditions given in equations 3 to 6 result in the diffusion current $i_d$ as

$$i_d = n\Im\pi R^2 D_m\left(\frac{\partial C}{\partial Z}\right) \quad Z = -\delta_m \qquad \text{(I-7)}$$

Where n is the number of electrons transferred, and $\Im$ is Faraday's constant. The permeability of the membrane is defined as

$$P_m = \alpha \frac{D_m}{\delta_m} \qquad \text{(I-8)}$$

Pm and Dm are estimated from the gas-phase calibration process. Therefore, the sensor signal, $i_d$ is a measurement of the oxygen flux at the electrode surface and is defined as $i_d = K\frac{\partial C}{\partial Z}$ , where $K = n\Im\pi R^2 D_m$, and $\frac{\partial C}{\partial Z}$ is the oxygen flux at the electrode surface.

The steady-state solution for the oxygen signal current $i_o$ is,

$$i_o = \frac{n\Im A P_m C_B}{(1 + Bi^{-1})} \qquad \text{(I-9)}$$

where A is the electrode area, and Bi is the dimensionless ratio of external to internal mass transfer.

## I.C Underlying Physiology of Implanted Oxygen Sensor

An array of oxygen sensor is implanted *in vivo* in the subcutaneous tissue, and it takes periodic measurements of the tissue oxygen flux from the surrounding and local tissue environment over a short-term time scale of 30 to 90 minutes. The *in vivo* oxygen flux signals contain many different types of variations and dynamics that need to be characterized and explained. With the assumption that the short-term oxygen signal variations are due to biological sources, i.e., local or global physiological

phenomena, in order to characterize the signal variations, the possible biological sources of the oxygen signal variations need to be indentified. Therefore, to identify the possible biological sources of the signal variations, mechanisms of tissue oxygen regulation and physiological events that affect tissue oxygen flux on the short-term time scale are studied and presented in the following sections.

## I.C.1 Vasomotion

Vasomotion is a physiologic process in which microscopic blood vessels undergo rhythmic and spontaneous oscillations of the luminal diameter by dilation and constriction [10]. These oscillations can occur at frequencies that range from 2- to 25 cycles per minute, and are independent of cardiac and respiratory rhythmcity [10, 18]. The phenomenon of vasomotion has been extensively studied, and the current view implies that vasomotion is a basic mechanism that regulates the local blood flow rate and thus the local oxygen supply to the heterogeneous tissue environment [10]. Moreover, vasomotion is a highly advantageous mechanism that provides the tissue with the ability to adapt to changes in the blood flow rate and tissue oxygen demand. In addition, the overall effect of vasomotion creates an inherent decrease of the vessel resistance to flow. This can be mathematically explained from Poiseulle's law, which states that the flow rate of liquid through a vessel is proportional to the fourth power of the vessel's radius [9].

$$FlowRate = \frac{(\Pr essureDifference)}{R}, \qquad \text{(I-10)}$$

$$Resistance\ to\ Flow = R = \frac{8(vis\cos ity)(length)}{\pi(radius)^4} \qquad \text{(I-11)}$$

Using Poiseulle's law, it can be demonstrated that the resistance of a vessel with a constant diameter is greater than that of a vessel with a diameter that changes sinusoidally, but still maintains the same average diameter [9]. Therefore, vasomotion decreases a vessel's flow resistance and results in an increase in the average blood flow rate through a vessel and the oxygen supply to the surrounding tissue.

The mechanism of vasomotion provides a likely source for the observed oxygen sensor signal variations. When vasomotion rhythmically or spontaneously occurs microvasculature at different frequencies, it results in variable fluctuations in the blood flow rate, hence, in the continuous oxygen supply to local tissue. This translates into the oscillatory behavior observed in the acquired sensor signals.

## I.C.2 Physiologic Role of Vasomotion

Vasomotion is hypothesized to play an apparent role in the dynamic and oscillatory signal variations observed in the oxygen signal responses. More specifically, two types of the signal response features are most likely to be due to effects of arteriolar vasomotion. The first type of oxygen signal feature is the small amplitude, rapid oscillation occurring on the order of seconds. The second type of feature is large amplitude, slow oscillation occurring on the order of minutes. In the subcutaneous tissue, small arteries and arterioles are the main types of blood vessels

that transport oxygen to the surrounding tissue [15, 16]. Consequently, when vasomotion occurs in these small arteries and arterioles, the diffusion rate of oxygen to the tissue is also affected, and the oxygen signal response results in small amplitude, rapid oscillations, or large amplitude, slow oscillations.

The frequency and amplitude of the signal response variations are dependent on the size of the blood vessel which vasomotion is occurring in [10, 11, 12, 14, 17]. For small arteries and larger arterioles (A1 arterioles), with diameters of 70- to 100 μm, slow-wave vasomotion has been observed [12, 13]. These are oscillations that occur 1 to 3 cycles per minute, with amplitudes that increase by 10-20% of the mean diameter, resulting in slow, large amplitude blood flow oscillations and slow, large amplitude variation in the tissue oxygen supply. In direct contrast, the vasomotion that occurs in small terminal arterioles (A4 arterioles) with diameters of the order of 10 μm is called fast-wave vasomotion [12, 13]. Fast-wave vasomotion is characterized with an oscillatory frequency that ranges from 10 to 25 cycles per minute [10, 18], and can include possible changes in the vessel diameter of up to 100% that lead to the complete closure of the vessel. This effect has been observed when vasomotion occurs in the terminal arterioles and results in “stop and go” blood flow patterns [10, 13, 16, 17, 18]. This fast-wave vasomotion produces rapid, and large magnitude changes in the diameters of small arteriolar vessels, which results in rapid, small amplitude changes in the blood flow, leading to rapid, small amplitude changes in oxygen supply to the tissues. Therefore, the time intervals of slow-wave and fast-wave vasomotion in the small arteries and arterioles are hypothesized to play

a probable role in to two types of dynamic signal response features observed in the sensor signal data.

### I.C.3 Regulation of Regional Blood Flow

The regional blood flow rate is regulated in order to meet the metabolic demands, including oxygen demand, of the tissues [16]. Therefore, understanding the dynamics of regional blood flow and how it is regulated is critical to understanding the dynamics of oxygen flux in tissue, and the dynamics observed in the oxygen sensor signal response. The main effectors of blood flow regulation in the subcutaneous tissues are the arterioles and small arteries, and they can provide for tissues are located some distance away [15, 16]. The mechanisms that are known to be involved in regional blood flow regulation are automatic nervous stimuli, circulating substances, shear-dependent responses, metabolic responses, conducted responses propagated along the vessel, and communication between paired feeding and draining vessels [11, 17, 18]. The manner in which these various mechanisms combine and interact is exceptionally complex. Consequently, the control of regional blood flow and thus the control of regional oxygen perfusion are not yet well understood. This presents a difficult challenge in determining the precise physiologic source for the signal variations that are hypothesized to be due to changes in regional blood flow.

# Chapter II: Oxygen Sensor Signals

The short-term oxygen sensor signals were collected from oxygen sensor electrode arrays implanted in the subcutaneous tissue of hamsters and pigs. The sensor electrode signals were collected while the animals were awake, at rest, and unanesthetized.

## II.A Collection of the Hamster Oxygen Sensor Signals

The hamster oxygen sensor signal datasets analyzed in this project were provided from studies by Dr. Milan T. Mikale while working for the Dr. David A. Gough Biosensor Laboratory at the Department of Bioengineering, University of California, San Diego. The details of the sensor fabrication and sensor implantation can be found elsewhere [4, 5, 6, 7]. The following is a summary of the oxygen sensor electrode array and electrode signal collection as it pertains to this project.

*Animal Subjects.* Male Syrian golden hamsters weighing 60 to 200 g.

## II.B Collection of the Pig Oxygen Sensor Signals

The pig oxygen sensor signal datasets analyzed in this project where provided by GlySens Incorporated, and by Dr. Joe Lin and Dr. David Gough. The details of the sensor fabrication and sensor implantation can be found elsewhere. The oxygen sensors implanted into the pigs are hermetically sealed and function identically to the sensors implanted into the hamsters.

*Animal Subjects*. Yucatan miniature pigs.

## II.C Oxygen Sensor Array

A summary of the standard sensor array is taken from [2]. The oxygen sensor is a 12 mm diameter disc with thick-film electrodes in a specified pattern. The electrodes are composed of disc platinum working electrodes of 125 to 300 μm in diameter, four common Ag/AgCl disc reference electrodes of ~875 μm in diameter, and a ribbon-like common counter platinum electrode. There are 18 working electrodes separated by distances of 1-2 mm on each array. A 25 μm layer of conductive electrolyte is deposited by spin casting on the ceramic substrate, followed by spin casting a 25 μm layer of polydimethylsiloxane for specificity to oxygen, in total creating a 50 μm polymer membrane. Individual wire connections are made to each sensor from the back of the array disc. A rectangular ceramic plate having patterned conductive traces mated with a multipin fan connector, is connected via ribbon cables to a custom multichannel potentiostat instrument for polarization of the individual working electrodes and conveyance of the signal currents. Signals are collected by computer [1, 2].

## II.D Oxygen Sensor Calibration

Individual sensors electrode arrays are similar in their manufacture and in vitro response to oxygen concentration. The oxygen sensors arrays are calibrated pre- and post-implantation to ensure that each electrode on the sensor array functions

properly. The sensitivity if each sensor is determined individually [3], in which the calibrations are made in the gas-phase. This method allows the sensor electrode signals to be measured without error due to effects of variable mass transfer boundary layers found in a stirred liquid phase [2]. During the calibration process, the oxygen sensor samples the surrounding oxygen concentration and collects signals in units of voltage or current with a sampling rate of one sample every several seconds. Figure I-2 shows the calibration of an oxygen sensor array. The calibration begins at the initial time of zero where the sensor is surrounded by a buffer gas-phase for approximately 12 minutes. At the 12 minute time mark, the oxygen concentration is changed to 2% oxygen, which is the physiological tissue oxygen concentration. At the 20 minute time mark, the buffer oxygen concentration is changed to 15% oxygen, and at the 30 minute time mark the buffer oxygen concentration is changed to 5%. Lastly, the at the 48 minute time mark the oxygen concentration is set to zero.

The in vitro calibration process reveals a delay of one to three minutes in the sensor signal response time when the oxygen concentration is changed. For the purpose of this project, the delay is assumed to not play a role in the collected *in vivo* oxygen signals since significant changes in tissue oxygen concentration do not occur in normal, resting animals. In addition, a significant feature revealed by the calibration process is that the in vitro oxygen sensor electrode signals are relatively free of noise.

The sensor electrode signals are approximately linearly proportional with the change in oxygen concentration. Additionally, each signal has its own proportionally constant of oxygen concentration to the signal recorded in units of voltage or current.

The gas-phase calibration process allows the membrane permeability, $P_m$, to be estimated. Once the permeability of the membrane has been estimated, the membrane diffusion can also be estimated, and the conversion rate may be calculated. The sensor electrode signal is converted to oxygen flux by the conversion rate of constant K, where $K = n\Im\pi R^2 D_m$.

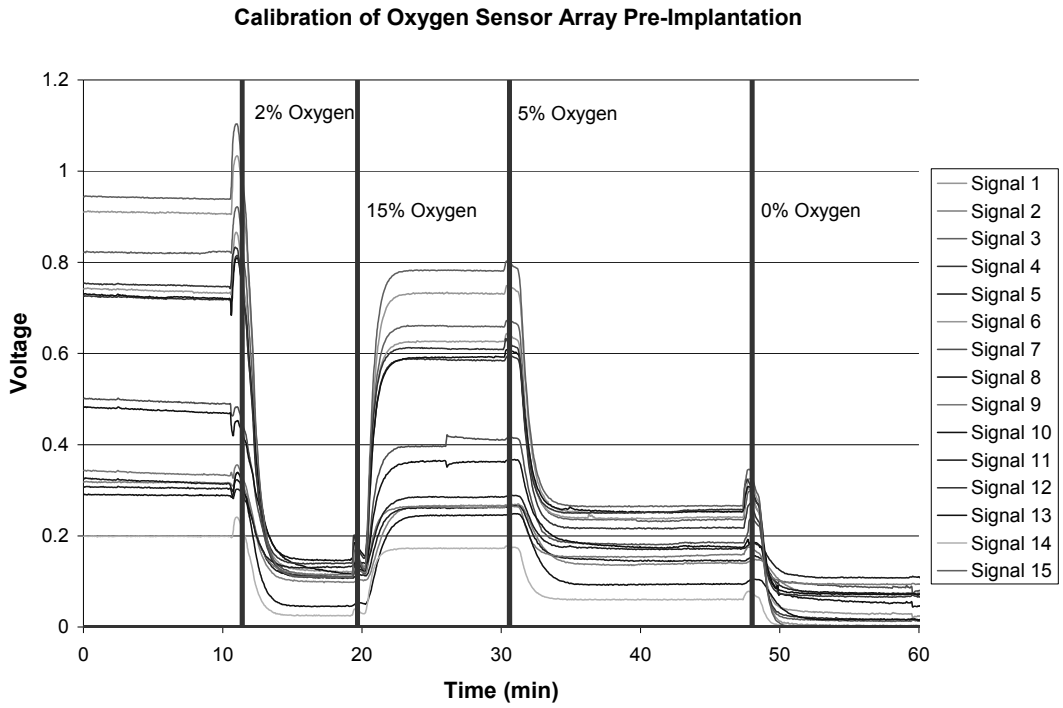


**Figure II-1. In vitro calibration process of the oxygen sensor array implanted in the pig, with four oxygen challenges of 2%, 15%, 5%, and 0% at times of 11.4 minutes, 19.7 minutes, 30.6 minutes, and 48.0 minutes.**

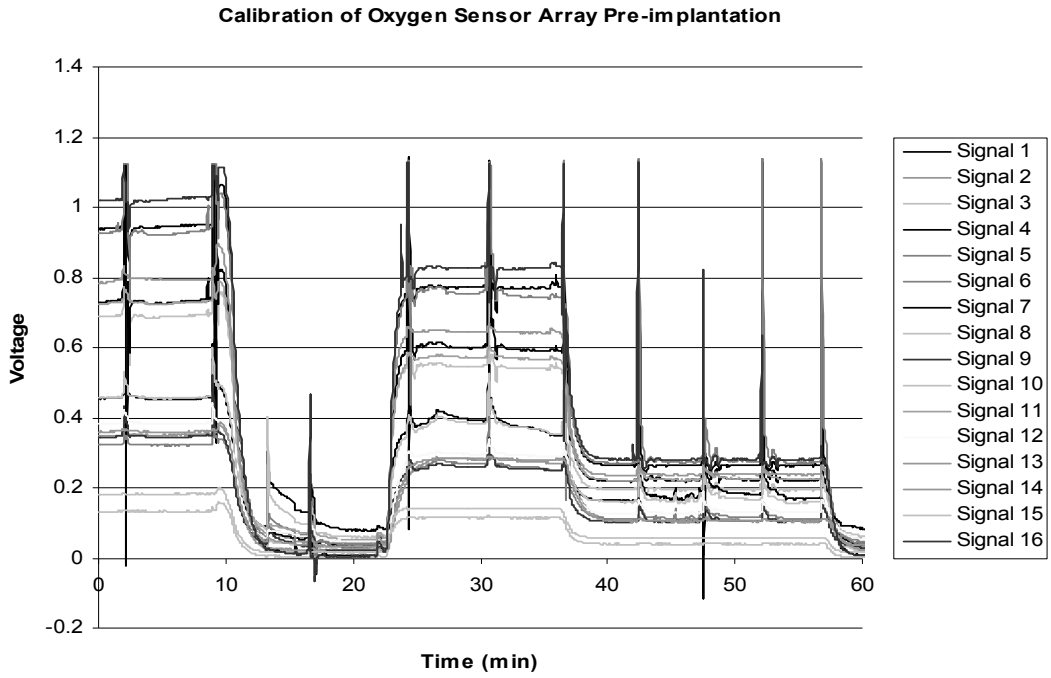


**Figure II-2. In vitro calibration process of the oxygen sensor array implanted in the hamster, with four oxygen challenges of 2%, 15%, 5%, and 0% at times of 9.62 minutes, 22.9 minutes, 35.9 minutes, and 56.9 minutes. Note that the collected in vitro signals contain noise in the form of electronic impulses.**

## II.E Implanted Oxygen Sensor Signal Datasets

The oxygen signal datasets analyzed in this project are presented in Table II.1. The oxygen signals are collected from sensor arrays implanted in two different hamsters and pigs. From each animal, a number of signals are chosen to represent the dynamics of the observed sensor array signal response. From the hamster datasets, four representative oxygen signals are chosen, and from the pig datasets, two representative oxygen signals are chosen.

**Table II-1. Table of Hamster and Pig Oxygen Signal Datasets**

| Hamster Oxygen Sensor Signals | Sampling Rate (seconds/sample) | Number of Samples Collected | Time Duration (minutes) |
|---|---|---|---|
| **Hamster A: Signals 1, 2, 3, 4** | 4.38 | 400 | 30 |
| **Hamster B: Signals 1, 2, 3, 4** | 4.38 | 976 | 71 |
| **Pig A: Signals 1, 2** | 1.24 | 3415 | 70 |
| **Pig B: Signals 1, 2** | 1.24 | 2901 | 60 |

# Chapter III: Methods of Analysis

The implanted oxygen sensor array produces sets of sampled, discrete time signals that represent the dynamics of oxygen flux within the tissue. In order to characterize the signal response features observed in the collected time signals, an engineering approach was used. Methodologies developed by the signal processing and time-series analysis fields present the best approach to analyze the biosensor data. These established and well-recognized methodologies have been relied upon to analyze, characterize, and study both time-varying and spatial-varying signals. The appropriate and applicable methods will be drawn on to analyze the oxygen sensor array signal data and characterize the observed signal response features. In this section, the applied signal processing and time-series analysis methods will be presented and reviewed.

## III.A Sampling Rate of the Implanted Oxygen Sensor

The oxygen sensors implanted in the subcutaneous tissue of hamsters and pigs collect samples of the tissue oxygen flux once every several seconds creating a dynamic picture of the *in vivo* tissue oxygen flux. The collected samples of the implanted oxygen sensors produce a discrete time signal that represents the original and continuous oxygen flux that occurs in real live tissue. With an appropriate sampling rate, the original signal can be reconstructed from the discrete time signal, and used to investigate, characterize, and explain the tissue oxygen flux signal

variations. From this investigation we can learn how a sensor implanted in the subcutaneous tissue responds to measuring a metabolite as ubiquitous as oxygen, and how oxygen dynamics affect the sensor array signal response. Furthermore, these result will be enormously valuable for other implanted biosensors, as wells as tissue engineered cellular devices.

The main theoretical postulate that underlies signal processing is the Shannon-Nyquist sampling theorem [22, 23]. The theorem states that to correctly reconstruct the original continuous signal the sampling rate must be greater than twice the highest frequency occurring within the original signal. Thus, to choose an appropriate sampling rate for the implanted oxygen sensor, we must know the highest frequency of natural variation for oxygen flux that occurs in the living tissue.

The implanted oxygen sensor array signal variations are hypothesized to be due to spatial and temporal arteriolar vasomotion. Based on the current literature [10, 13, 18] the maximum rate of vasomotion in arteriolar vessels is about 25 cycles per minute (416.7 mHz). Vasomotion can therefore theoretically affect the oxygen flux by causing fluctuations of up to 25 cycles per minute. Accordingly, the sensor sampling rate must be at least twice the highest frequency, resulting in the ideal sampling rate of at least 1 sample every 1.2 seconds.

The implanted oxygen sensor array samples the *in vivo* tissue oxygen flux with varying sampling rates ranging from approximately from 1.24 to 4.38 seconds per sample. For the oxygen sensors implanted in the awake hamster window chamber model, the sampling rate was approximately 1 sample every 4.38 seconds or a sampling frequency of 228 mHz. For the oxygen sensors implanted in the pigs, the

sampling rate was 1 sample ever 1.24 seconds, resulting in a sampling frequency of 893 mHz. According the Nyquist theorem, the limit on the highest frequency that can be correctly reconstructed from the discrete time signal is half the sampling frequency, or 114 mHz. This means that the highest frequency of oxygen flux that can be measured by the implanted oxygen sensor in hamsters is 114 mHz, and 447 mHz for the pigs, and any frequency greater than 125 mHz or 447 mHz contained within the discrete time signals of the hamsters and pigs may be considered erroneous.

The implanted oxygen sensor array is able to sense small and rapid changes in the local tissue oxygen flux, resulting in different types of variations in the collected signal responses. This high level of sensitivity to changes in oxygen concentration is due to the design of the oxygen sensor array. The sensor contains an extremely thin membrane of very permeable material (PDMS), resulting in relating rapid oxygen mass transfer in the membrane compared to the slower mass transfer in the tissues. Thus, small changes in local mass transfer are expected to have a large effect on the signals [1, 2, 3].

In order to identify and explain all the signal variations and patterns observed in the implanted oxygen signal data, time series analysis methods are applied. The first and simplest method of analysis involves plotting the collected oxygen signal response samples versus the sample time. The resulting plot of signal versus time allows any patterns in the time-domain to be displayed and identified. Based on this data, it is observed that the oxygen signal response contains many different types of variations that we will call the implanted oxygen sensor signal features.

### III.A.1 Biological Signal Response Features

The first type of feature observed in the sensor array signal response is the variability in range of steady state signal amplitudes produced by each individual electrode on the implanted sensor array. Figure III-1 shows an example of the different steady state levels for each signal response from an implanted oxygen sensor array after 2 weeks of implantation. The steady state levels vary from low to high (0.01 to 0.9 V). As mentioned previously, all compared electrodes are nearly identical in manufacture, and maintain stability of sensitivity to oxygen as indicated by negligible difference between pre-implantation and post-explantation calibrations [3]. Therefore, the different steady state signal amplitudes are hypothesized to be due to the differences in the microvasculature environment local to each electrode on the sensor array. Figure III-2 presents an image of the implanted oxygen sensor array and the overlaying heterogeneous microvasculature.

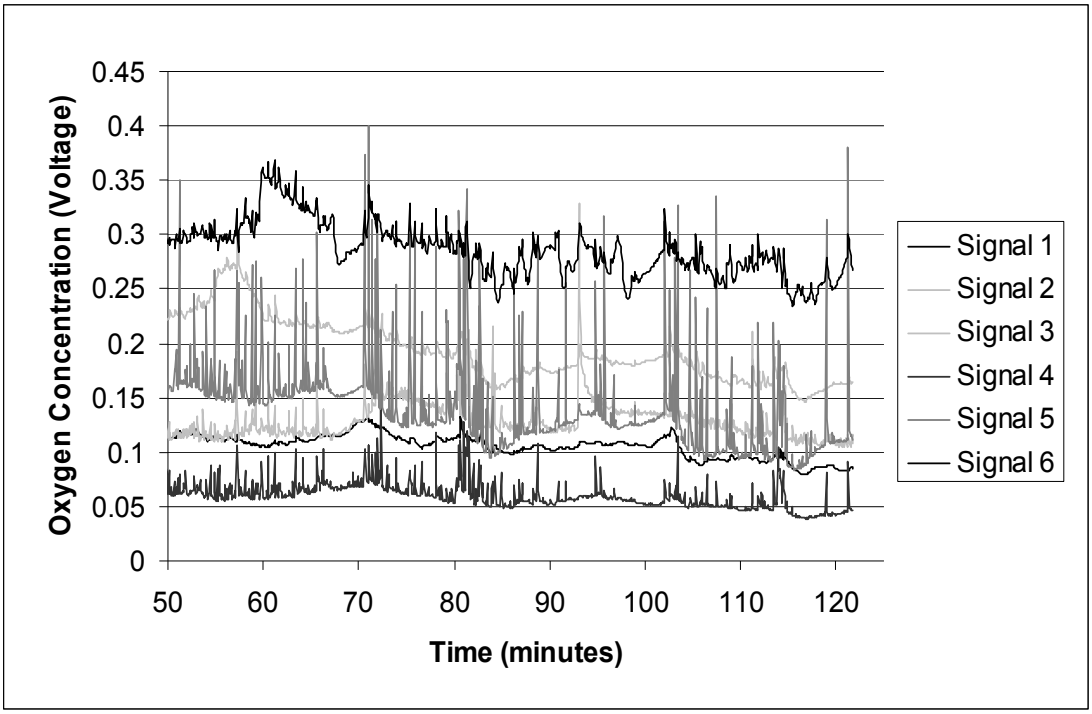


**Figure III-1. Example of the unfiltered implanted oxygen sensor signal responses of Hamster-B. The graph demonstrates the different steady-state signal amplitudes, ranging 0.05 to 0.2 V of six electrodes on the implanted sensor array. The signal responses of certain electrodes have been removed for clarity.**

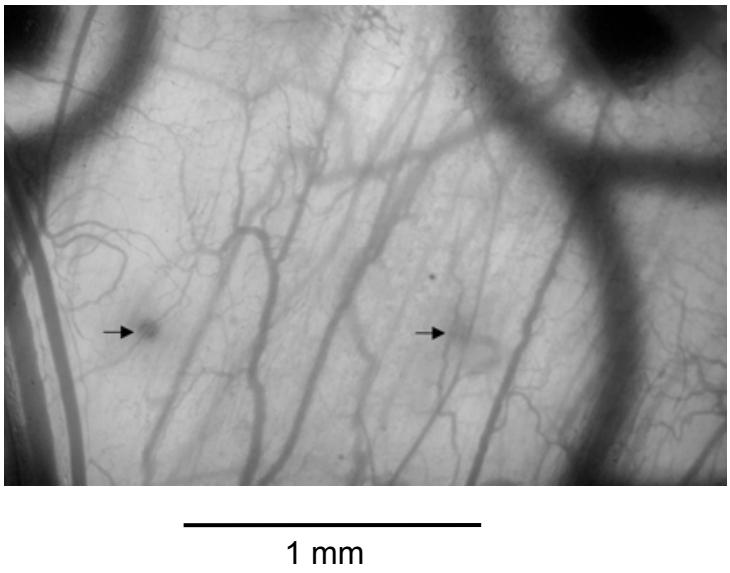


**Figure III-2. Image of the implanted oxygen sensor array in the hamster window chamber and the overlying heterogeneous microvasculature. The two arrows point at two electrodes on the oxygen sensor array, the unique microvasculature local to each electrode is clearly observed [1].**

The second type of feature observed in the sensor array signal response are rapid, small amplitude oscillations occurring on the order of seconds. The frequency of signal oscillations collected from each electrode on the implanted sensor array varies over time, and ranges approximately from 2 to 10 cycles per minute. Figure III-2 shows examples of this feature.

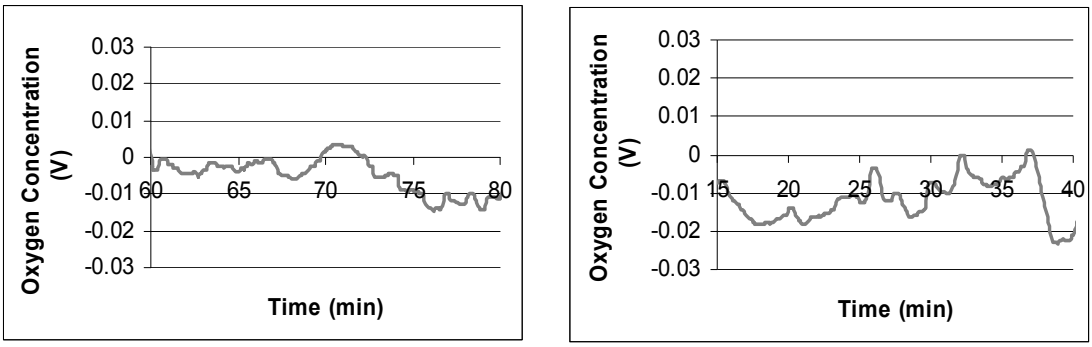


**Figure III-3**. **Examples of rapid, small amplitude oscillations observed in detrended, smoothed, and filtered oxygen sensor signals collected from Hamster-A (left), and Hamster-B (right).**

These rapid, small amplitude oscillations are hypothesized to be due to spatial and temporal arteriolar vasomotion occurring in the local tissue microvasculature of each respective electrode on the implanted sensor array. The physiologic basis of arteriolar vasomotion is the regulation of blood flow to the nearby tissues. Since the oxygenated arteriolar blood delivers the oxygen to the surrounding tissue, any fluctuations in the blood flow rate or diversion of blood flow from one region to another may result in fluctuations in the tissue oxygen perfusion rate. Therefore it is arteriolar vasomotion that is believed to be a possible source for the rapid, small amplitude fluctuations observed in the oxygen sensor signal response. Moreover, experiments conducted using the awake hamster skinfold model show that the

fundamental frequency of vasomotion in arterioles can range from 2 to 25 cycles per minute [10, 13, 18]. The observed oxygen signal oscillate at frequencies of 2 to 10 cycles per minute, which falls neatly within the arteriolar vasomotion range found in the literature. This further strengthens the assumption that it is arteriolar vasomotion that serves as a cause for the rapid, small amplitude signal oscillation observed in the collected oxygen signal.

The third type of biological signal feature found in the sensor array signal response is slow, large amplitude oscillations occurring on the order of minutes. Figure III-4 shows examples of four slow wave oscillatory signals collected from the sensor array implant in Hamster-B.

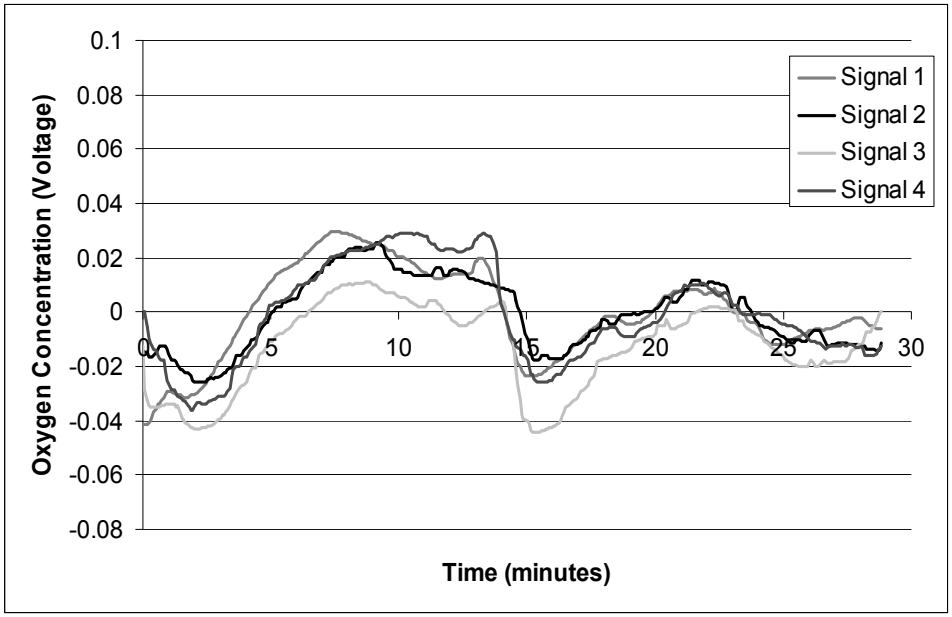


**Figure III-4**. **Hamster-B, Representative Signals 1-4. Signals have been detrended, smoothed, and filtered using the processing algorithm. Two slow, large amplitude oscillations occur over an approximate 25 minutes, starting from time of 2 minutes to 27 minutes. These oscillations are also correlated among all four representative signals.**

These oscillations are found to be coordinated among multiple signal responses from the electrode sensor array. It is hypothesized that the observed slow, large amplitude oscillations of oxygen flux could be due to changes in the regional tissue oxygen perfusion surrounding an area of the implanted oxygen sensor array. In effect, changes in the regional vascular perfusion would affect a larger tissue microenvironment, and it could be simultaneously detected multiple by electrodes on the sensor array that are located in the affected area. As a result, any electrodes near the area of oxygen perfusion would produce similar signal responses that would be correlated since they are measuring similar changes of tissues oxygen levels. Interestingly, much slower oscillations of the order of 1 to 2 weeks are observed in telemetry-based sensor observation in pigs that contain the sensor implant for over a year-long period. These features are being studied by other researchers.

## III.A.2 Non-Biological Signal Response Features

The second class of signal response features identified from the sensor signal time-domain plots are non-biological features. The first type of non-biological features are motion artifacts, identified is positive and negative impulses originating from the baseline level of the sensor signal. These impulses rise and fall too rapidly and sharply, over several sample periods (3 to 10 sample points to 30) to be considered anything but noise. Current literature postulates [12, 15, 16, 17] that there is a 2 to 3 factor change in the oxygen content from inside the arteriolar vessel to the surrounding local tissue environment over a 100 μm distance. As the distance from the vessel increases, the tissue oxygen content reaches a steady state plateau.

Consequently, over a 1000 μm tissue block, the maximum change in oxygen levels would be by a factor of 3 [21]. The positive and negative signal impulses, representing rapid, sharp changes of the oxygen flux in the local tissue environment, are observed to reach magnitudes 2 to 10 times greater than the signal steady state level over several sample periods (10 to 30 seconds). Such a rapid and large change in the oxygen flux over a time period of seconds is not physically possible in biology, and clearly a non-biological artifact of the oxygen signal. The source of the positive and negative impulses is hypothesized to be due to movement of exposed wire connections from the sensor to the signal collection device. The impulses can occur individually or consecutively, and can also be correlated with other impulses occurring in signals collected from the other electrodes on the sensor array. The impulses that are correlated among multiple signals from the same sensor array are due to movement in a group of the exposed wires. The impulses that occur consecutively are due to the movement of external connections over a certain interval of time.

The second type of non-biological signal features are erratic, jagged spikes that that rapidly rise above, sharply change direction, and then rapidly fall below the steady-state level, before returning to the signal baseline, all within a time interval of seconds. The erratic, sharp spikes in oxygen flux that characterize this feature are analogous to the electronic artifacts observed in signals collected from other implanted biosensors. This gives support to the assumption that the erratic spikes in the signal are electronic artifacts and of non-biological origin. Furthermore, there is

no reasonable biological explanation to rationalize these types of erratic changes in the tissue oxygen flux.

## III.B Digital Filtering

Once the time-domain features of the implanted oxygen sensor signal response have been identified, it is necessary to filter the collected signals. The type of features identified includes possible target biological features and artifactual non-biological features that distort the signal. To properly analyze the oxygen signal data, the unwanted non-biological features need to be suppressed or removed from the signal; otherwise the results of the time series analysis could be significantly biased and distorted. The application of a designed filter to the oxygen signal will remove the unwanted features, and provide a processed and 'cleaned' signal that will be used for analysis of the signal.

There are two general methods of filtering in signal processing [23]. The first and simplest method is to design a basic digital filter. A basic digital filter is a *frequency-selective filter* that is designed to have specific characteristics for the frequency domain in terms of the desired magnitude and phase response of the filter. Examples of such digital filters include low-, high-, bandpass, bandstop, low-shelf, high-shelf, etc. filters. These digital filters are designed based on known prior design criteria, where the specific frequency properties of the signal need to be known in advance in order to construct the desired filter. Also, basic digital filters are static filters, meaning that they are fixed throughout their application to the signal and

cannot respond to changes that might occur in the duration of the signal. Since there is no a priori qualitative knowledge of the oxygen signal properties, designing a digital filter to accurately remove the signal non-biological signal features and noise will be difficult. Alternatively, the filter can be designed by trial and error, but this is not an effective method of selecting an appropriate digital filter and the corresponding frequency characteristics.

The second method of filtering is called *adaptive filtering*. Adaptive filters are complex digital filters that are capable of adapting to the input signal by making self-adjustments and optimizing their filtering algorithm. In order to design such a filter certain properties about the input signal to need to known, such as what is the noise signal distorting the input signal (the reference signal), or what is the desired output signal. In the case of designing an adaptive filter to remove the non-biological features from the oxygen signal, the properties of the oxygen signal need to be known. However, the noise signal affecting the oxygen signal is not known, and the desired output of the filter, a noise-free and artifact-free oxygen signal response is not known. The only information about the sensor that is known is that there are two identified types of non-biological signal features distorting the oxygen signal, and that those features need to be removed. Any further information about non-biological features, such as specific frequency or statistical properties, is not known. As a result, there is not enough information known about properties of the collected oxygen signal response to design an adaptive filter and remove the unwanted signal features.

## III.C Designed Filtering Algorithm

Traditional methods of digital filtering can not be applied to the implanted oxygen sensor signal response because not enough design requirements, such as the frequency or impulse response, are known about the of the collected oxygen signals. Instead, to filter the oxygen sensor signal data and remove the non-biological signal features, an algorithm was designed to target, suppress, and remove the unwanted features of the signal. The algorithm accepts as input the original collected sensor signal that contains both the biological and non-biological features, and outputs a filtered oxygen signal with the unwanted features suppressed. The algorithm is outlined as series of processing steps shown in Figure III-5. The following is a discussion of filtering approach applied in the designed filtering algorithm. For full details of the oxygen signal filtering process, the Matlab code [26] of the designed filtering algorithm, called *baseline.m*, is provided in Appendix B. (For the purpose of designing the filtering algorithm, the collected oxygen sensor signals are assumed to have Gaussian statistical properties.)

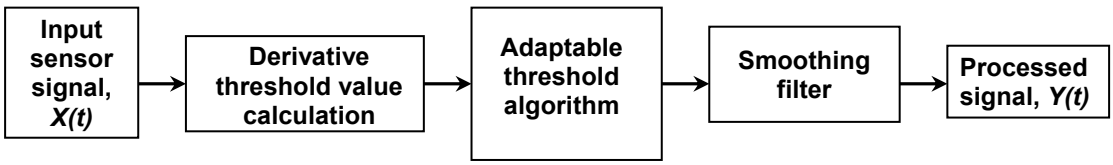


**Figure III-5**. **Designed filtering algorithm diagram.**

The designed filtering algorithm steps are shown in Figure III-5. The first diagram box is described as 'Derivative threshold value calculation.' This is the basis of the method used to distinguish non-biological signal features from the biological

signal features. The purpose of the derivative threshold value box is to indicate the locations of the non-biological signal features within the oxygen sensor signal by assessing the rate of change, or the derivative, over consecutive pairs of sample points.

The second box is the 'Adaptable threshold algorithm.' The purpose of the adaptable threshold algorithm is to determine all of sample points involved in the non-biological signal features and then to replace them with interpolated signal values. The adaptable threshold algorithm involves examining the surrounding sample points around each marked sample point, and re-calculating the derivative threshold value specifically to that non-biological signal feature's characteristics; thus, adapting the derivative threshold value. The surrounding sample points are then re-evaluated with the new threshold value and the sample points that span the non-biological signal are determined.

The third and last box uses applies a 'Smoothing filter,' either an appropriate moving average filter or a median filter, to the smooth the interpolated signal points that replaced the non-biological signal features with the rest of the oxygen signal. This is an important step because if the replaced points are not 'smoothed' with the rest of the signal, they could be interpreted as significant features of during the oxygen signal analysis and bias the results.

Calculation of the rate of change, or the derivative, of consecutive pairs of sample points of the oxygen sensor signal is a key part of the filtering algorithm. The main characteristic property of the non-biological signal features are sharp, rapid changes in the signal direction, which can also be mistaken for the biological signal

features of rapid, small amplitude fluctuations. This problem is addressed by having a derivative threshold value calculated from the variance of derivatives of consecutive pairs of sample points from the oxygen signal. The decision to use the variance of the derivatives was obvious because the derivative values of the non-biological signal features are at least five greater than the derivative values of the rest of oxygen signal sample point pairs. From the biological standpoint, the oxygen signal features must be within a certain range of biological feasibility. Since the non-biological features include changes in the oxygen flux that increase and decrease too rapidly, and to large magnitudes, those oxygen signal changes must be considered as a non-biological event. Therefore, calculating the derivatives for pairs of sample points of the oxygen signal was the best method to locate the non-biological signal features within the oxygen sensor signal.

The non-biological signal features of positive or negative impulses within the oxygen signal are identified by evaluating the first-derivatives (rates of change) of the impulses. The absolute derivative value for each consecutive pair of oxygen signal sample points is calculated for the entire signal duration. The average and standard deviation of the signal derivatives is also calculated and used to identify the maximum value for the rate of change between pairs of sample points. This value is chosen to be the derivative threshold value. Any pair of sample points that has an absolute derivative value greater than the defined derivative threshold value is recognized as an indicator where a non-biological signal feature, a large positive or negative impulse may have occurred. However, the impulse may span several sample point and only the derivative of one pair of sample points that is part of the impulse

exceeds the defined derivative threshold value. To address this issue, the algorithm is designed to have an *adaptable* derivative threshold value. The means that the pairs of sample points surrounding the identified derivative point are re-evaluated using a new threshold derivative value determined specifically for those local points. The number of surrounding sample points re-evaluated is dependent on many sample points away the next nearest non-biological signal feature is located and visual inspection of the non-biological signal features types found within the signal being processed. In general, the number of points re-evaluated varies from 10 to 40 sample points. The new derivative threshold value is calculated from the statistical properties of derivatives of the surrounding pairs of sample points before and after the indentified sample points with large-valued derivative. From the surrounding pairs of sample points, if any exceed the new calculated threshold, all the points between it and original identified pair of points are considered to be part of the impulse duration. Therefore, those points determined to be part of a non-biological signal features and are marked for processing (i.e. suppression of the unwanted signal feature).

The identification of the non-biological signal features of noise artifacts is similar to the method of identification of the positive and negative impulses features. First, the derivative of each consecutive pair of sample points in the oxygen signal is calculated. The derivatives of consecutive sample points that follow the pattern of having values that are positive, negative, positive or negative, positive, negative, are identified. The absolute value of the derivatives are examined in a second iteration using a derivative threshold value calculated from the statistical properties of the derivative values of surrounding pairs of sample points. The derivative threshold

value is used to evaluate if the surrounding sample points represent sharp, rapid, erratic changes in oxygen signal, and are therefore part of the non-biological artifact feature. The points that are determined to be part of the non-biological feature are then marked for suppressed in the filtering algorithm.

Once the sample points that make up the non-biological signal features in the oxygen signal have been located, the sample points must be adjusted. As the identifying feature of the non-biological signal features are rapid and large magnitude impulses, the ideal adjustment is to remove the impulse points from the signal and replace them with a connecting line of signal values that spans the base of the impulse, or a baseline. The baseline is calculated by taking the value of the sample point right before the start of the impulse, and the value of the sample point at the end of impulse, and calculating the cubic spline interpolation for the points that span the impulse. By interpolating the points that span the impulse, an estimate can be made of what the oxygen signal would look like if the impulse had not distorted the signal. The end result of adjusting all the identified artifact points is a 'cleaned' oxygen signal where all the identified non-biological features are removed and replaced with an estimate of the oxygen signal at those sample times.

After the removal of the non-biological signal features, it is beneficial to smooth the new oxygen signal to reduce any discontinuities between the replaced and interpolated signal points and the remaining oxygen signal points. By smoothing the signal, it prevents any possible discontinuities created by the interpolated signal values from being interpreted as features of the oxygen signal. The oxygen signal data is smoothed using a moving median transformation (median filter) or a moving

average transformation (mean filter). The median filter is a non-linear windowing filter that smoothes large magnitude impulses from the oxygen signal without affecting the small magnitude signal fluctuations. The mean filter is very similar to a low-pass filter. It is linear moving average digital filter that computes the average of a moving window of signal points. The filter is useful in that it smoothes the signal fluctuations and emphasizes any long-term periodicities within the signal. Both types of smoothing methods have advantageous properties, and the method applied to each individual oxygen signal was chosen based on the observed non-biological features distorting the signal. The window sample size of the filters was determined from the average number of sample points involved in the non-biological signal features of an oxygen signal.

## III.D Signal Preparation Prior to Analysis

In order to prepare the oxygen signal data for analysis, first the mean is subtracted from the signal, and then the linear trend is removed. If the mean is not removed and the signal is not detrended, these effects have the potential of masking any useful periodicities or real (biological) oxygen signal features in the data. Secondly, the oxygen signal is filtered using the designed filtering algorithm to remove the non-biological signal features. Thus, the resulting oxygen signal is demeaned, linearly detrended, and 'cleaned' of the non-biological signal features. This oxygen signal is free of any biasing effects distorting signal features, and is prepared for further analysis.

## III.E Power Spectral Analysis

Power spectral analysis is a principle tool of signal processing, and is commonly the first method applied in the process of analyzing a time signal. The power spectrum is used to identify any frequency-dependent variability, called periodicity, within a signal. It is calculated by squaring the magnitude of the Fourier transform (FT) of a series,

$$\text{Power}(S_1) = | \text{FT}(S_1) |^2 \qquad \text{(III-1)}$$

And the spectrum is plotted as power (energy per unit frequency) as a function of frequency. By locating the high power peaks in the power spectrum, the corresponding frequencies signify an equivalent periodicity within the signal.

The collected oxygen sensor signals are data sets of finite time sample points, and the calculation of the power spectrum requires infinite integration with time. Alternatively, if the discrete time Fourier transform was used to calculated the power spectrum, spectral bias would be introduced because of sharp truncation of the finite signal. Therefore, power spectral estimation methods must be used to acquire an estimate of the power spectral density for a finite time signal.

The method of spectral estimation applied to the oxygen signal data is the Welch method because it is robust non-parametric approach. Non-parametric methods do not make assumptions about the structure and probability distribution of the signal to be analyzed. This is a useful property because the probability distribution of the noise-free and artifact-free oxygen signal data is not known. The Welch method involves segmenting the time signal into overlapping sections and

windowing each segment such that the center of the segments is weighted more than the tail ends. To prevent loss of information, the adjacent windowed segment tail ends are overlapped. Next, the individual periodogram for each segment is calculated by taking the square magnitude of the discrete time Fourier transform, and the power spectrum is estimated by the time-averaging all of the periodograms. Although the averaging of the periodograms may reduce the variance of the power, it also reduces any noise in the finite time signal [22, 23].

## III.F Correlation Analysis

Correlation analysis and the calculation of the Pearson's correlation coefficient are excellent statistical signal processing tools to measure the similarity among the oxygen time signals collected from the same implanted sensor array. These tools can be used to measure the strength and direction of any linear relationship between the oxygen signals and to determine if there are any repeating patterns or features shared between the signals, and at what time-shifts they occur at. The *cross-correlation* is the correlation between two different signals time-shifted against one another as function of time-shift periods. The *autocorrelation* of a time-signal is the correlation of a signal's own past values with its future values time-shifted against one another. Calculation of the normalized cross-correlation function involves normalizing the oxygen signals, time-shifting one of the signals, $S_1$, and multiplying it by the other signal, $S_2$.

$$\text{Cross-Correlation Function of } (S_1[t], S_2[t]) = \sum_{n=-\infty}^{\infty} S_1^*[n] \cdot S_2[n+t], \qquad \text{(III-2)}$$

Where $S_1^*[n]$ is the complex conjugate of $S_1[n]$.

The autocorrelation function is calculated in the same manner as the cross-correlation, but the signal is crossed with itself. The autocorrelation function has a maximum correlation coefficient of one at the time-shift period of zero. The normalized cross- and autocorrelations are plotted as Pearson's correlation coefficient as function of time-shifts [23].

*Pearson's correlation coefficient* is used as a unit of measurement of the correlation for the oxygen signals. The values of the correlation coefficient can range from 1 to -1. When the value nears 1 or -1, it indicates a greater positive or greater negative linear relationship between the oxygen signals. A correlation coefficient of zero indicates that there is no linear relationship between the oxygen signals. When the cross- or autocorrelation of the oxygen signals is calculated, there may be transient time periods of strong and weak correlation, indicating significant correlation for only certain periods of time. Additionally, when evaluating the cross- and autocorrelations of the discrete time oxygen signals, it is important to determine confidence bounds for the correlation coefficient. The calculation of confidence bounds determines the range of values for which correlation coefficient may be considered significant for the correlational analysis of oxygen signal data.

The statistical significance of the correlation coefficient depends on the probability distribution of oxygen signal data, and on the number collected sample points in oxygen signal dataset. The Pearson's correlation coefficient of the signal

data is considered to be most accurate estimate of the population data when the time signal has a normal distribution and when the dataset is moderate to large in size. For the oxygen signal data, the probability distribution of the artifact-fee and noise-free oxygen signal is unknown. However, the signal data set sizes are large, where the short-term data set sizes vary from 400 to 3000 sample points, and the long-term data sets have sizes from 55,000 to 80,000 sample points. Therefore, for the oxygen signals with an unknown, and possibly non-normal probability distribution, and with a large data set size, the Pearson's correlation coefficient is considered to be unbiased and a consistent estimator of the correlation.

Another type of correlation analysis tool that is applied to the oxygen sensor signal data is the *lagged scatterplot* (lag plot) analysis. The lag plot is a graphical tool that is used to determine whether the oxygen signal data points are random or non-random, meaning there is spatial dependence between the oxygen signal sample points. The lag plot can also help identify the type and strength of the non-random correlation the signal points have with each other, for example linear, curvilinear, or sinusoidal. In addition, the lag plot can show whether the correlation is driven by one or more outliers within the oxygen signal data set. This is a valuable feature and distinct from the autocorrelation function which can not distinguish non-linearity within the oxygen signals [23].

The lagged scatterplot of the oxygen sensor signal is determined by plotting the oxygen signal against itself offset by $k$ data points. Therefore, for an oxygen signal that has $N$ sample points, the lagged scatterplot would be a plot of the last $N - k$ signal points against the first $N - k$ signal points. If the plotted points have an

organized pattern of curvature, it suggests a nonlinear correlation between the oxygen sensor signal points. If a straight line can be fitted to the lagged scatterplot, it suggests a linear dependence between the oxygen signal points, and the correlation coefficient of the fitted line evaluates the strength of the linear relationship.

## III.G Continuous Wavelet Transform Analysis

Wavelet analysis is a considered to be a new method of signal processing and time series analysis that allows the oxygen sensor signal's time and frequency domain characteristics to be represented simultaneously. This is an especially useful feature as it permits the stationarity of the discrete time oxygen signal to be evaluated. A signal is considered to be stationary only if the probability distribution, for example statistical parameters such as the mean and variance, do not change with time and space. By establishing the stationarity of the implanted oxygen sensor signal, it can determined whether the signal variations which represent the biological dynamics of the oxygen flux, have a constant probability distribution or whether the variations have different probability distributions. If the oxygen signal is determined to be stationary, such that the probability distributions for the entire signal are constant, then it may be assumed that the variations are due to a singular biological affect on the tissue oxygen flux. If the oxygen signal is found to be non-stationary, such that the signal variations are found to have different probability distributions at different times, it may signify different biological events affecting the tissue oxygen flux.

The wavelet analysis of the oxygen sensor signal involves the mathematical transformation of the signal into amplitudes called wavelet coefficients. Each calculated wavelet coefficient represents an equal area of the time-frequency plane, providing an amplitude measurement for range of frequencies, during a specific time window of the signal. Fundamentally, exact measurements at a specific time and frequency are not possible due to Heisenberg's uncertainty principle. However, wavelet analysis overcomes this problem by segmenting the collected oxygen signal into windows of finite time intervals and determining the frequency content of each time window. For a frequency to be detected in specific time window of the signal there must be at least one period of oscillation at that frequency. As a result, the resolutions for the time and frequency domain are dependent on the size of the time windows. In order to have good resolution for both the time and frequency, the length of the time windows is adjusted for each frequency that is detected. Hence, slow frequency events are examined with long windows, and fast frequency events are examined with short windows.

The continuous wavelet transform (CWT) of the discrete time oxygen sensor signal, S[t], with N sample points, is defined as:

$$CWT(S[t]) = \sum_{n=0}^{N-1} S[n]\psi^* \left[ \frac{(t-n)\delta t}{s} \right] \qquad \text{(III-3)}$$

Where $\psi$ is the mother wavelet, (*) indicates the complex conjugate, and $s$ is the wavelet scale (inverse of the frequency). The mother wavelet is a waveform that

is a function of time and frequency, and has finite length with zero mean. The mother wavelet is scaled (dilated) and translated (shifted in time) to create daughter wavelets. The daughter wavelets are applied to each time window of the oxygen signal and used to determine the existing frequencies. Taken together, the wavelet transform decomposes the oxygen time signal variations into wavelets, allowing us to see the different types of variability within the signal and how they change with time [24, 25].

The mother wavelet chosen for the continuous wavelet transform of the oxygen signal is the Morlet waveform. The Morlet wavelet is a Guassian function modulated by a sine wave, and was chosen as the mother wavelet because of its advantageous features. Firstly, the Morlet wavelet is nonorthogonal which is considered favorable because it produces smooth, continuous variations in the wavelet transform regardless of any periodic or aperiodic variations within the oxygen signal. An orthogonal wavelet would produce discrete 'blocks' in the wavelet amplitude, and would result in compact representation of the signal with a different wavelet spectrum for any apreiodic shift in the oxygen signal. Second, the Morlet wavelet is a complex wavelet and provides information about the phase and amplitude of the oxygen signal being transformed. This is useful as it will capture the oscillatory information of the oxygen signal variations. Third, a valuable feature of the Morlet wavelet is its shape. The shape of the chosen mother wavelet is important because that waveform will be used to decompose the oxygen signal in calculation of the wavelet transform. By choosing a mother wavelet that optimally reflects the features of the oxygen signal, the wavelet analysis will produce more precise results.

Morlet waveform is a Gaussian modulated sinusoidal curve, and it is most similar to the sinusoidal variations observed in the oxygen sensor signal. Therefore, the Morlet wavelet would be an optimal choice as the mother wavelet for wavelet analysis of the oxygen signals.

The expression for the Morlet wavelet in the time domain is:

$$\psi(u) = \frac{1}{\sqrt[4]{\pi}}\left(e^{-1\omega_0 u} - e^{-\omega^2/2}\right)\cdot e^{u^2/2} \qquad \text{(III-4)}$$

The value of $\omega_0$ is chosen carefully because smaller values of $\omega_0$ ($\omega_0 = 1$) form a waveform that best suits the localization of singular time events, and a larger values for $\omega_0$ are better suited for frequency localization. For the oxygen signal analysis, we are interested in localization of both time and frequency. Therefore, when using the Morlet wavelet, a compromise is made where $\omega_0$ is chosen such that the ratio of the highest and second highest value of $\psi(u)$ is ½ ($\omega_0 \cong 5.3364$). With a $\omega_0 \cong 5.3364$ , the expression for the Morlet wavelet in the time domain is simplified and approximated by Matlab Mathworks:

$$\psi(u) = Ce^{-u^2/2}\cos(5x) \qquad \text{(III-5)}$$

Where the constant *C* is used for normalization of the wavelet. [24, 25].

## III.H Probability Distribution Analysis

Determination of the probability distribution function of the implanted oxygen sensor signals would be useful in describing the *in vivo* statistics of tissue oxygen flux measured by an implanted sensor. It would establish the probability distribution density of the oxygen signals, which describes how signal points cluster together and the probability of a particular point having a certain value. Additionally, the statistical information of the oxygen signals would be extremely useful in evaluating the data sets for outlier points that could be a result of a biological event affecting the tissue oxygen flux, or could be due to noise.

There are various types of probability distributions and the task of testing the oxygen signal data against every possible distribution is inefficient; therefore, we have chosen to test the oxygen signal data against the *Gaussian distribution (normal distribution)*. The normal distribution is a simple probability function that has a high prevalence in real world datasets. This is due to the *central limit theorem* which states that as the as the number of independent random variables with unknown identical distribution increases the distribution of the dataset approximates the normal distribution. Therefore, if the assumption is made that the collected oxygen signal data points are independent and have near identical distributions, then the central limit theorem may be applied and it can be concluded that as the number of oxygen signal sample points increases, the signals may near a normal distribution. Moreover, by applying the central limit theorem to the oxygen signal datasets, an implication is made that the oxygen signals are stationary. In reality, the assumption of independence between the oxygen signal sample points is inaccurate as any changes

in tissue oxygen flux must depend on its past signal values. As a result, the central limit theorem cannot be applied to the oxygen signal data. However, the decision to test the oxygen signal against the normal distribution still remains valuable and informative as it will show how well the oxygen signal dataset follows a normal distribution, and any deviations will indicate a *non-normal probability distribution*. Furthermore, many statistical methods include the assumption that the datasets are normally distributed, making it an excellent probability distribution to test the oxygen signal data against.

The normal probability plot will be used to determine whether the oxygen signal data follows a normal distribution. The plot is made by graphing the observed oxygen signal data points against the expected probability values of a theoretical dataset with the same sample size that has a normal distribution. If the probability plot of the oxygen signal approximates the linear plot of the expected probabilities for the normal theoretical dataset, then the oxygen signal data is considered to be approximately normal. Alternatively, any deviations of the oxygen signal probability plot from linear normal plot specify the parts of the signal which do not follow a normal distribution.

In addition to the normal probability plot, to statistically test the normality of the oxygen signal datasets the *Lilliefors test* is applied. Lilliefors test is used to evaluate the null hypothesis that the oxygen signal data comes from a normally distributed population with unknown mean and variance. The Lilliefors test involves estimating the mean and variance of the oxygen signal dataset and determining the oxygen signal's empirical distribution. This empirical distribution function is

compared with a normal distribution that has the same values of mean and variance. If the difference between the empirical distribution function and the normal distribution function with the same mean and variance values is significant at the 5% level, then the null hypothesis of the oxygen signal being normally distributed is rejected. By applying Lilliefors test we include a statistical method of evaluation, in addition to the normal probability plot's graphical evaluation of the normality of the collected oxygen sensor signal data.

A *quantile-quantile plot (Q-Q plot)* is another type of probability plot can be used to compare the probability distributions of the collected oxygen signals of with each other. In effect, the Q-Q plot allows us to determine if the collected oxygen signals, with different sample sizes, have the same probability distribution. The Q-Q plot is made by graphing the quantiles of two oxygen signals against each other. If the plot approximates a linear line, then the two signals have approximately the same probability distribution. Otherwise, the oxygen signals are considered to have dissimilar probability distributions. The results of the Q-Q plot are useful as it can reveal whether the surrounding local area of tissue that the implanted oxygen sensor array measures the *in vivo* tissue oxygen flux from has sections with different statistical probability.

If one can consider the oxygen signals collected from the implanted sensor array to be stationary, non-deterministic, and a random variable, then the *cumulative probability distribution (cdf)* of the signal may be estimated. The cumulative probability distribution is the statistic that describes the distribution function of a real-valued random variable. Basically, by determining the cumulative probability

distribution the oxygen signals, then one can determine the probability of the oxygen signal to have any value less than or equal to the value x. An empirical estimate of the cumulative distribution of the oxygen signal data is made by calculating the proportion of oxygen signal data values that is less than each possible signal value occurring within the dataset. A plot of the proportion values are made as a function of the signal values and the shape of the plot can suggest a certain probability distribution for the oxygen sensor signals. [27, 28].

## III.I Autoregressive Modeling and Model Validation

A common parametric modeling approach of a random process in statistics and signal processing is the *autoregressive (AR) model*. The AR model is a valuable modeling tool for a random process signal, in this case the discrete time oxygen signal, with value points that are highly correlated with the points that precede and succeed them. The AR model of the discrete time series, $X_t$, is represented as $X_t$ being a function of one or more lagged time points within the series, and a error term, $\varepsilon_t$.

$$X_t = f(X_{t-1}, X_{t-2}, ..., X_{t-\alpha}, \varepsilon_t) \qquad \text{(III-6)}$$

By designing an AR model of the highly correlated time series, it can explain the relationship between the highly correlated points and also be used to predict future points of the time series.

The AR model is applicable to random process signals, and any random process is also classified as stationary. Thus, the AR modeling may be used for any oxygen signal that is found to be stationary. More specifically, the AR model is especially useful for modeling stationary time signals that have power spectrums with sharp peaks and no deep valleys. Other modeling approaches such as the *moving average (MA) model* or *autoregressive moving average (ARMA) model* are also available. The MA model is best for stationary signals with power spectrums that contain valleys and no sharp peaks, and the ARMA model is best for signals with power spectrums that contain valleys as well as sharp peaks. The selection of an adequate model for a stationary time signal may be determined from the evaluation of the power spectrum or autocorrelation plots, or by an iterative trial and error procedure and using a goodness-of-fit statistic to evaluate the model. For the analysis of the oxygen sensor signals, selection of the most appropriate model is determined from the knowledge of the power spectrum features, and it will be shown that signals collected from the implanted oxygen sensors best fit the AR model approach. Thus, the AR model will be used to model and ultimately to predict the future values of any stationary oxygen signal that satisfies the AR criteria for the power spectrum.

The AR model of a stationary oxygen signal is linear model composed of one or more prior values of the oxygen signal points. The AR(n) refers to an AR model with order number of n, and is written as:

$$X_t = b_0 + \sum_{i=1}^{n} b_i X_{t-i} + \varepsilon_t \qquad \text{(III-7)}$$

$$X_t = b_0 + b_1 X_{t-1} + b_2 X_{t-2} + \ldots + b_n X_{t-n} + \varepsilon_t \qquad \text{(III-8)}$$

Where $X_t$ is the oxygen signal time points, $\varepsilon_t$ is error (white noise), $b_i$ are the constant coefficients of the prior oxygen signal points the model is linearly dependent on, and $n$ is the AR model order.

The first step in creating an AR(n) model for the stationary oxygen signal, $X_{t,}$ is to determine the model order, n, or how many lagged $X_{t-i}$ terms to use as predictors in linear regression model. The method used to determine the AR model order is calculating the partial autocorrelation of the signal. Recall that the autocorrelation function is a measure of the correlation of a time signal with itself while being time-shifted. The partial autocorrelation is the autocorrelation of signal $X_{t,}$ with a time-shifted version of same signal, $X_{t-k,}$ where k is lag. When a suitable lag k is chosen, the partial autocorrelation will lessen and ideally render the autocorrelation within the not significant. The chosen lag k is then equal to the AR model order.

The second step in creating the AR(n) model of the oxygen signal is to estimate the coefficients of the model using least squares method. Least squares estimation method of the model coefficients, $b_i$, for the random process signal, $X_t$, with N data points:

$$X_t = \begin{bmatrix} X_{n+1} \\ X_{n+2} \\ \cdot \\ \cdot \\ \cdot \\ X_N \end{bmatrix}, \; b_i = \begin{bmatrix} b_1 \\ b_2 \\ \cdot \\ \cdot \\ \cdot \\ bn \end{bmatrix}, \text{ and } X_{t-i} = \begin{bmatrix} 1 & X_n & X_{n-1} & \cdot & \cdot & \cdot & X_1 \\ 1 & X_{n+1} & X_n & \cdot & \cdot & \cdot & X_2 \\ \cdot & \cdot & \cdot & \cdot & \cdot & \cdot & \cdot \\ \cdot & \cdot & \cdot & \cdot & \cdot & \cdot & \\ \cdot & \cdot & \cdot & \cdot & \cdot & \cdot & \\ 1 & X_{N-1} & X_{N-2} & \cdot & \cdot & \cdot & X_{N-b} \end{bmatrix} \qquad \text{(III-9)}$$

Where by ordinary least squares the AR(n) model coefficients may be solved:

$$b_i = \left(X_{t-i}^T X_{t-i}\right)^{-1} X_{t-i}^T X_t \qquad \text{(III-10)}$$

The third and last step is to diagnostically check and verify the model. This is done by first determining if the estimated coefficients are statistically different from zero. If a coefficient is evaluated and found to not be significant, then the AR model may be simplified by, for example, reducing the model order. Second, the model is verified by checking if the residual errors (real $X_t$ – model $X_t$) are random and uncorrelated in time. If the residual errors are not random then it indicates that the AR model does not successfully describe the correlation between oxygen signal points. The residuals are checked for randomness using four different graphical techniques which are summarized in a 4-plot. The 5-plot includes an autocorrelation plot, run chart, lagged scatterplot, histogram, and normal probability plot. The autocorrelation plot of the residual errors will test for any correlation between the residual error terms. The run chart is a plot of the residuals against the sample time, and will graphically summarize the behavior of residual errors. It will determine whether the residuals are from a random drawing, have a fixed distribution, a

common scale, a common location, and identify any outliers. The lagged scatterplot, described in detail earlier, will test for randomness of the residuals, and show any organized (linear or non-linear) behavior between the residual points. The histogram plot will graphically summarize the distribution of residuals. The histogram of the residual error terms is obtained by segmenting the range of the residual error terms into equal-sized bins, and counting the number of error terms that fall into each bin. The histogram is plotted as a bar graph, where the x-axis represents the range of the residual error terms, and the y-axis represents the number of counts. The shape of the histogram indicates features of the distribution. A histogram that presents a distribution shape that is fixed and bell-shaped indicates normality. If the distribution is not normal, the histogram can also show if the distribution of residuals are centered, spread out, or skewed, and expose any outliers or multiple modes. The normal probability plot will determine if the residuals follow normal probability distribution by how well the residuals follow the linear normal reference line. Thus, the 5-plot graphical summary will indentify any possible underlying non-random features of the residual errors, and it will also help determine the effectiveness of the AR model [22, 23, 28].

# Chapter IV: Results of Implanted Oxygen Sensor Signal Analysis for the Hamster

## IV.A Filtering the Hamster Oxygen Signals

The following of Figures IV-1 to Figure IV-4 present plots of the original Hamster-A oxygen sensor signals, plotted against the same signal that has been processed by being linearly detrended, filtered using the designed filtering algorithm to suppress the non-biological artifacts distorting the signal, and lastly, smoothed using a moving median filter. In order to better visualize the original signal plotted against the processed signal, the original signals were also linearly detrended in order for both signal to have the same oxygen concentration scale on the y-axis.

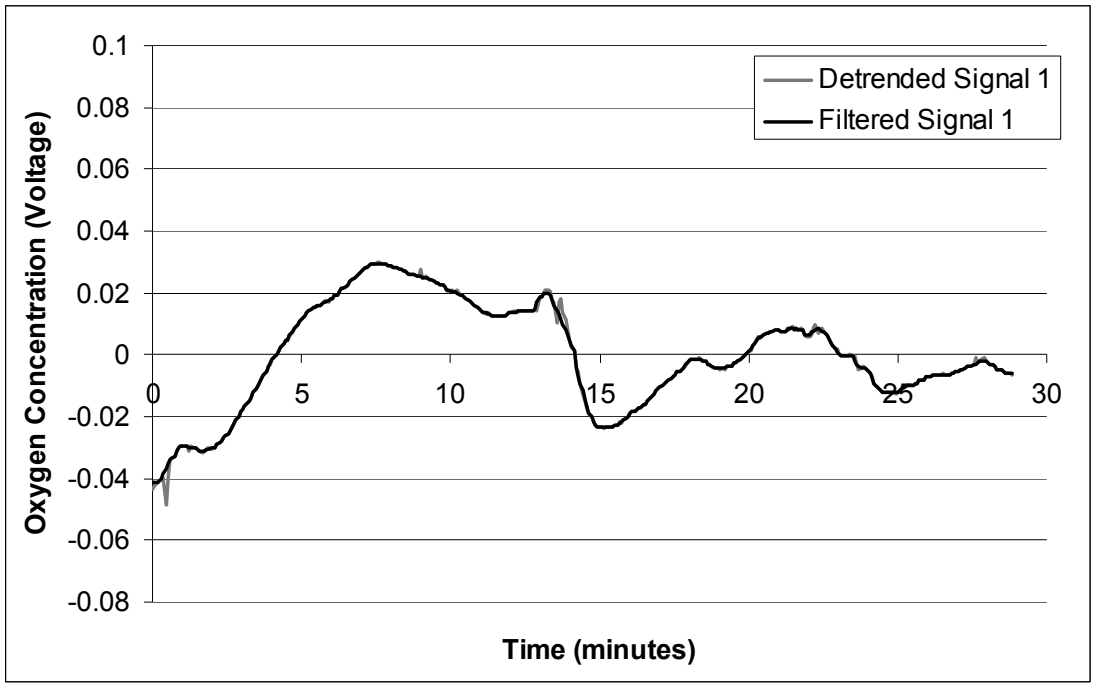


**Figure IV-1. Hamster-A, Signal 1**

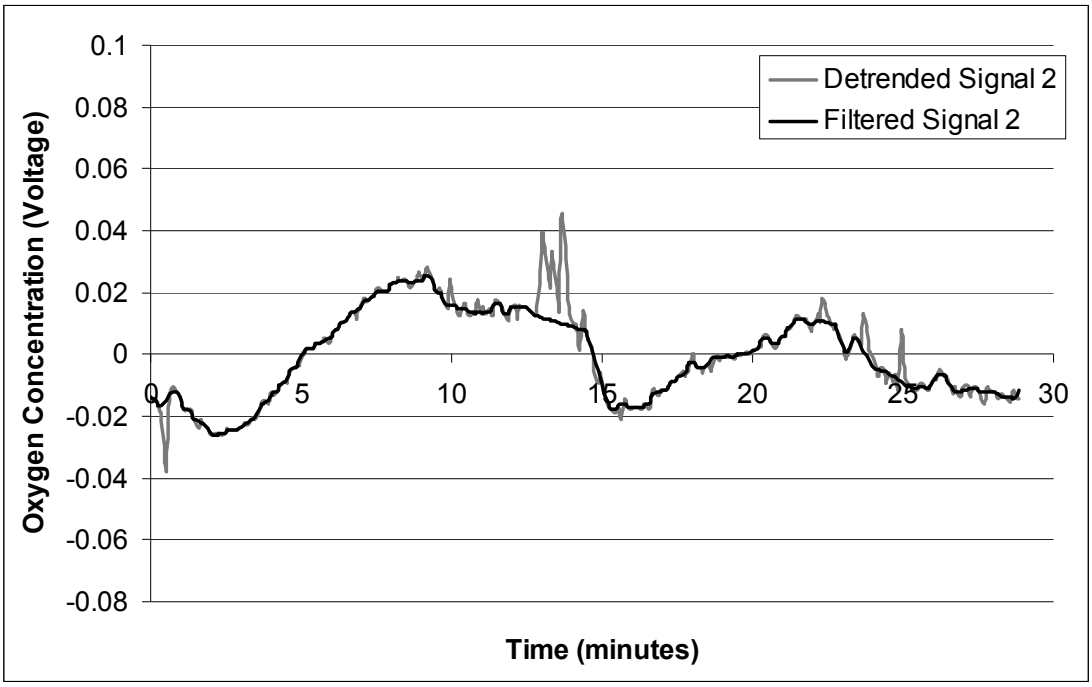


**Figure IV-2. Hamster-A, Signal 2**

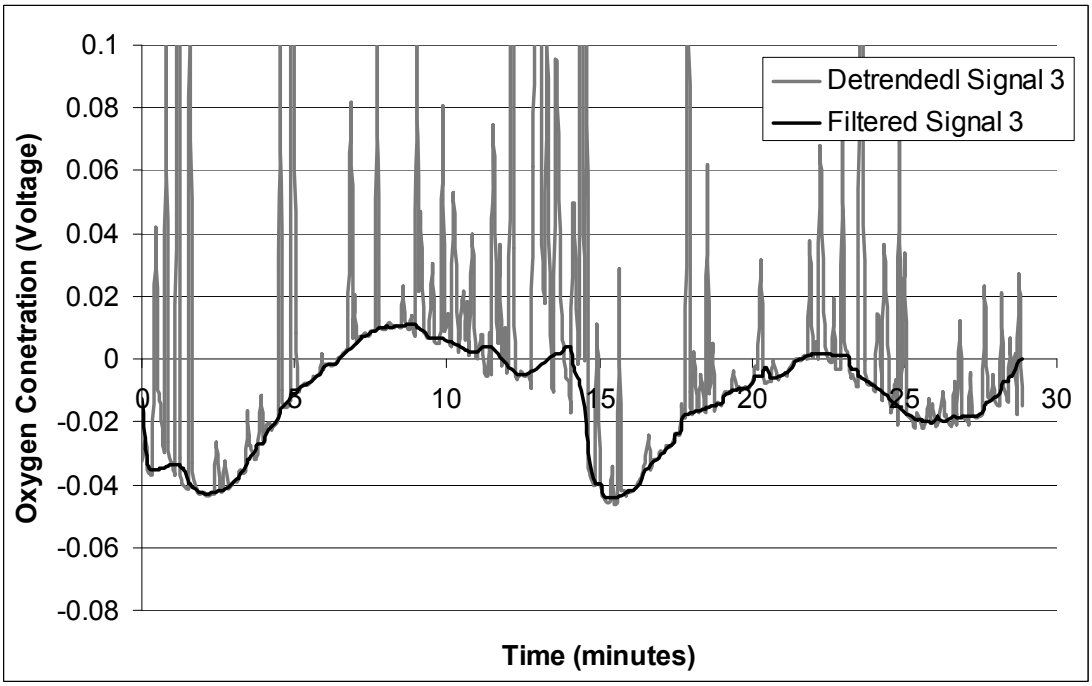


**Figure IV-3. Hamster-A, Signal 3**

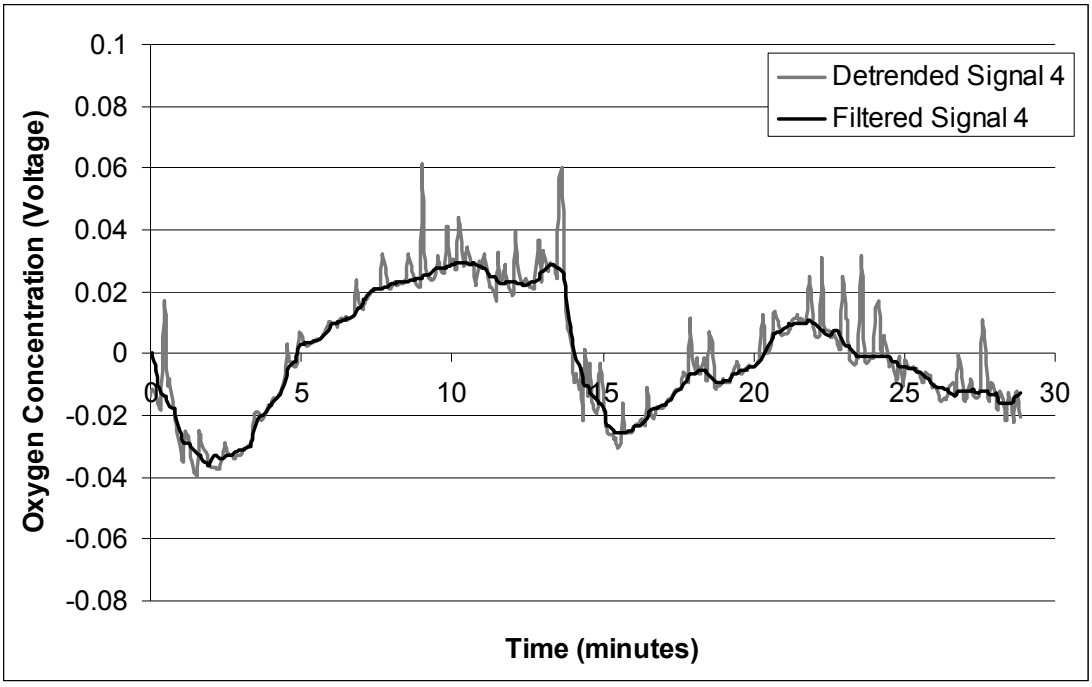


**Figure IV-4. Hamster-A, Signal 4**

The original signals plotted against the filtered signals for Hamster-B, Signals 1 – 4 are shown in Appendix A, Figures A-1 to Figure A-4.

## IV.B Results of Power Spectral Analysis

The oxygen signals from the short-term oxygen sensor array were collected a minimum of 14 days after sensor implantation into the hamster window. This is considered sufficient time duration to mitigate the hamster tissue response to the sensor implant. From the oxygen signals collected, four different signals were chosen to represent sensor signal response. Prior to the spectral analysis, the signals are detrended (linear trend is removed), smoothed, and filtered to remove the identified non-biological features, and the power spectrums are estimated via the Welch

method. The normalized power spectra estimated via the Welch method of representative Signals 1-4 for Hamster-A and Hamster-B, are shown in Figure IV-5 and Figure IV-6.

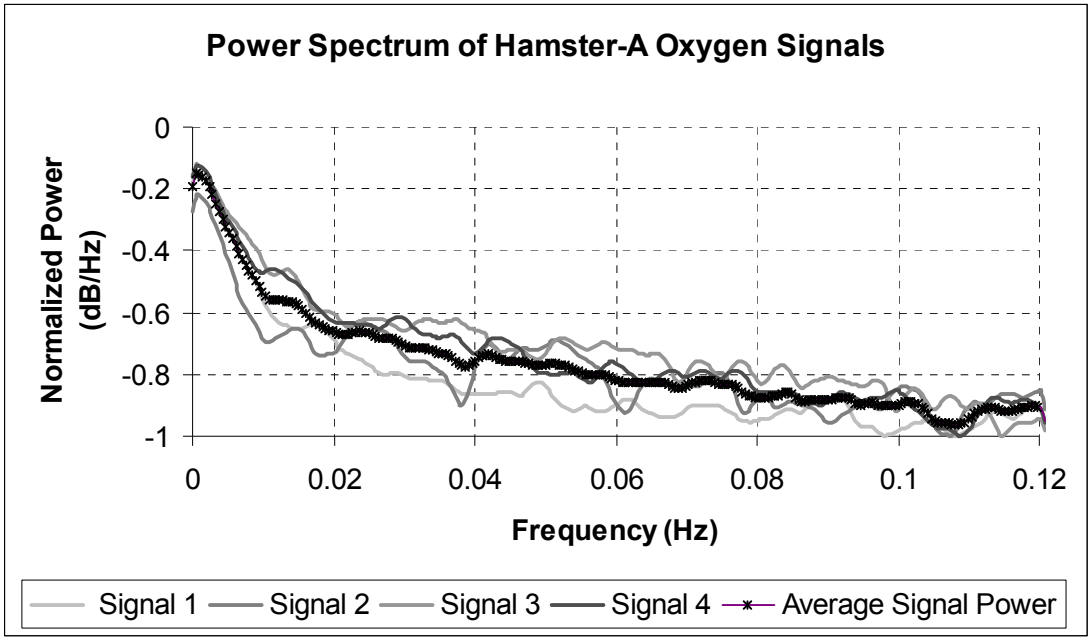


**Figure IV-5. Normalized power spectrums of Hamster-A, Signals 1-4.**

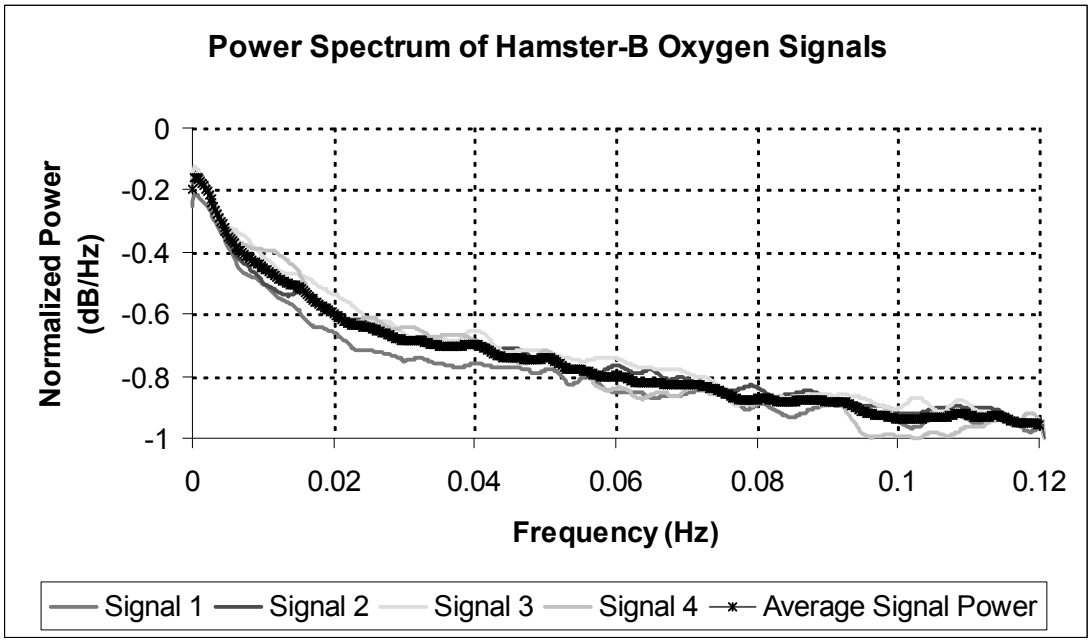


**Figure IV-6. Normalized power spectrums of Hamster-B, Signals 1-4.**

The power spectra for Hamster-A representative signals contains greater spectral variation than the spectra of Hamster-B signals. Each of the power spectrums for Hamster-A, Signals 1-4 shows an observable sinusoidal oscillation. A possible source for the oscillations in the Hamster-A power spectra is that the Hamster-A representative signals span over shorter time duration, and as a result, the signals are composed of fewer points. Both Hamster-B representative signals contain almost twice as many signal points than the Hamster-A signals. In order to minimize of calculation error for the power spectra estimation via the Welch method, the signal have a large sample size. Therefore, the Welch power spectral estimate for Hamster-A may be confounded by increased estimation error, corresponding to the observed power spectral variations in Figure IV-5, due to Hamster-A Signals 1-4 significantly fewer points (containing 400 points) than the signals of Hamster-B (976 points).

In general, the average power signal of the filtered and representative oxygen signals for Hamster-A, and -B, are remarkably similar despite the fact that the representative oxygen signals of Hamster-A and -B have recognizable differences in their time signal variations and fluctuations. The power spectra for Hamster-A, and -B have similar trends in the power over frequency, where as the frequency increases the power exponentially decays to a common power level. Additionally, for every frequency, for each hamster, all the oxygen signals share similar level of normalized power. This shared trend in the power spectrum is called low-frequency power spectrums and is indicative of positive autocorrelation with the time signals. For the spectrums of each of the hamster oxygen signals, there are no obvious dominant or distinguished peaks at any frequency in the power spectra of Hamster-B. However,

there is also an observed oscillatory behavior in the power level as frequency increases. For Hamster-A, the more pronounced oscillations are assumed to be mostly due to spectral estimation error. Nevertheless, the spectral oscillations for Hamster-A and -B may represent periodicity within the signals at various frequencies, noise within the signal, spectral estimation error or a combination of these effects. The observed local spectral peaks in the Hamster-A and Hamster-B oxygen signals occur approximately every 10 ± 5 mHz, suggesting that the hamster oxygen signals have periodic component, a fundamental frequency. In conclusion, the spectral analysis shows both hamster signal sets to have similar low-frequency spectrum trends; that there are no dominant peaks representing distinguishable frequencies; and that there is a pervasive periodicity within the spectrums occurring with an approximate fundamental frequency of 10 ± 5 mHz.

## IV.C Results of the Correlation Analysis

Correlation analysis is completed for the oxygen signals collected from the oxygen sensor arrays implanted in the hamster window chamber after a minimum of 14 days of implantation. From each sensor array implanted in each hamster, four oxygen signals were chosen to represent the various types of dynamics measured by implanted sensor. The short-term oxygen signals are collected over a time period that varies from approximately 30 to 70 minutes. Prior to the correlational analysis, the signals are detrended (linear trend is removed), smoothed, and filtered to remove the identified non-biological features. The representative oxygen signals are collected

from the same sensor array are analyzed for any type of correlation within individual signals, and for correlation among multiple signals collected from the same sensor array. The correlation analysis includes the plots and discussion of the autocorrelation, cross-correlation, and the lagged scatterplot of the collected sensor signals.

### IV.C.1 Correlation Analysis of Hamster-A Signals

Figure IV-7 shows the plot of the normalized autocorrelation of the four representative signals, Signals 1-4, collected from the sensor array implanted in Hamster-A. The horizontal lines at value 0.1 and -0.1 correlation coefficients are the 95% confidence bounds, and any correlation coefficient value of the autocorrelation that falls between 0.1 and -0.1 is considered to be not statistically significant. The autocorrelation plot shows each of four of the representative signals from Hamster-A contains statistically significant periodicity. This is observed as the sinusoidal pattern in each signal's autocorrelation analysis and plot. The duration of one sinusoidal cycle signifies the cycle of periodicity within the signal, and is measured as the number of sample points starting from the sample time of zero to the first sinusoidal peak. From the autocorrelation plots of Hamster-A, signals 1-4, each signal is observed to contain periodicity of approximately 185 to 200 sample points, corresponding to a periodic cycle of 13.5 to 14.6 minutes. Theoretically, the number of sample points from the first peak at ~185-200 sample points, to the second peak at ~330-345 sample points, should be equal to ~185-200, the number of sample points

from sample time zero to the first peak. However, the oxygen sensor signal is a finite and discrete time signal with 400 collected sample points and the autocorrelation results will reflect these characteristics. In calculation of the autocorrelation, after the final 400th sample point of the oxygen sensor signal is reached, the value of zero is used in all calculations thereafter. As a result, the occurrence second sinusoidal peak takes place at an earlier sample time, and the normalized correlation coefficient of the second sinusoidal peak will be decreased. In summary, the normalized autocorrelation shows that for Hamster-A, Signals 1-4, there is clear periodicity within each signal of 1 cycle every 13.5 to 14.6 minutes, which corresponds to a frequency of 1.1 mHz to 1.2 mHz.

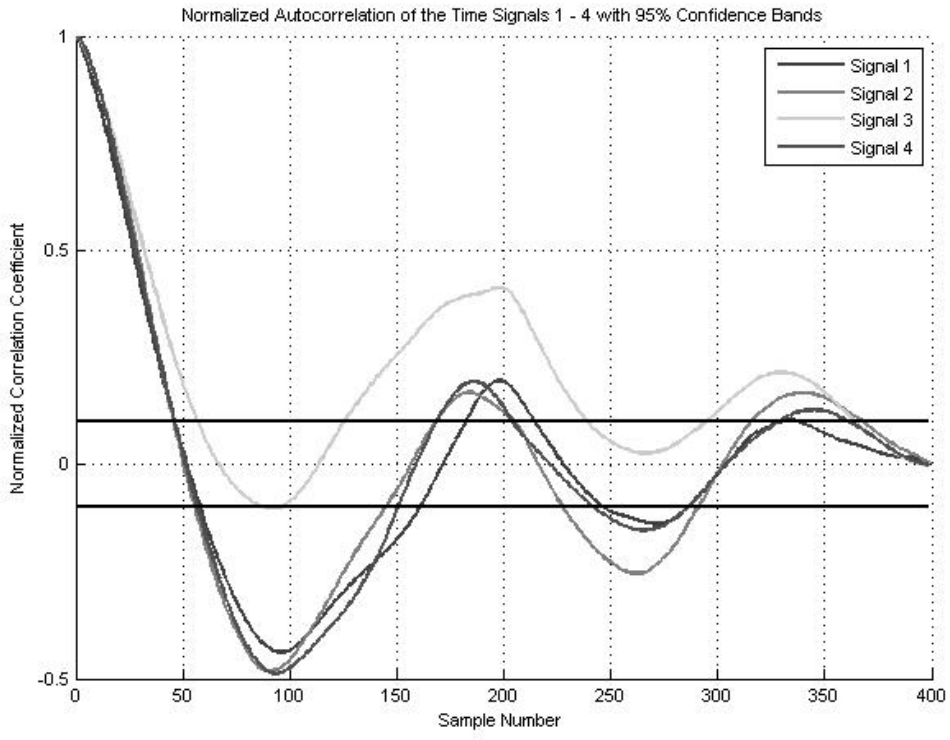


**Figure IV-7. Normalized autocorrelation plot for Hamster-A, Signals 1 – 4.**

Figure IV-8 shows the plot of the normalized cross-correlation for every combination of cross between the Hamster-A representative oxygen sensor Signals 1 – 4. The horizontal lines at correlation coefficient values of 0.1 and -0.1 are the 95% confidence bounds, and any correlation coefficient value that falls between 0.1 and -0.1 is considered to not be statistically significant. The Hamster-A cross-correlation plot shows a clear sinusoidal pattern characterizing periodicity for every combination of cross between the oxygen signals. What is more, the sinusoidal pattern, and therefore the periodicity, appears to be remarkably similar for every cross-correlation indicating a definite correlation between each of the four signals. The cross-correlation periodicity is observed to be one cycle every 185 to 190 sample points (13.5 to 13.9 minutes), corresponding to a sinusoidal frequency of ~1.2 mHz.

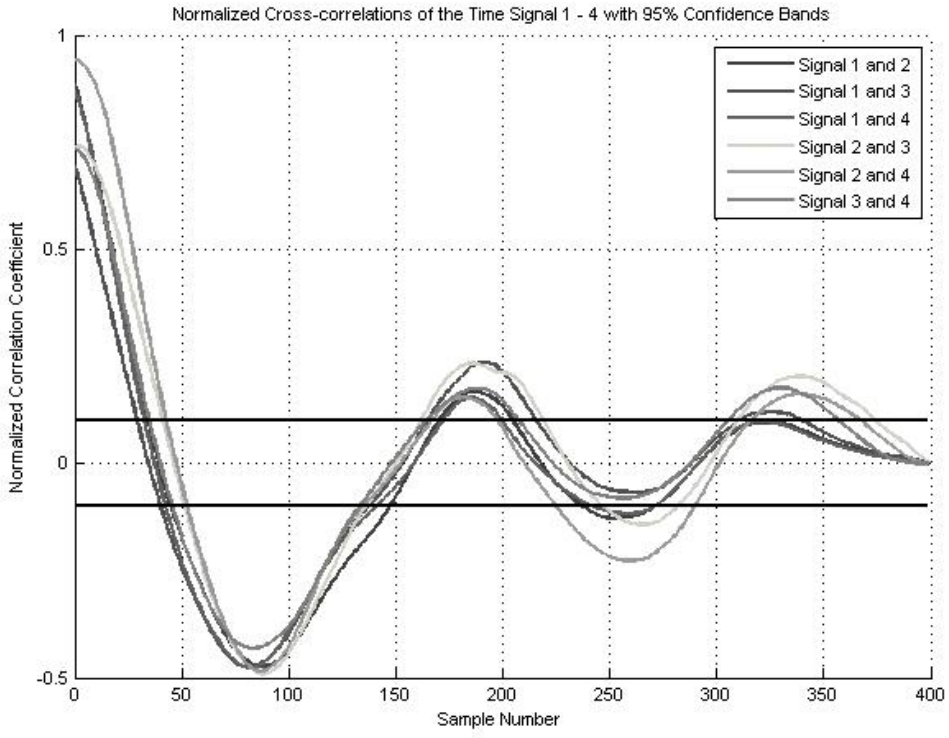


**Figure IV-8. Normalized cross-correlation plot for Hamster-A, Signals 1 – 4.**

The autocorrelation and cross-correlation plots of the Hamster-A, Signals 1-4 representative oxygen sensor signals reveals a definite statistically significant periodicity within each individual signal and between every combination of two signals. The frequencies of periodicity for the auto- and cross-correlation are approximately the same, and found to be 1.2 mHz. Therefore, it can be said that the Hamster-A representative signals that demonstrate different time signal variations, are periodic with a frequency of 1.2 mHz, and correlate in a comparable manner with themselves, and with each other.

Figure IV-9 to Figure IV-12 present the lagged scatterplots for each of the Hamster-A representative oxygen sensor Signals 1-4. The lag plots were calculated for lag k at 1, 5, 10, 20, 50, and 100. The multiple lags of increasing times are chosen in order to indentify the origin of any spatial dependence between the collected sensor signal sample points, and to determine if there is dispersion in the lagged scatterplot as the lag is increased. Figure IV-9 presents the lagged scatteplots for Hamster-A Signal 1. The lag plot with a lag of one shows an clear linear dependence between consecutive points of Signal 1, demonstrated by the y=x linear graph of the collected sample points. At the lag of 5, the scatterplot pattern maintains a linear pattern albeit with some small dispersions among the signal points. As the lag k is increased, the lag plot shows further dispersion among the samples points. At the largest lag k of 100, there is the greatest dispersion of points in the lagged scatterplot and an ambiguous pattern is observed which could be a sign of a non-linear dependence or random behavior among the signal points. The lagged scatterplots for Hasmter-A

Signals 2-4, shown in Figure IV-10 to Figure IV-12 display similar lagged scatterplot behavior as seen for Signal 1. At a lag of one, the scatterplots for each signal demonstrate linearity shown by the y=x linear graph of the signals points. The linear pattern of points indicates an obvious linear dependence between consecutive oxygen signal points. As the lag k is increased, the scatterplot pattern becomes increasingly dispersed, and displays an ambiguous pattern suggesting that the signals could have non-linear dependence at larger lags. Overall, the lagged scatterplots for Hamster-A Signals 1 – 4 shows linear dependence at small lags, and as the lags increase, there is an increase in the dispersion of the points. However, the dispersion pattern of the signal points at larger lags has an ambiguous plot pattern which could represent non-linear dependence between the signal points.

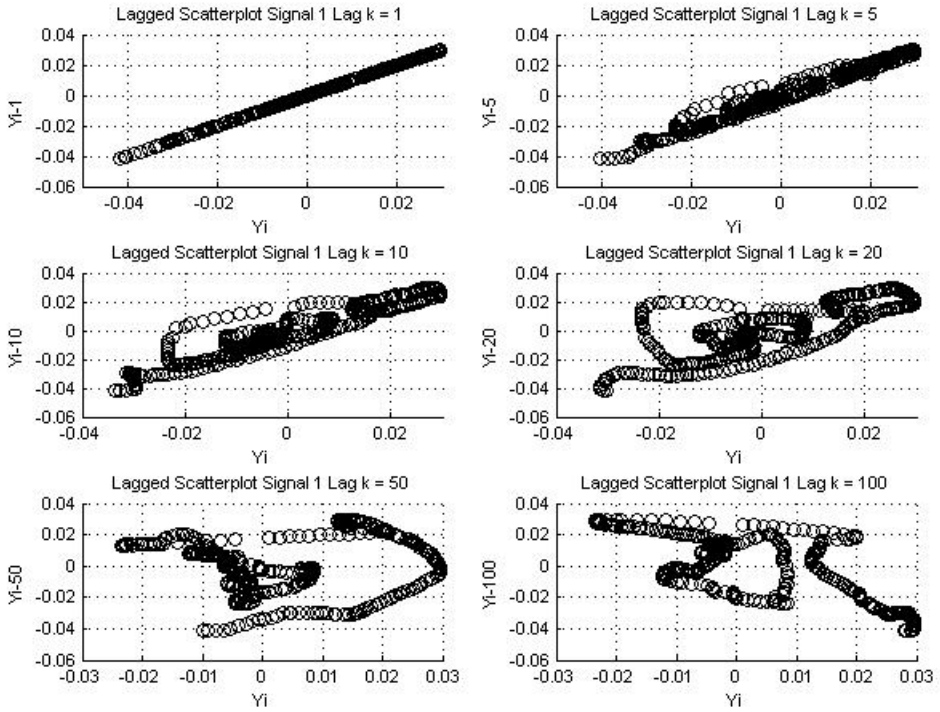


**Figure IV-9. Lagged Scatterplot of Hasmter-A, Signal 1 for lags of 1, 5, 10, 20, 50 and 100.**

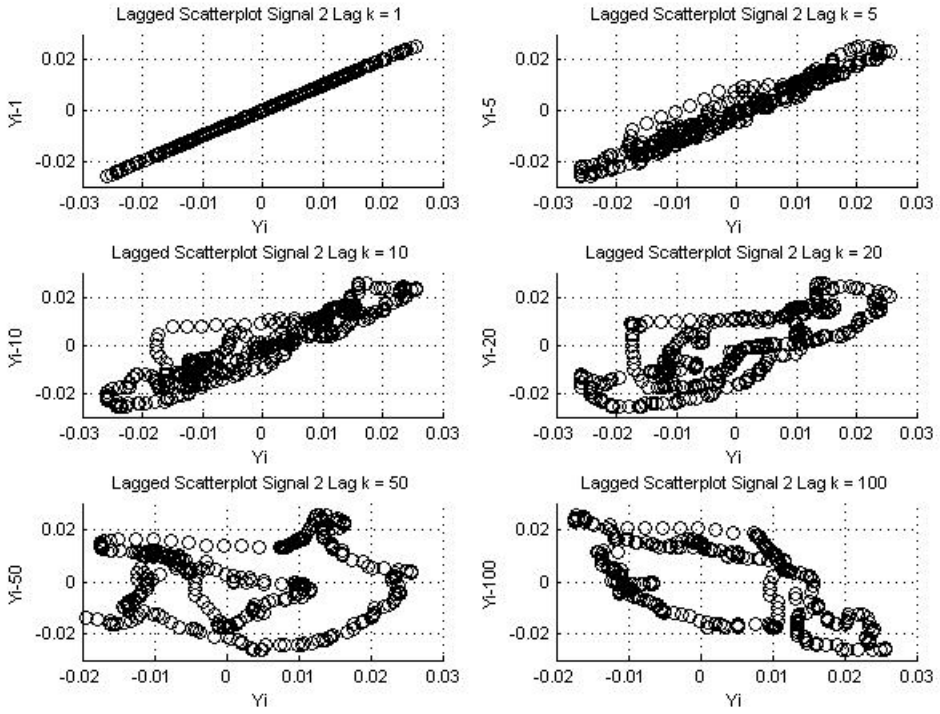


**Figure IV-10. Lagged Scatterplot of Hasmter-A, Signal 2 for lags of 1, 5, 10, 20, 50 and 100.**

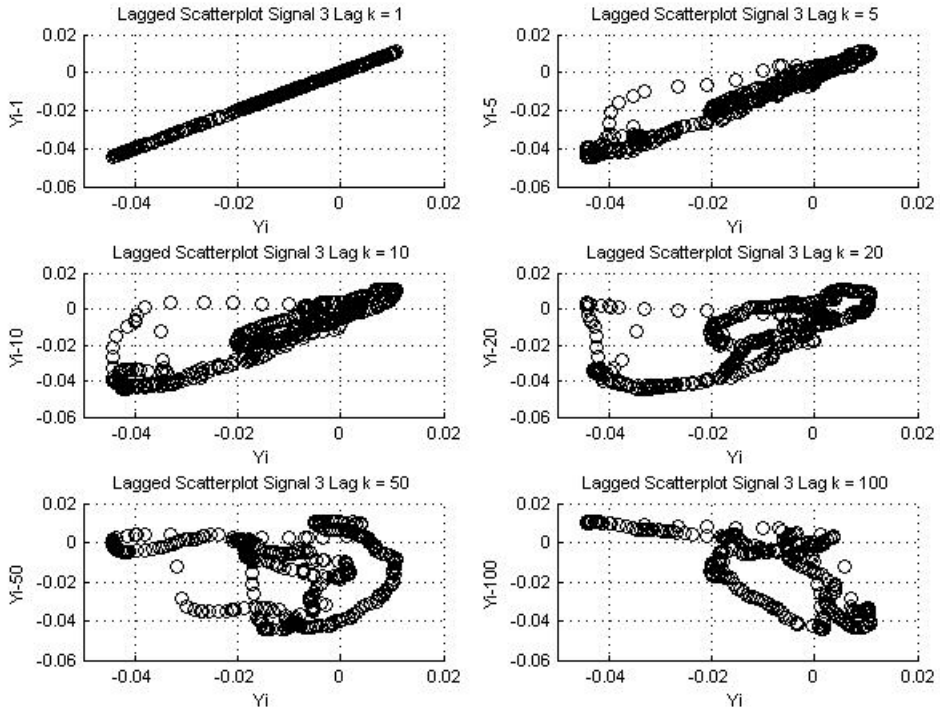


**Figure IV-11. Lagged Scatterplot of Hamster-A, Signal 3 for lags of 1, 5, 10, 20, 50 and 100.**

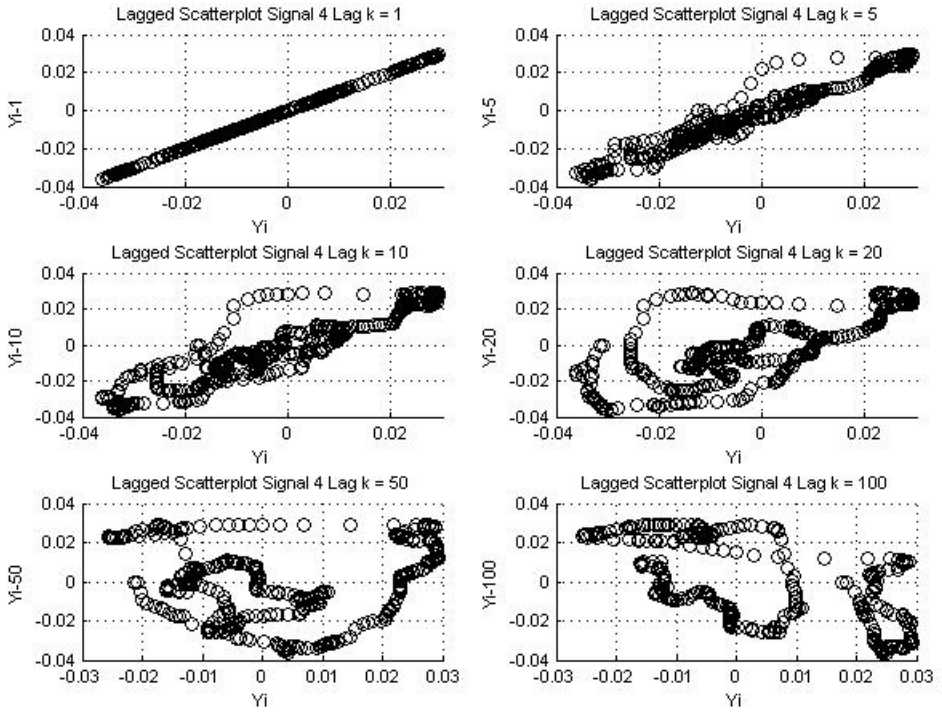


Figure IV-12.Lagged Scatterplots of Hamster-A, Signal 4 for lags of 1, 5, 10, 20, 50 and 100.

## IV.C.2 Correlation Analysis of Hamster-B Signals

Figure A-5 in Appendix A presents the plots of the normalized autocorrelation of the four representative oxygen time signals collected from the oxygen sensor array implanted in Hamster-B. The horizontal lines at correlation coefficient values of 0.064 and -0.064 are the 95% confidence bounds and any correlation coefficient value of the autocorrelation that falls between 0.064 and -0.064 are considered to not be statistically significant. The autocorrelation of the Hamster-B representative signals shows to be signals have different frequencies of periodicity and to be moderately autocorrelated. Signals 1, 2 and 4 all display a sinusoidal-like pattern within the autocorrelation, indicating periodicity within the signals. The period time of the

periodicity appears to vary for each of the Signals 1, 2 and 4; Signal 1 is determined to have periodic frequency of one cycle every 415 sample points (30.3 minutes); Signal 2 is determined to have periodic frequency of one cycle every 635 points (46.4 minutes); Signal 4 is determined to have a periodic frequency of one cycle every 222 sample points (16.2 minutes). Interestingly, the periodicity seems to have a fundamental period of approximately 15 to 16 minutes per periodic cycle (1.1 to 1.0 mHz). This is evidenced as the autocorrelation cycling periods to be approximate multiples of 15 to 16 minutes. The autocorrelation plot of Signal 3 displays a positive correlation between consecutive signal points which suggests a moderate linear correlation within the signal. This is inferred from the positive correlation coefficient at every sample, and the overall descending trend in the autocorrelation plot. In summary, the autocorrelation plots of Hamster-B Signals 1 through 4 all display autocorrelation behavior that varies for each signal. Signal 4, 1 and 2 contain periodicity occurring at the fundamental period of 1 cycle every 15 to 16 minutes (1 cycle every 16.2 minutes, 30.3 minutes, and 46.4 minutes) and Signal 3 displays a moderate linear autocorrelation between its sample points.

Figure A-6 in Appendix A presents the cross-correlation plots for every combination of cross between the Hamster-B representative oxygen sensor signals. The horizontal lines at correlation coefficient values of 0.064 and -0.064 are the 95% confidence bounds and any correlation coefficient value of the cross-correlation that falls between 0.064 and -0.064 are considered to not be statistically significant. The cross-correlation plots display sinusoidal behavior indicating that each combination of crossed signals contains periodicity and is therefore periodically correlated. The

frequencies of sinusoidal behavior in the cross-correlation plots range from one cycle every 100-120 sample points (~8.0 minutes) for crossed Signals 2 and 3, Signals 2 and 4, and Signals 3 and 4, up to one cycle every 430 sample points (~31.4 minutes) for crossed Signals 1 and 3. Cross-correlated Signals 1 and 2, and Signals 1 and 4 display cycles of oscillations that occur every 100 to 120 samples points throughout the sample duration. The observance of sinusoidal behavior in the cross-correlation plots agrees with the results of the autocorrelation plots. The autocorrelation plots indicate the existence of a possible fundamental cycling period for the signals. The cross-correlation results show plentiful amount of sinusoidal behavior for each combination of signal crossing with a minimum periodic cycle every 8.0 minutes. This suggests that the fundamental period for the Hamster-B Signals may around 8.0 minutes (2.1 mHz), which is approximately half of the smallest cycle of periodicity (~15-16 minutes/cycle) determined from the autocorrelation plots. In general, the cross-correlation plots of the Hamster-B signals show that the collected oxygen sensor signals are correlated with each other, and there may be a fundamental cycling period for the signals that is estimated to around 8.0 minutes per cycle (2.1 mHz).

Figure A-7 to Figure A-10 in Appendix A shows the lagged scatterplots calculated for lags k of 1, 5, 10, 20, 50, and 100 for each of the four representative oxygen signals collected from the sensor array implanted in Hamster-B. Figure A-7 show the lagged scatterplots for Hamster-B, Signal 1. The lagged scatterplot with a lag k = 1 demonstrates that the Signal 1 sample points have a clear linear dependence between consecutive points. This is observed as the y = x line in the lag k = 1 scatterplot. For the lag k = 5 scatterplot, the plot displays a linear arrangement of the

signal sample points however there is some dispersion among the plotted points. As the lag k is increased to 10 and 20, the dispersion of the plotted points continues to increase. For lag k = 10, the plot still maintains a linear-like pattern of points, but for lag k = 20, the plotted points take on a non-linear pattern. For lags k = 50 and 100, the scatterplot has a random appearance with the many points concentrated at intersection of $Y_i = 0$, and $Y_{i-50,\ 100} = 0$. Figure A-8 shows the lagged scatterplots for Hamster-B, Signal 2. At the lag k = 1, the scatterplot demonstrates linear behavior as seen by the y = x plot. This pattern indicates that consecutive signal points are linearly dependent. As the lag is increased to lag k = 5, the scatterplot includes some small dispersions of points but maintains its linear pattern of points. At the lag of k = 10 and 20, the scatterplot points becomes further dispersed, and takes on a non-linear pattern. For a lag k = 50, the scatterplot has a concentrated number of points at $Y_i = 0$, and $Y_{i-50} = 0$, but there are two outer loops of points that branch out from the clustered concentration of points. The two outer loops indicate a non-linear pattern in the points. At lag k = 100, there is a star-like pattern in the lagged scatterplot, which could be interpreted as a random or non-random pattern. Figure A-9 and Figure A-10 present the lagged scatterplots for Hamster-B, Signal 3 and Signal 4. For both signals, the scatterplots display similar behavior as described for Signal 2. In general, for each signal, the lagged scatterplot at lag k = 1, there is linear pattern indicated a clear linear dependence between consecutive signal points. As the lag k is increased, the points become dispersion and begin to stray away from the linear pattern seen in the smaller lags of k = 1, and k = 5. Finally, at the largest lag of k = 100, there the points are clustered at $Y_i = 0$, and $Y_{i-100} = 0$, with points wandering in

star-like pattern away from the main cluster of points. The lagged scatterplots of the Signal 1-4 for Hamster-B allow the conclusion to be made that the signal points are linearly dependent at small lags, and take on a non-linear, star-like pattern as the lag k increases.

## IV.D Results of the Continuous Wavelet Transform Analysis

Wavelet analysis is completed for the oxygen signals collected from the oxygen sensor arrays implanted in the hamster window chamber. The signals analyzed are collected from two different oxygen sensor arrays after 14 days of implantation in the hamster window chamber. From each sensor four oxygen signals were chosen to represent the various types of dynamics measured by implanted sensor. The short-term oxygen signals are collected over a time period that varies from approximately 30 to 70 minutes. Prior to the wavelet analysis, the signals are detrended, smoothed, and filtered to remove the identified non-biological features. The continuous wavelet transform of the oxygen signal are completed using the Morlet wavelet and the transforms are plotted in terms of time and frequency, with the wavelet coefficient as the amplitude

The frequency range of the wavelet transform, represented by a discrete set of scales, is chosen such that the plot of the transformed oxygen signal is most complete and can be best visualized. Each set of signals set will contain a different number of samples points, collected over a different duration of time, and with a different sampling rate, and these differences affect the visualization of the frequency domain

on the wavelet transform. Therefore, the range of frequencies and scales for each set of oxygen signals collected from a different sensor arrays are individually chosen in order to build the best visual wavelet transform plot.

### IV.D.1 Wavelet Analysis of Hamster-A Signals

The oxygen signals for Hamster A are collected over a 30 minute time duration, and the average sampling rate of the signals is one sample every 4.38 seconds. The normalized wavelet transforms for each signal is shown in the corresponding Figure IV-13 to Figure IV-16. For each figure, there is a plot of the filtered time-signal, and two different types of plots of the normalized wavelet transform are shown, one as a two-dimensional (2-D) image plot, and the second as a three-dimensional (3-D) mesh plot. The wavelet transform for each oxygen signal demonstrates an on overall weak stationary behavior over the 30 minute time period.

The normalized wavelet transforms of Hamster-A, Signals 1 – 4 shown in Figures IV-13 to IV-16, display an overall oscillation occurring throughout the total duration of each oxygen signal for the frequency range of approximately 0.0001 Hz to 0.12 Hz. This is observed in wavelet transform 2-D image plots as similarly spaced parallel white and grayish white oval areas of different sizes that span the entire time duration of the signal. For the wavelet transform 3-D mesh plots, the evenly spaced peaks spanning the entire length of the signals also suggest an overall oscillation occurring throughout the entire duration of the signal. The existence of a common and shared frequency of oscillation occurring within all the short-term oxygen signals of Hamster A suggests that the signals may be stationary. In closer detail, the wavelet

transforms of the oxygen signals for the collected samples of 150 to 250, corresponding to time range of 11 to 18 minutes, have significantly higher wavelet coefficient magnitudes for the frequency range 0.0001 Hz to 0.12 Hz, than the rest of the transformed signal. This is observed in samples 150 to 250 as large, white parallel ovals areas in the 2-D image plots, and as large prominent peaks in the 3-D mesh plots of the normalized wavelet transform for each oxygen signal. Comparing the wavelet transform plots with the oxygen time signal plots, it can be seen that for samples 150 to 250 there is a noticeable oscillation in the time-signal for that correlates with the observed patterns of higher magnitude wavelet coefficients, indicating a strong oscillatory behavior in the wavelet transform plots.

In summary, the plots of the wavelet transform suggest that there is an overall oscillatory behavior with a frequency range of 0.0001 to 0.12 Hz throughout the total duration of each oxygen signal, implying the Hamster A collected signals are some what stationary. In addition, for each oxygen signal sample points of 150 to 250 (11 to 18 minutes), the wavelet coefficients are significantly larger in magnitude, indicating the presence of a distinct and more prominent oscillatory behavior within the oxygen signal for same frequency range of 0.0001 to 0.12 Hz. Although there is an observed oscillatory behavior of 0.0001 to 0.12 Hz within the collected oxygen signals, the 11 to 18 minute time period within the oxygen signals demonstrates significantly stronger oscillatory behavior, suggesting that the Hamster-A oxygen signals may be weakly stationary.

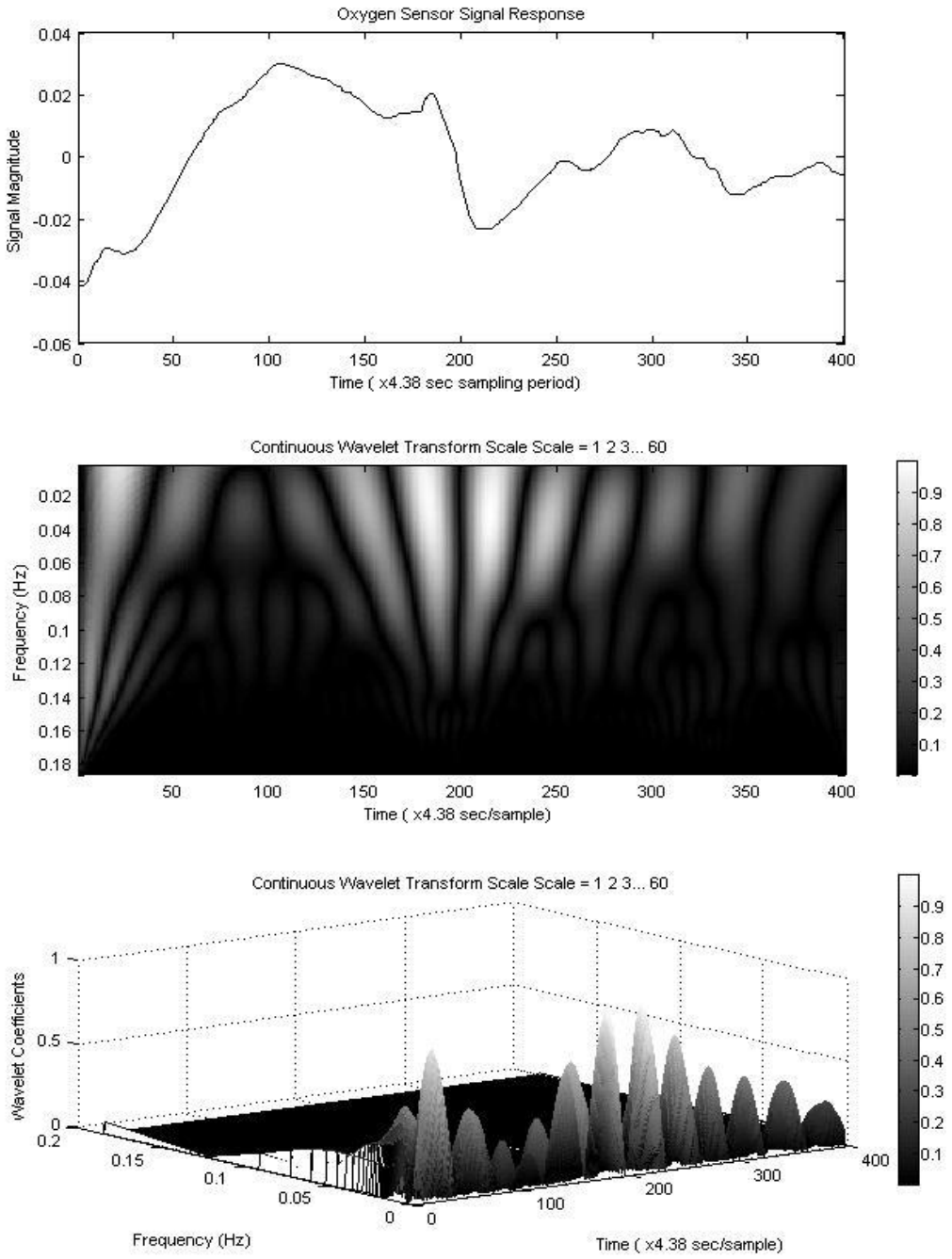


**Figure IV-13. Continuous wavelet transforms for Hamster-A, Signal 1. The first plot is a plot of the Signal 1 magnitude with respect to sample time. The second plot is the 2-D wavelet transform of the Signal 1. The third plot is the 3-D wavelet transform of Signal 1.**

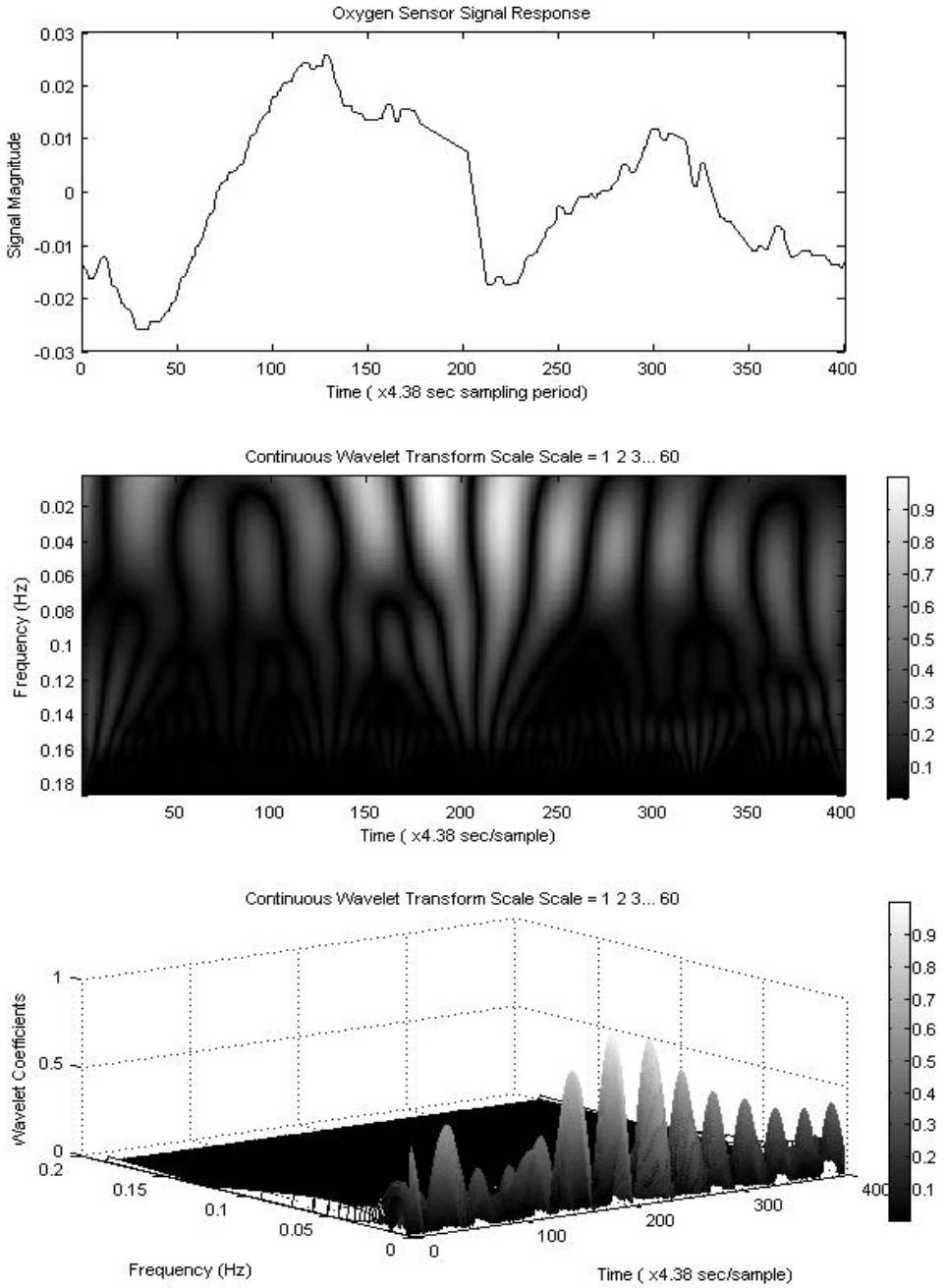


**Figure IV-14. Continuous wavelet transforms for Hamster-A, Signal 2. The first plot is a plot of the Signal 2 magnitude with respect to sample time. The second plot is the 2-D wavelet transform of the Signal 2. The third plot is the 3-D wavelet transform of Signal 2.**

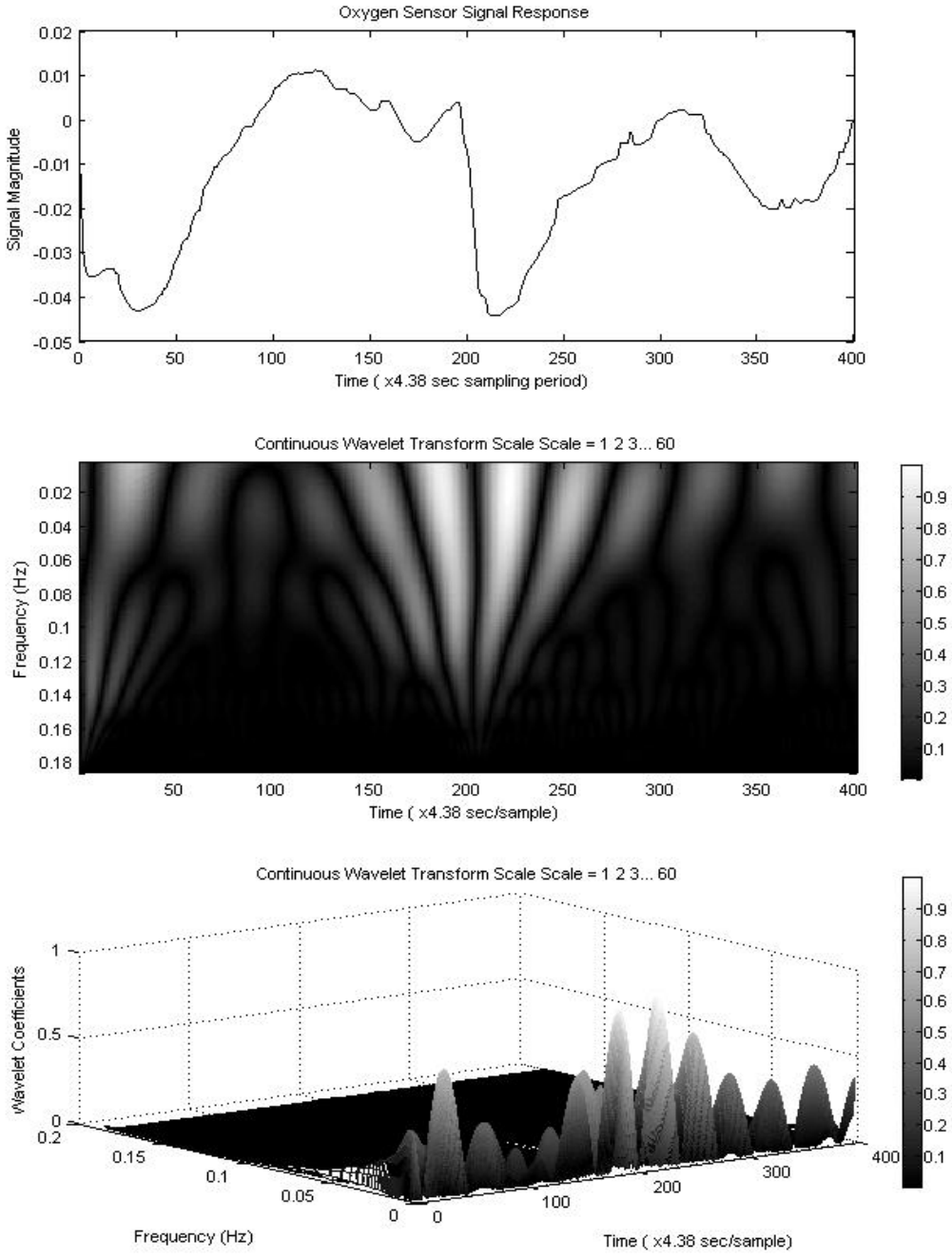


**Figure IV-15. Continuous wavelet transforms for Hamster-A, Signal 3. The first plot is a plot of the Signal 3 magnitude against the sample time. The second plot is the 2-D wavelet transform of the Signal 3. The third plot is the 3-D wavelet transform of Signal 3.**

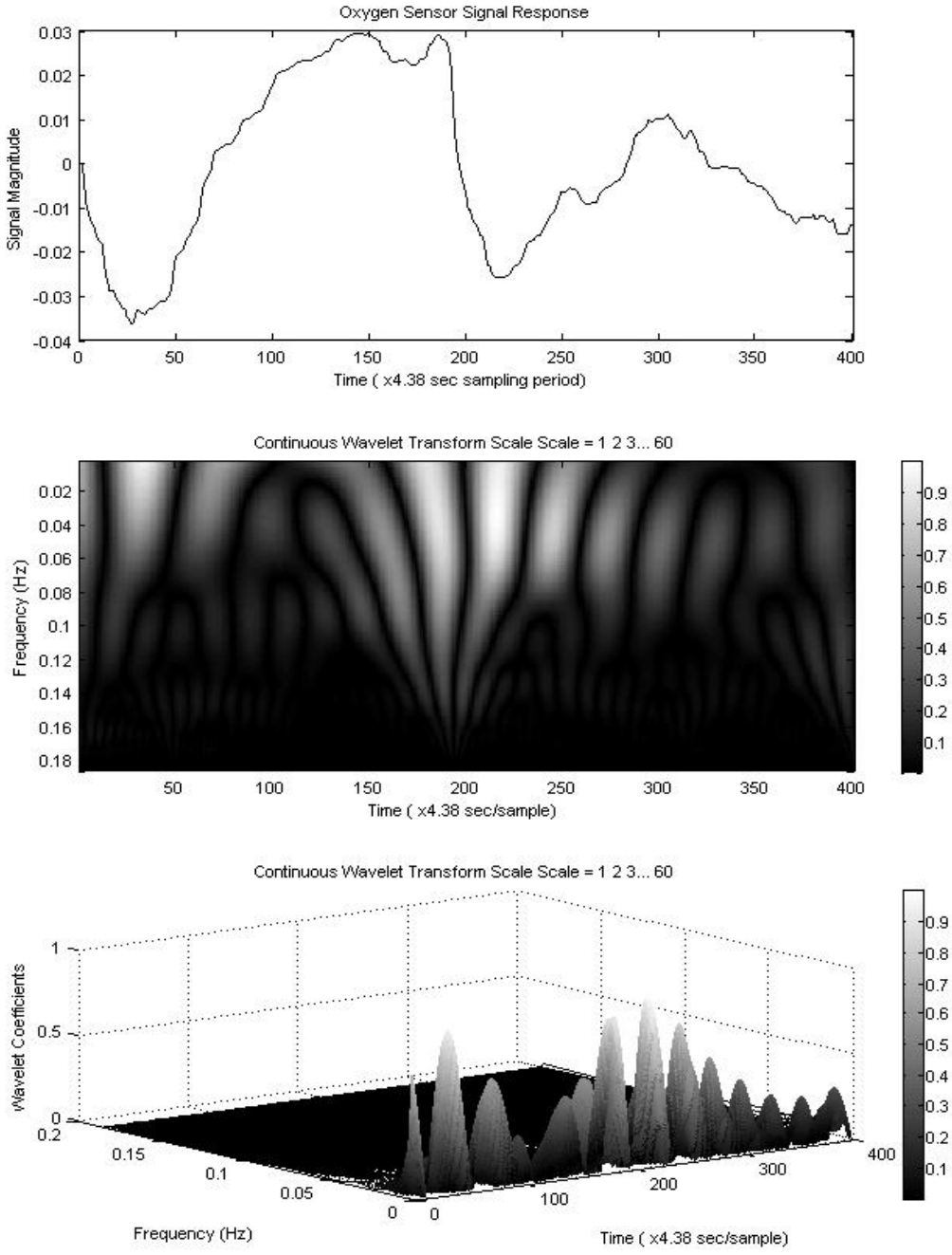


**Figure IV-16. Continuous wavelet transforms for Hamster-A, Signal 4. The first plot is a plot of the Signal 4 magnitude with respect to sample time. The second plot is the 2-D wavelet transform of the Signal 4. The third plot is the 3-D wavelet transform of Signal 4.**

### IV.D.2 Wavelet analysis of Hamster-B Signals

The oxygen signals for Hamster B are collected over a 70 minute time duration, and the average sampling rate of the signals is one sample every 4.38 seconds. The normalized wavelet transforms for Hamster-B, Signal 1 – 4 are in Appendix A as Figure A-11 to Figure A-14. For each figure, there is a plot of the filtered time-signal, and two different types of plots of the normalized wavelet transform are shown, one as a two-dimensional (2-D) image plot, and the second as a three-dimensional (3-D) mesh plot. The wavelet transform for each oxygen signal demonstrates non-stationary behavior over the 70 minute time period.

For Hamster B, Signal 1, shown in Figure A-11 in Appendix A, there is a period of sample points from 650 to 970 (47 to 70 minutes) where the normalized wavelet transform indicates a prominent oscillatory behavior with a frequency of 0.0001 to 0.09 Hz in the oxygen signal. This can be observed in the wavelet transform 2-D image plot as high magnitude wavelet coefficients represented by parallel, evenly spaced white oval areas for the sample points of 650 to 970, spanning the frequencies of 0.0001 to 0.09 Hz. In the wavelet transform 3-D mesh plot, it may be clearer to see the oscillatory behavior of the oxygen signal 1, represented by the high magnitude consecutive peaks for the sample points of 650 to 970, in the 0.0001 to 0.09 Hz frequency range. The wavelet transform also displays two other smaller time periods where oscillatory behavior may be occurring within the oxygen time signal. This can be more clearly seen in the normalized wavelet transform 3-D mesh plot for the sample points of 240 to 320 (18 to 24 minutes), and for 475 to 580 (35 to 42 minutes). During those two time periods, there are groups of higher magnitude

peaks for a frequency range of 0.0001 to approximately 0.08 Hz which represent an oscillatory behavior occurring within the oxygen signal. When the filtered oxygen time signal is compared to its wavelet transform, the three time periods of oscillatory behavior occurring at the frequency range of 0.0001 to ~0.09 Hz exposed by the normalized wavelet transform correspond to specific time periods of variations in filtered oxygen signal. Additionally, the identified frequency range reveals the frequencies at which those variations are occurring. Overall, for Hamster B, oxygen signal 1, there are three time periods, 18 to 24 minutes, 35 to 42 minutes, and 47 to 70 minutes which demonstrate oscillatory behavior occurring within the oxygen signals with frequency ranges of 0.0001 to ~0.09 Hz. This suggests that the Hamster-B, oxygen signal 1 is a non-stationary signal.

For Hamster-B, Signal 2, shown in Figure A-12 in Appendix A, there are three separate time periods within the oxygen signal that display strong oscillatory behavior represented by high magnitude wavelet coefficients from the normalized wavelet transform. The time periods of high magnitude wavelet coefficient are indentified as white strips or areas in the 2-D image plot, and as high magnitude peaks in the 3-D mesh plot. The time ranges for which the high wavelet magnitude coefficients occur are observed to span sample points of approximately 30 to 180 (2 to 13 minutes), 380 to 600 (28 to 44 minutes), and 750 to 970 (55 to 70 minutes). The frequency ranges of the identified ranges of sample points are estimated to be approximately equal, and range from 0.0001 to 0.12 Hz. When the filtered oxygen time signal is compared with the time periods of oscillatory behavior identified in the wavelet transform plots, the oxygen time signal also displays distinct variations that

occur during the same time intervals. As a result, the frequency ranges of 0.0001 to 0.12 Hz may be said to specify the frequencies of the various oscillations which take place during the identified time intervals. In summary, the three separate and distinct time periods of oscillatory behavior in the oxygen time signal exposed by the wavelet transform allow us to conclude that the Hamster-B, signal 2 is non-stationary.

For Hamster-B, Signal 3, shown in Figure A-13 in Appendix A, there are two separate time periods within the oxygen signal that display strong oscillatory behavior represented by high magnitude wavelet coefficients of the normalized wavelet transform. From the wavelet transform plots, the two time periods are identified by areas of white stripes in the 2-D image plot, and peaks in the 3-D mesh plot, and span the sample points of approximately 200 to 500 (15 to 44 minutes), and 700 to 950 (51 to 69 minutes). The corresponding frequencies for the identified time intervals, representing the frequencies of variations and oscillation in the filtered oxygen time signal, range from 0.0001 to 0.15 Hz. In closer detail of the wavelet transform 2-D image plot, it is observed that the largest wavelet coefficient magnitude occurs for the sample points 800 to 920 with the frequency range 0.08 Hz to 0.15 Hz. In examination of the filtered oxygen time signal during the identified sample point intervals of 200 to 500, and 700 to 950, many different types of oscillations, including high frequency oscillations superimposed over lower frequency oscillation, are observed. To sum up for Hamster B, signal 3, there are two time intervals of significant oscillatory behavior occurring within the filtered oxygen time signal, and the frequency of the oscillations ranges from 0.0001 to 0.15 Hz. Therefore, the conclusion can be made that Hamster B, signal 3 is non-stationary

because there are distinct and separate time intervals that exhibit different oscillatory frequencies.

For Hamster-B, Signal 4, shown in Figure A-14 in Appendix A, the normalized wavelet transform plots show three intervals of time with high magnitude wavelet coefficients. From the normalized wavelet transform plot, the 3-D mesh plot best reveals the time intervals of strong oscillatory behavior occurring in the filtered oxygen time signal 4. By searching the wavelet transform 3-D mesh plot for consecutive high magnitude peaks grouped together, the sample point intervals may be located, and for signal 4 they are estimated to be 5 to 320 (0.5 to 24 minutes), 425 to 700 (31 to 51 minutes), and 850 to 950 (62 to 69 minutes). The range of frequencies that correspond with the identified sample point intervals is best revealed by the wavelet transform 2-D image plot. The frequency ranges may be indentified by finding the groups of white stripes in the 2-D image, which are a representation of the high magnitude wavelet coefficients, and identifying the frequencies that span the length of the white stripe. For the sample point intervals, corresponding range of frequencies are 0.0001 to 0.14 Hz. This represents the range of frequencies for the observed oscillations and variations occurring in the filtered oxygen time signal during the identified time intervals. In summary, because there the results of the wavelet transform showing certain time intervals with different frequencies of oscillation, the Hamster B, signal 4 is considered to be non-stationary.

In conclusion, for the Hamster-B, Signals 1 – 4, each signal is classified to be non-stationary. Also, there is overlap between the indentified time intervals where high magnitude wavelet coefficients are found among all the signals. Furthermore,

the range of frequencies for the variations observed in the Hamster B, oxygen time signals 1 – 4 are extremely similar, where the lowest frequency of oscillation is found to be of 0.0001 Hz, and the highest frequency of oscillation is found to be 0.15 Hz.

## IV.E Results of the Probability Distribution Analysis

The probability distribution analysis was determined for the oxygen sensor signals collected from the sensor arrays implanted in the hamster window chamber. The probability distribution analysis includes the calculation of the normal probability plots and the quantile-quantile plot (Q-Q plots) a using the collected oxygen sensor signals that have been detrended, smoothed and filtered to remove the indentified non-biological artifacts. The normal probability plots will determine if the oxygen signals are normally distributed, and the Q-Q plots will answer the question of whether the oxygen signals come from populations with the same probability distribution.

### IV.E.1 Probability Distribution Analysis for Hamster-A Signals

In Figure IV-17.A-D shows the normal probability plots for Hamster-A, Signals 1-4. Figures IV-17.A-D all show similar trends in the normal probability plot by having a long-tail end trend. The normal probability plots displays moderate linear pattern in the center of the data. In closer detail, it is observed that the middle groups of points display a mild to moderate S-like pattern. For the tail ends of the normal probability plot, there is an observed departure from the reference normal line.

Specifically, the first group of tail end points shows increasing departure from the reference normal line below the line, and the last group of tail end points shows increasing departure from the reference normal line above the line. These noticeable tail ends that depart from the reference normal line are called long-tails. The long-tails trend observed in the normal probability plots indicates that a distribution other than the normal distribution would be a good model for the Hamster-A Signal 1-4 datasets. The Lilliefors test calculated for the each of the signals corroborates with the normal probability plot results, where the null hypothesis of the oxygen signals being normally distributed is rejected on the 5% significance level. Thus, it is concluded that all of Hamster-A signals do not fit the normal distribution. However, because the normal probability plots for each signal displays similar long-tails trends, the oxygen signal datasets may all come from similar or same unknown distribution.

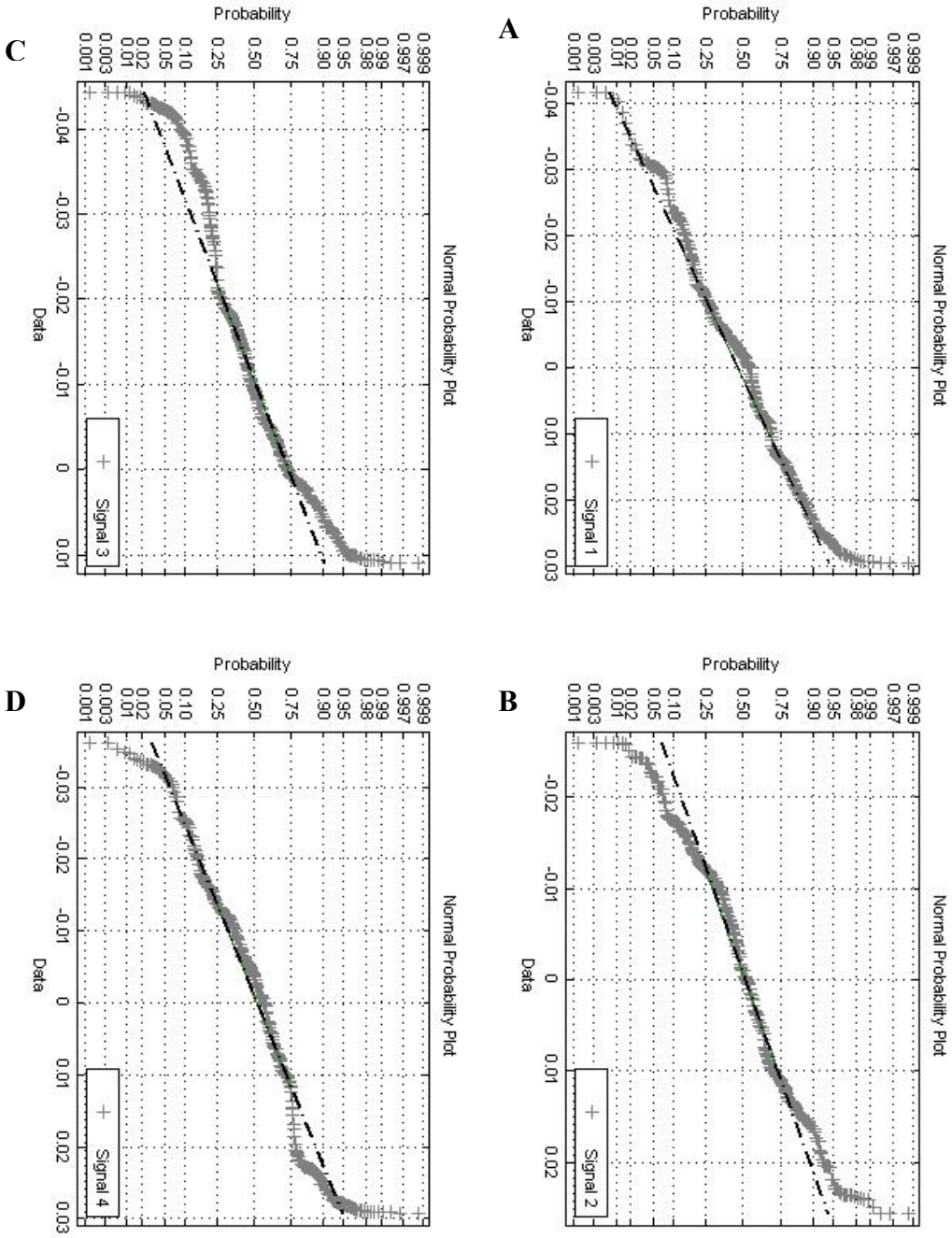


**Figure IV-17.A-D Normal Probability Plots for Hamster-A, Signals 1 – 4.**

In IV-18.A-F, the Q-Q plot for Hamster-A, Signals 1-4 are shown. The Q-Q plots are determined for every two set combinations of Hamster-A, Signals 1-4. Figure IV-18.A shows the Q-Q plot for Hamster-A Signals 1 and 2. The plot displays a left-skewed tail, where the Signal 2 quantiles from -0.026 to -0.012 are larger than for Signal 1. This means that the signal values for Signal 2 are, initially, larger in value than Signal 1. From -0.012 to 0.026 both signals follow the reference line fairly well suggesting the probability distribution is similar for the corresponding points. Figure IV-18.B shows the Q-Q plot for Signals 1 and 3. The plot displays a slight S-pattern, and is considered to be light-tailed. This suggests that the two signals may have a common probability distribution. Figure IV-18.C shows the Q-Q plot for Signals 1 and 4. The plot may be considered to be slightly left-skewed as all the quantiles for Signal 4 are above the reference line. However, the middle group of points follows the reference well and the departures from the reference are small, indicating that Signal 1 and 4 may have a shared probability distribution. Figure IV-18.D shows the Q-Q plot for Signals 2 and 3. The Q-Q plot is right-skewed for the beginning group of tail points, indicating the signal values of Signal 2 are larger than Signal 3. The remainder of the plot follows the reference linear line very well, and it indicates that the corresponding points from Signals 2 and 3 have a near equivalent probability distribution. Figure IV-18.E shows the Q-Q plot for Signals 2 and 4. This is plot is long-tailed, where the beginning group the quantiles falls below the reference line, and the end group of quantiles rises above the reference line. The middle group of points is observed to have a mild S-pattern. This pattern suggests that the Signal 2 and 4 may not come from the same probability distribution. Lastly,

Figure IV-18.F shows the Q-Q plot for Signal 3 and 4. This plot has heavy left-skewed tails and a middle section that falls below that the reference line. This plot indicates that Signal 3 and 4 may not have a shared probability distribution. In summary, the Q-Q plots for Hamster-A Signals 1-4 share the trend of having middle sections of points that follow the reference line fairly well. The Q-Q plots for Signal 1 and 3 and Signals 1 and 4 follow the linear reference line the best, and this indicates that those signals may have the same probability distributions. The Q-Q plots of remaining combinations of signals do follow the linear reference line to some degree, but have tail ends that are lightly skewed above and below the reference line. This indicates that the probability distributions of all of the Hamster-A oxygen signals may be similar.

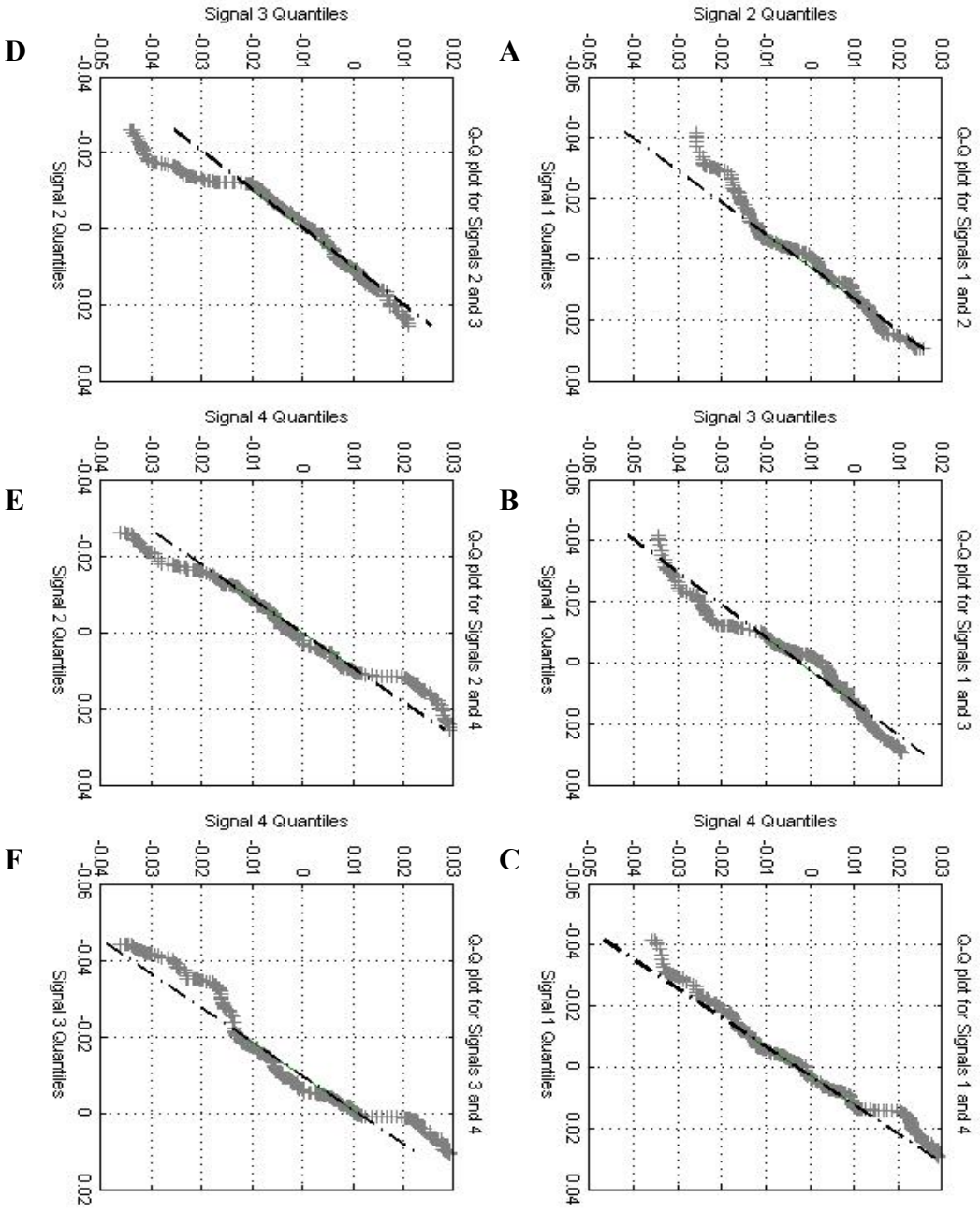


**Figure IV-18.A-F Quantile-Quantile Plots for Hamster-A, Signal 1 – 4.**

## IV.E.2 Probability Distribution Analysis for Hamster-B Signals

Figure A-15.A-D in Appendix A show the normal probability plots for Hamster-B, Signals 1-4 are shown. Figure A-15.A shows the normal probability plot of Hamster-B, Signal 1. The plot has a subtle S-like curvature and the tail ends of the plot show increasing departure from the normal distribution reference line. This suggests that the normal distribution may not be the best model for the Hamster-B, Signal 1 dataset. Figure A-15.B shows the normal probability plot for Hamster-B, Signal 2. The normal plot displays heavy-tailed, non-linear shaped departures from the normal reference line. The lower tail displays a left skewed pattern, and the upper tail displays a right skewed pattern. Moreover, the general shape of the Signal 3 normal probability plot contains an obvious curvature. This indicates with certainty that Signal 3 does not come from a normal distribution. The normal plots for Hamster-B, Signals 3 and 4, presented in Figure A-15.C-D, are similar in shape in that the middle group of points follows the normal reference line, albeit with some S-like curvature among the plotted points. The tails ends depart in a non-linear fashion above and below the reference line, with the upper tail displaying greater degree of departure in a right-skewed pattern. Overall, this indicates that the normal distribution is not the best fit distribution for the Hamster B, Signals 3 and 4 data sets. A noticeable feature shared between all of the Hamster B signal's normal probability plots is that the upper tails are all significantly skewed to the right in a quadratic pattern. This suggests that the points that make up the upper tail may follow a right-skewed distribution. The Lilliefors test calculated for the each of the Hamster-B signals corroborates with the normal probability plot results. The null hypothesis of

the oxygen signals being normally distributed is rejected on the 5% significance level. As a result, it is concluded that all of Hamster-B oxygen signals are not normally distributed.

Figure A-16.A-F shown in Appendix A displays the Q-Q plots for the Hamster-B oxygen Signals 1 – 4. The Q-Q plots are determined for every two set combinations of the Hamster-B Signals 1-4. Figure A-16.A shows the Q-Q plot for Signals 1 and 2. The plot displays a heavy long-tail pattern, where the lower tail points are increasing in departure below the reference line, and the upper tail points are increasing in departure above the above the reference line. This Q-Q plot demonstrates that Hamster-B Signals 1 and 2 do not come from the same distribution. Figure A-16.B shows the Q-Q plot for Hamster-B Signals 1 and 3. The plot is mostly right-skewed where most of the points fall below the reference line with the exception of eight outlier points in the upper tail that rise above the reference line with increasing departure. In addition to the right-skewed pattern of points, the overall shape of the plot contains a minor S-like curvature. However, the Q-Q plot does appear to be somewhat linear, and does follow the reference line suggesting that Signal 1 and 3 could have the probability distribution. Figure A-16.C shows the Q-Q plot for Signals 1 and 4. The plot has light long-tailed pattern, where the lower tail points fall below the reference line, and the upper tail points lay above the reference line. In general, the Q-Q plotted points follow the linear reference line, and this indicates that the Signal 1 and 4 share the same probability distribution. Figure A-16.D and A-16.E presents the Q-Q plot for Signals 2 and 3, and 2 and 4. Both plots display fat-tailed, also called short-tailed behavior where the lower tails rise above the

reference line, the upper tails fall below the reference line, and middle segments non-linear S-like plot shape. What's more, the upper tail of the Q-Q plot for Signals 2 and 3, and the lower tail of the Q-Q plot for Signals 2 and 4 both have distinct non-linear patterns. Overall, this indicates that neither Signals 2 and 3 or Signals 2 and 4 share a common distribution. Figure A-16.F presents the Q-Q plot for Hamster-B Signals 3 and 4, and the plot is lightly left-skewed where the majority of plotted points lay above the reference line indicating that the Signal 4 values are larger than the Signal 3 values. There are several outlier points observed in the lower and upper tails that do not follow the left-skewed trend of the Q-Q plot and fall below the reference line. Overall, the Q-Q plot does follow the reference with some non-linear departures from the reference line, suggesting that Signals 3 and 4 could have common probability distribution. In general, the Q-Q plot for Signals 1 and 3, 1 and 4, 3 and 4 follow the reference line fairly well, and may all have similar or common probability distributions. The Q-Q plots for the other signal combinations, 1 and 2, 2 and 3, and 2 and 4 have larger departures from the linear reference line, and this suggests these oxygen signals do not share a common probability distribution.

## IV.F Autoregressive Modeling of the Implanted Oxygen Sensor Signals

In order to model the *in vivo* oxygen signals collected from the implanted oxygen sensor arrays, the oxygen signals must satisfy the criteria of being stationary. Wavelet analysis of the detrended, smoothed, and filtered oxygen signals collected from the oxygen sensor arrays implanted in the hamster window chamber showed that

Hamster-A, Signals 1-4 are stationary, and hence, the signals may be modeled. Moreover, the power spectral analysis of the four representative signals collected from the oxygen sensor implanted in Hamster-A, were shown to contain peaks and no deep valleys. As a result of the Hamster-A, representative signals 1, 2, 3, and 4 displaying stationary behavior, and possessing specific power spectral features, may be modeled using an autoregressive model.

Once the AR model for each appropriate signal is designed, it must be validated to ensure stability of the model, meaning that over time the model predicted values do not expand to infinite or decrease to zero. Also, the model must be validated to ensure that it effectively describes the correlation within the signal. In order to validate the model, the model coefficients are tested for statistical significance using 95% confidence limit. Second, the residual error terms, calculated as the difference between the real signal values and the model predicted values, are tested to for randomness. Using the five different graphical analysis methods, autocorrelation plot, the run chart, lagged scatterplot, histogram, and normal probability plot of the residual errors, residual errors will be tested for randomness, and the model effectiveness will be checked.

### IV.F.1.i Autoregressive Model and Coefficient Validation for Hamster A, Signal 1

To determine the order of the AR model, the normalized partial autocorrelation plot of Hamster-A Signal 1 is calculated. The partial autocorrelation

plot identifies the model order by showing at which lag k that the correlation coefficients become statistically insignificant. The significance of the correlation coefficients in the partial autocorrelation plot are indentified by 95% confidence bounds where any correlation coefficient greater than -0.1 and less than 0.1 is considered to not be statistically significant. Figure IV-19 presents the normalized partial autocorrelation plot of Hamster-A, Signal 1, and it is observed that at lag k = 4 the correlation coefficients become insignificant.

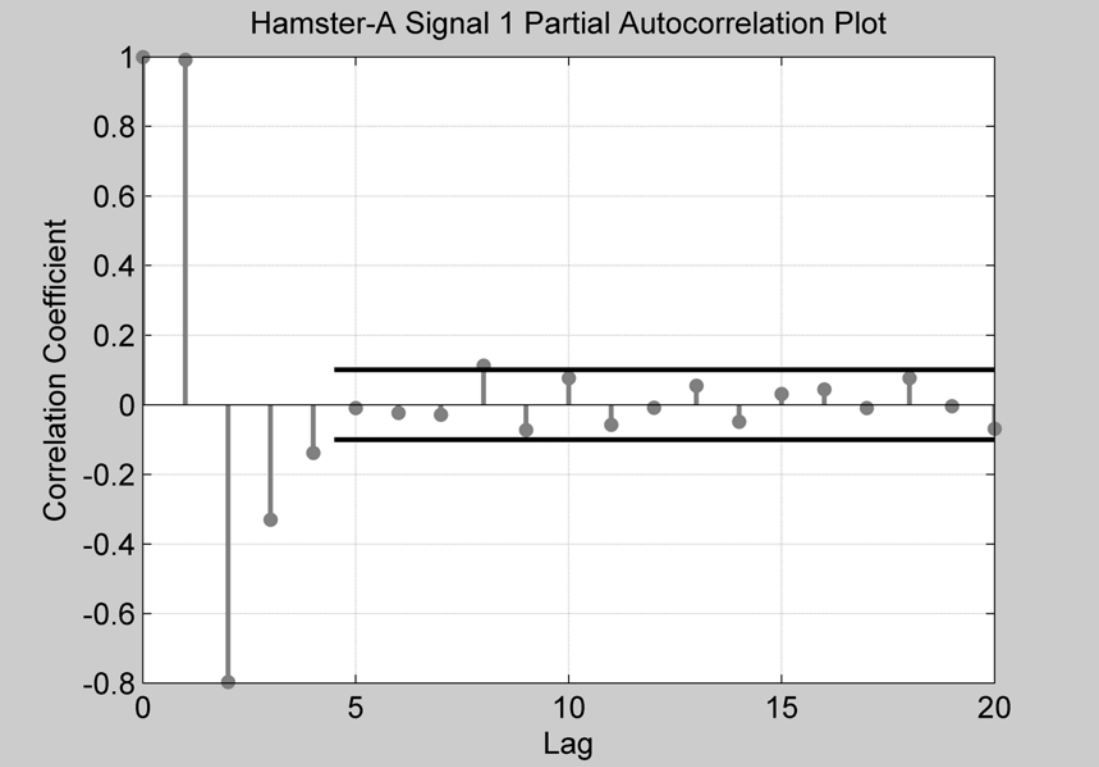


**Figure IV-19. The normalized partial autocorrelation plot for Hamster-A, Signal 1 calculated with a lag of 4. The 95% confidence bounds are marked by parallel black lines starting at lag of 4, and indicate the significance bounds for the correlation coefficient values.**

AR(4) model form: $X_t = b_0 + b_1 X_{t-1} + b_2 X_{t-2} + b_3 X_{t-3} + b_4 X_{t-4} + \varepsilon_t$

Matlab ® Mathworks is used to compute the AR(4) model coefficients $b_i$ using least squares method.

The coefficients with 95% confidence limits are:

$b_0 = 1.014 \times 10^{-5} \pm 4.333 \times 10^{-5} = -3.407 \times 10^{-5} < 1.014 \times 10^{-5} < 5.347 \times 10^{-5}$

$b_1 = 1.482 \pm 0.09727 = 1.383 < 1.482 < 1.578$

$b_2 = -0.2289 \pm 0.1745 = -0.4034 < -0.2289 < -0.05446$

$b_3 = -0.1175 \pm 0.1739 = -0.2919 < -0.1175 < 0.05685$

$b_4 = -0.1380 \pm 0.09651 = -0.2345 < -0.1380 < -0.04149$

The AR(4) model designed for the Hamster-A Signal 1 must be validated to ensure that the model effectively describes the correlation within the signal. Presented above, the model coefficient values with the 95% coefficient limits are listed. If the confidence limit includes the zero value, then that coefficient is considered to not be statistically significant. The 95% confidence intervals for the AR(4) coefficients shows that $b_0$ is not significant because the 95% confidence limit intervals includes the zero value. Therefore the $b_0$ term may be removed from the AR(4). However, as $b_0$ it is a constant term the AR model order is not affected. Therefore, the autoregressive model for Hamster-A Signal 1, $X_t$, is:

$$X_t = 1.482X_{t-1} - 0.2289X_{t-2} - 0.1175X_{t-3} - 0.1380X_{t-4} + \varepsilon_t$$

### IV.F.1.ii Autoregressive Model Validation of Residual Errors Terms for Hamster A, Signal 1

Second, in order to validate the AR model for Hamster-A Signal 1, the residual error terms must be analyzed. The residual error terms are calculated as the difference between the real signal values and the model predicted values for each sample time. In order to determine the effectiveness the AR(4), the residual error terms must tested for randomness. Figure IV-20.A-F presents six different plots that check the effectiveness of the model.

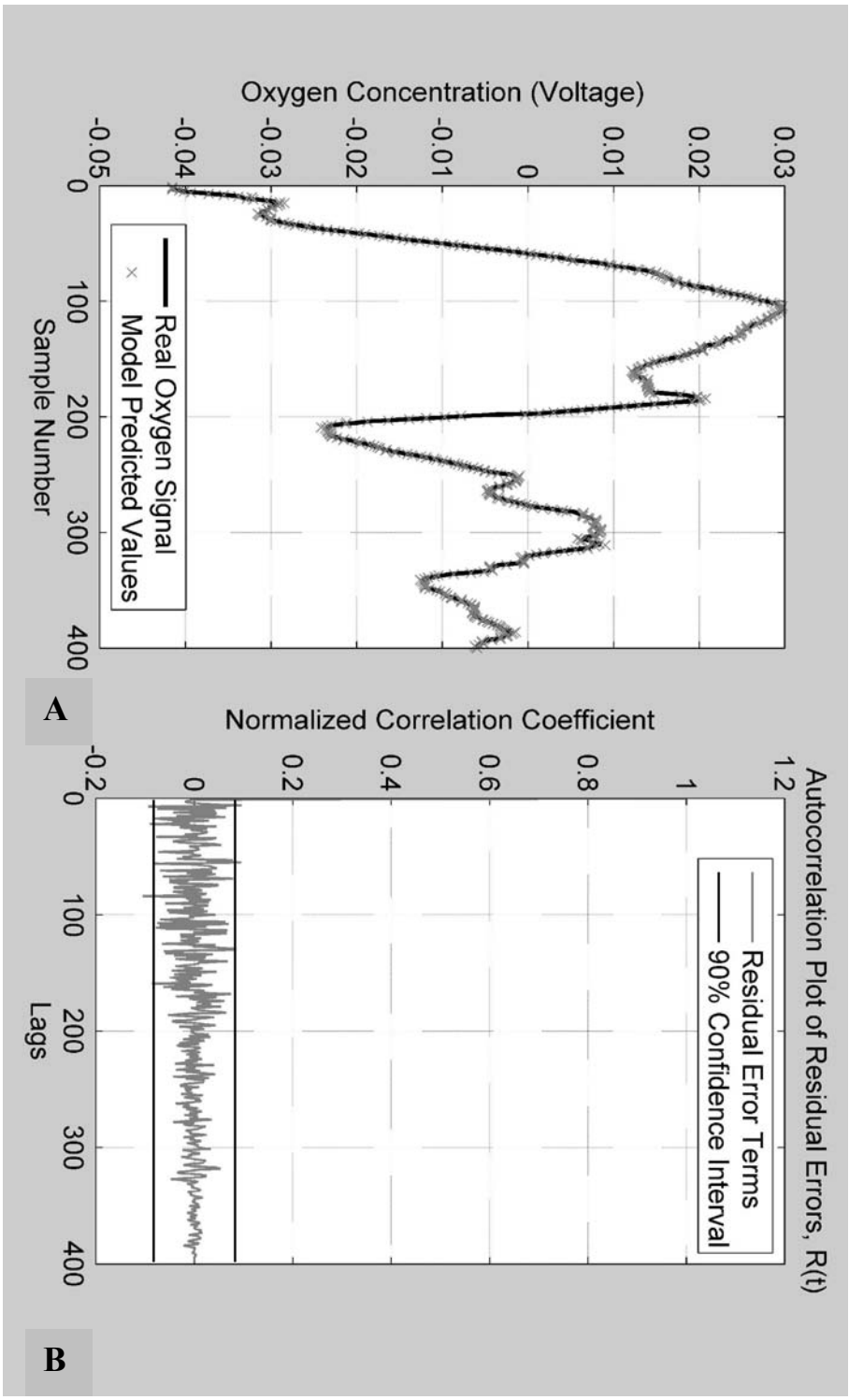


**Figure IV-20.A-B. Residual error analysis plots to validate the AR model for the Hamster-A Signal 1. A. Comparison plot of the model predicted values for the oxygen signal, vs. the real collected oxygen signal values. B. Autocorrelation plot of the residual error terms.**

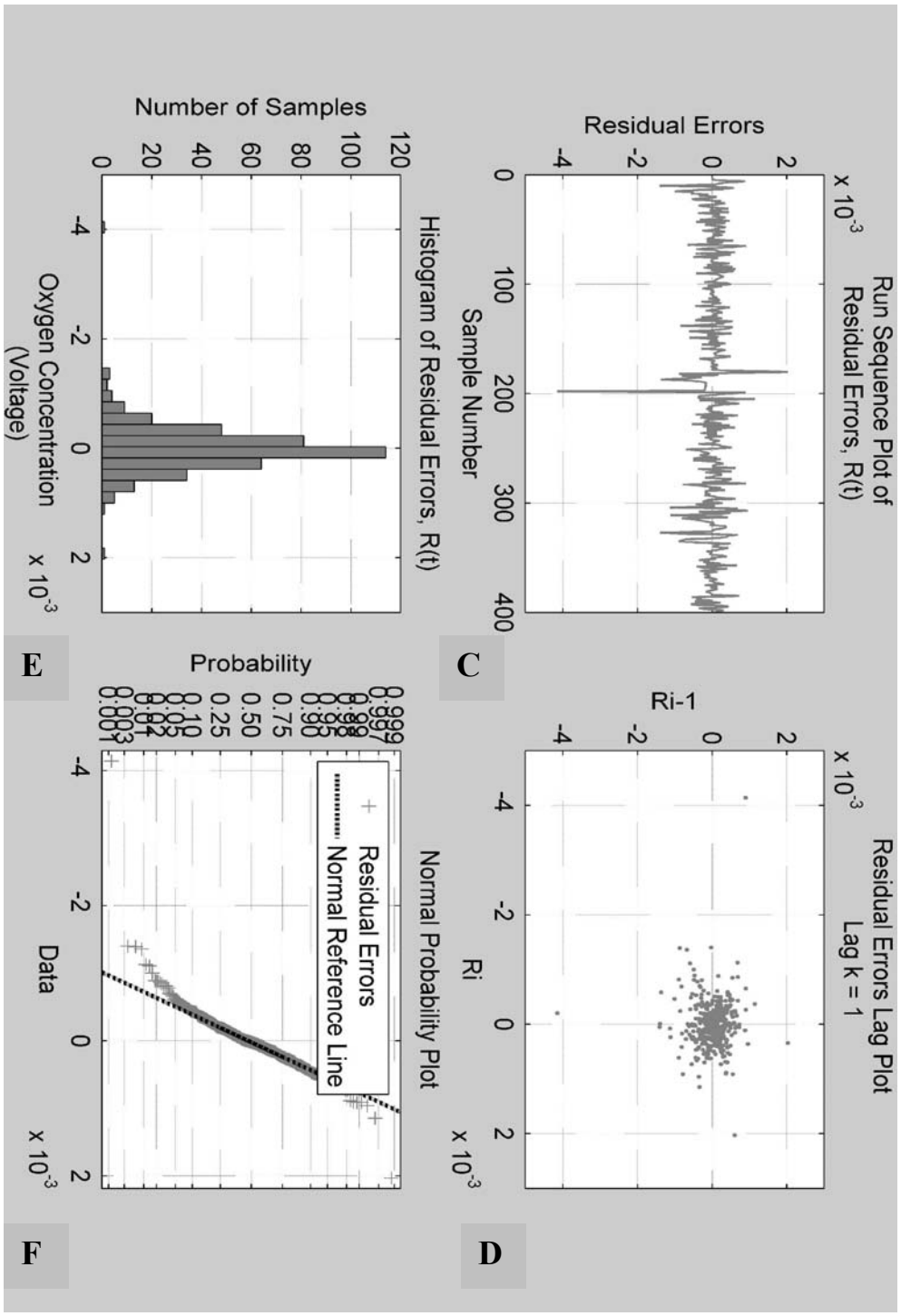


**Figure IV-20.C-F. Plots of the residual error analysis to validate the AR model for the Hamster-A Signal 1. C. Run Sequence Plot. D. Lagged Scatterplot, lag k = 1. E. Histogram plot. F. Normal Probability Plot.**

Figure IV-20.A presents a plot the AR(4) model predicted signal values with respect to time, and the values are compared to the to real (filtered) oxygen signal values with respect to time. It is observed from the figure that the model predicted values closely follows the real signal values

Figure IV-20.B-F presents five different graphical analysis methods, the autocorrelation plot, run sequence plot, lagged scatterplot, histogram, and normal probability plot that will analyze the residual error terms for randomness. Figure IV-20.B presents the autocorrelation plot of the residual error terms with 90% confidence interval bounds. The 90% confidence intervals place bounds on the correlation coefficients, where any values greater than the 0.0825 or less than -0.0825 are considered to statistically significant and indicative of autocorrelation within the residual error terms. Overall, the autocorrelation plot shows that none of the residual error terms peak significantly over the confidence bounds. Thus, the residual error terms contain no statistically relevant autocorrelation.

Figure IV-20.C presents the run sequence plot of the residual error terms. The run sequence plot is an essential tool for checking for outliers and for detecting shifts in location and scale among the residual error terms. From the Figure IV-20.C, it is apparent that residual error terms behave randomly because there is no observable pattern in the run sequence plot. In addition, the run sequence plot displays no significant shifts in location and scale over time. It is observed that almost all of the residual error terms share a common location and scale by existing within the approximate range of $-1.4 \times 10^{-3}$ and $1 \times 10^{-3}$, with the exception of two outlier points

occurring at sample time 180 and 198. Overall, the run sequence plot shows that the residual error terms are random, and share a common scale and location.

Figure IV-20.D presents the lagged scatterplot of the residual error terms. The lagged scatterplot is calculated with a lag of 1, because the small lag would best show any type correlation, linear or non linear, between the residual error terms. The lagged scatterplot of the residual error terms does not show any underlying shape or pattern, indicating that the residual error terms are random. The lagged scatterplot does show the presence of two outliers, where the points at $(0.3 \times 10^{-3}, 2 \times 10^{-3})$ and $(2 \times 10^{-3}, 0.3 \times 10^{-3})$ represent the same outlier point, and $(-0.2 \times 10^{-3}, -4 \times 10^{-3})$ and $(-4 \times 10^{-3}, 0.9 \times 10^{-3})$ represent the second outlier point. Therefore, the lagged scatterplot shows that there is no underlying correlation between the residual error terms, and that overall, the error terms are random.

Figure IV-20.E presents the histogram plot of the residual error terms. The histogram is a valuable tool that can graphically summarize the distribution of a residual error terms. In Figure IV-20.E, the range of the residual error terms are segmented into 30 equal-sized bins and the number of error terms that fall into each bin is counted. The histogram displays a symmetric bell-shape, with short tails on each side. Moreover, two outliers in are observed in the histogram, one at oxygen concentration (V) of -4 bin, and the second at the 2 bin. In general, the shape of the histogram is centered, symmetric, and not skewed. However, due to the existence of the short tails, a conclusive statement about the normality of the residual error terms can not be made. The normal probability plot would be the definitive method to test if the residual errors terms come from a normal distribution.

Figure IV-20.F presents that normal probability plot of the residual error terms. The normal probability plot provides a comparison of the probability distribution of residual error with the normal probability distribution, which is a plotted as linear reference line. Figure IV-20.F shows the middle section of the residual errors probability distribution to closely follow the normal reference line. However, the tail ends of the residual errors probability distributions exhibits departure from the normal reference line. The tail end on the left displays increasing departure above the reference line, and the tail end on the right displays increasing departure below the reference line. This type of tail end departure from the normal reference line is classified as short-tails. Therefore, the short-tail behavior of the residual errors probability distribution indicates that the normal probability distribution may not be the best fit distribution.

In summary, the five graphical methods of the residual error analysis suggest that as a whole the residual error terms behave randomly. The autocorrelation plot indicates that there is no autocorrelation between the residual error terms, and the run sequence plots shows the error terms to be random with two outlier points. The lagged scatterplot also shows the error terms to be random with no underlying correlation. The histogram and normal probability plot confirm that the probability distribution of residual error terms does not completely follow normal distribution. This is likely due to two residual error outlier points which were identified by run sequence plot, lagged scatterplot, and histogram. If the two outlier points were removed, the histogram plot would be expected to satisfy the symmetric, bell-shape of a normal distribution, and the normal probability plot of the residuals would be

expected to fit the normal distribution. As a result, the AR(4) model of the Hamster-A Signal 1 may be considered adequate, but a more effective model may be designed with the removal of the signal points that are the source of the outlier two points.

### IV.F.2.i Autoregressive Model and Coefficient Validation for Hamster A, Signal 2

To determine the order of the AR model, the normalized partial autocorrelation plot of Hamster-A Signal 2 is calculated. The partial autocorrelation plot identifies the model order by showing the lag k for which the correlation coefficients are considered statistically insignificant. The significance of the correlation coefficients in the partial autocorrelation plot are indentified by 95% confidence bounds where any correlation coefficient greater than -0.1 and less than 0.1 is considered to not be statistically significant. Figure IV-21 presents the normalized partial autocorrelation plot of Hamster-A, Signal 1, and it is observed that after lag k = 3 the correlation coefficients can be considered insignificant. At lag 7, and 16, the correlation coefficients are equivalent to -0.1, and are considered to not be significant. At the lag of 12, the correlation coefficient value is -0.149 and outside the 95% confidence bounds. However, taking into consideration that the next lag after the lag of 3 that the correlation coefficient is outside the 95% confidence bounds is lag of 12, and at that the lag of 12 the correlation coefficient is not radically beyond the -0.1 confidence bounds, the significant at lag of 12 is ignored and an AR model order of 3 is chosen.

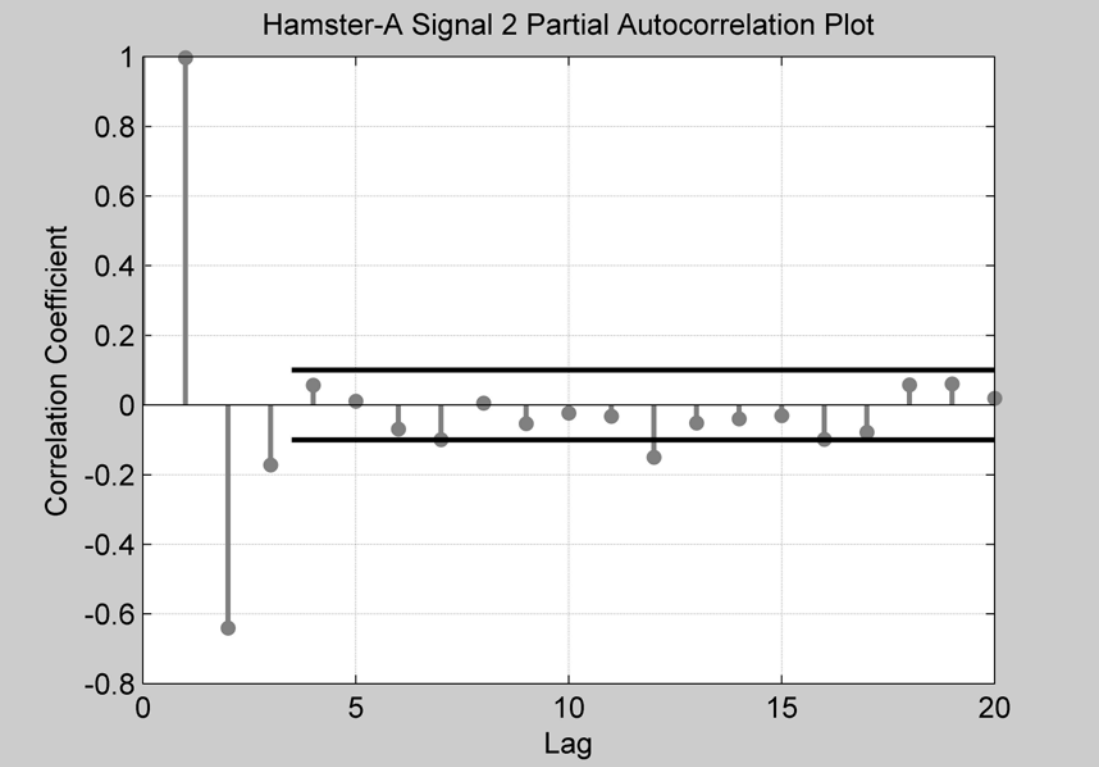


**Figure IV-21. The normalized partial autocorrelation plot for Hamster-A, Signal 2 calculated with a lag of 3. The 95% confidence bounds starting at lag of 3 are marked by parallel black lines, and indicate the significance bounds for the correlation coefficient values.**

AR(3) model form: $X_t = b_0 + b_1 X_{t-1} + b_2 X_{t-2} + b_3 X_{t-3} + \varepsilon_t$

Matlab ® Mathworks is used to compute the AR(3) model coefficients $b_i$ using ordinary least squares method.

The coefficients with 95% confidence limits are:

$b_0 = 5.0497 \times 10^{-6} \pm 6.389 \times 10^{-5} = -5.884 \times 10^{-5} < 5.050 \times 10^{-6} < 6.894 \times 10^{-5}$

$b_1 = 1.527 \pm 0.09756 = 1.429 < 1.527 < 1.624$

$b_2 = -0.3593 \pm 0.1762 = -0.5355 < -0.3593 < -0.1831$

$b_3 = -0.1718 \pm 0.09756 = -0.2694 < -0.1718 < -0.07424$

The AR(3) model designed for the Hamster-A Signal 2 must be validated to ensure that the model effectively describes the correlation within the signal. Presented above, the model coefficient values with the 95% coefficient limits are listed. If the confidence limit includes the zero value, then that coefficient is considered to not be statistically significant. The 95% confidence intervals for the AR(3) coefficients shows that $b_0$ is not significant because the 95% confidence limit intervals includes the zero value. Therefore the $b_0$ term may be removed from the AR(3). However, as $b_0$ it is a constant term the AR model order is not affected. Therefore, the autoregressive model for Hamster-A Signal 2, $X_t$, is:

$$X_t = 1.527X_{t-1} - 0.3593X_{t-2} - 0.1718X_{t-3} + \varepsilon_t$$

## IV.F.2.ii Autoregressive Model Validation of Residual Errors Terms for Hamster A, Signal 2

After the AR(3) model coefficients for Hamster-A, Signal 2 are checked for significance, the AR model is further tested for validation by checking the residual error terms for randomness. Figure IV-22.A-F presents six different plots that check the randomness of the residual error terms, hence, the effectiveness of the model.

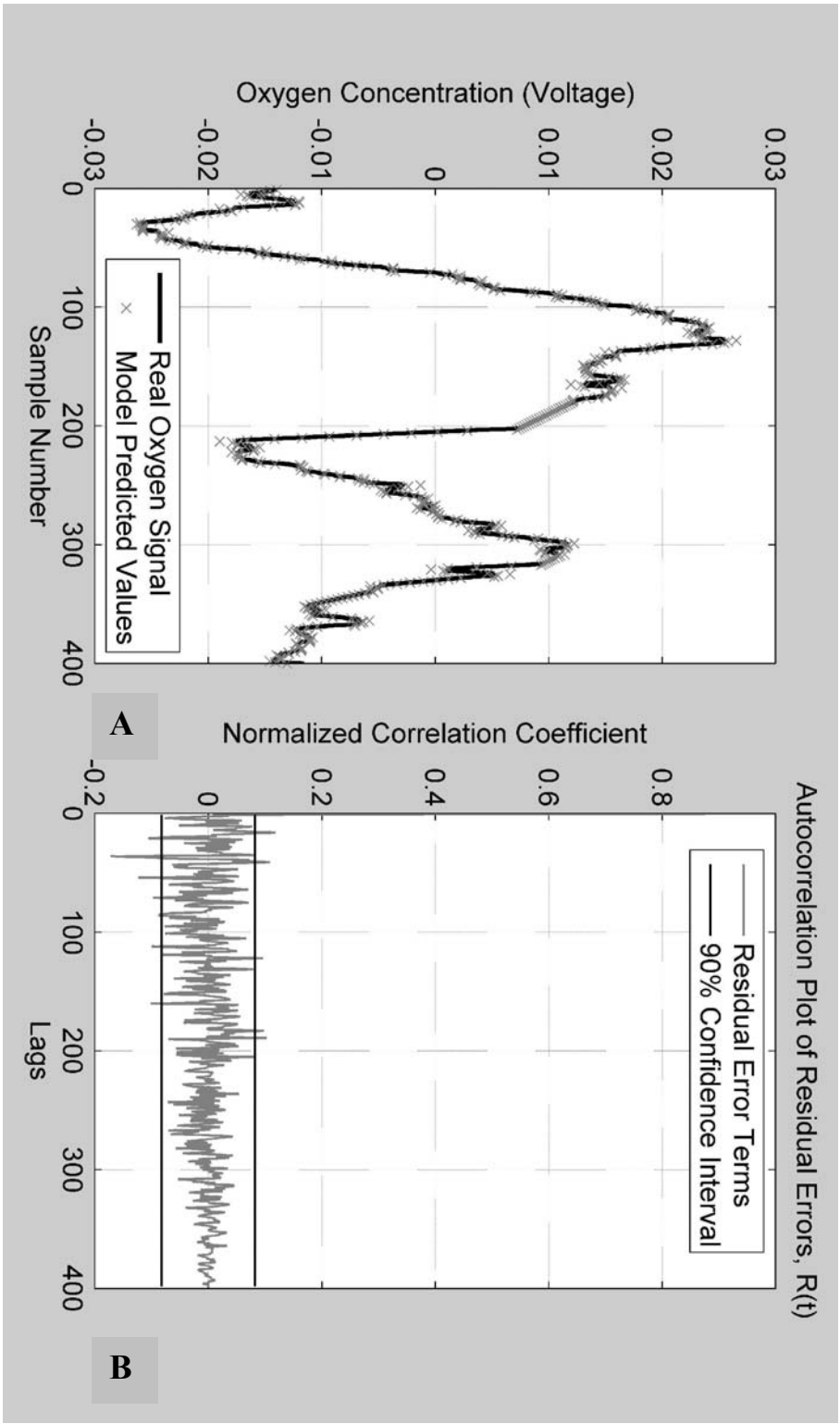


**Figure IV-22..A-B. Residual error analysis plots to validate the AR model for the Hamster-A Signal 2. A. Comparison plot of the model predicted values for the oxygen signal, vs. the real collected oxygen signal values. B. Autocorrelation plot of the residual error terms.**

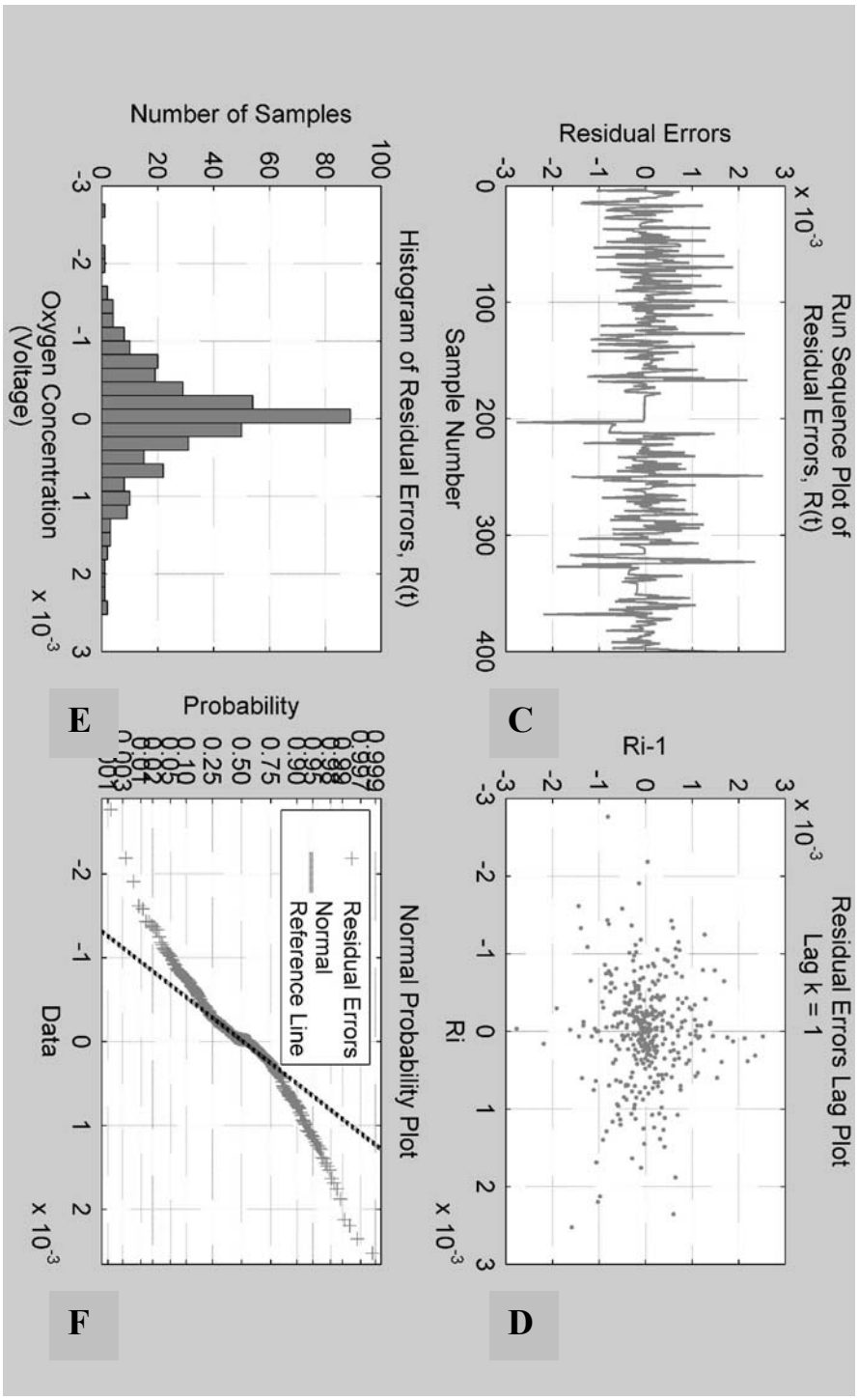


**Figure IV-22.C-F. Plots of the residual error analysis to validate the AR model for the Hamster-A Signal 2. C. Run Sequence Plot. D. Lagged Scatterplot, lag k = 1. E. Histogram plot. F. Normal Probability Plot.**

Figure IV-22.A presents a plot of the AR(3) model predicted signal values with respect to time, and it is compared to the to real, filtered oxygen signal values with respect to time. It is observed that the model predicted values do follow the real signal values. As a result, the AR(3) model does accurately predict the actual signal values from the implanted oxygen sensor array.

Figure IV-22.B-F presents five different graphical analysis methods, the autocorrelation plot, run chart, lagged scatterplot, histogram, and normal probability plot that will analyze the residual error terms for randomness. Figure IV-22.B presents the autocorrelation plot of the residual error terms with 90% confidence interval bounds. The 90% confidence intervals place bounds on the correlation coefficients, where any values greater than the 0.0825 or less than -0.0825 are considered to be statistically significant and indicative of autocorrelation within the residual error terms. The autocorrelation plot shows some small departure outside the 90% confidence bounds at lags of 16, 21, 36, 41, 54, 74, 122, 169, 183, and 189. The greatest correlation coefficient that is outside the 90% confidence bounds is at the lag of 36, with a correlation coefficient value of -0.17. However, if the statistical significance is increased from 90% to 99%, the new bounds for significance will be between 0.13 and -0.13, and all the correlation coefficient values except at lag of 36 can be considered insignificant. In general for the autocorrelation, the correlation coefficient values of the residual errors display some minor departures beyond the 90% confidence bounds. However, the number of points outside the confidence bounds can be decreased by increasing the level of statistical confidence. As a result,

there is at least one point that lies outside the confidence bounds, but the residual error terms present no obvious autocorrelation pattern.

Figure IV-22.C presents the run sequence plot of the residual error terms. The run sequence plot is an essential tool for checking for outliers and for detecting shifts in location and scale among the residual error terms. From the Figure IV-22.C, the run sequence plot displays an overall random-like behavior and there are no shifts in location are over time. For points 178 to 201, the run plot does show a shift in scale over time. The residual error values for points 178 to 201 are of the order of $10^{-5}$, two orders of magnitude smaller than all other residual error values that range from $-2.7 \times 10^{-3}$ and $2.5 \times 10^{-3}$. As a result, the run sequence plot shows that the residual error terms of Hamster-2 Signal 2 are random with the exception for the sample points of 178 to 201 which display a shift in the scale.

Figure IV-22.D presents the lagged scatterplot of the residual error terms. The lagged scatterplot is calculated with a lag of 1 because the small lag best shows any type correlation, either linear or non linear, among the residual error terms. From from Figure IV-22.D, the lagged scatterplot of the residual error values looks like a random scattering of points. As a result, no underlying shape or pattern is identified to indicate correlational behavior between the residual error terms. Moreover, no distinct outliers are identified. Therefore, the lagged scatterplot at lag of 1 shows that the residual error terms behave randomly and that there is no underlying correlation between the residual error terms.

Figure IV-22.E presents the histogram plot of the residual error terms. The histogram is a valuable tool that can graphically summarize the distribution of a

residual error terms. In Figure IV-22.E, the range of the residual error terms are segmented into 30 equal-sized bins and the number of error terms that fall into each bin is counted. In general, the histogram shows the residual errors distribution to be symmetric, centered, shape, with long tails on each end. However, due to the existence of the long, symmetric tails, a conclusive statement about the normality of the residual error terms can not be made. The normal probability plot would be the definitive method to test if the residual errors terms come from a normal distribution.

Figure IV-22.F presents that normal probability plot of the residual error terms. The normal probability plot provides a comparison of the probability distribution of residual error with the normal probability distribution, which is a plotted as linear reference line. Figure IV-22.F shows the residual errors values from $-3.5 \times 10^{-4}$ to $3.5 \times 10^{-4}$ to follow the normal reference with a slight S-shape. The residual error values less than $-3.5 \times 10^{-4}$ show departure above the normal reference line, and the error values greater than $3.5 \times 10^{-4}$ show departure below the normal reference line. This normal probability plot departure pattern is called short-tails and it indicates that the variance of the residual error terms is less than what is expected for a normal distribution. Thus, the short-tailed behavior of the residual errors probability distribution suggests that the normal probability distribution may not be the best fit distribution.

In summary, the five graphical methods of the residual error analysis suggest that the residual errors terms may not all behave randomly. The autocorrelation plot, run sequence plot, and normal probability plot reveal specific residual error points that diverge from random behavior. The lagged scatterplot and histogram show that

despite some residual error terms that deviate from randomness, the residual error terms behave in a random manner as a whole, and present a distribution that is symmetric, bell-shaped with no discernable outliers. As a result, the residual error values are only 'weakly' random, and the AR(3) model of the Hamster-A Signal 2 may be not be an effective model. A better AR model may be designed by removing of the signal points that are the source of the non-random residual error terms.

### IV.F.3.i Autoregressive Model and Coefficient Validation for Hamster A, Signal 3

The partial autocorrelation plot is used to identify the model order for Hamster-A Signal 3, by revealing the lag k for which the correlation coefficients are considered statistically insignificant. The significance of the correlation coefficients in the partial autocorrelation plot are indentified by 95% confidence bounds where any correlation coefficient greater than -0.1 and less than 0.1 is considered to not be statistically significant. Figure IV-23 presents the normalized partial autocorrelation plot of Hamster-A, Signal 3, and it is observed that after lag k of 2 the correlation coefficients can be considered insignificant. At the lag of 4, the correlation coefficient value is -0.133, and only slightly outside the 95% confidence bounds. If the statistical confidence is increased from 95% to 99%, setting the confidence bounds at ± 0.13, the correlation coefficient at lag of 4 can be considered insignificant. Hence, after the lag of 2, the correlation coefficients for all greater lag

k's are considered to not be statistically significant. Therefore, an AR model order of 2 is chosen.

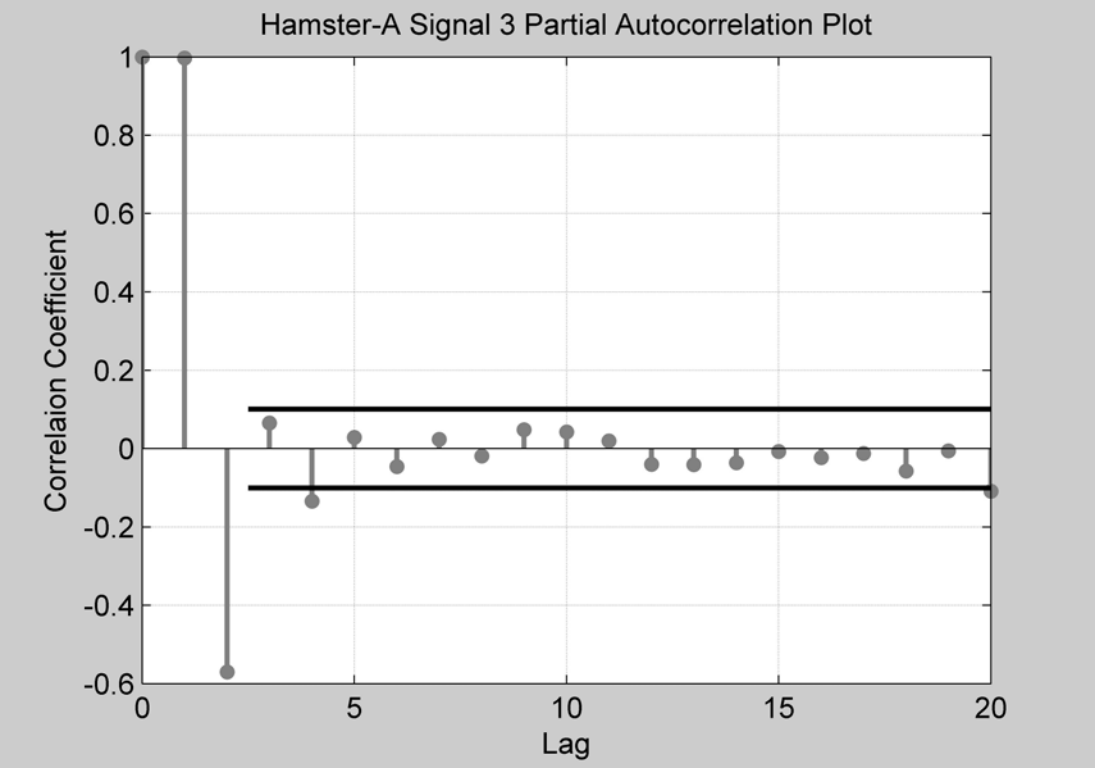


**Figure IV-21. The normalized partial autocorrelation plot for Hamster-A, Signal 3 calculated with a lag of 2. The 95% confidence bounds are marked by parallel black lines starting at the lag of 2, and indicate the significance bounds for the correlation coefficient values.**

AR(2) model form: $X_t = b_0 + b_1 X_{t-1} + b_2 X_{t-2} + \varepsilon_t$

Matlab ® Mathworks is used to compute the AR(2) model coefficients $b_i$ using ordinary least squares method.

The coefficients with 95% confidence limits are:

$b_0 = -1.000 \times 10^{-5} \pm 9.223 \times 10^{-5} = -1.0411 \times 10^{-5} < -1.000 \times 10^{-5} < 8.4127 \times 10^{-5}$

$b_1 = 1.566 \pm 0.05405 = 1.5115 < 1.566 < 1.620$

$b_2 = -0.5705 \pm 0.05409 = -0.6246 < -0.5705 < -0.5164$

The AR(2) model designed for the Hamster-A Signal 3 must be validated to ensure that the model effectively describes the correlation within the signal. Presented above, the model coefficient values with the 95% coefficient limits are listed. If the confidence limit includes the zero value, then that coefficient is considered to not be statistically significant. The 95% confidence intervals for the AR(2) coefficients shows that $b_0$ is not significant because the 95% confidence limit intervals includes the zero value. Therefore the $b_0$ term may be removed from the AR(2). However, as $b_0$ it is a constant term the AR model order is not affected. Therefore, the autoregressive model for Hamster-A Signal 3, $X_t$, is:

$$X_t = 1.566X_{t-1} - 0.5705X_{t-2} + \varepsilon_t$$

## IV.F.3.ii Autoregressive Model Validation of Residual Errors Terms for Hamster A, Signal 3

The AR(2) model for Hamster-A Signal 3 is further tested for validation by checking the residual error terms for randomness. Figure IV-24.A-F presents six different plots that check the randomness of the residual error terms, hence, the effectiveness of the model.

Figure IV-24.A presents a plot of the AR(2) model predicted signal values with respect to time, and it is compared to the to real, filtered oxygen signal values

with respect to time. It is observed that the model predicted values do follow the real signal values. As a result, the AR(2) model does accurately predict the actual signal values from the implanted oxygen sensor array.

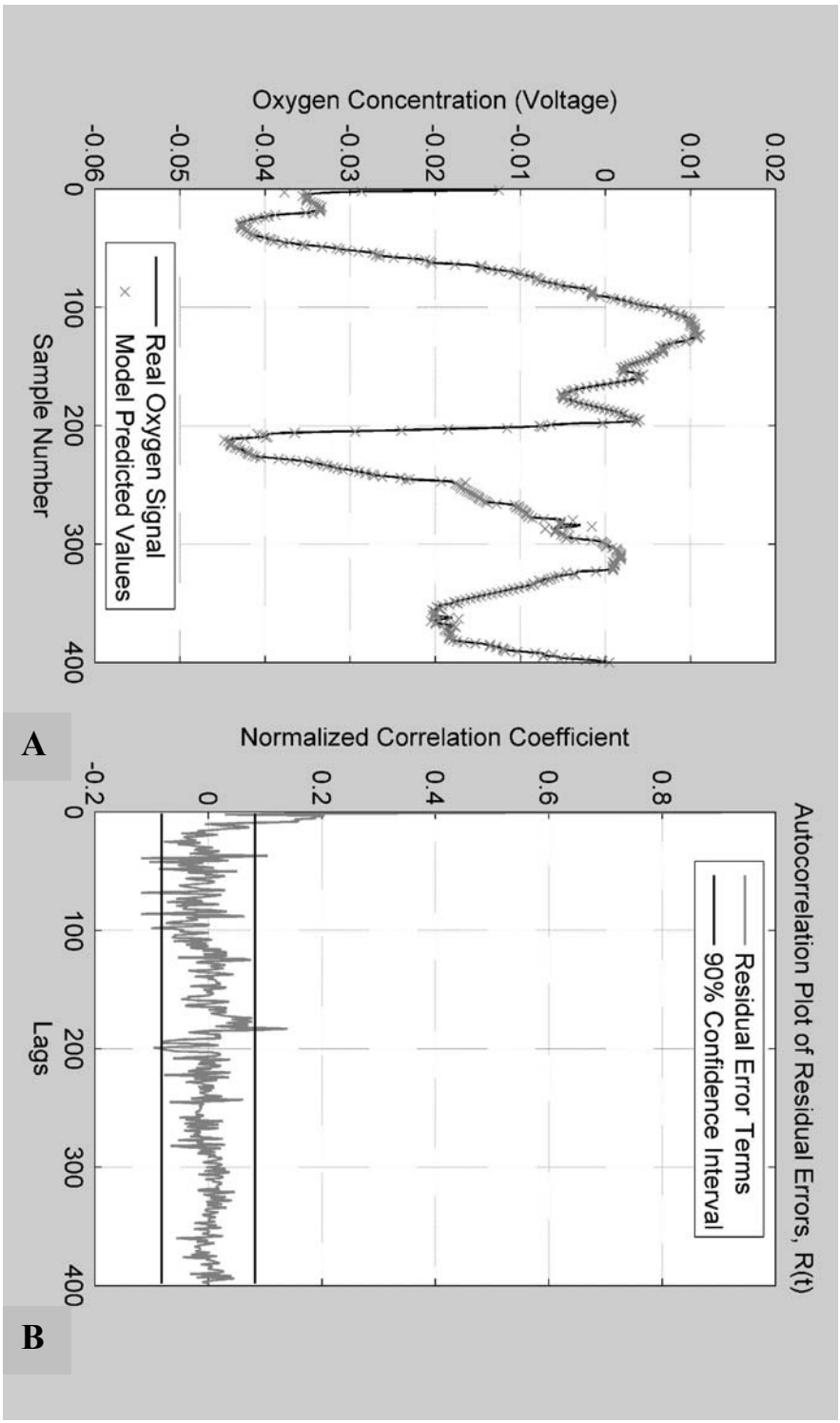


**Figure IV-22.A-B. Residual error analysis plots to validate the AR model for the Hamster-A Signal 3. A. Comparison plot of the model predicted values for the oxygen signal, vs. the real collected oxygen signal values. B. Autocorrelation plot of the residual error terms.**

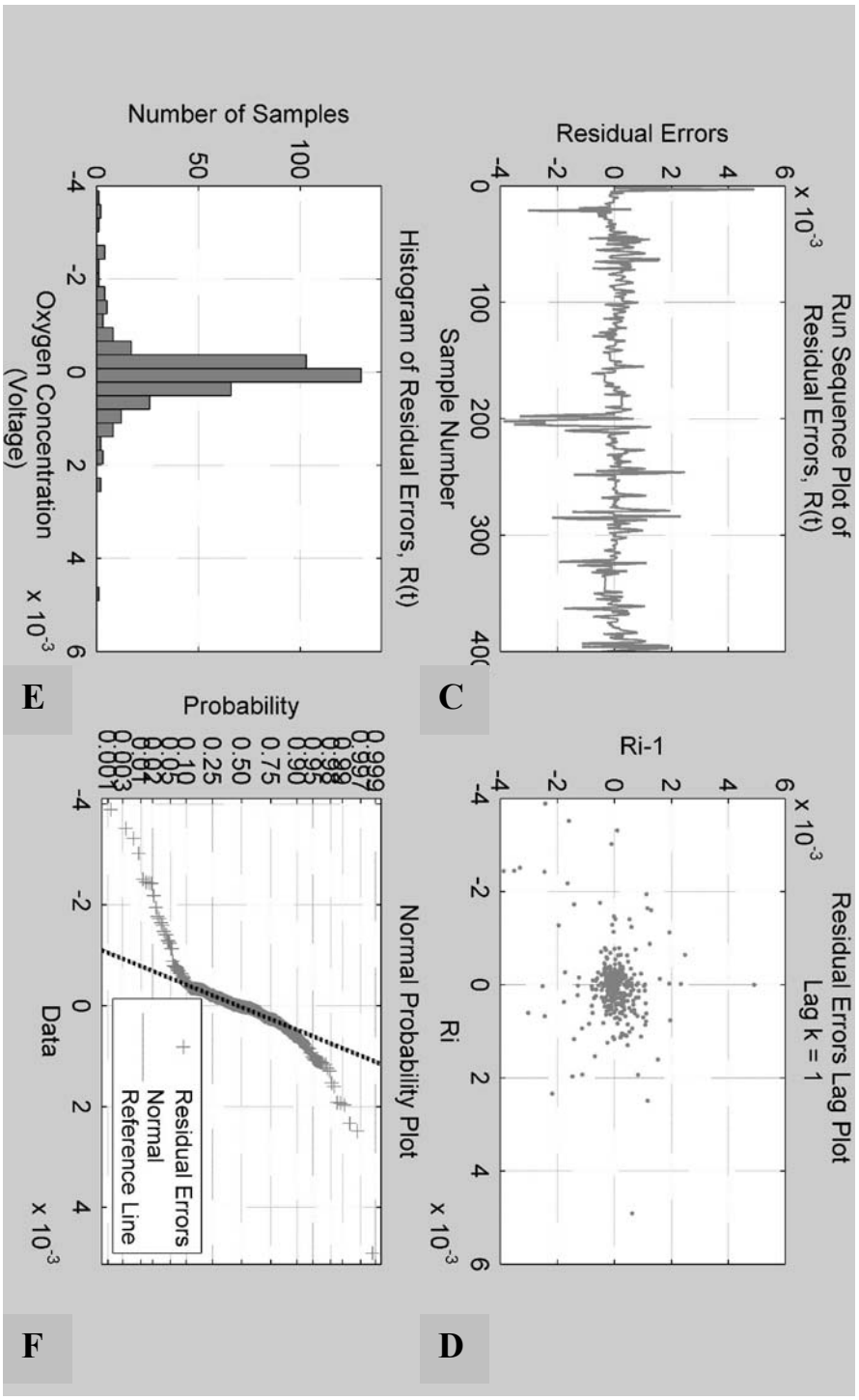


**Figure IV-24.C-F. Plots of the residual error analysis to validate the AR model for the Hamster-A Signal 3. C. Run Sequence Plot. D. Lagged Scatterplot, lag k = 1. E. Histogram plot. F. Normal Probability Plot.**

Figure IV-24.B-F presents five different graphical analysis methods, the autocorrelation plot, run chart, lagged scatterplot, histogram, and normal probability plot that will analyze the residual error terms for randomness. Figure IV-24.B presents the autocorrelation plot of the residual error terms with 90% confidence interval bounds. The 90% confidence intervals place bounds on the correlation coefficients, where any values greater than the 0.0825 or less than -0.0825 are considered to be statistically significant and indicative of autocorrelation within the residual error terms. The autocorrelation plot shows some small departure outside the 90% confidence bounds at lags of 3 to 8, and 37, 39, 41, 68, 86, 184, and 199. The greatest correlation coefficient that is outside the 90% confidence bounds is at the lag of 3, with a correlation coefficient value of 0.20. If the statistical significance is increased from 90% to 99%, the new bounds for significance will be between 0.13 and -0.13, and the correlation coefficient values at lags 37, 39, 41, 68, 86, 184, and 199, can be regarded as statistically insignificant. However, even with a 99% confidence, the coefficients for lags 3 to 8, are statistically significant and indicate that there is correlation for those 6 points. As a result, with 99% statistical confidence, the residual error values may be considered uncorrelated if sample points 3 to 8 are excluded.

Figure IV-24.C presents the run sequence plot of the residual error terms. The run sequence plot is an essential tool for checking for outliers and for detecting shifts in location and scale among the residual error terms. From the Figure IV-24.C, the run sequence plot of the residual error terms does not display random behavior. While the residual error values show no observed shift in location over time, there is

an observed shift in scale over time. There is an observed pattern of intervals, most clearly observed over samples time 200 to 400, where the residual error values shift by one order of magnitude, from $10^{-3}$ to $10^{-4}$ and vice versa. As a result, the run sequence plot shows that the residual error terms of Hamster-2 Signal 3 are not random, and that is a observable shift in scale over time.

Figure IV-24.D presents the lagged scatterplot of the residual error terms. The lagged scatterplot is calculated with a lag of 1 because the small lag best shows any type correlation, either linear or non linear, among the residual error terms. From from Figure IV-24.D, the lagged scatterplot of the residual error terms appears as small cluster of random points surrounded by more distant, additional scattered points. These more distant scattered points are classified as outliers since they do not group with the smaller, random cluster of scattered points. Moreover, the outlier points are determined to be the points that shift in scale identified in run sequence plot. In conclusion, there is no clear underlying shape that describes the lagged scatterplot and the ensuing correlation, but there is pattern in way the points are scattered. This pattern indicates that the lagged scatterplot is composed of a random cluster of points with numerous surrounding outlier points.

Figure IV-24.E presents the histogram plot of the residual error terms. The histogram is a valuable tool that can graphically summarize the distribution of a residual error terms. In Figure IV-24.E, the range of the residual error terms are segmented into 30 equal-sized bins and the number of error values that fall into each bin is counted. In general, the histogram shows the residual errors distribution to be symmetric and centered, with short tails on each end. The majority of the residual

error values fall within 6 bins located in the middle of the distribution. The remaining bins make up the tail-ends of the distribution and contain the residual error outlier values. As a result, the histogram plot shows the distribution of the residual error terms to be symmetric, centered, with tail-ends that are made up of outlier points.

Figure IV-24.F presents that normal probability plot of the residual error terms. The normal probability plot provides a comparison of the probability distribution of residual error with the normal probability distribution, which is a plotted as linear reference line. Figure IV-24.F shows the residual errors values from $-4.0 \times 10^{-4}$ to $4.0 \times 10^{-4}$ to closely follow the linear normal reference. The residual error values less than $-4.0 \times 10^{-4}$ show departure above the normal reference line, and the error values greater than $4.0 \times 10^{-4}$ show departure below the normal reference line. This normal probability plot departure pattern is called short-tails and it indicates that the variance of the residual error terms is less than what is expected for a normal distribution. Thus, the short-tailed behavior of the residual errors probability distribution suggests that the normal probability distribution may not be the best fit distribution.

In summary, the five graphical methods of the residual error analysis suggest that the residual errors terms do not behave randomly. Each of the graphical analysis methods indicates non-random behavior among the residual error terms. The autocorrelation plot shows that for 6 points there is statistically significant correlation, and the run sequence plot displays a pattern of shifting scales over time. Furthermore, the lagged scatterplot and histogram indicate that the non-random behavior could be due to the residual error terms that shift in scale. As a result, the

residual error values are not random and the AR(2) model of the Hamster-A Signal 3 may be not be an effective model. A better AR model may be designed by removing of the outlier signal points that are the source of the non-random residual error terms.

### IV.F.4.i Autoregressive Model and Coefficient Validation for Hamster A, Signal 4

The partial autocorrelation plot is used to identify the model order for Hamster-A Signal 4, by revealing the lag k for which the correlation coefficients are considered statistically insignificant. The significance of the correlation coefficients in the partial autocorrelation plot are indentified by 95% confidence bounds where any correlation coefficient greater than -0.1 and less than 0.1 is considered to not be statistically significant. Figure IV-25 presents the normalized partial autocorrelation plot of Hamster-A, Signal 4, and it is observed that after lag k of 6 the correlation coefficients can be considered insignificant. Therefore, an AR model order of 6 is chosen.

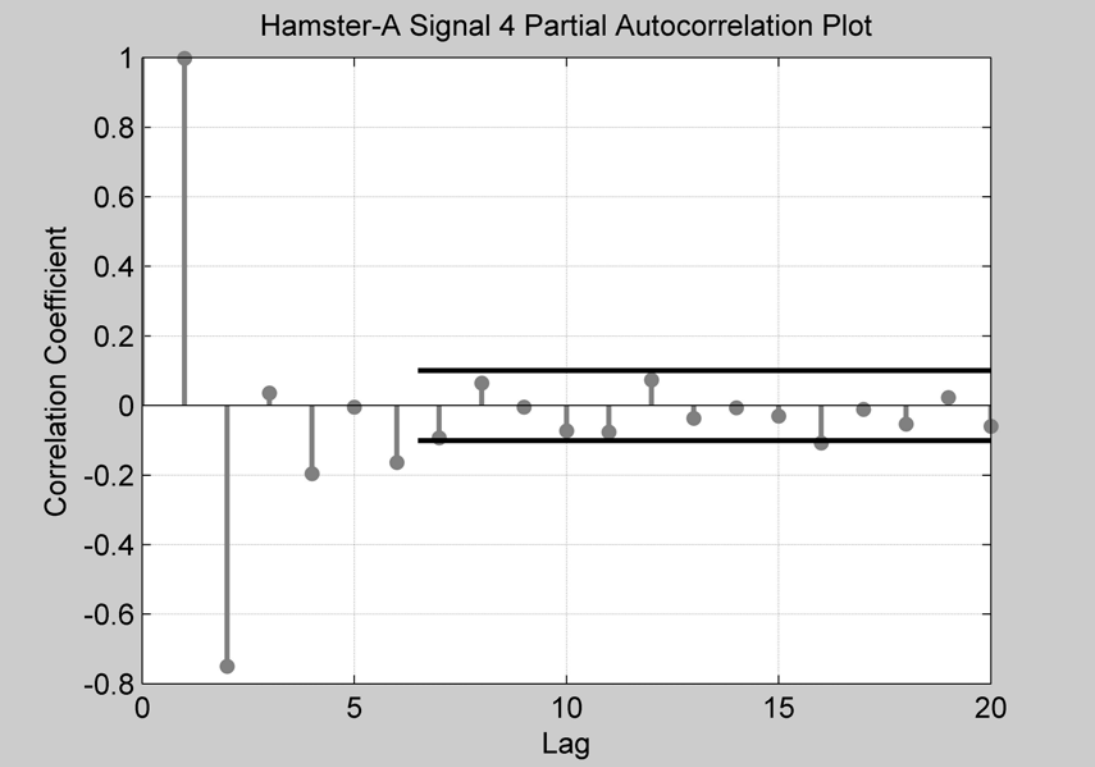


**Figure IV-23. The normalized partial autocorrelation plot for Hamster-A, Signal 4 calculated with a lag of 6. The 95% confidence bounds are marked by parallel black lines, and indicate the significance bounds for the correlation coefficient values.**

AR(6) model form:

$$X_t = b_0 + b_1 X_{t-1} + b_2 X_{t-2} + b_3 X_{t-3} + b_4 X_{t-4} + b_5 X_{t-5} + b_6 X_{t-6} + \varepsilon_t$$

Matlab ® Mathworks is used to compute the AR(6) model coefficients $b_i$ using ordinary least squares method.

The coefficients with 95% confidence limits are:

$b_0 = 6.206 \times 10^{-6} \pm 6.5552 \times 10^{-5} = -5.935 \times 10^{-5} < 6.206 \times 10^{-6} < 7.176 \times 10^{-5}$

$b_1 = 1.785 \pm 0.09793 = 1.6856 < 1.785 < 1.8814$

$b_2 = -1.003 \pm 0.2015 = -1.205 < -1.003 < -0.8016$

$b_3 = 0.4470 \pm 0.2243 = 0.2226 < 0.4470 < 0.6712$

$b_4 = -0.3639 \pm 0.2217 = -0.5856 < -0.3639 < -0.1422$

$b_5 = 0.2960 \pm 0.1912 = 0.1048 < 0.2960 < 0.4872$

$b_6 = -0.1637 \pm 0.09195 = -0.2557 < -0.1637 < -0.07176$

The AR(6) model designed for the Hamster-A Signal 1 must be validated to ensure that the model effectively describes the correlation within the signal. Presented above, the model coefficient values with the 95% coefficient limits are listed. If the confidence limit includes the zero value, then that coefficient is considered to not be statistically significant. The 95% confidence intervals for the AR(6) coefficients shows that $b_0$ is not significant because the 95% confidence limit intervals includes the zero value. Therefore the $b_0$ term may be removed from the AR(6). However, as $b_0$ it is a constant term the AR model order is not affected. Therefore, the autoregressive model for Hamster-A Signal 4, $X_t$, is:

$$X_t = 1.785X_{t-1} - 1.003X_{t-2} + 0.4470X_{t-3} - 0.3693X_{t-4} + 0.2960X_{t-5} - 0.1637X_{t-6} + \varepsilon_t$$

## IV.F.4.ii Autoregressive Model Validation of Residual Errors Terms for Hamster A, Signal 4

AR(6) model for Hamster-A Signal 4 is further tested for validation by checking the residual error terms for randomness. Figure IV-26.A-F presents six

different plots that check the randomness of the residual error terms, hence, the effectiveness of the model.

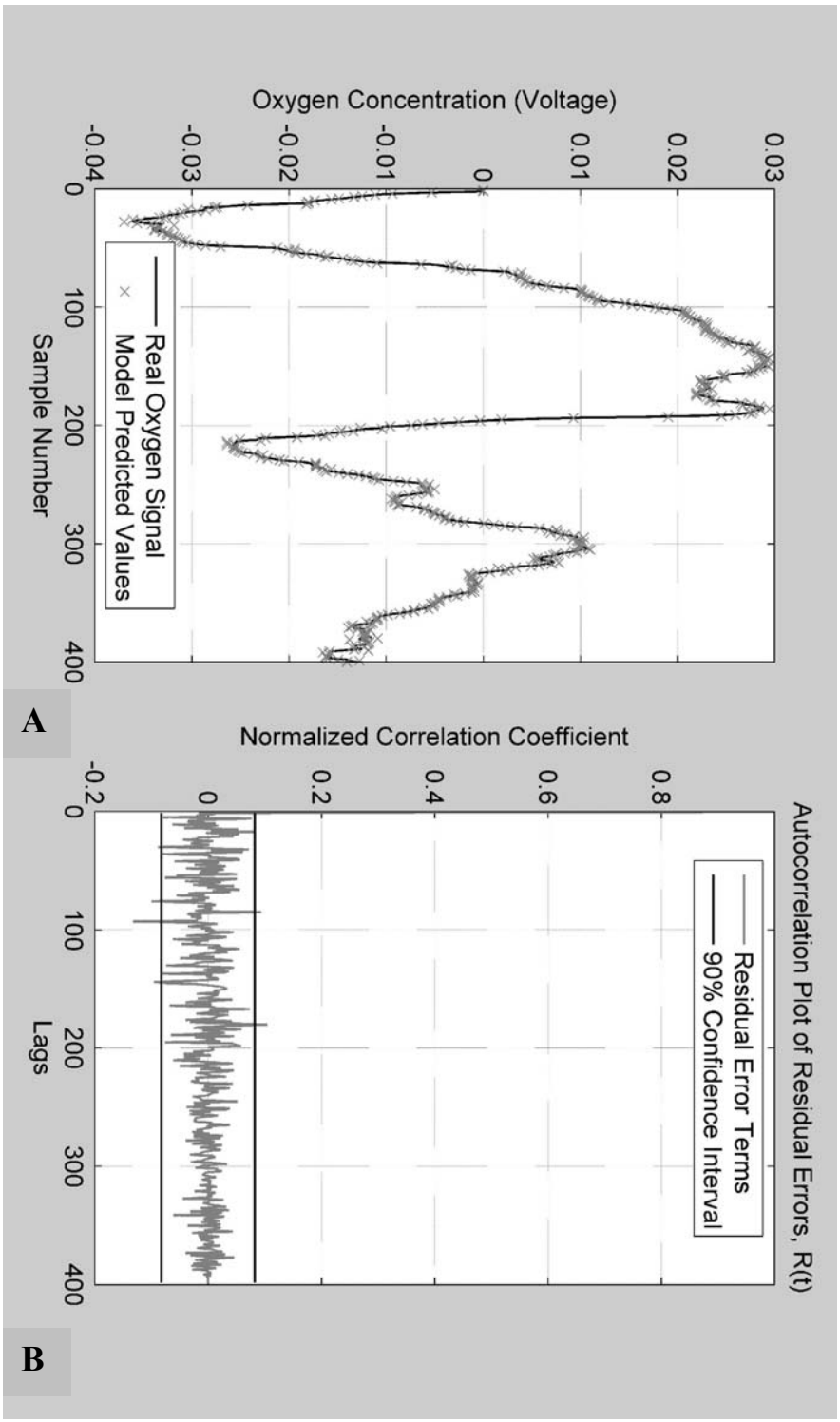


**Figure IV-24.A-B. Residual error analysis plots to validate the AR model for the Hamster-A Signal 4. A. Comparison plot of the model predicted values for the oxygen signal, vs. the real collected oxygen signal values. B. Autocorrelation plot of the residual error terms.**

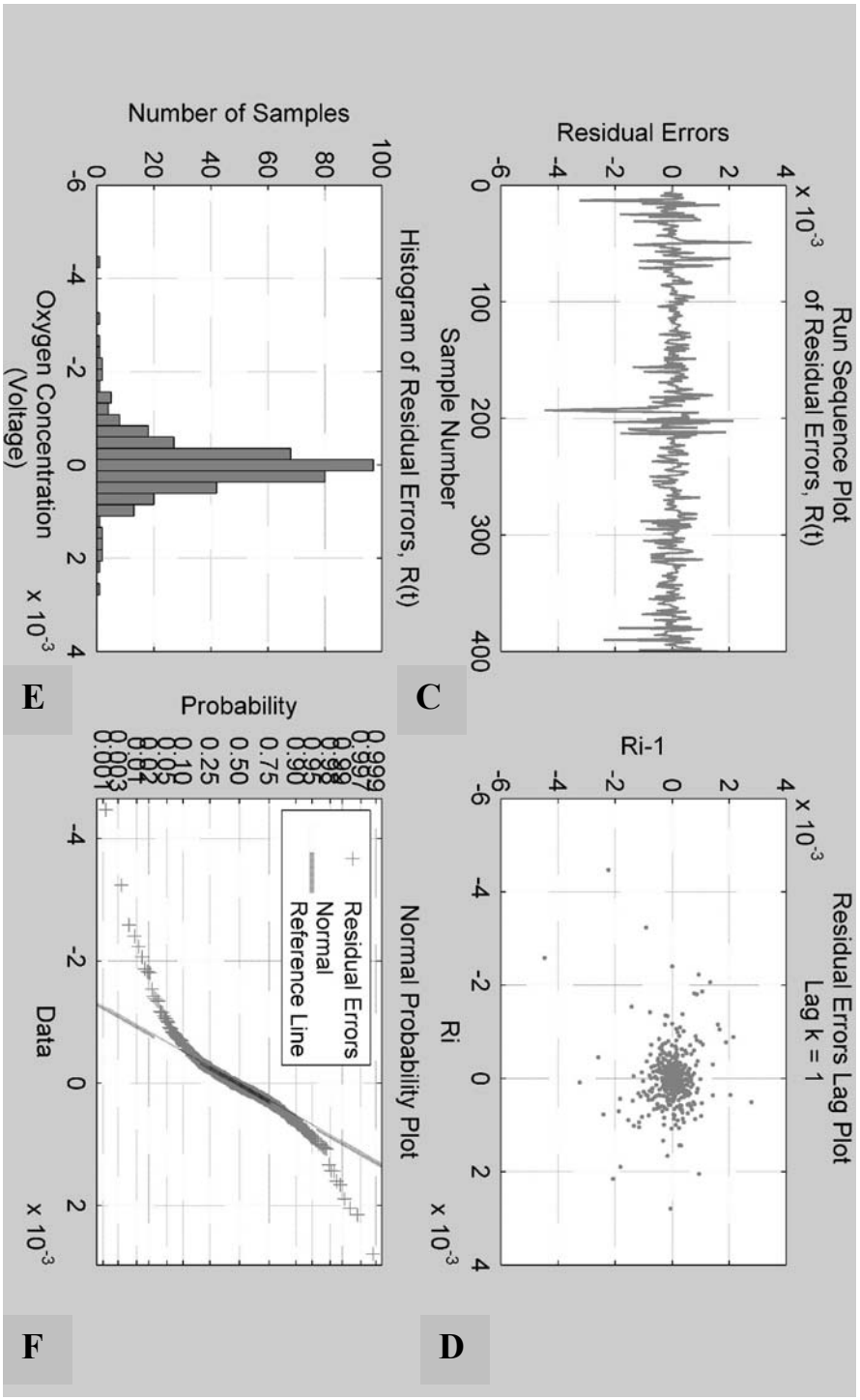


**Figure IV-26.C-F. Plots of the residual error analysis to validate the AR model for the Hamster-A Signal 4. C. Run Sequence Plot. D. Lagged Scatterplot, lag k = 1. E. Histogram plot. F. Normal Probability Plot.**

Figure IV-26.A presents a plot of the AR(6) model predicted signal values with respect to time, and it is compared to the to real, filtered oxygen signal values with respect to time. It is observed that the model predicted values closely follow the real signal values. As a result, the AR(6) model does accurately predict the actual signal values from the implanted oxygen sensor array.

Figure IV-26.B-F presents five different graphical analysis methods, the autocorrelation plot, run chart, lagged scatterplot, histogram, and normal probability plot that will analyze the residual error terms for randomness. Figure IV-26.B presents the autocorrelation plot of the residual error terms with 90% confidence interval bounds. The 90% confidence intervals place bounds on the correlation coefficients, where any values greater than the 0.0825 or less than -0.0825 are considered to be statistically significant and indicative of autocorrelation within the residual error terms. The autocorrelation plot shows six isolated departures outside the 90% confidence bounds, where the greatest magnitude correlation coefficient of 0.132 occurs at lag of 93. By increasing the statistical significance from 90% to 99%, the new bounds for significance will be at ± 0.13 and the correlation coefficient values of every lag other than lag of 93 can be considered statistically insignificant. Moreover, the lag at 93 is minimally outside the 99% confidence bound, and can be considered an outlier and removed. As a result, with 99% statistical confidence and removing the point at lag of 93, the residual error values may be considered uncorrelated and random.

Figure IV-26.C presents the run sequence plot of the residual error terms. The run sequence plot is an essential tool for checking for outliers and for detecting shifts

in location and scale among the residual error terms. From the Figure IV-26.C, the run sequence plot of the residual error terms displays random-like behavior. In addition, there is no observed shift in location or scale with time. However, there are distinct outlier points that are greater in magnitude than the rest of the residual error values and fall outside the range of $\pm 1.5 \times 10^{-3}$. The outliers are observed at sample times of 13, 17, 25, 49, 63, 193, 202, 212, 380, and 390, with the greatest residual error outlier value of $4.472 \times 10^{-3}$ occurring at sample time of 193. As a result, the run sequence plot shows the Hamster-A Signal 4 residual error terms to be random, and identifies approximately 10 outlier points that could be removed to make the AR(6) model more effective.

Figure IV-26.D presents the lagged scatterplot of the residual error terms. The lagged scatterplot is calculated with a lag of 1 because the small lag best shows any type correlation, either linear or non linear, among the residual error terms. From from Figure IV-26.D, the lagged scatterplot of the residual error terms is observed as a random cluster of points surrounded by more distant, additional scattered points. The more distant scattered points are determined to be the outliers identified in the run sequence plot. Specifically, the outlier points at $(2.259 \times 10^{-3}, 4.472 \times 10^{-3})$ and $(4.472 \times 10^{-3}, 2.223 \times 10^{-3})$ originate from the outlier point at sample time 193, with residual error value of $4.472 \times 10^{-3}$. In conclusion, the lagged scatterplot of the residual error terms is observed as randomly scattered points and outliers.

Figure IV-26.E presents the histogram plot of the residual error terms. The histogram is a valuable tool that can graphically summarize the distribution of a residual error terms. In Figure IV-26.E, the range of the residual error terms are

segmented into 30 equal-sized bins and the number of error values that fall into each bin is counted. The histogram shows the residual errors distribution to be symmetric and bell-shaped, with tails on each end. The majority of the residual error values fall within the bins that span from $-1 \times 10^{-3}$ to $1 \times 10^{-3}$. The remaining bins make up the tail-ends of the distribution and contain the residual error outlier values. As a result, the histogram plot shows the distribution of the residual error terms to be symmetric, and bell-shaped with tail-ends that are made up of outlier points.

Figure IV-26.F presents that normal probability plot of the residual error terms. The normal probability plot provides a comparison of the probability distribution of residual error with the normal probability distribution, which is a plotted as linear reference line. Figure IV-26.F shows the residual errors values from $-4.0 \times 10^{-4}$ to $5.0 \times 10^{-4}$ to closely follow the linear normal reference. The residual error values less than $-4.0 \times 10^{-4}$ show departure above the normal reference line, and the error values greater than $5.0 \times 10^{-4}$ show departure below the normal reference line. This normal probability plot departure pattern is indicative of short-tails and suggests that the variance of the residual error terms is less than what is expected for a normal distribution. Thus, the short-tailed behavior of the residual errors probability distribution means that the normal probability distribution may not be the best fit distribution.

In summary, the five graphical methods of the residual error analysis suggest that the residual errors terms behave randomly with the exception of the outlier points. The autocorrelation plot indicated that there is no correlation among the residual error terms. The run sequence plot shows that the residual error terms are

random, and identified ten outlier points. The lagged scatterplot and histogram confirm the randomness of the residual error terms, as well as the existence of outliers. The normal probability plot shows that the residual error terms somewhat follow the normal distribution, and if the outliers points were removed the normal distribution may be become a better fit with the distribution of the residual error terms. As a result, the residual error terms are determined to be random with outliers, and the AR(6) model for Hamster-A Signal 6 can be designed to be more effective if the source of the residual error outlier points are removed.

# Chapter V: Results of Implanted Oxygen Sensor Signal Analysis for the Pig

The oxygen signals were collected from hermetically sealed oxygen sensors implanted in the dorsal side of the pig in subcutaneous tissue. The sensor signals were collected after a sufficient amount of time had passed post-implantation to mitigate any signal bias caused by the surrounding tissue wound healing process. The sensor implantation and signal collection were completed by GlySens Incorporated. GlySens Inc. was able to provide two sets of oxygen signals, consisting of two signals each, from two different pig sensor implants for analysis. The implanted oxygen sensor sampled the local tissue oxygen level at the rate of 1 sample every 1.24 seconds for approximately 60 to 70 minutes. Prior to any analysis the pig oxygen signals were detrended (removal of the linear trend), smoothed, and filtered to remove the indentified non-biological signal features.

## V.A Filtering of the Pig Oxygen Signals

The following Figures V-1 and Figure V-2 presents plots of the linearly detrended Pig-A oxygen sensor signals, plotted against the processed signal that has been linearly detrended, filtered using the designed filtering algorithm to suppress the non-biological artifacts distorting the signal, and lastly, smoothed using a moving median filter. In order to better visualize the orighinal signal plotted against the processed signal, the original signals were also linearly detrended in order for both signal to have the same oxygen concentration scale on the y-axis.

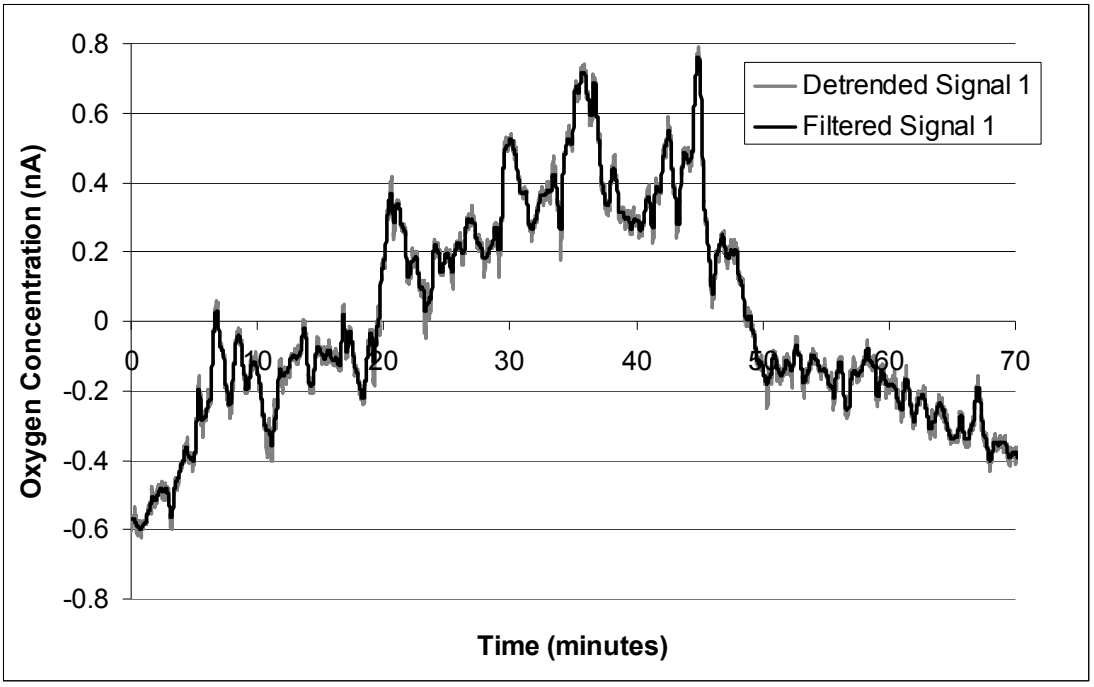


**Figure V-1. Pig-A, Signal 1**

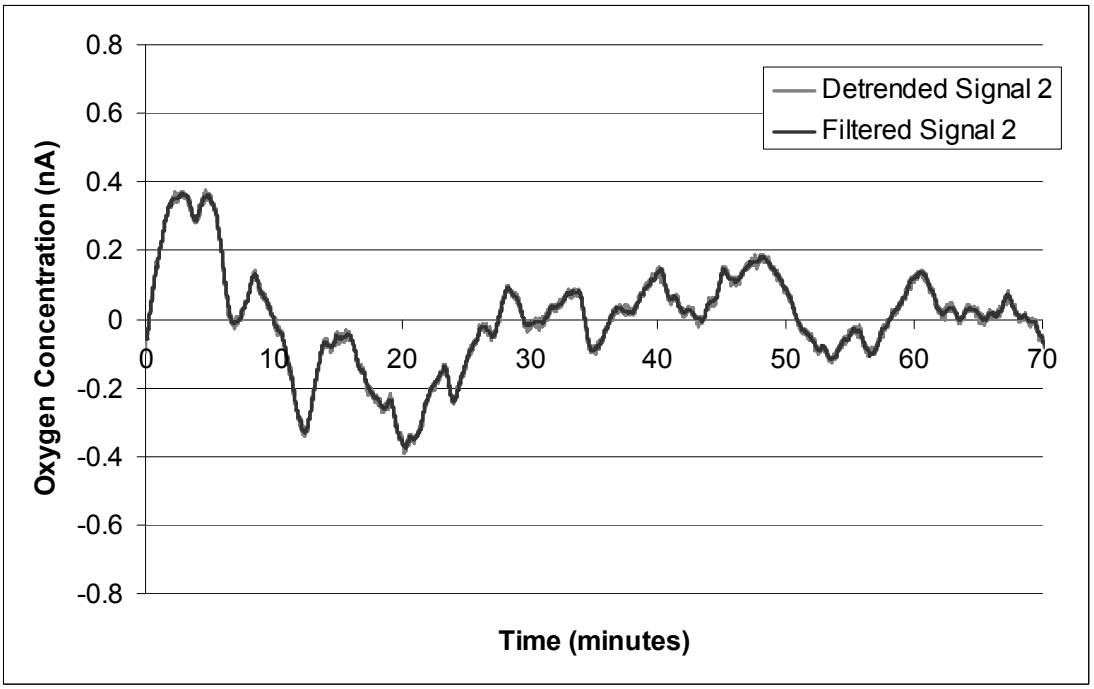


**Figure V-2. Pig-A, Signal 2**

The original signals plotted against the filtered signals for Pig-B, Signals 1 – 2 are shown in Appendix A, in Figures A-17 and Figure A-18.

## V.B Results of Power Spectral Analysis

The oxygen signals collected from hermetically sealed oxygen sensor arrays implanted in the dorsal side and subcutaneous tissue of pigs. From the oxygen signals collected, two different oxygen signals represent the pig sensor signal response from each pig, and the power spectrums of the filtered signals were estimated via the Welch method. The power spectra of the representative signals collected from Pig-A and Pig-B are presented in Figure V-3.

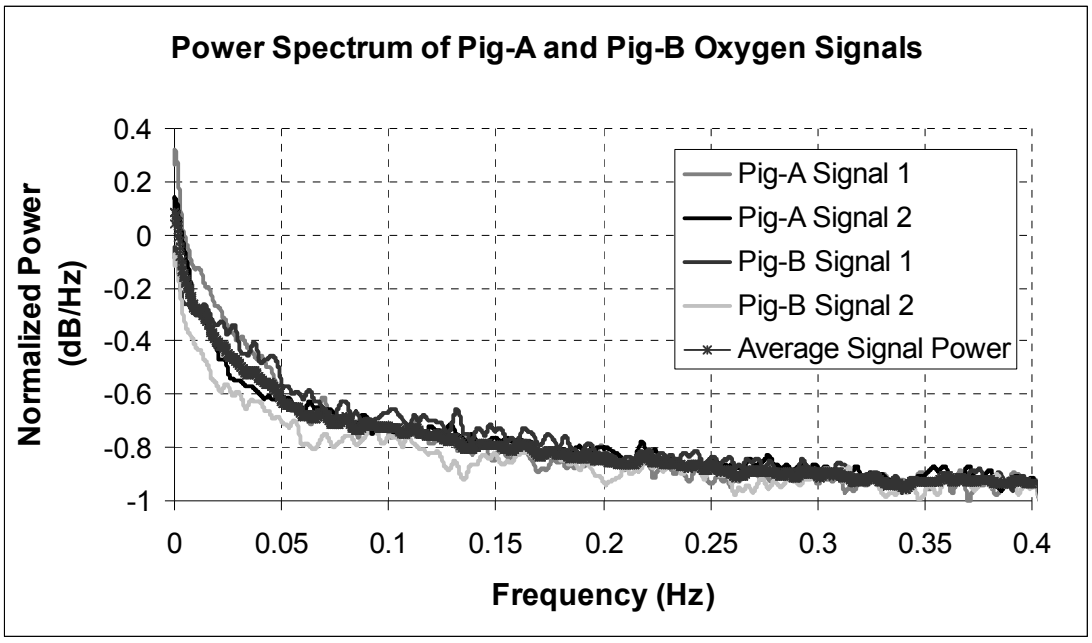


**Figure V-3. Normalized estimated power spectra of the representative signals from the oxygen sensor array implanted in Pig-A and Pig-B.**

The normalized power spectra of the filtered pig oxygen signals ranges in descending power from 0.33 dB/Hz to approximately -1 dB/Hz, over increasing frequency. This range of values from positive to negative power is specifically due to the removal of the linear trends from the signals prior to analysis. The detrending of the oxygen signals removes the influence of the different steady-state levels on the oxygen signal analysis, resulting in signals that fluctuate about the zero-axis, and the power spectra to include positive and negative values. The normalized power spectrums of the filtered pig oxygen signals have the maximum power at very low frequencies. This indicates that the pig oxygen signals have relatively high variance at low frequencies and that the time signals contain positive autocorrelation. Furthermore, the power spectrum of the oxygen signals display no distinguishable differences from each other even though the time-signals of the representative oxygen signals contain notable differences in the signal variations. In addition, the power spectra show similar trends in the power versus frequency, where as the frequency increases, the power exponentially decays to a common power level. Moreover, for every frequency, all the oxygen signals share similar level of normalized power. As a result, the estimated spectrums of Pig-A and Pig-B signals may be labeled as low-frequency spectrums. The spectral analysis of the pig signals also shows there to be no dominant and distinguishable peaks representing a significant oxygen signal event with an identifiable frequency. Instead, there is an observed oscillatory behavior in the spectral power level that spans the total frequency range. These oscillations may represent periodicity in the signal at various frequencies, or noise in the signal, or a

combination of both effects. The spectral oscillations are observed as local peaks in the power spectrums of Pig-A Signal 1 and 2, and Pig-B, Signal 1 and 2, that occur approximately every 10 ± 5 mHz. Therefore, the spectral analysis of Pig-A and Pig-B oxygen signals reveals the signals to have a periodic component, identified as a fundamental frequency. Conclusively, the spectral analysis shows the Pig-A and Pig-B oxygen signals to have low-frequency spectrums, that there are no dominant spectral peaks, and for the spectrums to have a fundamental frequency of 10 ± 5 mHz, representing an obvious pervasive periodicity within each of the pig oxygen signal.

## V.C Results of the Correlation Analysis

Correlational analysis is completed for the short-term oxygen signals collected from the oxygen sensor arrays implanted in the pig subcutaneous tissue. The oxygen sensor arrays are implanted in two pigs, and the signals are collected after a sufficient time period post implantation in order to minimize the effects of tissue immune response on the sensor signal response. From each sensor two oxygen signals represent the various types of dynamics measured by implanted sensor. The oxygen signals are collected over a time period of 60 to 70 minutes, with a sampling rate of 1 sample every 1.24 seconds. Prior to the correlational analysis, the signals are detrended, smoothed, and filtered to remove the identified non-biological features.

The representative oxygen signals collected from the same sensor array are analyzed for any type of correlation within individual signals, and for correlation among multiple signals collected from the same sensor array. The correlational analysis plots include the autocorrelation, cross-correlation, and lagged scatterplots.

## V.C.1 Correlation Analysis of Pig-A Signals

Figure V-4 shows the plot of the normalized autocorrelation of the two representative signals collected from the sensor array implanted in Pig-A. The horizontal lines at value 0.034 and -0.034 correlation coefficients are the 95% confidence bounds, and any correlation coefficient value of the autocorrelation that falls between 0.034 and -0.034 is considered to be not statistically significant. The autocorrelation plot shows each of the two representative signals from Pig-A contains statistically significant periodicity and are autocorrelated. This is observed as the sinusoidal pattern in each signal's autocorrelation analysis and plot. The duration of one sinusoidal cycle signifies the cycle of periodicity within the signal, and is measured as the number of sample points starting from the sample time of zero to the first sinusoidal peak. For Pig-A, Signals 1, the signal is observed to contain one full periodic cycle that spans from sample number 0 to approximately 2835 sample points, corresponding to a periodic cycle of approximately 59 minutes. For Pig-A, Signal 2, there is one periodic cycle starting from sample 0 to sample 2115, corresponding to a periodic cycle of 44 minutes. Pig-A, Signal 2 autocorrelation plot presents an additional sinusoidal cycle starting from sample number 2115 to 2775,

corresponding to a periodic cycle of 660 samples, and approximately 14 minutes. The significant different between to the two sinusoidal cycles within the autocorrelation of Signal 2, first a 59 minute periodic cycle, and the second a 14 minute periodic cycle, cannot be attributed to inherent autocorrelation calculation error due to the finite length and discrete nature of signal. The two different periodic cycles within Pig-A, Signal 2 are attributed to the non-stationarity of the signal and indicative of the different frequencies of oscillations occurring over different sampling periods. In summary, the normalized autocorrelation shows that for Pig-A, Signals 1-2 are autocorrelated and have clear periodicity. Signal 1 displays a 59 minute periodic cycle, equivalent to a frequency of oscillation of 0.28 mHz, and Signal 2 displays a 44 minute and 14 minute periodic cycle, equivalent to frequencies of oscillation of 0.38 mHz and 1.2 mHz.

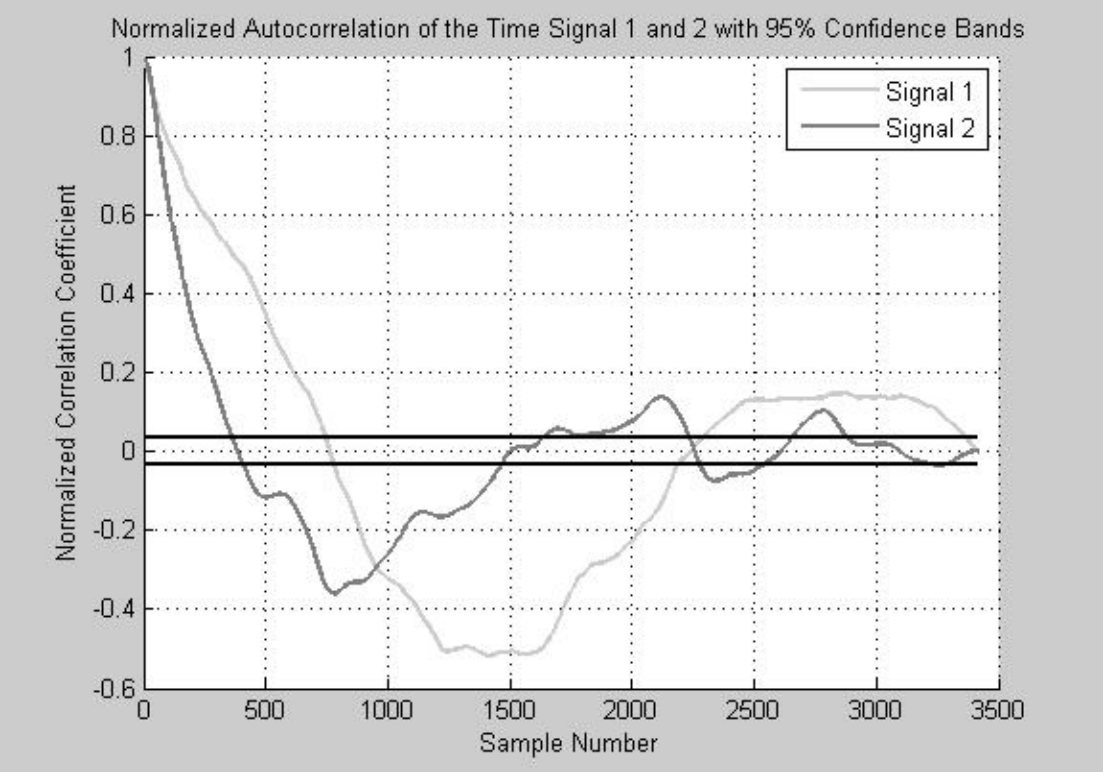


**Figure V-4. Normalized Autocorrelation Plot for Pig-A, Signals 1-2.**

Figure V-5 shows the plot of the normalized cross-correlation for the cross between the Pig-A representative oxygen sensor Signals 1 and 2. The horizontal lines at correlation coefficient values of 0.034 and -0.034 are the 95% confidence bounds, and any correlation coefficient value that falls between 0.034 and -0.034 is considered to not be statistically significant. The Pig-A cross-correlation plot suggests that the two signals are negatively correlated with each other because at the sample zero, the correlation coefficient is negative. As the sample number increases a sinusoidal pattern emerges indicating that the two signals are periodically correlated. The periodicity is determined by calculating the duration of one periodic cycle within the cross-correlation plot. This cycle is estimated to start at sample number 700 to 3020,

and corresponds to a periodicity of 48 minutes, which is equivalent to a frequency of 0.35 mHz. In general, Pig-A, Signal 1 and 2 are found to be negatively and periodically correlated, with a periodic cycle of 48 minutes (0.35 mHz).

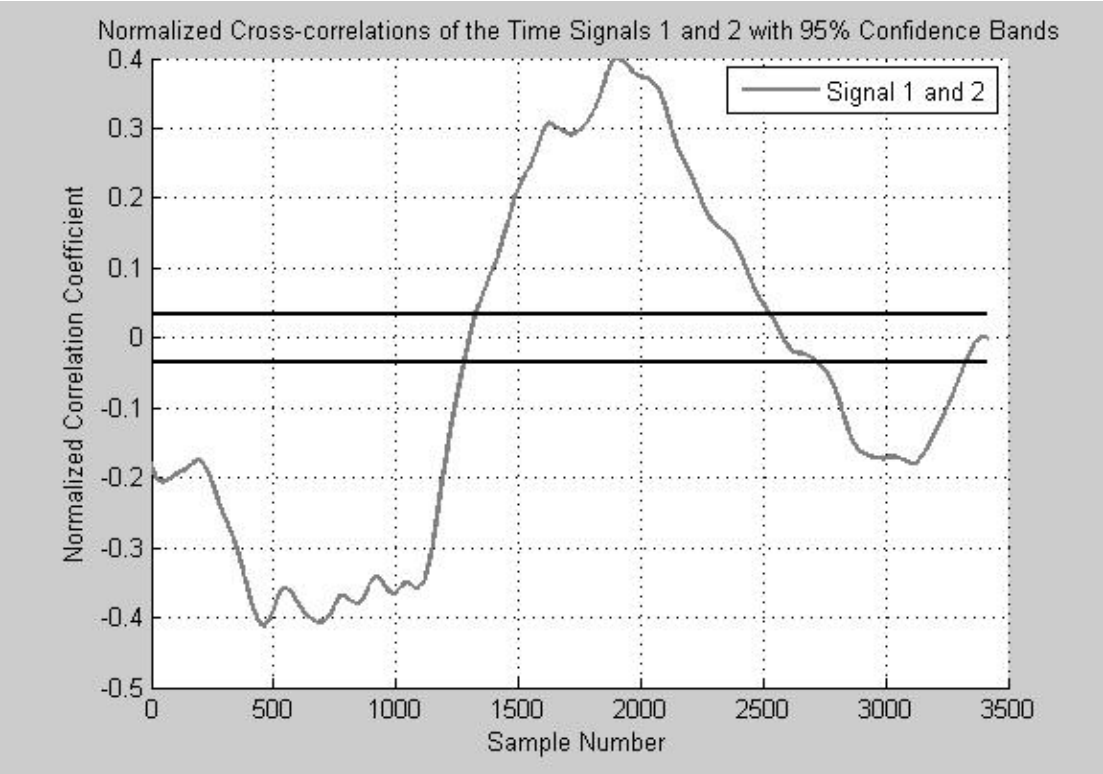


**Figure V-5. Normalized Cross-correlation Plot for Pig-A, Signals 1-2.**

The autocorrelation and cross-correlation plots of the Pig-A, Signals 1 and 2 representative oxygen sensor signals reveals that the signals are autocorrelated and demonstrate cross-correlation. In addition, the signals demonstrate statistically significant periodicity within each individual signal and between the two signals, where the frequencies of periodicity for the auto- and cross-correlation are within one order of magnitude.

Figure V-6.A-B presents the lagged scatterplots for the Pig-A representative oxygen sensor Signals 1 and 2. The lag plots were calculated for lag k at 1, 5, 10, 20, 50, and 100. The multiple lags of increasing times are chosen in order to indentify the origin of any spatial dependence between the collected sensor signal sample points, and to determine if there is dispersion in the lagged scatterplot as the lag is increased. Figure V-6.A presents the lagged scatteplot for Pig-A, Signal 1. The lag plot with a lag of one shows a clear linear dependence between consecutive points of Signal 1, demonstrated by the y=x linear graph of the collected sample points. At the lag of 5, the scatterplot pattern maintains a linear pattern albeit with some small dispersions among the signal points. As the lag k is increased, the lag plot shows further dispersion among the samples points but the linear pattern is maintained. The linear behavior of the Pig-A Signal 1 lagged scatterplot suggests a linear dependence between the signal points. Figure V-6.B presents the lagged scatterplot for Pig-A Signals 2. At a lag of one, the scatterplot for the signal demonstrates linearity shown by the y=x linear graph of the signals points. The linear pattern of points indicates an obvious linear dependence between consecutive oxygen signal points. As the lag k is increased, the scatterplot pattern maintain linearly up to lag of 20. At the lag of 50 and lag of 100, the scatterplot becomes increasingly dispersed, and displays an ambiguous pattern suggesting that the signals could have non-linear dependence at larger lags. Overall, the lagged scatterplots for Pig-A Signal 1 shows linear dependence between signal points for every lag, and the lagged scatterplot for Pig-A

Signal 2 displays linear dependence at lower lags, and non-linear dependence between signal points at large lags.

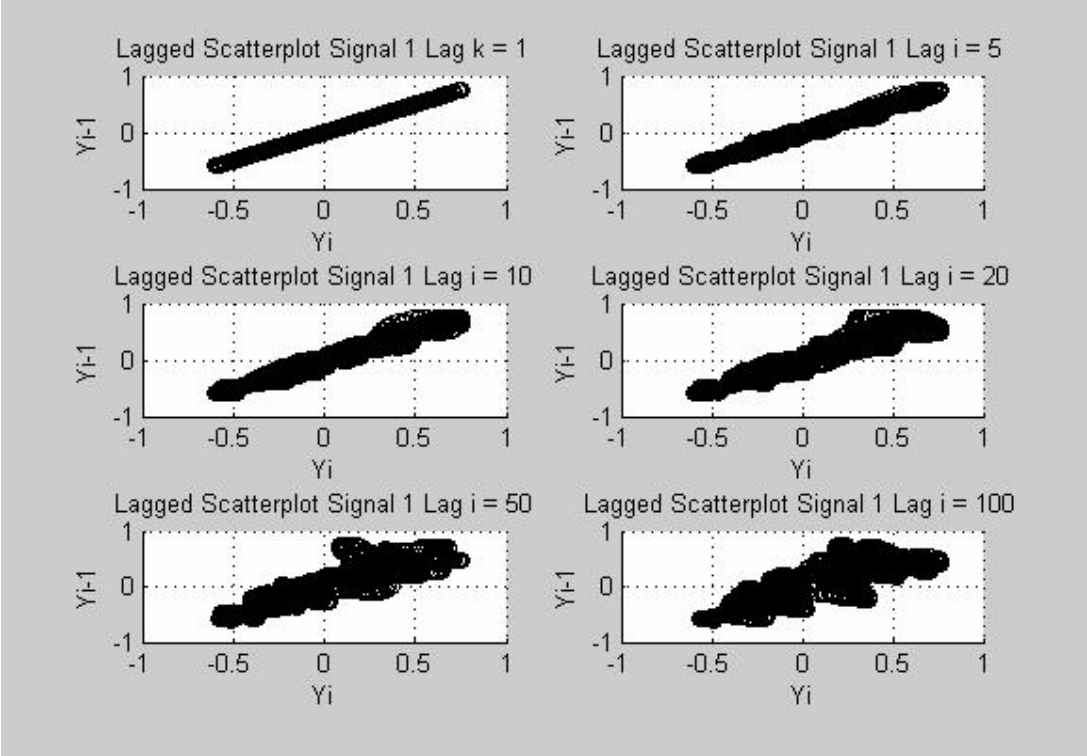


**Figure V-6.A. Lagged Scatterplots of Pig-A, Signal 1 for lags of 1, 5, 10, 20, 50 and 100.**

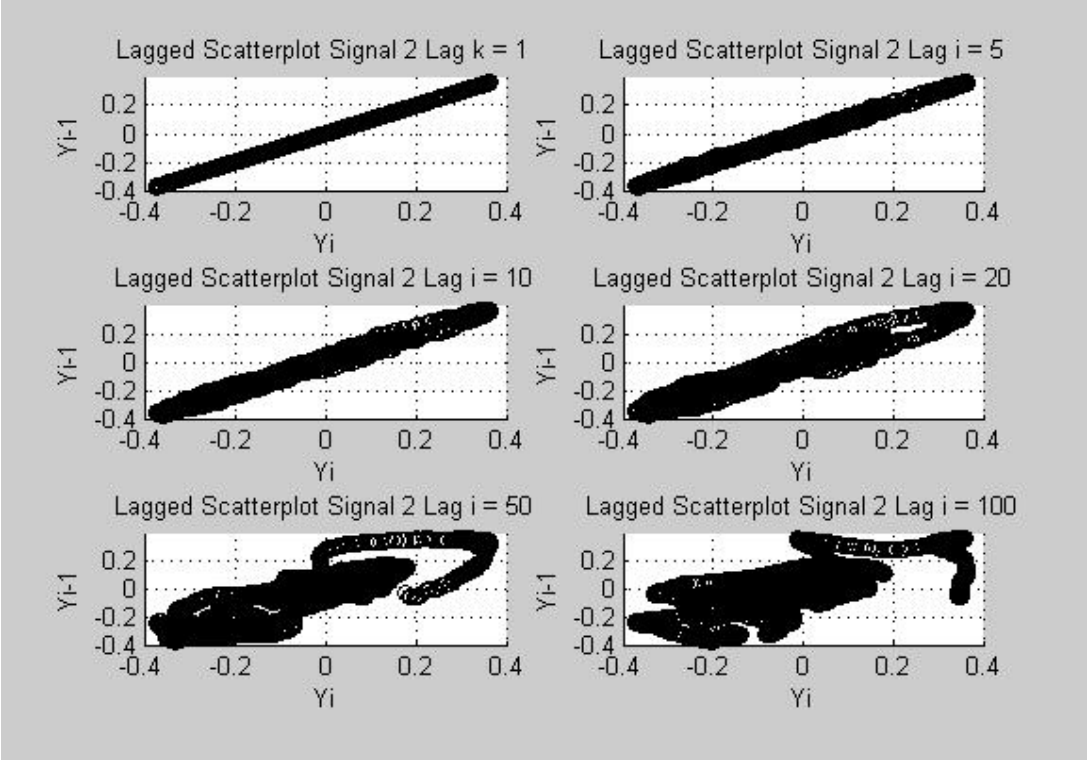


**Figure V-6.B. Lagged Scatterplots of Pig-A, Signal 2 for lags of 1, 5, 10, 20, 50 and 100.**

## V.C.2 Correlation Analysis of Pig-B Signals

Figure A-19 presented in Appendix A presents the plots of the normalized autocorrelation of the two representative oxygen time signals collected from the oxygen sensor array implanted in Pig-B. The horizontal lines at correlation coefficient values of 0.037 and -0.037 are the 95% confidence bounds and any correlation coefficient value of the autocorrelation that falls between 0.037 and -0.037 are considered to not be statistically significant. The autocorrelation of the Pig-B representative signals shows the signals to be autocorrelated and to display similar periodicity. The autocorrelation of Pig-B, Signal 2 displays a clear sinusoidal pattern indicating periodicity within the signal, with the sinusoidal cycle starting from sample number 0 to 2308, corresponding to a periodic cycle of approximately 48 minutes.

Signal 1 is observed to have a similar overall sinusoidal pattern as Signal 2, with the sinusoidal-like cycle starting at sample 0 to 2765, corresponding to periodic cycle of 57 minutes. However, the autocorrelation plot of Signal 1 is observed to have a high frequency fluctuation superimposed over the larger sinusoidal cycle. This could be a result of the non-stationarity of the Signal 1 or a result of noise within Signal 1. In summary, the autocorrelation plots of Pig-B Signals 1 and 2 both display similar autocorrelation and periodic behavior within the signals. Signal 1 contains 57 minute periodic cycle, equivalent to a 0.29 mHz frequency of oscillation, and Signal 2 displays a 48 minute periodic cycle, equivalent to a 0.35 mHz frequency of oscillation.

Figure A-20 presented in Appendix A presents the plot of the normalized cross-correlation for the cross between the Pig-B representative oxygen sensor Signals 1 and 2. The horizontal lines at correlation coefficient values of 0.037 and -0.037 are the 95% confidence bounds, and any correlation coefficient value that falls between 0.037 and -0.037 is considered to not be statistically significant. The Pig-B cross-correlation plot suggests that the two signals are strongly positively correlated with each other because at the sample zero, the correlation coefficient is positive and has the maximum normalized correlation coefficient of 0.68. As the sample number increases a sinusoidal pattern becomes apparent indicating that the two signals are periodically correlated. The periodicity is determined by calculating the duration of one periodic cycle within the cross-correlation plot. This cycle is estimated to start at sample number 0 to 2587, and corresponds to a periodicity of 53.5 minutes, which is

equivalent to a frequency of 0.31 mHz. The cross-correlation plot also shows variations superimposed over the larger sinusoidal cycle. These imposed variations could be due to differences in periodicity within the individual signals, the non-stationary behavior of the both signals, and/or due to noise within the signals. In summary, Pig-B, Signal 1 and 2 are found to be positively and periodically correlated, with a periodic cycle of 53.5 minutes (0.31 mHz).

The autocorrelation and cross-correlation plots of the Pig-B, Signals 1 and 2 representative oxygen sensor signals reveals that the signals are autocorrelated and demonstrate cross-correlation. In addition, the signals demonstrate statistically significant periodicity within each individual signal and between the two signals, where the frequencies of periodicity for the auto- and cross-correlation lie within the range of 0.29 mHz to 0.35 mHz.

Figure A-21.A-B shown in Appendix A presents the lagged scatterplots for the Pig-B representative oxygen sensor signals 1-2. The lag plots were calculated for lag k at 1, 5, 10, 20, 50, and 100. The multiple lags of increasing times are chosen in order to indentify the origin of any spatial dependence between the collected sensor signal sample points, and to determine if there is dispersion in the lagged scatterplot as the lag is increased. Figure A-21.A presents the lagged scatteplot for Pig-B Signal 1. The lag plot with a lag of one shows a clear linear dependence between consecutive points of Signal 1, demonstrated by the y=x linear graph of the collected sample points. As the lag k is increased, the lag plot loses its linear behavior and takes on a non-linear globular pattern where the signal points become grouped closed

together. At the lag k of 50 and 100, the scatterplots are very similar and there is a definite non-linear dependence between the signal points. Figure A-21.B presents the lagged scatterplot of Pig-B Signal 2. The lag plot with a lag of one shows a clear linear dependence between consecutive points of Signal 2. At the lag of 5, the scatterplot pattern maintains a linear pattern albeit with some small dispersions among the signal points. As the lag k is increased to 10 and 20, the lag plot shows further dispersion among the samples points but a linear-like is maintained among the signal points. At the lag of 50 and lag of 100, the scatterplots becomes increasingly dispersed, and displays an ambiguous pattern suggesting that the signal has non-linear dependence at larger lags. In summary, the lagged scatterplots for Pig-B Signal 1 and 2 demonsrtates linear dependence between signal points at lower lags, and as the lags are increased the scatterplots take on a non-linear pattern indicating non-linear dependence between the signal points.

## V.D Results of the Continuous Wavelet Transform Analysis

Wavelet analysis is completed for the short-term oxygen signals collected from the oxygen sensor arrays implanted in the pig subcutaneous tissue. The oxygen sensor arrays are implanted in two pigs, and the signals are collected after a sufficient time period post implantation in order to minimize the effects of tissue immune response on the sensor signal response. From each sensor two oxygen signals were chosen to represent the various types of dynamics measured by implanted sensor. The oxygen signals are collected over a time period of 60 to 70 minutes. Prior to the

wavelet analysis, the signals are detrended (removal of the linear trend), smoothed, and filtered to remove the identified non-biological features. The continuous wavelet transform of the oxygen signal are completed using the Morlet wavelet and the transforms are plotted in terms of time and frequency, with the wavelet coefficient as the amplitude

The frequency range of the wavelet transform, represented by a discrete set of scales, is chosen such that the plot of the transformed oxygen signal is most complete and can be best visualized. Each set of signals will contain a different number of samples points, collected over a different duration of time, and with a different sampling rate, and these differences affect the visualization of the frequency domain on the wavelet transform. Therefore, the range of frequencies and scales for each set of oxygen signals are collected from sensor arrays that are individually chosen in order to build the best visual wavelet transform plot.

### V.D.1 Wavelet Analysis of Pig-A Signals

The oxygen signals for Pig-A are collected over a 70 minute time duration, and the average sampling rate of the signals is one sample every 1.24 seconds. The normalized wavelet transforms for each signal is shown in the corresponding Figures 1 – 2. For each figure, there is a plot of the filtered time-signal, and two different types of plots of the normalized wavelet transform are shown, one as a two-dimensional (2-D) image plot, and the second as a three-dimensional (3-D) mesh plot.

The wavelet transform for each oxygen signal demonstrates a non-stationary behavior over the 70 minute time period.

The normalized wavelet transforms of Pig-A Signal 1 are presented in Figure V-7, and shows that the pig oxygen signal is non-stationary. From the 2-D normalized wavelet transform image, the non-stationarity of the signal is demonstrated by unequal, and irregular distribution of peak wavelet coefficient values over the total duration of pig oxygen signal. The peak wavelet coefficient values are determined to be within the range of 0.65 to 1, and are represented by parallel white stripes or white elongated ovals over the sample time periods of 0 to 100 (0 to 2 minutes) and 775 to 2400 (16 to 50 minutes) for the frequency range of 0.0001 Hz to 0.5 Hz. The 2-D wavelet transform of the pig oxygen signal also shows that the identified sample time periods to occur with different ranges of frequencies which vary and overlap. This feature of varying and overlapping frequency ranges is most clearly observed for the sample time period of 775 to 1200, which has a frequency range of 0.0001 Hz to 0.25 Hz, and for the sample period of 2000 to 2400, which displays an overlapping frequency range of 0.1 Hz to 0.5 Hz. From the wavelet transform 3-D mesh plots, the peaks wavelet coefficients are observed over the specified time periods of 0 to 100 and from 775 to 2400, and this correlates with the results 2-D wavelet transform of the signal. In conclusion, the wavelet transform of the Pig-A Signal 1 shows that the oxygen signal is non-stationary because there is an unequal and irregular distribution of peak wavelet coefficient values indicating that

during certain time periods of the oxygen signal, there are specifically occurring frequencies.

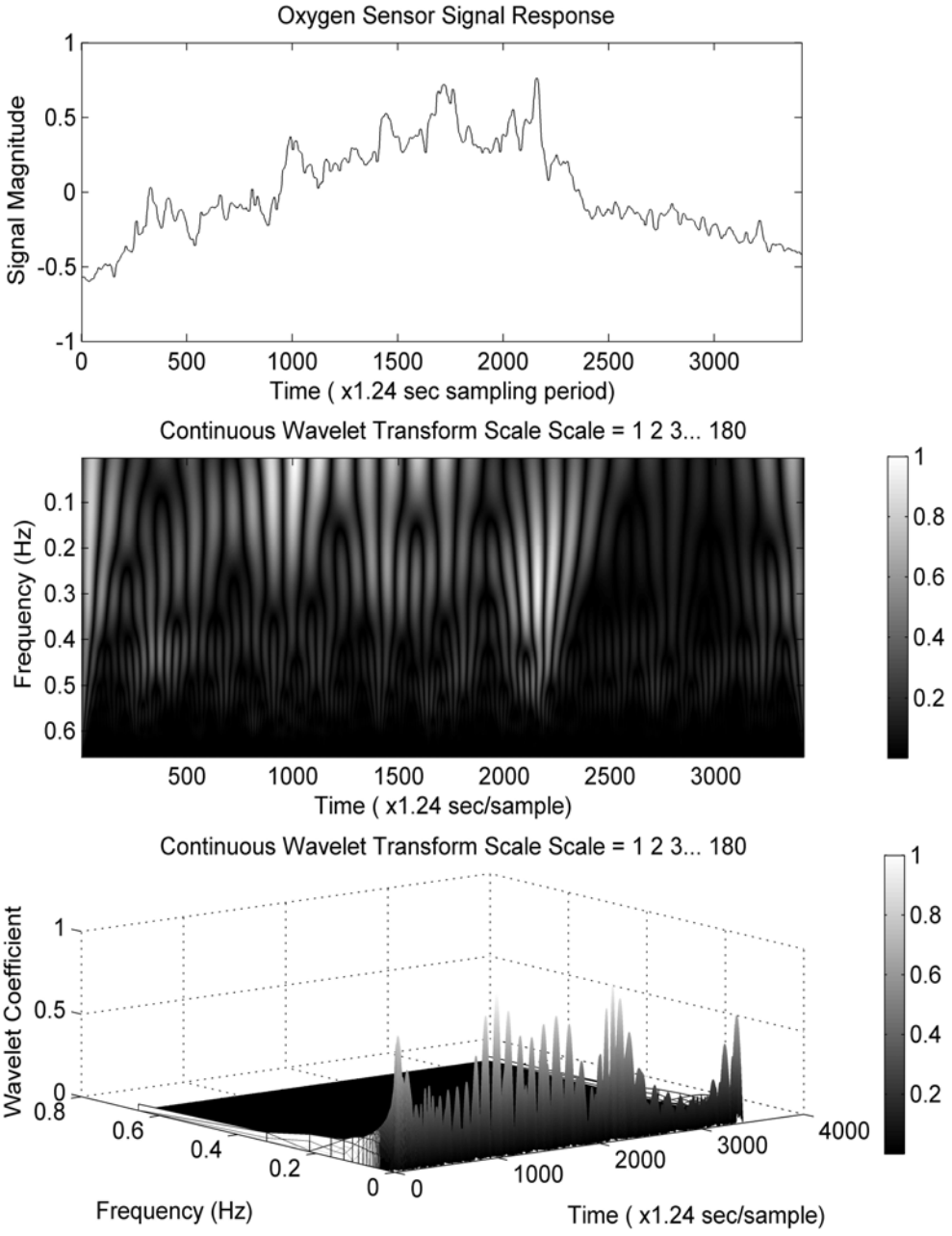


Figure V-7. Continuous wavelet transforms for Pig-A, Signal 1.

The normalized wavelet transforms of Pig-A Signal 2 are presented in Figure V-8, and shows that the pig oxygen signal is non-stationary. The 2-D normalized wavelet transform reveals that there is one time sample period of 65 to 730 (approximately 1 to 15 minutes) during the oxygen signal which has the peak wavelet coefficients ranging from 0.52 to 1.0. This is observed as a series of elongated white ovals occurring for the sample period 65 to 730 with the frequency range of 0.0001 Hz to 0.35Hz. From the 3-D normalized wavelet transform, it is observed that there are three other time sample periods where there are peaks in wavelet coefficient values that range from 0.45 to 0.25. The first and greatest set of wavelet coefficient that ranges from 1.0 to 0.52 occurs for the sample period of 65 to 730, which was also revealed by the 2-D wavelet transform plot. The second and third sample periods of peak wavelet coefficients values that range from 0.45 to 0.25 is from 800 to 1950 (16.5 to 40.3 minutes), and from 2600 to 3000 (~ 54 to 62 minutes). The range of frequencies observed for the identified sample time periods of peak wavelet coefficients range from 0.0001 Hz to 0.35 Hz. In conclusion, Pig-A Signal 2 displays three time periods of different lengths, occurring at irregular intervals that are found to have frequencies of oscillation which range from 0.0001 to 0.35 Hz. Thus, the pig oxygen signal is considered to be non-stationary.

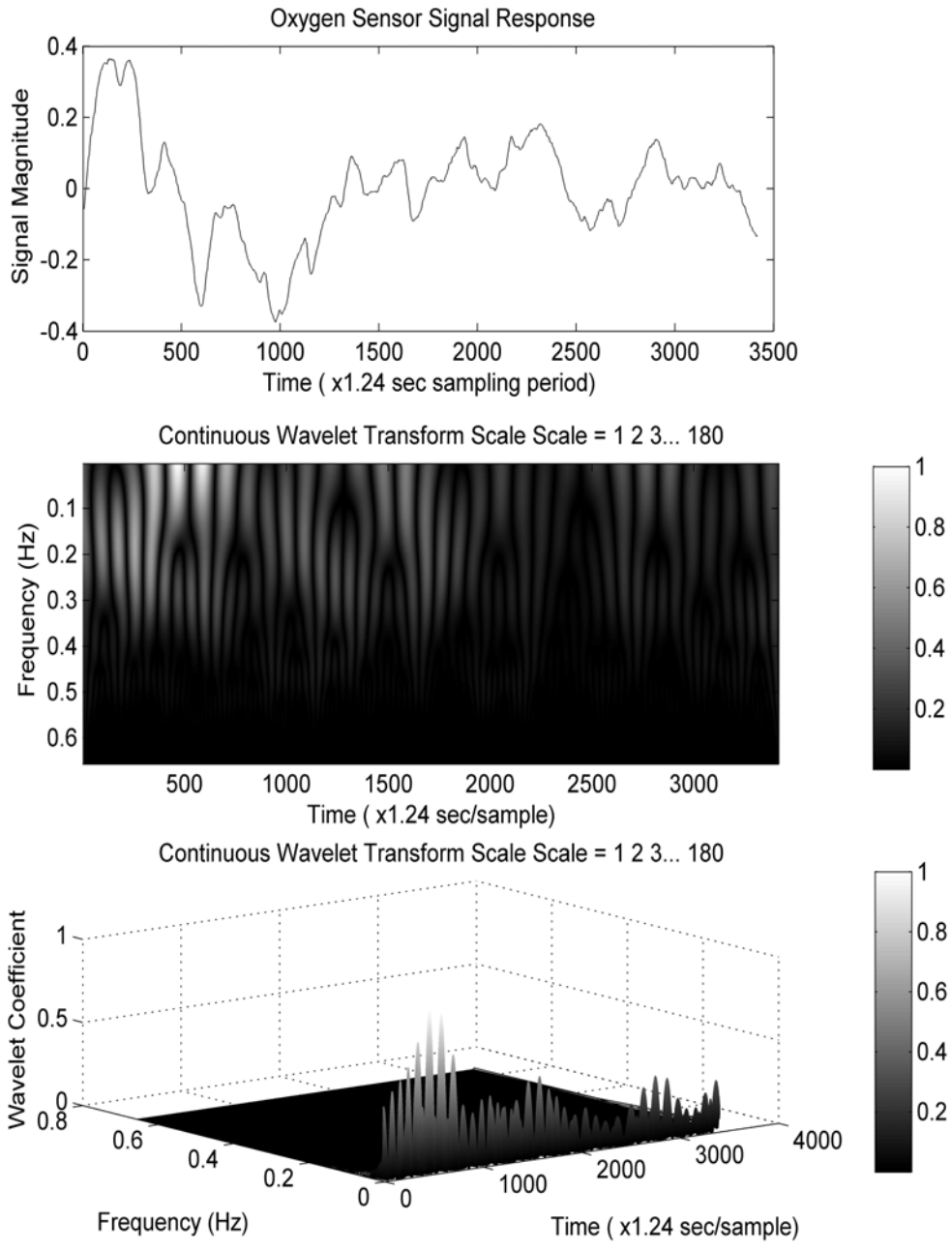


**Figure V-8. Continuous wavelet transforms for Pig-A, Signal 2.**

In summary, the Pig-A representative oxygen signals are both non-stationary. Both Pig-A Signal 1 and Signal 2 have identified sample periods where peak wavelet coefficient values occur for specific ranges of frequencies. In effect, the wavelet transforms of the non-stationary Pig-A oxygen signals reveals the pig oxygen signal to have different, and irregularly spaced time sample periods, for which each time period has specifically occurring frequencies identifying the oxygen signal oscillations and dynamics within that individual time period.

## V.D.2 Wavelet Analysis of Pig-B Signals

The oxygen signals for Pig-B are collected over a 60 minute time duration, and the average sampling rate of the signals is one sample every 1.24 seconds. The normalized wavelet transforms for each signal are presented in Appendix A, as Figure A-22 and Figure A-23. For each figure, there is a plot of the filtered time-signal, and two different types of plots of the normalized wavelet transform are shown, one as a two-dimensional (2-D) image plot, and the second as a three-dimensional (3-D) mesh plot. The wavelet transform for each oxygen signal demonstrates a non-stationary behavior over the 40 minute time period.

The normalized wavelet transforms of Pig-B Signal 1 are presented in Figure A-22 in Appendix A, and show the pig oxygen signal to be non-stationary. From the 2-D normalized wavelet transform plot, two sample time periods are observed to have peak wavelet coefficient values ranging from 0.65 to 1.0, which are represented by long elongated white stripes or ovals. The two sample periods of high wavelet

coefficient values occur at time samples 145 to 250 (~3 to 5 minutes), and 1050 to 1225 (~22 to 25 minutes), for the frequency range of 0.0001 to 0.44Hz. The 2-D wavelet transform also reveals time sample periods with peak wavelet coefficient values ranging from 0.67 to 0.45. These peak values are represented by unequal groups of gray-white stripes in the 2-D plot which occur at approximately irregular intervals of throughout the duration of the oxygen signal. Since the 2-D normalized wavelet transform plot shows the peak wavelet coefficients values to be irregularly spaced in time and frequency throughout the entire signal, it indicates that pig oxygen signal is non-stationary. The 3-D normalized wavelet transform reveals three time sample periods with peaks in the wavelet coefficient values. The first peaks are found within the sample time period of 175 to 230 (~3.5 to 5 minutes), frequency range of approximately 0.38 to 0.45 Hz, and has wavelet coefficient values ranging from 0.54 to 0.70. The second observed peaks are found within the sample time period of 1100 to 1200 (~23 to 25 minutes), frequency range of 0.30 to 0.44 Hz, and has wavelet coefficient values ranging from 0.70 to 1.0. The thirds set of peaks occurs for the time sample period of 2300 to 2550 (~47.5 to 53 minutes), frequency range of 0.0001 to 0.27 Hz, with peak wavelet coefficient values that range from 0.4 to 0.7. The 3-D plot are reveals lesser peaks at different sample times during the pig oxygen signal. In general, the 2-D and 3-D normalized wavelet transform show the Pig-B Signal 1 to have several different time periods where various frequency ranges occur. Therefore, the Pig-B Signal 1 is considered to be non-stationary.

The normalized wavelet transforms of Pig-B Signal 2 are presented in Figure A-23 in Appendix A, and shows that the pig oxygen signal to be non-stationary. From the 2-D normalized wavelet transform, the areas of peak wavelet coefficient values ranges from 0.60 to 1.0 are observed during the sample time periods of 0 to 110 (0 to ~ 2.3 minutes), 470 to 700 (~10 to 14.5 minutes), 1750 to 2300 (~36 to 47.5 minutes) and 2500 to 2900 (~52 to 60 minutes). The frequency ranges for each identified sample time period of peak wavelet coefficients varies from 0.0001 to 0.45 Hz. The 2-D plot also reveals the pig oxygen signals to have the greatest variation in frequency dynamics for the sample time period of 1750 to 2900 (~36 to 60 minutes). The 3-D wavelet transform correlates with the 2-D wavelet transform and shows that there are groups of peak wavelet coefficient values with different magnitudes, occurring at different time periods which are irregularly spaced throughout the duration of oxygen signal. In conclusion, the normalized wavelet transform plots reveal Pig-B Signal 2 to be non-stationary because the signal is shown to have different time periods of unequal duration and irregularly spacing, with various associated frequency ranges.

In summary, the Pig-B representative oxygen signals are both non-stationary. Both Pig-B Signal 1 and Signal 2 have identified sample periods where the peak wavelet coefficients occur for different time periods, at irregular intervals, and for specific ranges of frequencies. Thus, the Pig-B representative oxygen signals display certain frequencies of oscillations and dynamics for specific time periods during the signal.

## V.E Results of the Probability Distribution Analysis

The probability distribution analysis was determined for the short-term oxygen sensor signals collected from the sensor arrays implanted in pig subcutaneous tissue. The probability distribution analysis includes the calculation of the normal probability plots and the quantile-quantile plot (Q-Q plots) a using the collected oxygen sensor signals that have been detrended, smoothed and filtered to remove the indentified non-biological artifacts. The normal probability plots will determine if the oxygen signals are normally distributed, and the Q-Q plots will answer the question of whether the oxygen signals come from populations with the same probability distribution.

### V.E.1 Probability Distribution Analysis for Pig-A Signals

Figure V-9.A-B shows the normal probability plots for Pig-A Signals 1 and 2. Figure V-9.A presents the normal probability plot of Pig-A, Signal 1, and it is observed that the center portion of data points moderately follows the reference normal probability distribution fit line. However, the tail-end points show increasing departures from the fitted reference normal line, where the negative valued tail-end points fall below the reference normal line, and positive valued tail-end points lie above of the reference normal line. The direction of tail-end departures from the reference normal line classifies the Signal 1 data points as long-tailed. Therefore, it

may be concluded that the normal probability distribution is not best fit distribution for Pig-A, Signal 1 data points. Figure V-9.B presents the normal probability plot for Pig-A, Signal 2. The normal probability plot for Signal 2 displays a linear pattern for the center portion of the Signal 2 data points between -0.11 and 0.17, and is observed to follow the reference normal probability fit line reasonably well. The Signal 2 data points greater than 0.17, and less than -0.11, there is an observed departure from the reference normal line. Specifically, the tail-ends of the normal plot display a quadratic pattern, or skewed tail-end pattern, in the departures from the reference line. The negative valued tail-end is left-skewed, where all the departures are above the reference line, and the positive valued tail-end is right skewed, where all the departures are below the reference line. The non-linear pattern observed in the tail-ends of the normal probability plot for Signal 2 indicates that a distribution other than the normal distribution would be a good model for the Pig-A Signal 2 dataset. The Lilliefors test calculated for the each of the signals corroborates with the normal probability plot results, where the null hypothesis of the oxygen signals being normally distributed is rejected on the 5% significance level. Therefore, it is concluded that all of Pig-A signals do not fit the normal distribution. In addition, since the normal probability plots for Signal 1 and Signal 2 are dissimilar in their patterns, it may be concluded the datasets for Signal 1 and Signal 2 do not follow the same probability distribution.

Figure V-9.C presents the Q-Q plot of Pig-A, Signals 1 and 2. The Q-Q plot shows the quantiles Signal 1 plotted against the quantiles of Signal 2. The plot points

do not follow along the reference line, demonstrating that the two datasets do not come from common probability distribution.

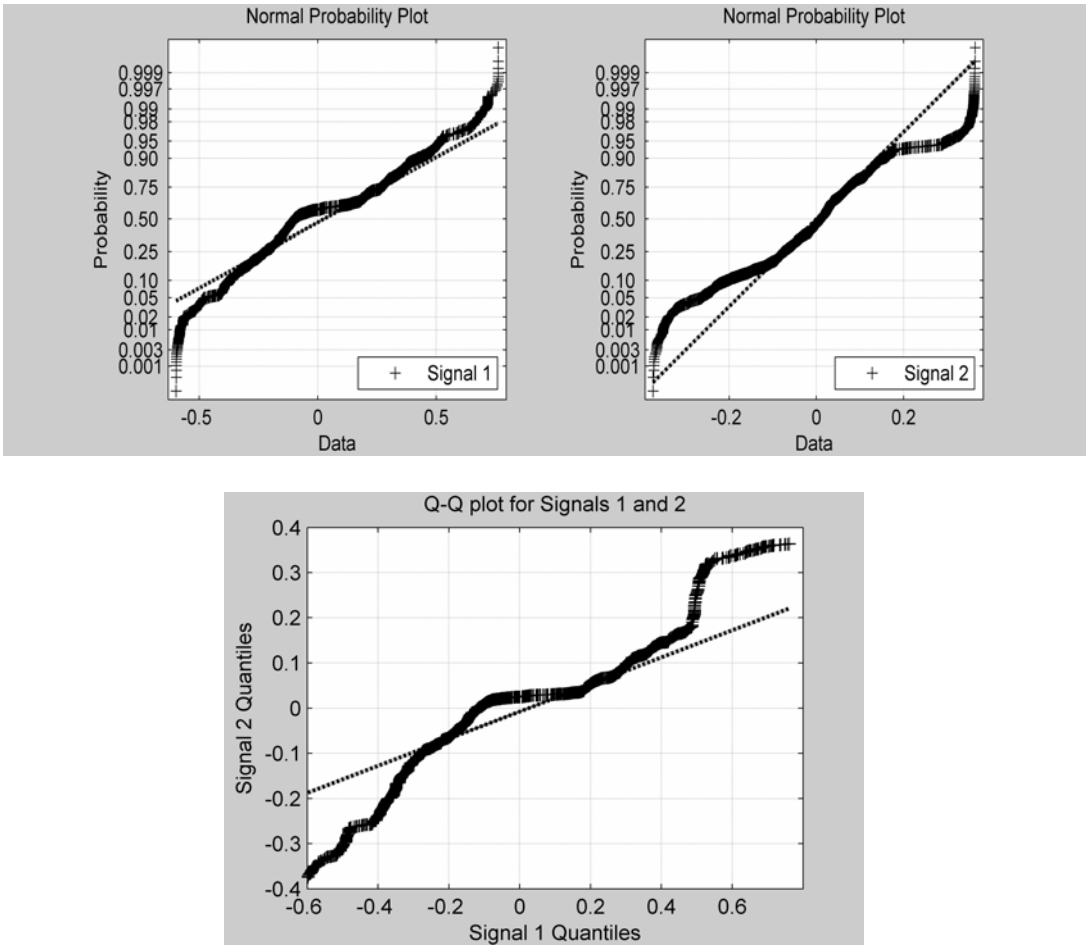


**Figure V-9.A-C. A. Normal Probability Plot for Pig-A, Signal 1. B. Normal Probability Plot for Pig-A, Signal 2. C. Q-Q Plot for Pig-A, Signals 1 and 2.**

## V.E.2 Probability Distribution Analysis for Pig-B Signals

Figure A-24.A-B shown in Appendix A present the normal probability plots for Pig-B Signals 1-2. Figure A-24.A presents the normal probability plot of Pig-B, Signal 1, and it is observed that the center portion of data points with values between -0.04 and 0.04, follow the reference normal probability distribution line reasonably well. However, for the data values greater than 0.04 and less than -0.04, there is an increasing departure from the reference normal line. The departures from the normal line take on a quadratic pattern, where both the positive valued and negative valued tail-end points display a quadratic-like departure above the normal line. As a result, the tail-end points are considered to be left-skewed because the departures rise above the reference normal line. Additionally, both tail-ends are observed to have a slight S-like shape. In conclusion, the normal probability plot of Pig-B, Signal 1 moderately follows the reference normal line, with non-linear departures in the tail-ends. Therefore, it may be concluded that the normal probability distribution is not best fit distribution for Pig-A, Signal 1 data points. Figure A-24.B presents the normal probability plot for Pig-B, Signal 2. The normal probability plot for Signal 2 displays a linear pattern for the center portion of the Signal 2 data points between -0.029 and 0.038, and is observed to closely follow the reference normal probability fit line. The Signal 2 data points greater than 0.038, and less than -0.029, there is an observed departure from the reference normal line. Specifically, the negative valued tail-end shows increasing departure below the normal reference line, and the positive valued tail end shows increasing departure above the normal reference line. The departure pattern of the tail-ends classifies the Signal 2 data set to be long-tailed, and

it indicates that a distribution other than the normal distribution would be a good model for the Pig-B Signal 2 dataset. The Lilliefors test calculated for the each of the Pig-B signals corroborates with the normal probability plot results. The null hypothesis of the oxygen signals being normally distributed is rejected on the 5% significance level. As a result, it is concluded that all of Pig-B oxygen signals are not normally distributed. Furthermore, the normal probability plots for Pig-B Signal 1 and 2 are not similar indicating that the two signals may have different probability distributions.

Figure A-24.C presents the Q-Q plot of Pig-B, Signals 1 and 2. The Q-Q plot displays the quantiles Signal 1 plotted against the quantiles of Signal 2. The center section of the Q-Q plot points follows closely along the reference line. However, the tail-ends of the Q-Q plot exhibit clear departure from the reference line, and due to the significant number of data points forming the tail-ends, those points may not be considered as outliers. As a result, the Q-Q plot indicates that the Pig-B, Signal 1 and Signal 2 come from different probability distributions.

## V.F Autoregressive Modeling of the Implanted Oxygen Sensor Signals

In order to model the *in vivo* oxygen signals collected from the implanted oxygen sensors in the pigs, the oxygen signals must satisfy the criteria of being stationary. Wavelet analysis of the linearly detrended, smoothed, and filtered oxygen signals collected from the hermetically sealed oxygen sensor arrays implanted in Pig-A and Pig-B are shown to be non-stationary, and discussed in detail in Chapter V.C.

As a result, the signals do not satisfy the criteria to be modeled using an autoregressive model.

# Chapter VI: Discussion

The objective of this thesis was to analyze and characterize the variations of the *in vivo* oxygen signals collected from sensor arrays that are implanted in hamsters or pigs. The signal variations could be due to a various factors, such as spatial and temporal differences in tissue microvasculature local to the oxygen sensor implant, differences in tissue mass transfer resistances, transient and variable changes in the local and systemic blood flow, and changes in the local metabolic rate. Here, by identifying the characteristics of the signal variations, we gained important information about *in vivo* oxygen dynamics which may be applied to the development of a long-term implantable sensor and to other tissue engineered cellular devices. To this purpose we applied several engineering methods of signal analysis including signal processing, statistical analysis, and time series analysis methods. These methods allowed us to quantitatively explore and characterize observed oxygen signal dynamics and variations..

First, before any of the oxygen signals can be analyzed, the non-biological signal features and noise needed to be suppressed or removed otherwise the results of the oxygen signal analysis would be significantly biased and distorted. Classical digital filtering methods could not be applied to the oxygen signals because important oxygen signal properties critical to designing the classical filters are unknown. Therefore, a filtering algorithm was designed and applied to each individual oxygen signal. The filtering algorithm was designed to specifically remove the unwanted non-biological signal features while preserving the biological signal features,

producing an output oxygen signal that is linearly detrended, cleaned of unwanted features, and sufficiently smoothed. Next, an engineering approach of digital signal processing and time series analysis was applied to each filtered oxygen signal in order to characterize the sensor signal variations. The applied methods included spectral analysis, correlation analysis, wavelet analysis, and probability distribution analysis that allowed for complete oxygen sensor signal analysis.

First, spectral analysis was completed in order to study the frequency domain of the oxygen signals. Spectral analysis allows for the frequency characterization of any dominant and distinguishable oxygen signal events, and the determination of any periodicity within the oxygen signals. From the spectral analysis, it was found that the oxygen sensor signals from both the hamsters and pig collected over 30 to 70 minute time duration have very similar trends, and may be classified as low-frequency spectrums. In addition, spectrums for both the hamster and pig oxygen signals contained no dominant peaks, which indicate that there was no singular oxygen event or dominant oxygen frequencies occurring during the time of the sensor signal collection. It was found that both the hamster and pig *in vivo* oxygen signals contained periodicity that has a fundamental frequency of 10 ± 5 mHz. We hypothesize that this fundamental frequency is fundamental frequency of vasomotion occurring in the microvasculature of the local tissue environment of the implanted sensor. A fundamental frequency of 10 ± 5 mHz corresponds to vasomotion of 0.6 ± 0.3 cycles per minute. In the power spectrums of both the hamster and pig oxygen signals, local power maximums at multiples of n, where n = 1, 2, 3… are observed and determined to be harmonic frequencies. For the hamster oxygen signals, the

maximum harmonic frequency was determined to be approximately 120 mHz, which translates to a maximum frequency of vasomotion of approximately 7 cycles per minute. For the pig oxygen signals, the maximum harmonic frequency was determined to be approximately 400 mHz, which translates into a maximum frequency of vasomotion of approximately 24 cycles per minute. Both the hamster and pig maximum harmonic frequencies are less than the pre-determined maximum frequency limits calculated from the sampling rates of the implanted sensor. As mentioned above the limits on the maximum frequency that can be correctly measured by the implanted oxygen sensor without aliasing is 114 mHz for the hamster signals, and 447 mHz for the pig signals according to the Nyquist sampling theorem. Therefore, the determined maximum harmonic frequency for the hamster and pig suit the Nyquist sample theorem. Furthermore, the determined fundamental frequency for vasomotion of 10 ± 5 mHz revealed by the spectral analysis correlates with the previously published data on *in vivo* vasomotion frequencies for animals awake, at rest or un-anaesthetized. As previously shown for small arteries and larger arterioles (A1 arterioles with diameters of 70- to 100 μm), vasomotion occurs with a frequency of approximately 1 to 3 cycles per minute [10, 18]. For the smallest terminal arterioles (A4 arterioles) with diameters of the order of 10 μm, vasomotion has been observed to occur with a frequency that ranges from 10 to 25 cycles per minute [12, 13]. In summary, the spectral analysis of the oxygen signals from hamster and pigs have very similar spectral characteristics and also have the same fundamental frequency of 10 ± 5 mHz for arteriolar vasomotion within the subcutaneous tissue local to the implanted oxygen sensor.

Correlation analysis of the hamster and pig oxygen signals included the calculation the autocorrelation plot and lagged scatterplots of each individual oxygen signal, and the cross-correlation between each oxygen signal collected from the same implanted sensor array. The autocorrelation and cross-correlation plots of the Hamster-A oxygen signals revealed statistically significant periodicity of approximately 1.2 mHz within each individual signal and between every combination of two signals collected from the same implanted oxygen sensor array. The 1.2 mHz frequency (13.8 minutes per cycle) is hypothesized to be due to a periodic regional perfusion of oxygen to the local tissue environment of the implanted sensor for the Hamster-A signals. This hypothesis is based on the fact that the 1.2 mHz frequency of periodicity (13.8 minutes per cycle) was found in each individual Hamster-A signal, and also in each possible signal cross-correlation. This suggests that the tissue environment local to entire sensor array was affected by a periodic oxygen perfusion occurring during the 30 minute signal collection time period. The 13.8 minutes per cycle is not considered to be arteriolar vasomotion since the periodic cycle is too slow and does not fall within identified physiological ranges of arteriolar vasomotion. The lagged scatterplots for Hamster-A oxygen signals showed strong linear dependence and strong autocorrelation at the small lags, where successive observations appear to be linearly correlated. This means that the oxygen signal data points come from an underlying autoregressive model at small lags. As the lags were increased, the lagged scatterplots for the Hamster-A signals demonstrated non-linear patterns. As a result, a linear AR model with small model order may be an appropriate model for the Hamster-A signals.

The autocorrelation plots of Hamster-B oxygen signals display autocorrelation behavior that varies for each signal. The Hamster-B Signals 1, 2, and 4 contain periodicity occurring at the fundamental period 15 to 16 minutes per cycle (1 cycle every 16.2 minutes, 30.3 minutes, and 46.4 minutes) and Hamster-B Signal 3 displays a moderate linear autocorrelation between adjacent sample points. The cross-correlation plots of the Hamster-B signals show that the collected oxygen signals from the same array sensor implant are correlated with each other, and that there may be a fundamental cycling period estimated to be approximately 8.0 minutes per cycle (2.1 mHz). The fundamental period of 8.0 minutes per cycle is half the harmonic period found in the autocorrelation of the Hamster-B signals, which suggests that the actual fundamental period of the Hamster-B signals was 8.0 minutes per cycle. We hypothesize that the Hamster-B oxygen signals reflected regional oxygen perfusion that has a fundamental period of 8.0 minutes per cycle. This hypothesis is based on the analysis that the majority of autocorrelations and all cross-correlation of the Hamster-B oxygen signals show periods of oscillations that are harmonics of the fundamental period of 8.0 minutes per cycle. The lagged scatterplots of the Hamster-B signals are linearly dependent and demonstrate strong linear autocorrelation at small lags. As the lags are increased, the lagged scatterplot presents a non-linear, star-like pattern. Therefore, the linear AR model with a small model order may be an appropriate model for the Hamster-B signals.

Pig-A, Signals 1 and 2 collected from the same sensor array implant display autocorrelation and cross-correlation behavior. Both methods of correlation analysis demonstrate periodicity in the signals that are approximate multiples of the

fundamental period of 14 minutes per cycle. Pig-A Signal 1 displays a 59 minute periodic cycle, approximately 4× the fundamental period of 14 minutes per cycle, which is equivalent to a frequency of oscillation of 0.28 mHz. Pig-A Signal 2 displays a 14 minute periodic cycle (1× 14 minute per cycle) and 44 minute periodic cycle (approximately 3× 14 minute per cycle) equivalent to frequencies of oscillation of 1.2 mHz and 0.38 mHz. Based on these results we hypothesize that the Pig-A signals reflect regional oxygen perfusion that has a fundamental period of 14 minutes per cycle (1.2 mHz). It is assumed that the periodicity observed in the auto- and cross-correlations of the Pig-A oxygen signals represents regional oxygen perfusion because the periodicity is found to affect the entire tissue environment local to the implanted oxygen sensor array, and also because the frequency of 0.38 mHz to 1.2 mHz is too slow to be considered as arteriolar vasomotion. The lagged scatterplots for Pig-A Signal 1 show successive linear dependence between signal points for every lag, which suggests that a linear model may be appropriate for Pig-A signal 1. The lagged scatterplot for Pig-A Signal 2 displays linear dependence at lower lags, hand non-linear dependence between signal points at the larger lags. This suggests that the linear AR model with a small model order may be an appropriate model for Pig-A Signal 2.

The autocorrelation and cross-correlation plots of the Pig-B Signals 1 and 2 demonstrate statistically significant periodicity within each individual signal and also correlated periodicity between the two signals. The ranges for the periodicity are found to be approximately one periodic cycle every 47 to 57 minutes (0.29 mHz to 0.35 mHz). We hypothesize that this periodicity represents the periodic frequency of

regional oxygen perfusion in the local tissue environment of the oxygen sensor implanted in Pig B. The lagged scatterplots for Pig-B Signal 1 and 2 demonstrate successive linear dependence and strong autocorrelation between the signal points at lower lags. As the lags are increased, the lagged scatterplots take on a non-linear pattern indicating non-linear dependence between the signal points at large lags. Therefore, the AR model with a small model order may be an appropriate model for the Pig-B signals.

In summary, the correlation analysis of the hamster and pig oxygen signals showed that regional oxygen perfusion occurred periods ranging from 8 to 57 minutes per cycle (≈ 2.1 mHz to 0.29 mHz), within the tissue environment local to the implanted oxygen sensor array. Furthermore, regional oxygen perfusion occurred with a periodic cycle in all of the hamster and pig oxygen signals.

The continuous wavelet transform was applied to the hamster and pig oxygen signal datasets. The wavelet transform of the oxygen signals was used to characterize the stationarity of the collected oxygen sensor signals. For Hamster-A Signals 1-4, an overall oscillatory behavior over the frequency range of 0.0001 Hz to 0.12 Hz was observed for the total duration of each oxygen signal suggesting that the Hamster-A signals are approximately stationary. In addition, for each oxygen signal, for the sample points of 150 to 250 (11 to 18 minutes), the wavelet coefficients are significantly larger in magnitude, indicating the presence of a prominent oscillatory behavior within the oxygen signals over the same frequency range of 0.0001 Hz to 0.12 Hz. Therefore, the Hamster-A signals demonstrate an oscillatory behavior of 0.0001 to 0.12 Hz over the total time duration of the collected Hamster-A oxygen

signals. In closer detail, the 11 to 18 minute time period within the oxygen signals display a larger wavelet coefficient magnitude than the rest of the signal. This suggests that the oscillatory behavior is more pronounced over this time period than over the rest of the time signal. Furthermore, the wavelet analysis of the Hamster-A oxygen signals shows that the sensor signals contain frequencies that range from 0.1 mHz to 120 mHz, and this correlates with the fundamental frequency identified for vasomotion by the spectral analysis (10 ± 5 mHz) and the fundamental frequency identified for regional oxygen perfusion of the tissue identified by correlation analysis (fundamental frequency of 1.2 mHz). In general, the continuous wavelet transformation of the Hamster-A short-term oxygen signals reveals the signals to be approximately stationary over the 30 minutes time period of signal collections. These results confirm the frequency ranges identified by the other spectral and correlation analysis methods.

For the Hamster-B, Signals 1-4, wavelet transformation reveals each signal to contain different time intervals that have different frequencies of oscillation. As a result, the Hamster-B short-term oxygen signals are determined to be non-stationary. For Hamster-B, Signal 1, there are three separate time periods over the duration of the signals that demonstrate oscillatory behavior with specific frequency ranges. These three separate time periods display frequencies that range from 0.0001 to ~0.09 Hz. For Hamster-B, Signal 2, the three separate time periods display frequencies that range from 0.0001 to 0.12 Hz. In summary, these three separate and distinct time periods of oscillatory behavior exposed by the wavelet transform of the Hamster-B Signals 1 and 2, show the signals to be non-stationary. For Hamster-B, Signal 3,

there are two time intervals of significant oscillatory behavior occurring within the oxygen time signal with frequencies of the oscillations that range from 0.0001 to 0.15 Hz. Therefore, the conclusion can be made that Hamster-B, Signal 3 is non-stationary. Finally, the Hamster-B, Signal 4 also contains several time periods with frequencies of oscillation that range from 0.0001 to 0.14 Hz, and is therefore determined to be non-stationary. The wavelet analysis of the Hamster-B oxygen signals shows the sensor signals to contain frequencies that range from 0.1 mHz to 150 mHz, and this correlates with the fundamental frequency for vasomotion identified by the spectral analysis (10 ± 5 mHz) and the fundamental frequency identified for regional oxygen perfusion of the tissue by correlation analysis (fundamental frequency of 2.1 mHz).

The wavelet transformations of the Pig-A and Pig-B oxygen signals revealed the signals to have different time periods, with specific frequency ranges. Therefore, the short-term Pig-A and Pig-B oxygen signals are determined to be non-stationary. Pig-A, Signal 1 was found to have frequencies of oscillation that range from 0.0001 Hz to 0.5 Hz, and Pig-A, Signal 2 was found to have frequencies of oscillation that range from 0.0001 to 0.35Hz. Pig-B was found to have frequencies of oscillation from 0.0001 Hz to 0.44 Hz for Signal 1, and 0.0001 Hz to 0.45 Hz for Signal 2. These identified time periods represent the time intervals that certain signal variations occur, and the identified frequency ranges represent the frequency of the variations that ocurr during that time interval. In summary, the continuous wavelet transforms results correlate with the frequency ranges identified by the spectral analysis and correlation analysis of the Pig-A and Pig-B oxygen signals.

Overall, the short-term oxygen signals for the hamsters and pigs were determined to be both stationary and non-stationary. However, a non-stationary short-term oxygen signal could be split into stationary and non-stationary time periods. As a result, the stationarity of the short-term oxygen signals was found to be dependent on the type of local and regional tissue oxygen changes occurring in the environment surrounding the implanted sensor array during the time of signal recording.

The probability distribution analysis of the hamster and pig oxygen sensor signals was found to not fit the normal distribution. Lilliefors test parameters were calculated for the each of the hamster and pig representative signals, and the null hypothesis of the oxygen signals being normally distributed was rejected on the 5% significance level. The normal probability plot analysis for each of the Hamster-A Signals 1 – 4 showed all the signals to have similar non-normal long-tailed trends in their normal plots. As a result, the Hamster-A oxygen signal dataset may be not be normally distributed, but all the signals collected from the same sensor array almost certainly come from the same unknown probability distribution. Q-Q plots were also determined for the Hamster-A signals. This method was used as a graphical tool to compare the unknown probability distributions of two different oxygen signals. The Q-Q plots of the Hamster-A oxygen signals all shared the same features and trends. This correlates with the normal probability plot results, indicating that the probability distributions of the all the Hamster-A oxygen signals may be the same. Furthermore, these results correspond to the correlation analysis results of the Hamster-A signals suggesting that all the Hamster-A signals are correlated with each other. From a

physiological standpoint, the fact that the Hamster-A oxygen signals may all come from the same non-normal distribution indicates that the electrodes on the implanted sensor array were similarly affected by the local heterogeneous tissue environment. Moreover, the correlation analysis shows that the implanted oxygen sensor measured a regional oxygen effect that was detected by all electrodes on the sensor array, and thus, affected all Hamster-A representative signals.

Similarly, for the Hamster-B Signals 1 – 4, the normal probability plot of each of the signals displays upper tails that are all significantly skewed to the right in a quadratic pattern. This suggests that the Hamster-B signals may all follow a non-normal right-skewed distribution. The Q-Q plots for the Hamster-B signals shows that signals 1, 3 and 4 have similar trends, and therefore, share the same probability distribution. Hamster-B Signal 2 was found to have different trends in its Q-Q plots. This suggests that Hamster-B oxygen signals may not all share the same probability distribution. The Hamster-B correlation results show that all the signals show a relationship with each other, and that there is a fundamental frequency of 2.1 mHz, where each signals contains periodicity at different harmonics of the fundamental frequency. From a physiological perspective, the Hamster-B oxygen signals display different frequencies of periodicity and different probability distributions which suggests that measurements made by each sensor array electrode were affected differently by the heterogeneity of the local tissue environment and by different local and regional tissue oxygen changes. Consequently, different groups of electrodes on the sensor measured distinct oxygen perfusion effects resulting in a set of oxygen signals with varying properties.

In contrast, Pig-A and Pig-B oxygen signals were found to not only be not normal, but the normal probability plots for of each signal from each pig displayed different and unique probability distribution patterns. As a result, we concluded that the Pig-A Signals 1 and 2, and the Pig-B Signals 1 and 2 are not normally distributed and have different probability distributions. The Q-Q plots for Pig-A and Pig-B confirm that the signals from each dataset do not have the same probability distribution. The correlation analysis of the Pig-A signals shows Signal 1 and Signal 2 are correlated to each other, and also contain a fundamental frequency of 1.2 mHz that represents the effect of regional oxygen perfusion on the local tissue environment of the implanted sensor. The correlation analysis of Pig-B Signals 1 and 2 showed the signals also to be correlated and to contain different frequencies of periodicity. Nevertheless, the probability distribution analysis finds the Pig-A and Pig-B signals to display different non-normal probability distributions, suggesting that the measurements of the oxygen signals were affected by the heterogeneity of the local tissue environment.

The modeling of the oxygen signals from the hamster and pig datesets was based on the criteria of stationarity. If an oxygen signal was found to be stationary, then it was modeled using the AR model. From all of the oxygen signal datasets, only the Hamster-A Signals 1-4 were determined to be fairly stationary. This was determined from the results of wavelet analysis of the oxygen signals. AR models were designed and the models were tested for validation for each of the Hamster-A oxygen signals. From the models, only the Hamster-A Signal 1, AR model, calculated as:

$$X_t = 1.482X_{t-1} - 0.2289X_{t-2} - 0.1175X_{t-3} - 0.1380X_{t-4} + \varepsilon_t$$

where the residual error terms were checked for randomness, and determined to sufficiently random. Therefore, the AR(4) model for Hamster-A Signal 1 is stable and valid.

The models designed for the Hamster-A Signals 2, 3, and 4, were found not to have sufficiently random residual error terms. The tests for residual error randomness showed the AR models for Hamster-A Signals 2, 3 and 4 not always to be random. Therefore, the AR models can not be considered totally stable and therefore, valid.

# Chapter VII: Conclusions and Future Directions

Implantable tissue enzyme sensors are critically valuable for variety of clinical applications including diabetes, pulmonary insufficiency, shock, extreme exertion, and other pathological conditions. A major obstacle in implantable tissue enzyme sensor development is the contamination of the sensor signal by local metabolite fluctuations. These fluctuations are caused by various factors, such as spatial and temporal heterogeneity of the tissue, differences in mass transfer resistance, variable local and systemic blood flow, and changes in the local metabolic rate. In addition, the sensor signal may be contaminated by added noise and artifacts due to the sensor function. Unfortunately, current methods of tissue sensor signal processing do not provide reliable correlation between tissue sensor signal and metabolite blood concentration.

Here, using digital signal processing and time series analysis tools, we developed an algorithm that allowed us to characterize short-term oxygen sensor signal response from tissue oxygen sensor arrays implanted in awake, at rest, and unanesthetized animals.

First, we showed that the collected short-term oxygen sensor signals contain different types of variations which that we categorized as biological and non-biological signal features. Second, we designed a filtering algorithm that was applied to each individual sensor signal to remove and suppress the non-biological signal features while preserving the biological ones. As a result, the filtering algorithm produced a 'cleaned' oxygen signal that is not distorted by the any unwanted signal

features. Third, these cleaned oxygen signals were analyzed in order to quantify and characterize the oxygen signal variations. Methods of signal analysis were specifically chosen from the fields of digital signal processing, time series analysis, and statistical signal processing to thoroughly examine every aspect of the oxygen time signals. These methods revealed important properties of the oxygen sensor signal variations.

- Oxygen sensor signals were found to contain small amplitude, rapid oscillation variations caused by local arteriolar vasomotion that occur at harmonics of the fundamental frequency of $10 \pm 5$ mHz.

- Oxygen signals were found to contain large amplitude, slow oscillation variations due to regional tissue oxygen perfusion that occur with frequencies ranging from 0.29 mHz to 2.1 mHz.

- Short-term oxygen sensor signals were determined to be stationary and non-stationary. However, a non-stationary short-term oxygen signal could be split into stationary and non-stationary time periods. As a result, the stationarity of the short-term oxygen signals was found to be dependent on the variable local and regional oxygen perfusion that occurs in the tissue environment surrounding the implanted sensor array.

- Oxygen signals collected from the same sensor array demonstrated normal and non-normal probability distributions.

Thus, the oxygen sensor signal features have been quantified, explained, and characterized. Using this, approach the oxygen signal variations induced by local tissue factors such as variable tissue oxygen changes and the heterogeneous tissue environment were removed from the sensor signal response revealing oxygen signal that is representative of the global oxygen level (blood oxygen concentration). Therefore, the removal of the signal variations that are caused by tissue oxygen factors from the short-term oxygen signal results in a relatively constant global oxygen level.

Future work in the field of implantable tissue enzyme sensor development includes the characterization of the collected short-term oxygen sensor signal response from an animal during physiologic challenges such as hypoxia, hyperoxia, exercise, or sleep. Using the findings from this project, the tissue factors that affect the oxygen signal response can be removed in order to evaluate the global oxygen level during the physiological challenge.

The characteristics of the short-term oxygen sensor signal response can also be applied to a 2-D or 3-D finite element model (FEM) of the subcutaneous tissue and the implanted oxygen sensor signal. These characteristics can be applied to a FEM model to simulate the local tissue environment of the sensor signal, and simulations of various tissue oxygen events and physiological challenges can be made in order to further study the short-term oxygen sensor signal response.

The designed filtering algorithm and established set of signal analysis methods will be tremendously beneficial for the characterization of the short-term sensor signal responses of implantable sensors that measure other key metabolites such as glucose, lactate, and pyruvate. Integration other physiological signals such as the heart rate, temperature, and circadian rhythm with the collected sensor signal will result in a better understanding of implanted tissue sensor signal response.

# Appendix A: Additional Results Figures

## Chapter VIII:

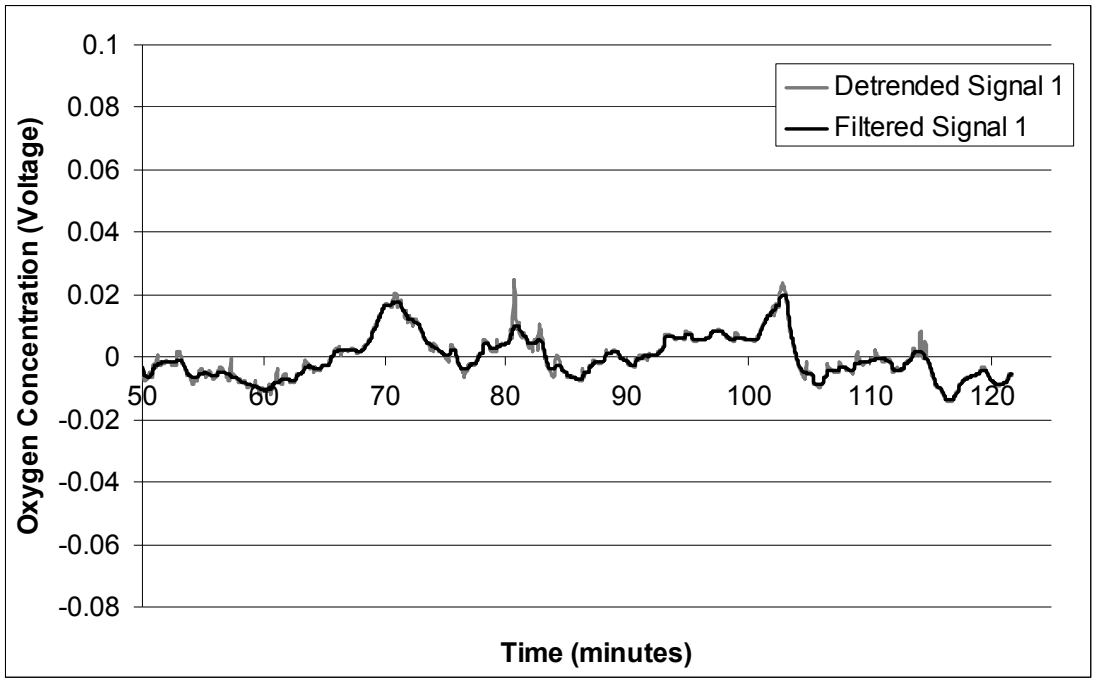


**Figure A-1. Hamster-B, Signal 1.**

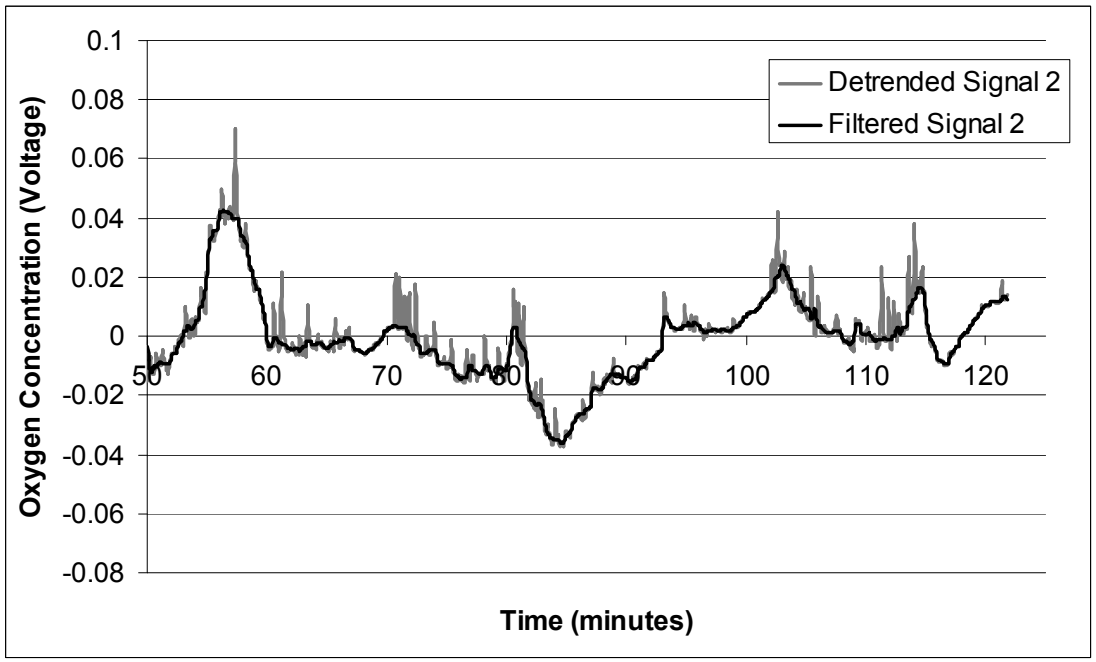


**Figure A-2. Hamster-B, Signal 2.**

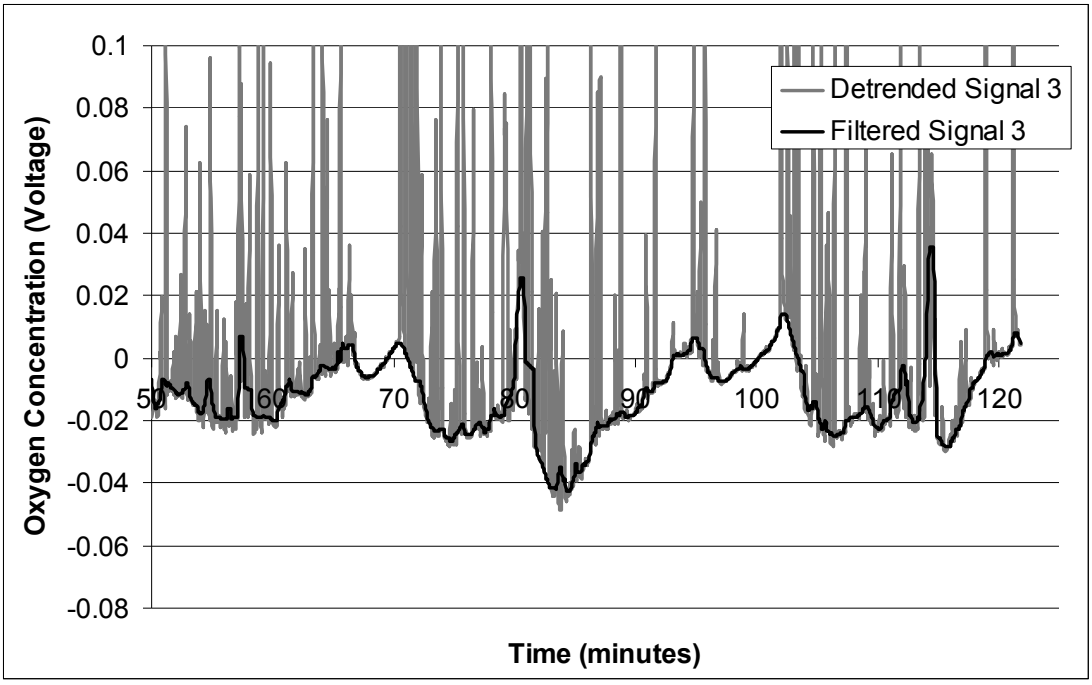


**Figure A-3. Hamster-B, Signal 3.**

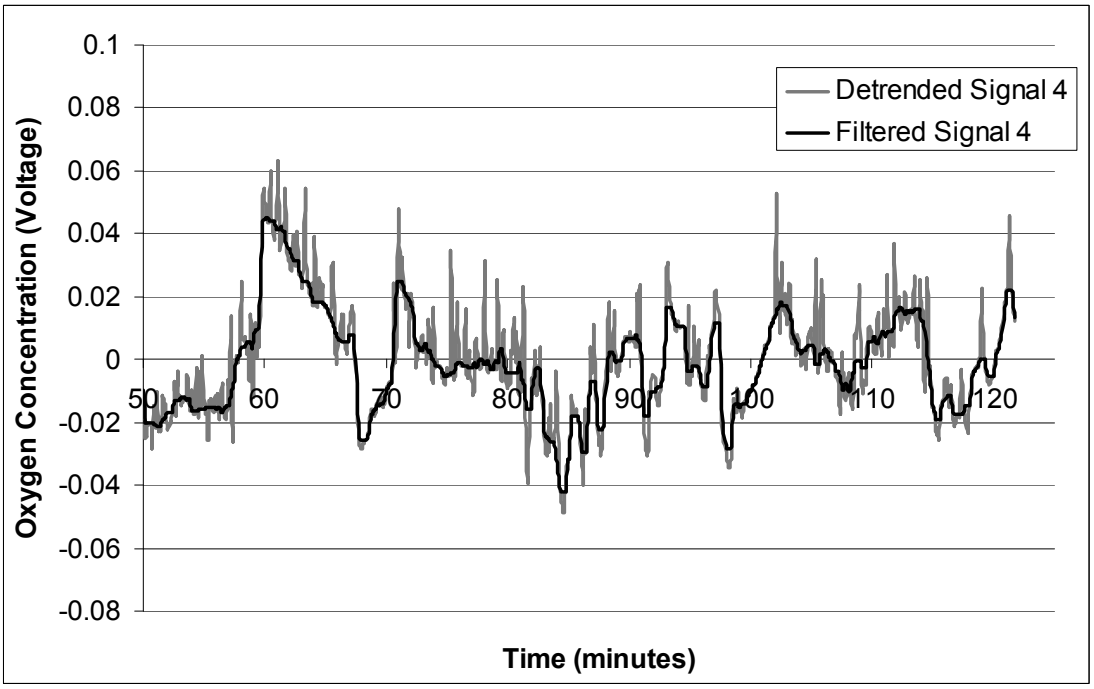


**Figure A- 4. Hamster-B, Signal 4.**

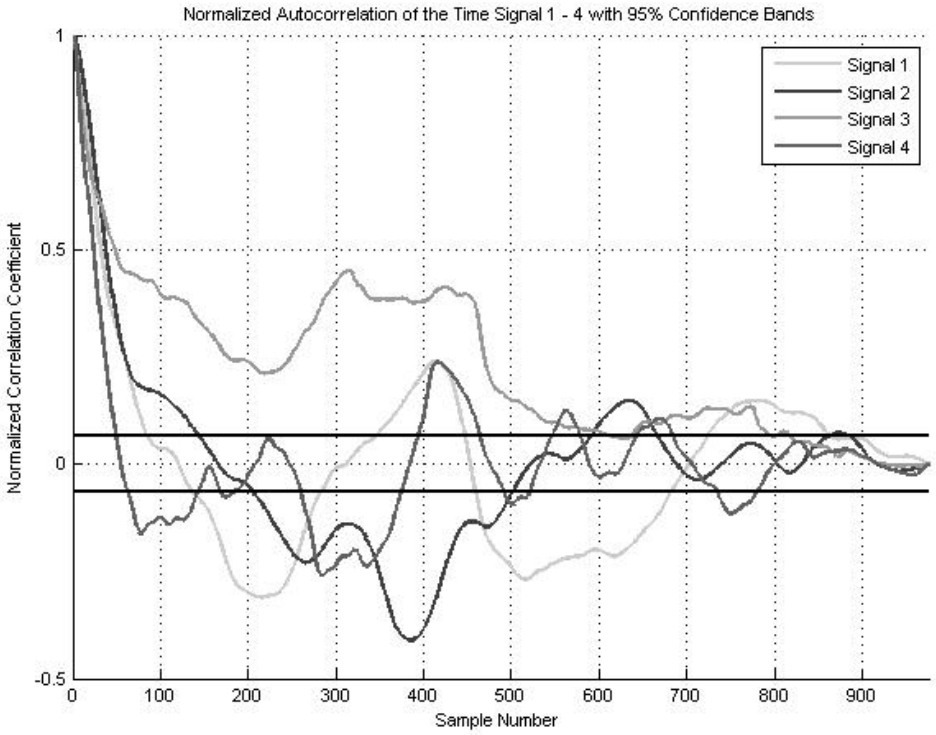


**Figure A-5. Normalized autocorrelation plot for Hamster-B, Signals 1 – 4.**

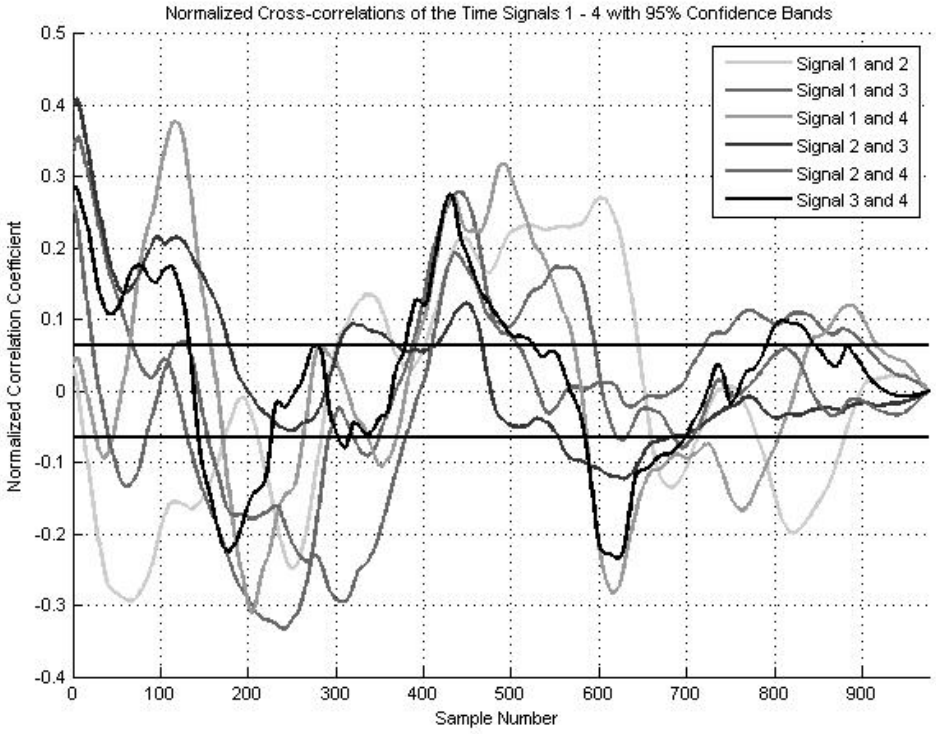


**Figure A-6. Normalized cross-correlation plot for Hamster-B, Signals 1 – 4.**

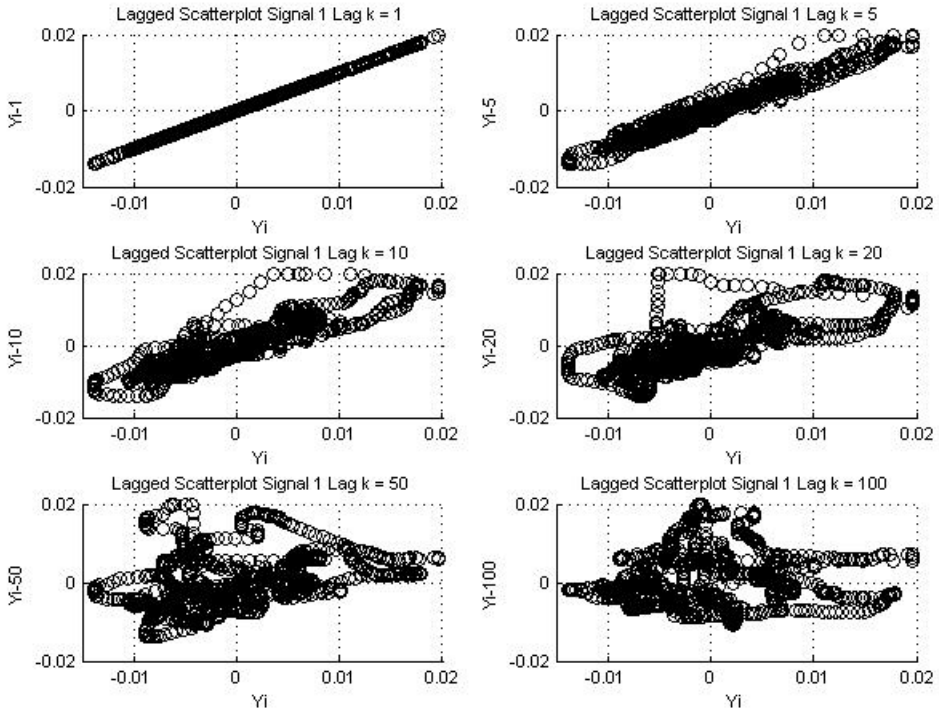


**Figure A-7. Lagged Scatterplot of Hamster-B, Signals 1 for lags of 1 5, 10, 20, 50 and 100.**

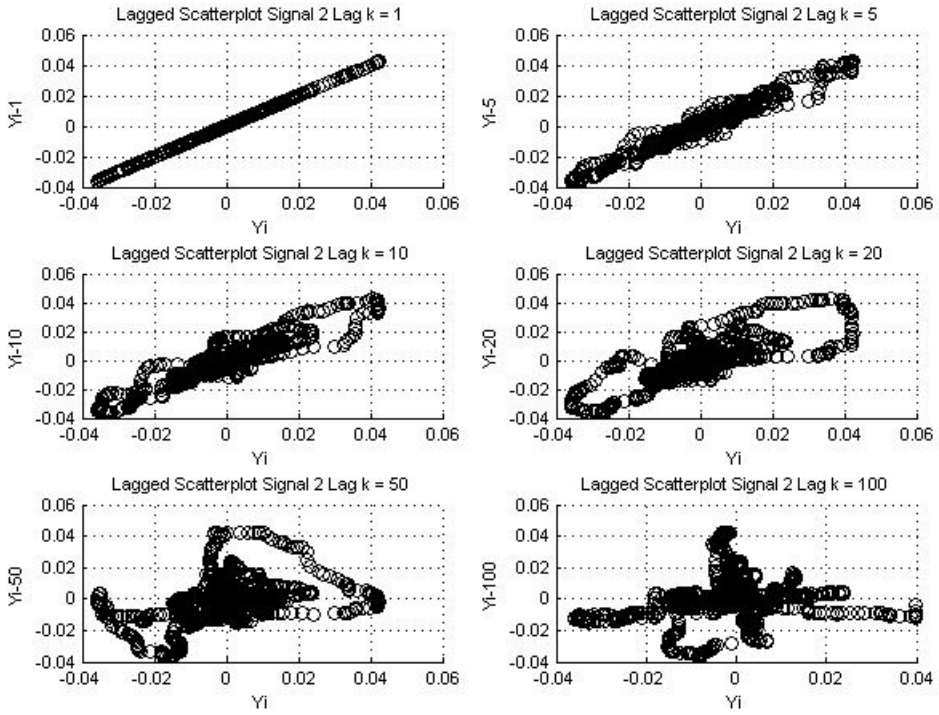


**Figure A-8. Lagged Scatterplot of Hamster-B, Signals 2 for lags of 1 5, 10, 20, 50 and 100.**

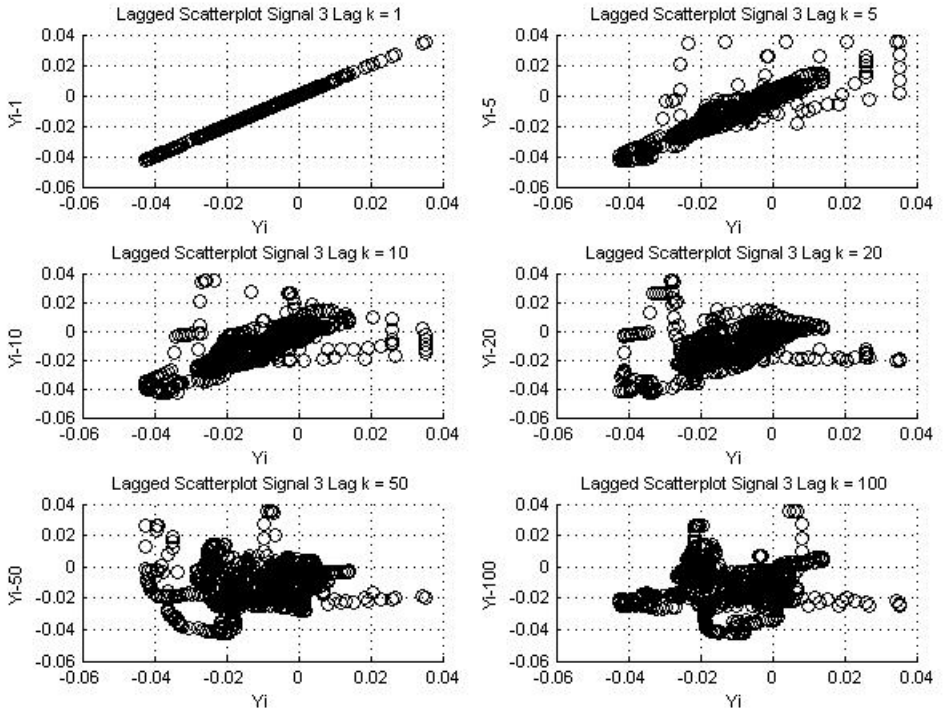


**Figure A-9. Lagged Scatterplot of Hamster-B, Signals 3 for lags of 1 5, 10, 20, 50 and 100.**

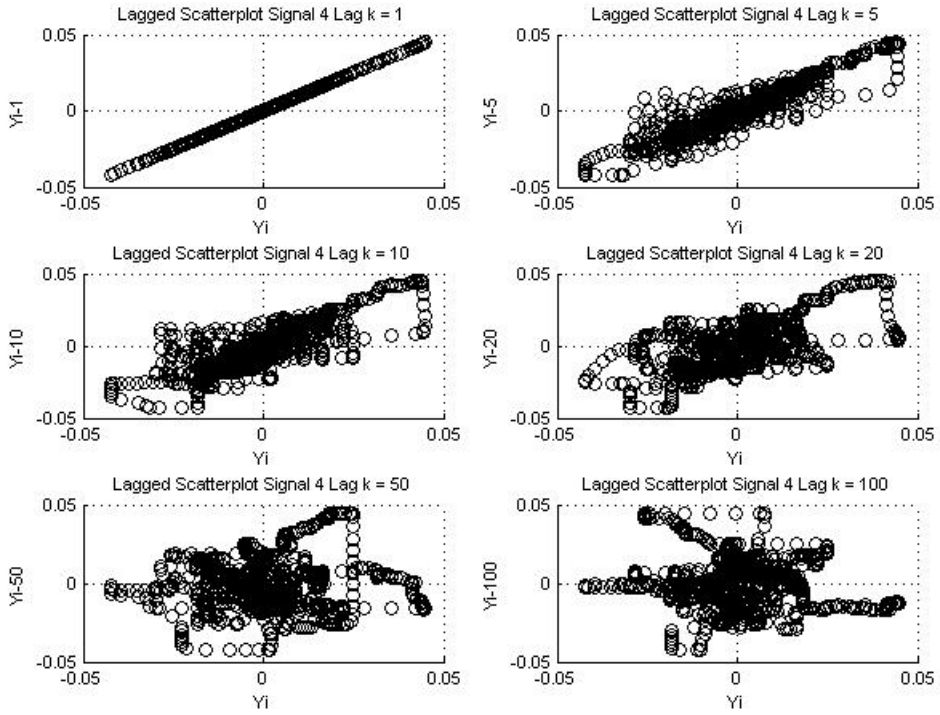


**Figure A-10. Lagged Scatterplot of Hamster-B, Signals 4 for lags of 1 5, 10, 20, 50 and 100.**

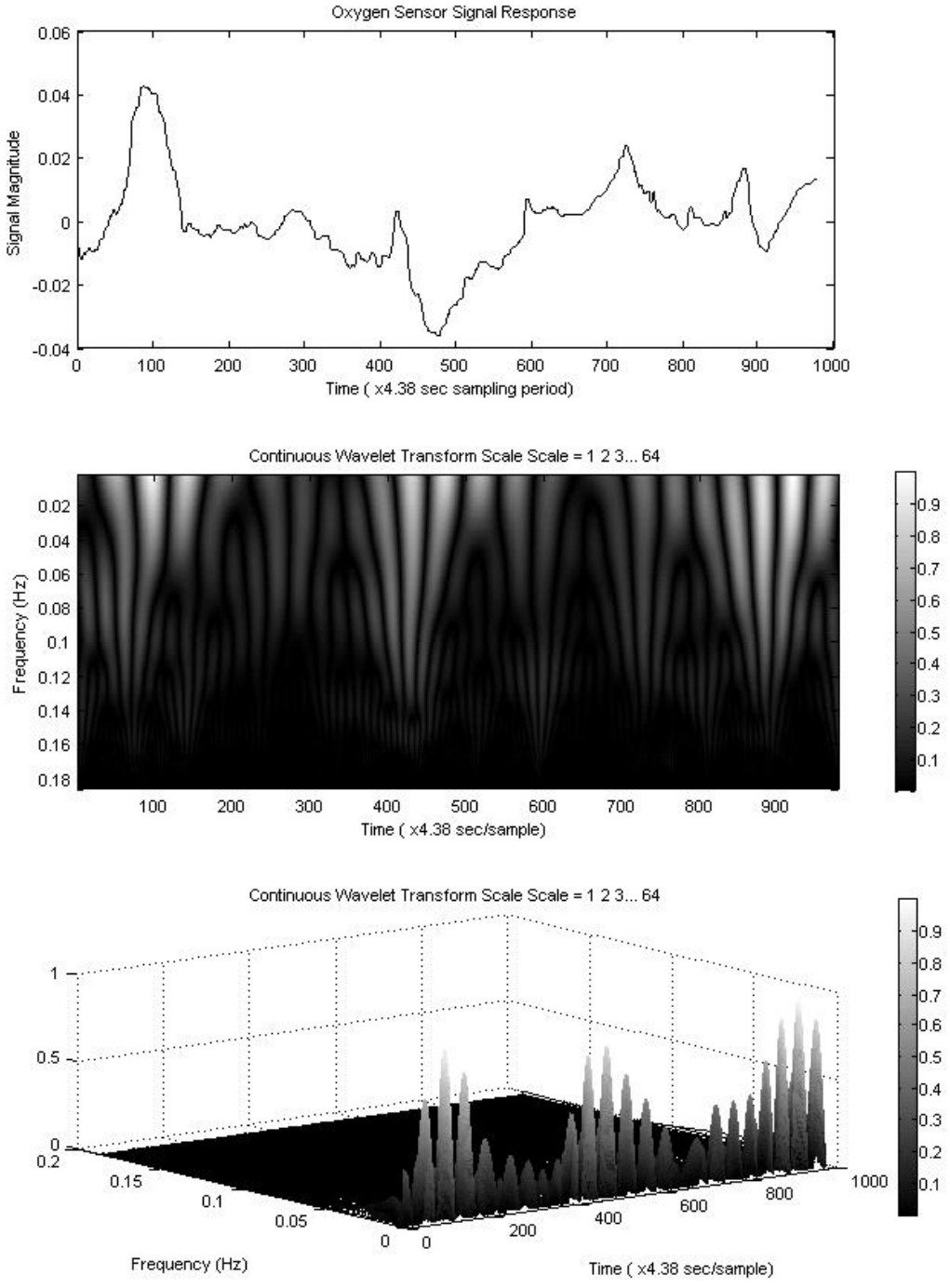


**Figure A-11. Continuous wavelet transforms for Hamster-B, Signal 1. The first plot is a plot of the Signal 1 magnitude against the sample time. The second plot is the 2-D wavelet transform of the Signal 1. The third plot is the 3-D wavelet transform of Signal 1.**

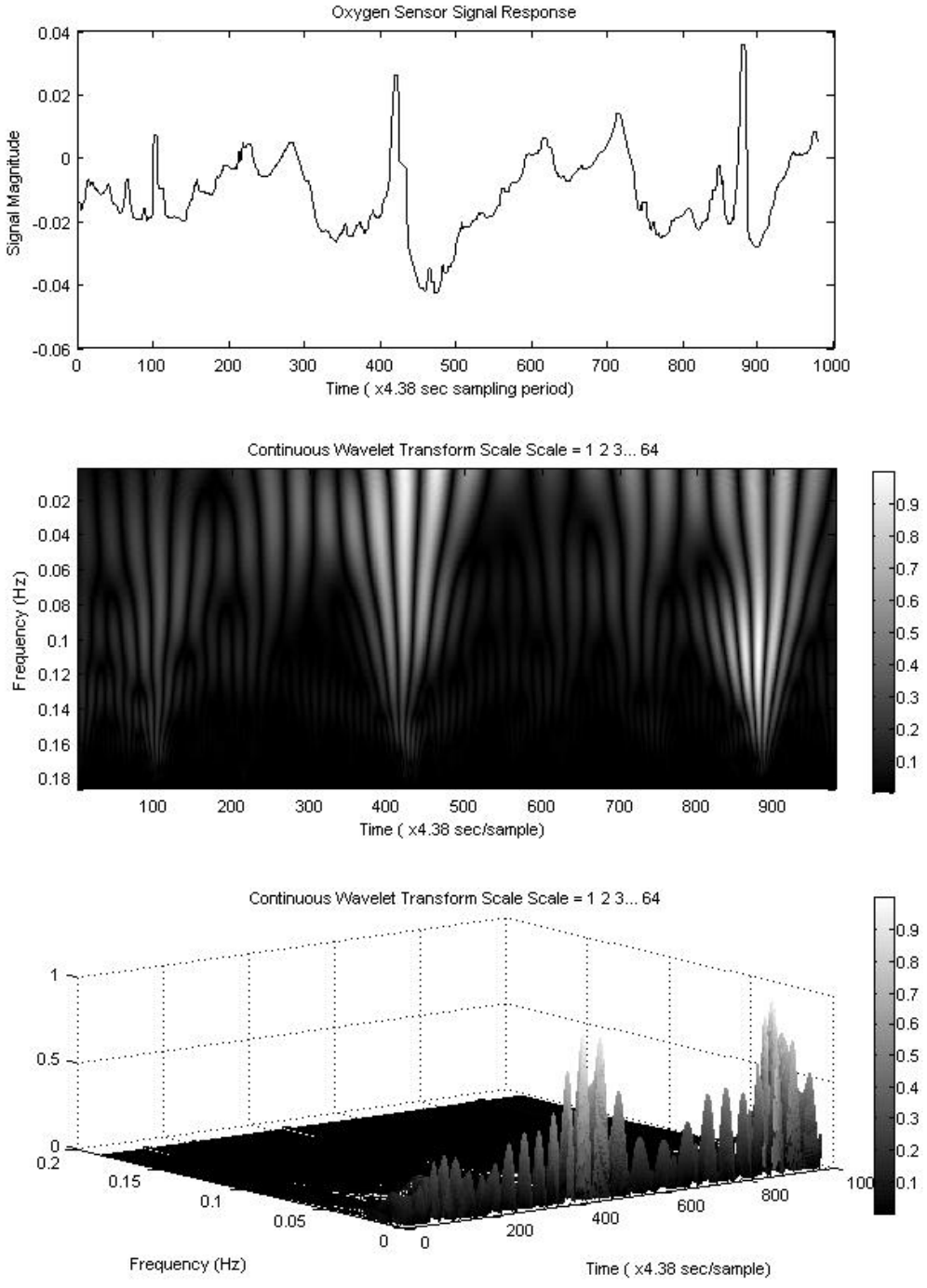


**Figure A-12. Continuous wavelet transforms for Hamster-B, Signal 2. The first plot is a plot of the Signal 2 magnitude against the sample time. The second plot is the 2-D wavelet transform of the Signal 2. The third plot is the 3-D wavelet transform of Signal 2.**

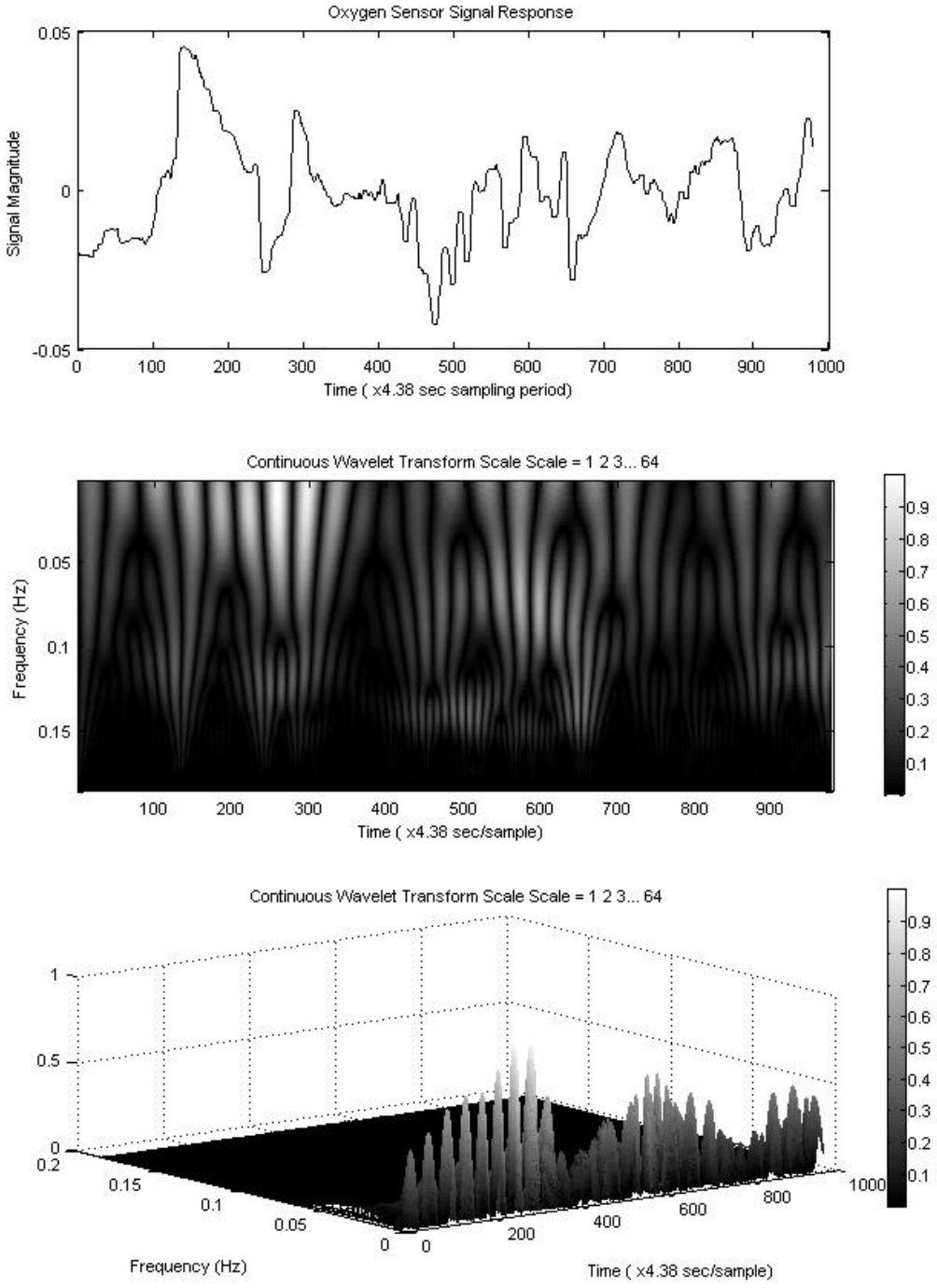


**Figure A-13. Continuous wavelet transforms for Hamster-B, Signal 3. The first plot is a plot of the Signal 3 magnitude against the sample time. The second plot is the 2-D wavelet transform of the Signal 3. The third plot is the 3-D wavelet transform of Signal 3.**

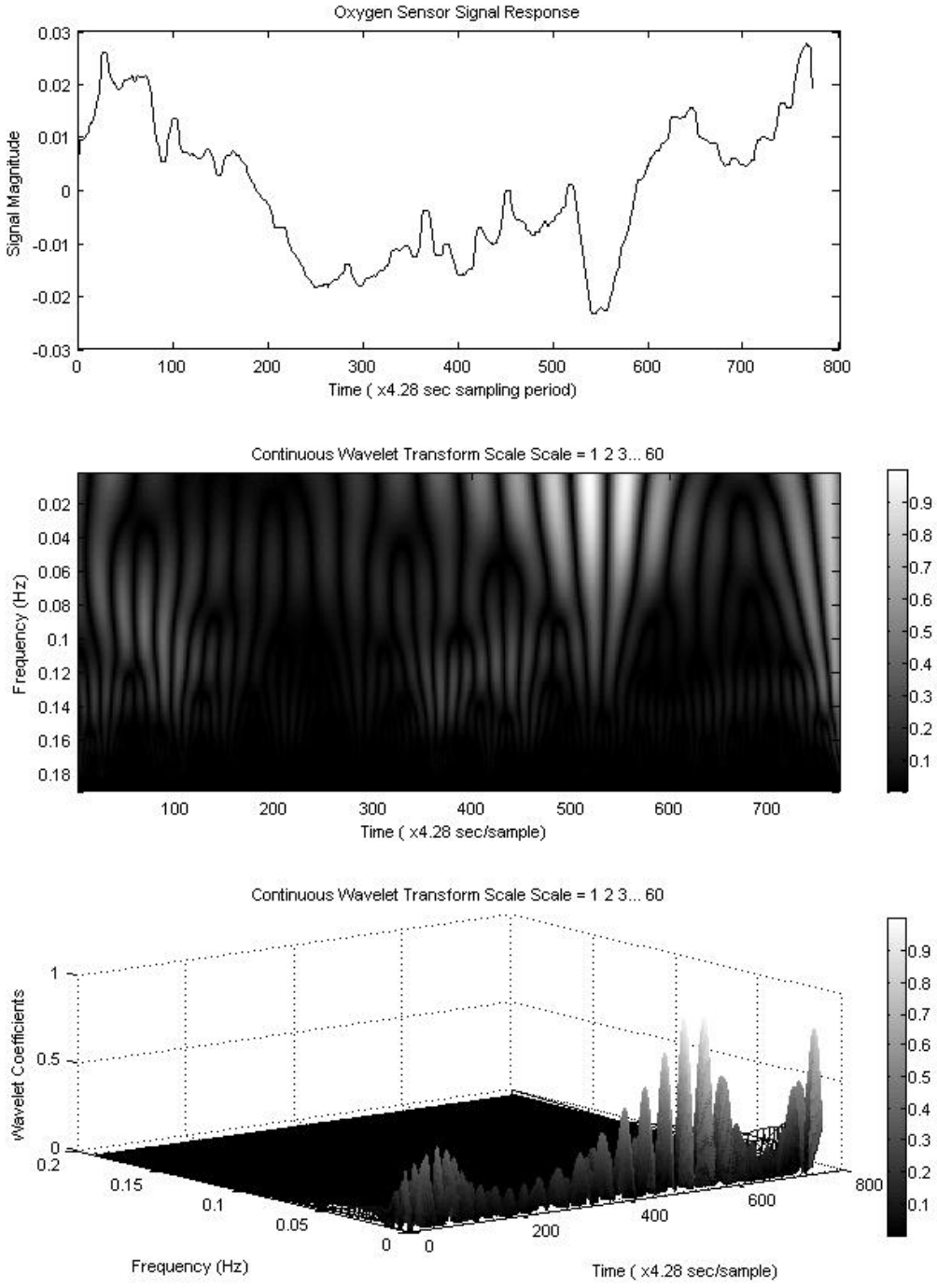


**Figure A-14. Continuous wavelet transforms for Hamster-B, Signal 4. The first plot is a plot of the Signal 4 magnitude against the sample time. The second plot is the 2-D wavelet transform of the Signal 4. The third plot is the 3-D wavelet transform of Signal 4.**

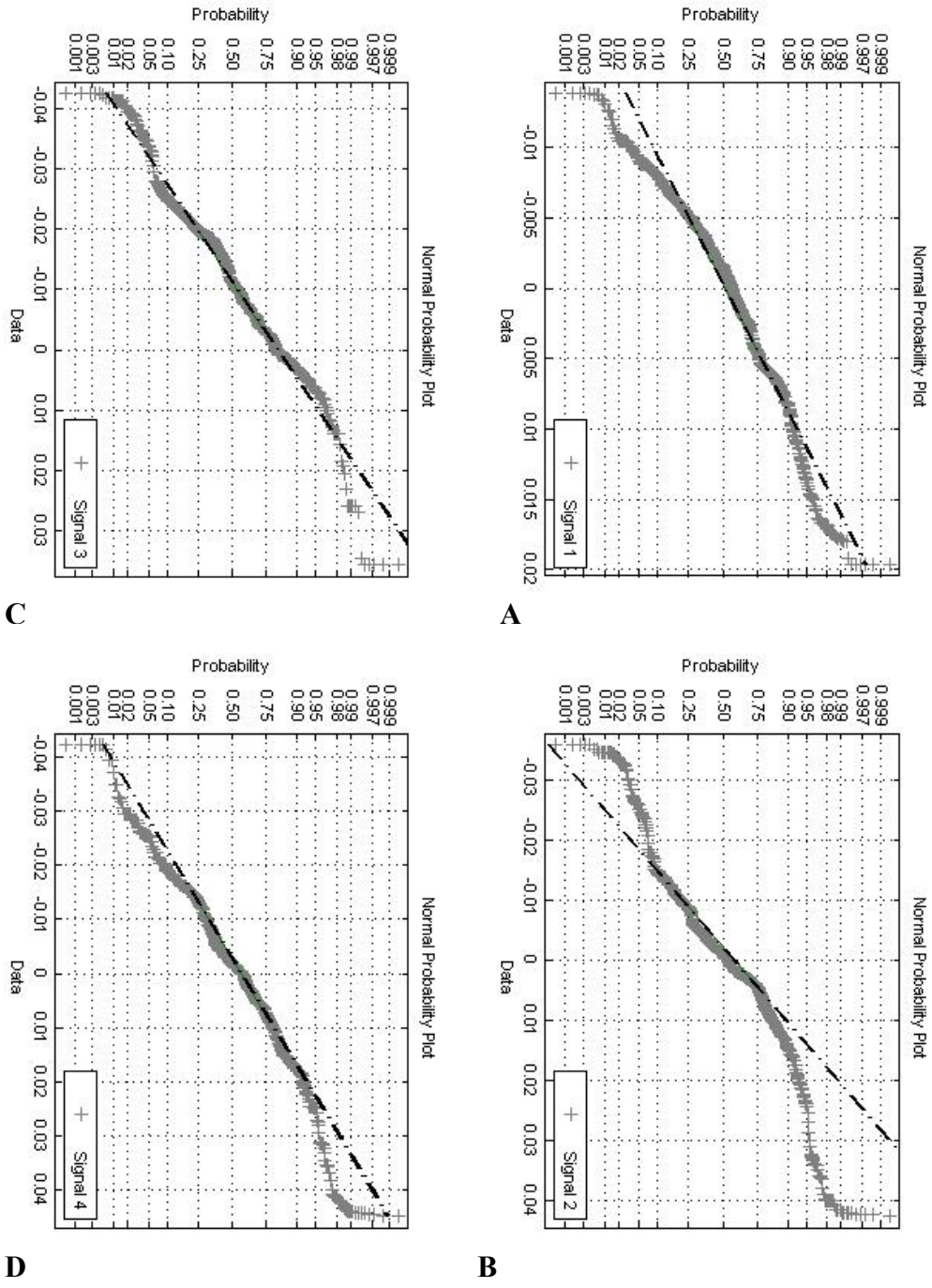


**Figure A-15.A-D Normal Probability Plots for Hamster-B, Signals 1 – 4.**

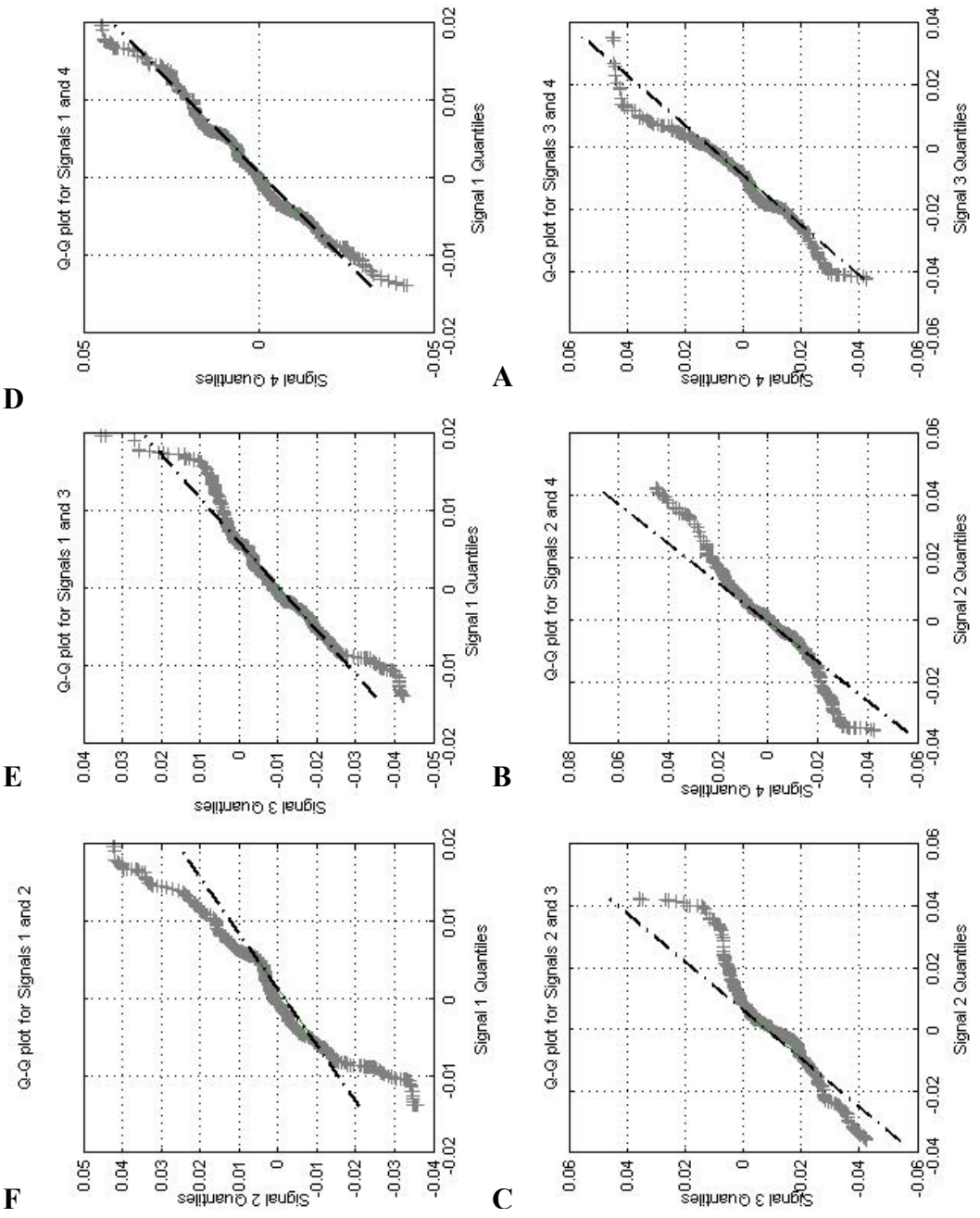


**Figure A-16.A-F Quantile-Quantile Plots for Hamster-B, Signal 1 – 4.**

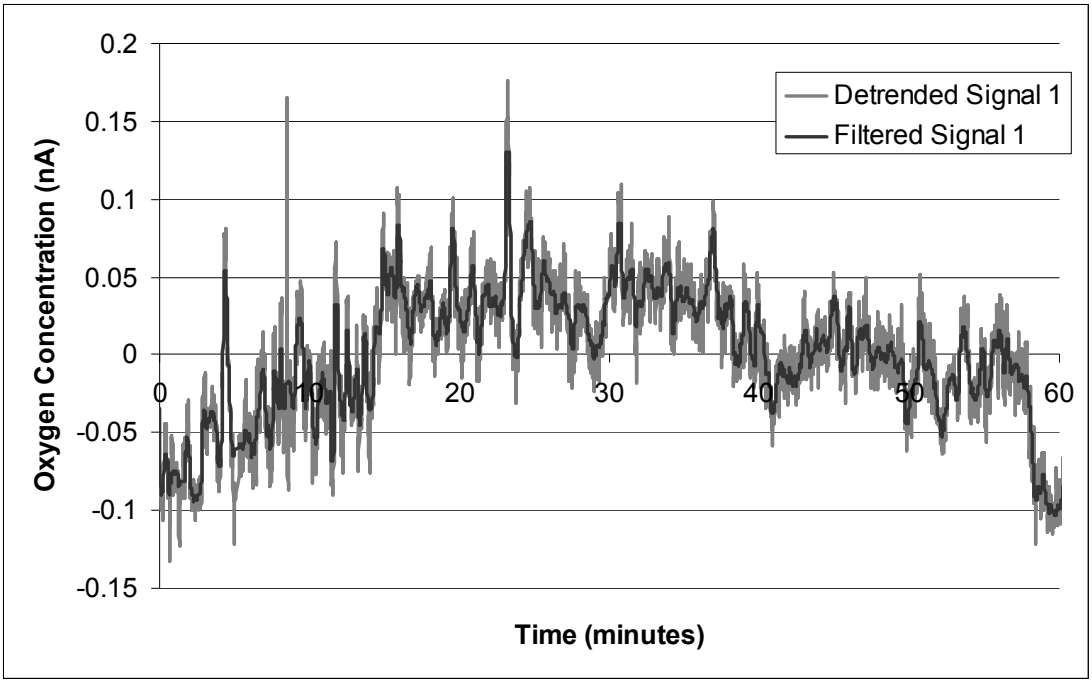


**Figure A-17. Pig-B, Signal 1**

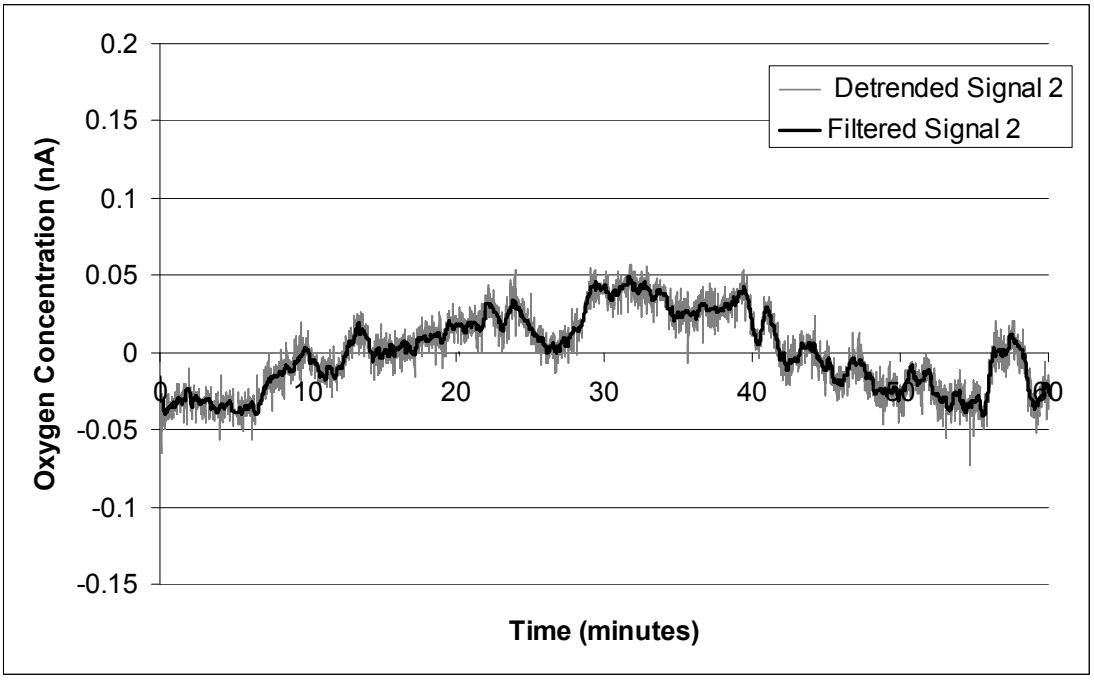


**Figure A-18. Pig-B, Signal 2**

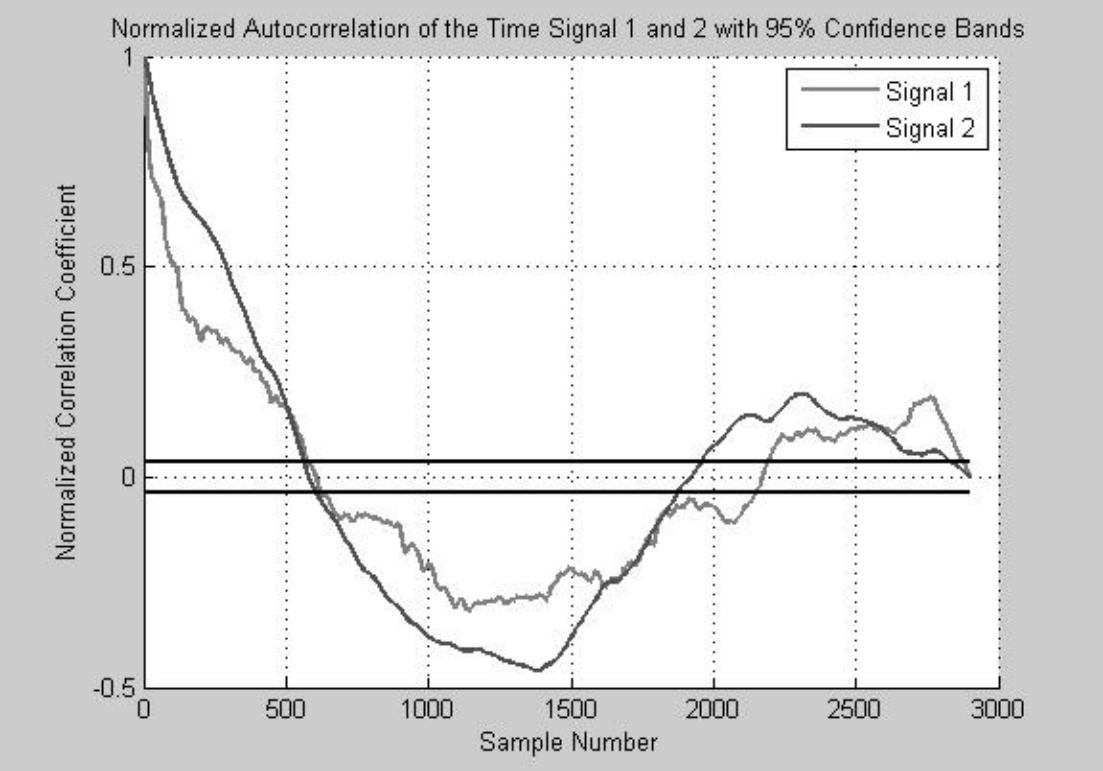


**Figure A-19. Normalized Autocorrelation Plot for Pig-B Signal 1.**

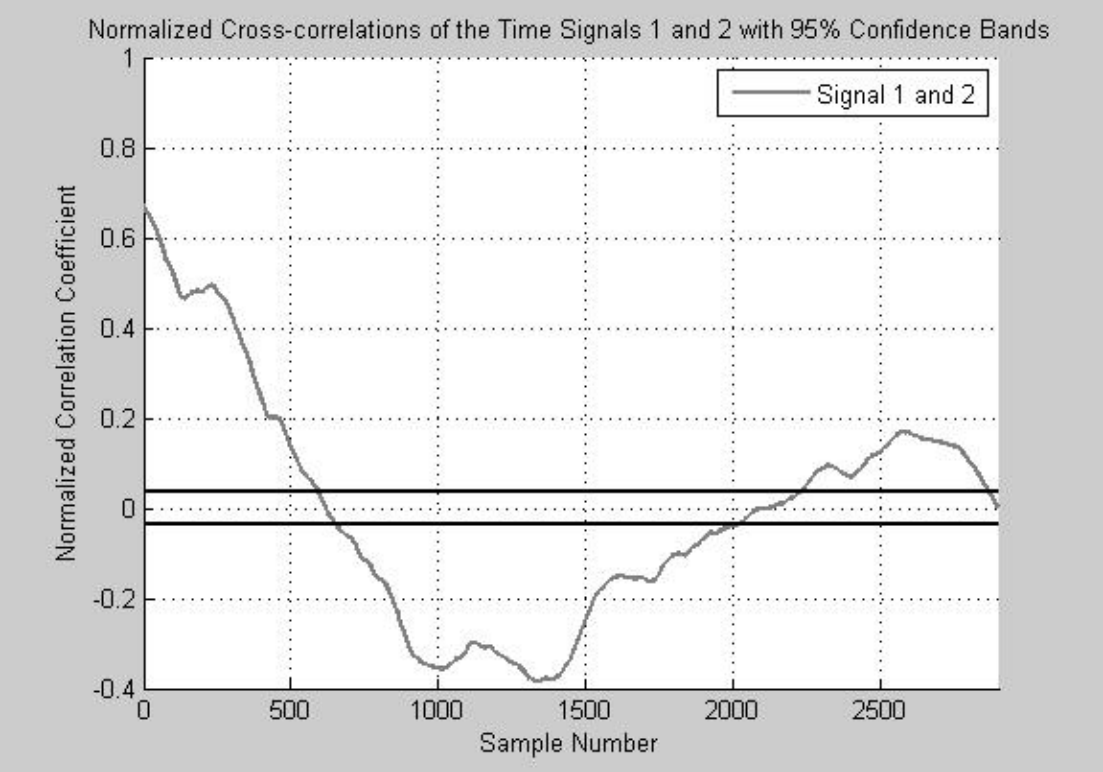


**Figure A-20. Normalized Cross-correlation plot for Pig-B Signal 2.**

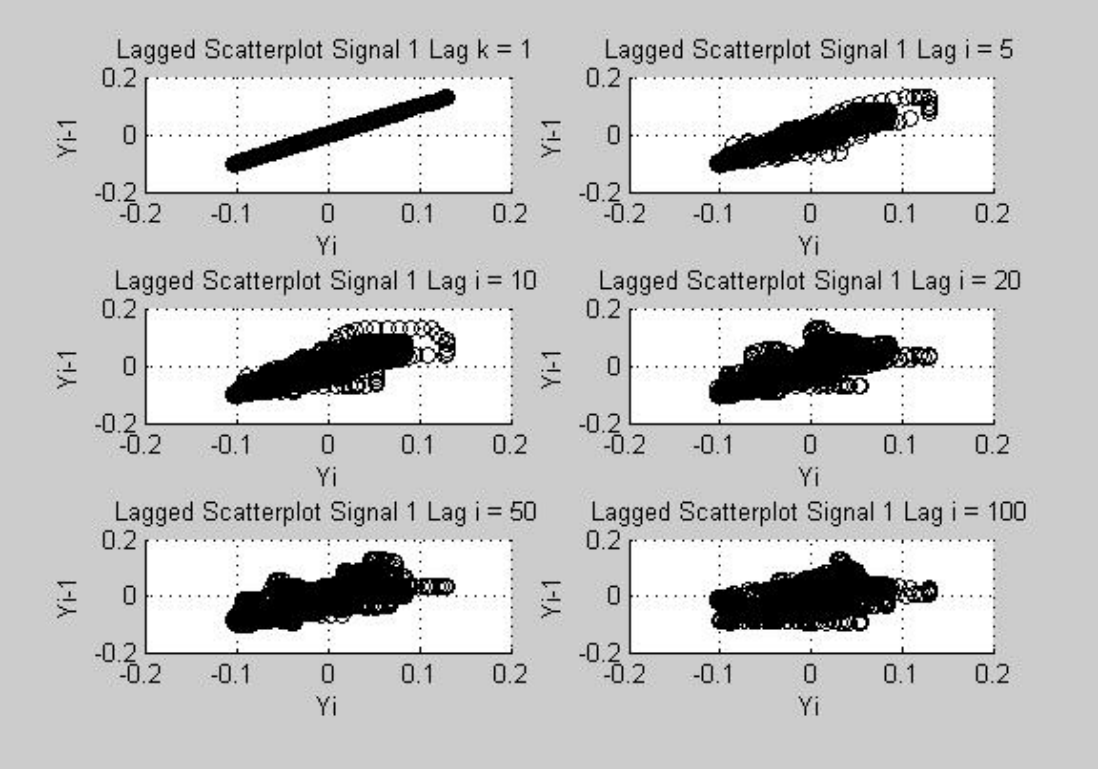


**Figure A-21. Lagged Scatterplots of Pig-B, Signal 1 for lags of 1, 5, 10, 20, 50 and 100.**

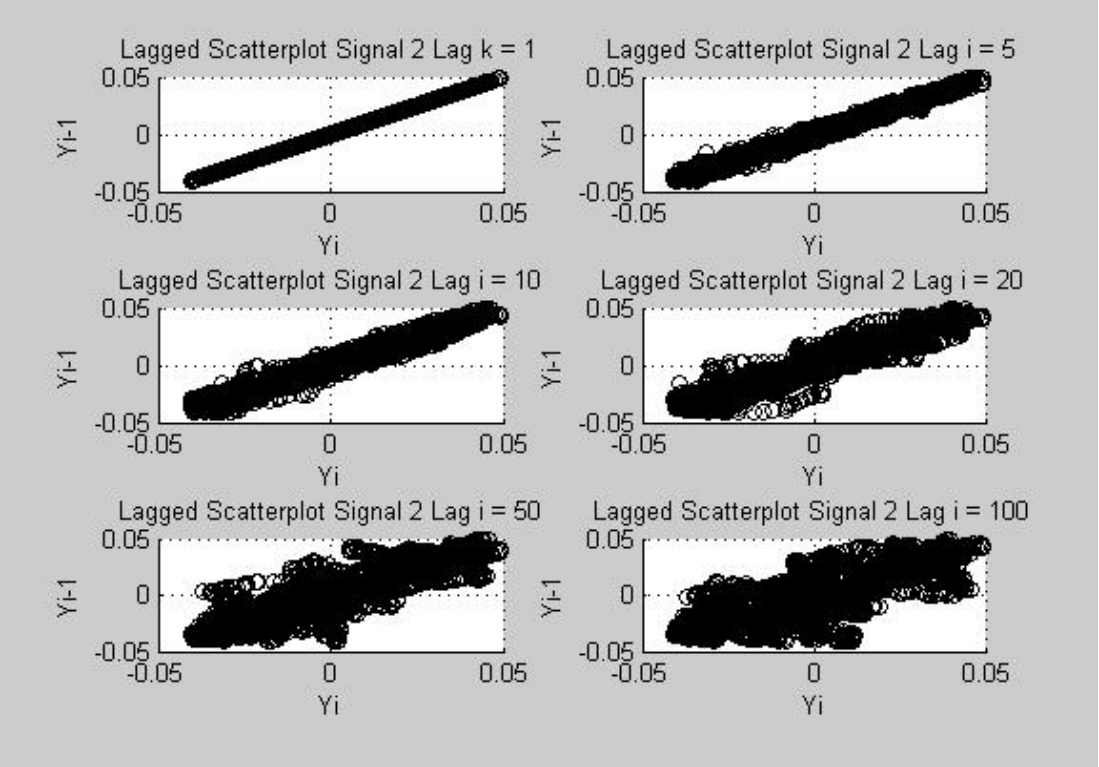


**Figure A-22. Lagged Scatterplots of Pig-B, Signal 2 for lags of 1, 5, 10, 20, 50 and 100.**

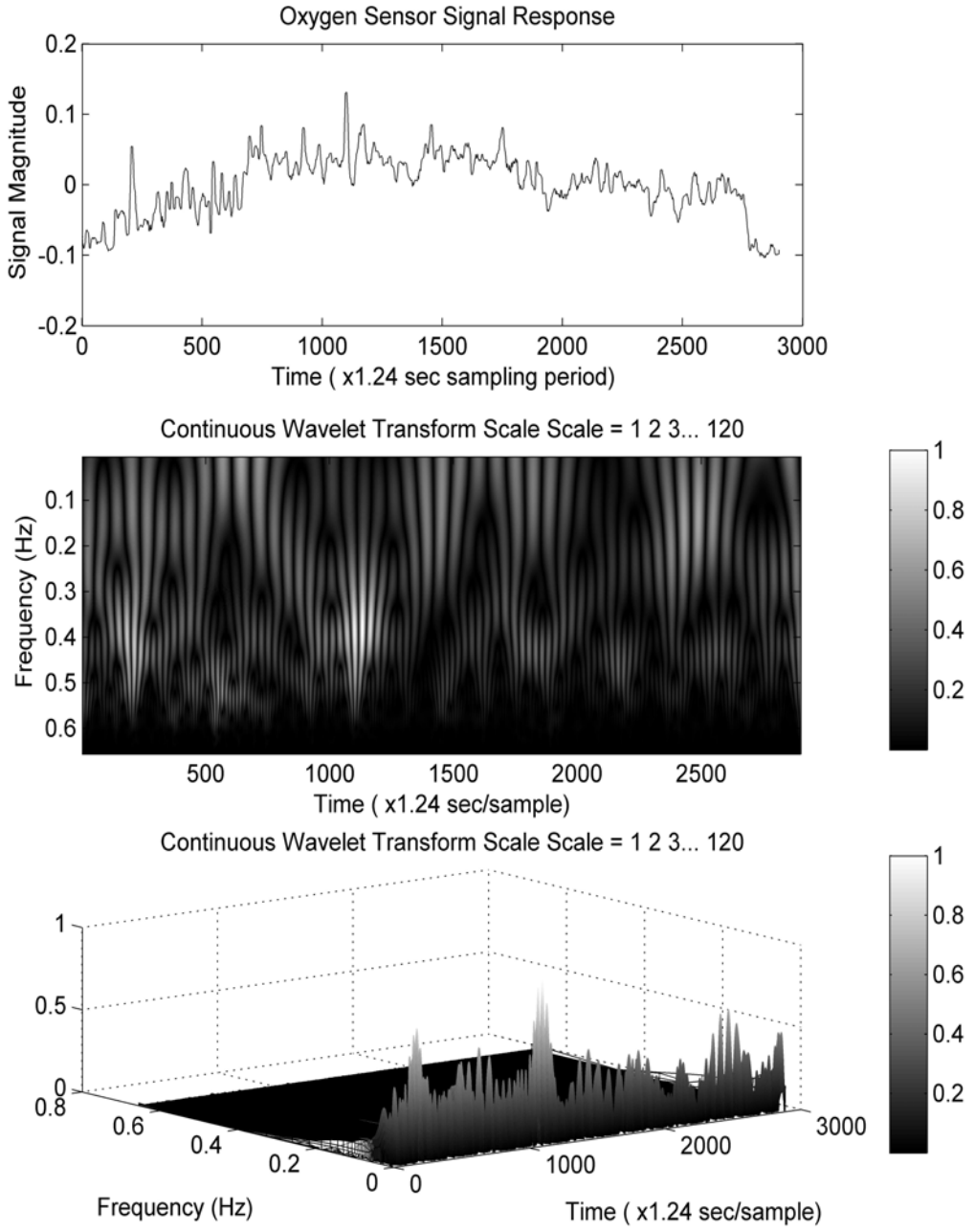


**Figure A-23. Continuous wavelet transforms for Pig-B, Signal 1.**

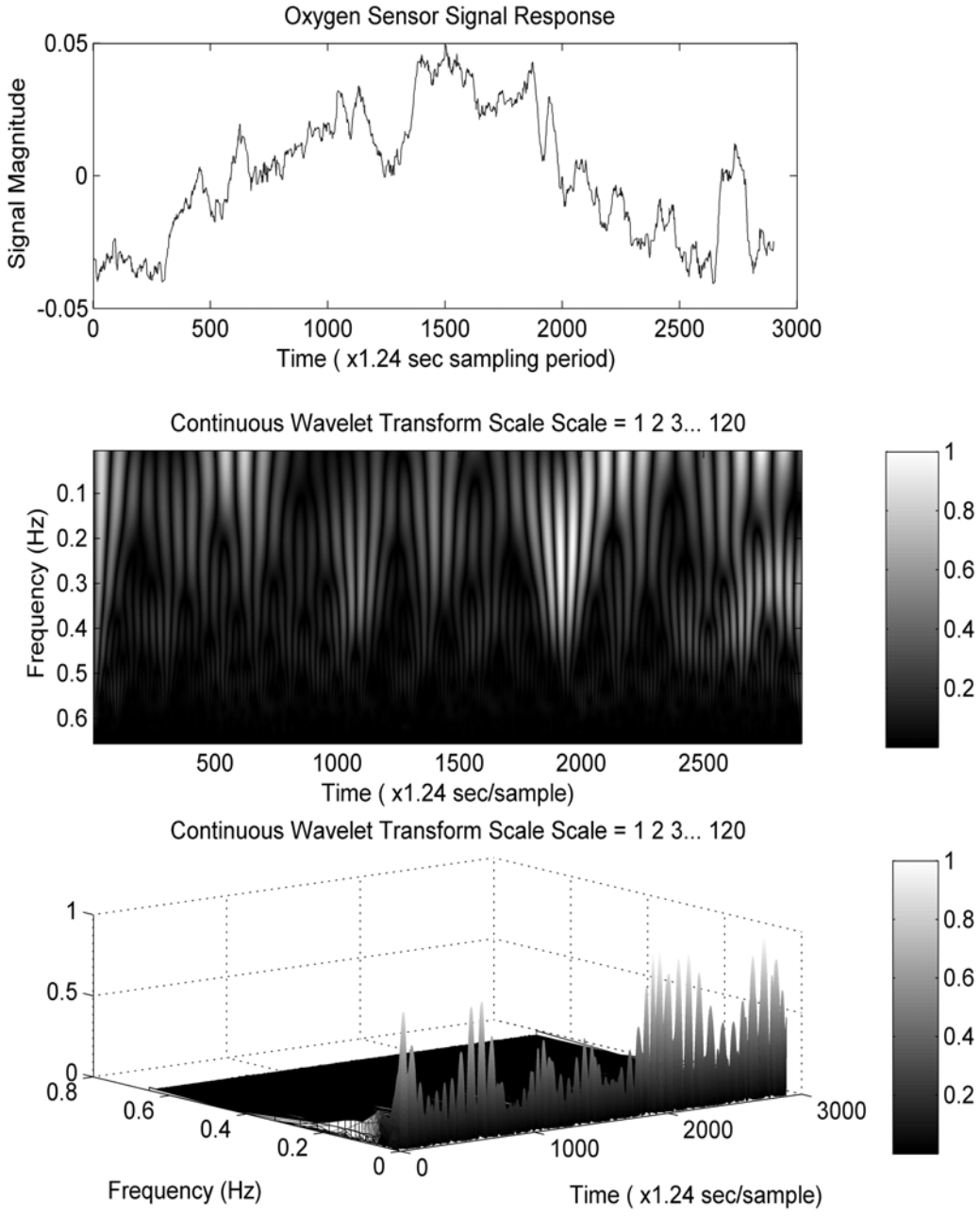


**Figure A-24. Continuous wavelet transforms for Pig-B, Signal 2.**

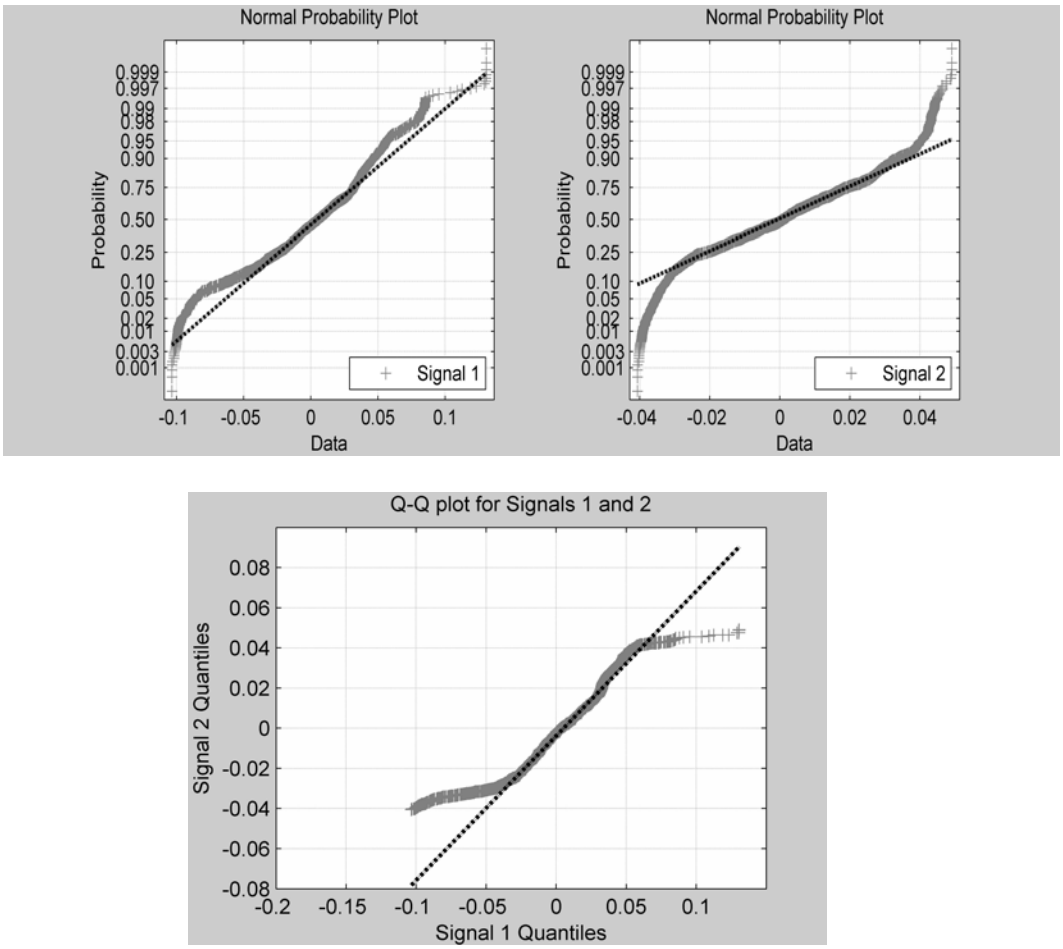


**Figure A-25. A-C. A. Normal Probability Plot for Pig-B, Signal 1. B. Normal Probability Plot for Pig-B, Signal 2. C. Q-Q Plot for Pig-B, Signals 1 and 2.**

# Appendix B: Programming Code for Oxygen Signal Analysis.

Software: Matlab ® Mathworks (Matlab R2009b Version 7.9.0.529)

## Designed Filtering Algorithm: baselinev6.m

```
function [sig9] = baselinev6(data)
% Data contains the incoming time array and matching data matrix
(signal set from an electrode) that needs to be filtered
(electronically caused spikes
% removed).

%What this program does: The data is detrended, baseline is
determined, and
%the a 4-point moving average filter is applied.

format long

%roc_thresh = 0.005;   % Constant slope threshold  (based off of %
realistic derivative c
%roc_pre_thresh = 1;  % Precent change in the threshold of the slope
between points with high slope.

[s1 s2] = size(data);

roc = zeros(s1 - 1, s2 - 1);  % Contains the first derivaties
(slopes) of the data series
%roc = [roc; zeros(10, 1)];
time = data(:, 1);

D_data = [time detrend(data(:, 2)) ];
data2 = D_data(:, 2:s2);

%Calculating the Rate Of Change (ROC) between consecutive points in
the data
%series - Can use the ROC as a thresholding method to filter the
data
%series.

for a = 1: s2-1

    for b = 1: s1-1
        roc(b, a) = (D_data(b+1, a+1) - D_data(b, a+1))/(time(b+1) -
time(b));
    end
end
roc = [roc; zeros(10, s2 - 1)];
```

```
% Look in the ROC where a point is between a positive and negative
slopes
% (i.e. The Roots!)
%Calculate the average and standard deviation of the incoming data
%set to use as thresholds.
avg = mean(D_data);
stdev = std(D_data);

%md = mode(roc);

%Obtain USER DEFINED THRESHOLD VALUES AFTER DISPLAYING THE STEM PLOT
%of the ROC (includes a default value)

close(figure(1));
figure(1);
stem(roc)
title('1st Derivative of Sensor Signal Data')
pos_Thresh = input('Enter the postive ROC threshold: ')
if isempty(pos_Thresh)
    pos_Thresh = 0.2; %Default value is a positive threshold value
of 0.2
end

neg_Thresh = input('Enter the negative ROC threshold: ')
neg_Thresh = abs(neg_Thresh);
if isempty(neg_Thresh)
    pos_Thresh = 0.15; %Default value is a negative threshold value
of 0.15
end
close

%Thresholding the sensor signal data based off the the user entered
%threshold values of the positive and negative ROC.

for (col = 1:s2-1)
    a1 = 0;
    a2 = 0;
    row = 1;


    while (row < s1-3)
        %Removing positive peaks/spikes
        if abs(roc(row + 1, col)) >= pos_Thresh %If the slope of the
next point is greater than the
            %the user-defined threshold value(based on looking at
the stem(roc).)
           a1 =  row;
           row = row +1;
        end
        %Rise in the spike.

        if a1 ~= 0
```

```
            while  abs(roc(row, col))  >= neg_Thresh & (row < s1 -
2) % | abs(roc(a1, col)) > .75*abs(roc(row + 1, col))
                %Next points are compared to another user defined
threshold
                %value based on stem(roc).
                row = row+1;
            end
            a2 = row;

        end

        %Check next two consecutive points and see if the roc of the
next
        %point surpasses the threshold again. If it does, then reset
a2, to
        %the new row position value.
        if a1 ~= 0 & a2 ~= 0
            while (abs(roc(row+2, col))  >= neg_Thresh & (row < s1 -
4))
                row = row + 2;
                while abs(roc(row, col))  >= neg_Thresh & (row < s1
- 3)
                    row = row +1;
                end
                a2 = row +1;
            end
%             if (abs(roc(row+2, col))  >= 0.15 & (row < s1 - 3))
%                 while (abs(roc(row+1, col))  >= 0.15 & (row < s1 -
3))
%                 %Next points are compared to another user defined
threshold
%                 %value based on stem(roc).
%                     row = row+1;
%                 end
%                 a2 = row + 2;
%             end
         end

        if a1 ~= 0 & a2 ~= 0
            xi = [a1 a2];
            yi = [data2(a1, col) data2(a2, col)];
            splne = csaps(xi , yi, .9, a1:a2);
            data2(a1:a2, col) = splne';
            a1 = 0;
            a2 = 0;
        end
        row = row+1;
    end
end

%
%
%
% for n = 1: s2 -1
```

```
%     r1 = 0;
%     r2 = 0;
%     m = 1;
%     while  m <= length(time) - 2
%
%        if roc(m, n) < 0  & roc(m + 1, n) > 0 & r1 == 0
%            root1 = m + 1;
%            r1 = 1;
%       % elseif roc(m, n) < roc_thresh  & roc(m, n) > roc_thresh*-1
& roc(m, n) > roc_thresh & r == 0
%
%
%        elseif roc(m, n) < 0 & roc(m + 1,n) > 0 & r1 == 1 & r2 == 0
%            root2 = m + 1;
%            r2 = 1;
%            m = m -1 ;
% %        elseif roc(m, n) < -1*roc_thresh & roc(m+ 1, n) > 0 &
roc(m + 1, n) < roc_thresh & r1 == 1
% %            root2 = m + 2;
% %            r2 = 1;
%        %elseif roc(m, n) > roc_thresh & roc(m+ 1, n) > 0 & r1 == 1
%        end
%       if (r1 == 1 & r2 == 1)
%           %if abs (root1 - root2) < 4
%              X = [time(root1)  time(root2)];
%              Y = [data2(root1, n) data2(root2, n)];
%              P = polyfit(X,Y, 1);
%              for z = root1: root2
%                 data2(z, n) = P(1)*power(time(z), 1) + P(2);
%              end
%              r1 = 0;
%              r2 = 0;
% %           else
% %              X = [time(root1)  time(root2)];
% %              Y = [data2(root1, n) data2(root2, n)];
% %              P = polyfit(X,Y, 4);
% %              for z = root1: root2+1
% %                 data2(z, n) = P(1)*power(time(z), 4) +
P(2)*power(time(z), 3) + P(3)*power(time(z),2) + P(4)*power(time(z),
1) + P(5) ;
% %              end
% %              r1 = 0;
% %              r2 = 0;
% %              r3 = 0;
% %           end
%       end
%       m = m+1;
%     end
% end

%NEW METHOD OF LOOKING FOR THE MINIMUM VALUES!!! and ORDERING THE
DATA
%POSSIBLY LOOKING FOR THE MINIMUM VALUE BETWEEN EVERY 3 to 10 POINTS
AND
%EXTRAPOLATING THE MINS TOGEHTER USING CSAPS!!!!
```

```
%DATA3: vector that will contain the new data set that has been re-
sampled to
%contain the baseline.

%OBTAIN USER DEFINED SAMPLING VALUE AFTER DISPLAYING STEM PLOT of
the DATA
%(includes a default value)
close(figure(2));
figure(2)
stem(D_data(:, 2))
title('Sensor Signal Data')
sample = input('Enter the re-sample value: ')
if isempty(sample)
    sample= 5; %Default value of sample is 5.

end
close

% 'The std of the signal is '
% stdev(2)
% std_x = input('Enter the standard deviation interval to be
excluded: ')
% if isempty(std_x)
%     std_x=3; %Default value of std_x is 3 (3 standard deviations
from mean)
% end

close(figure(1));
close(figure(2));


data3 = zeros(s1, s2-1); %Method for data interpolation using csaps
function
data4 = zeros(s1, s2-1); %Method for data interpolation using spline
function
data5 = zeros(s1-sample+1, s2-1); %Method for data interpolation
using interp1 function

for (col = 1:s2-1)

        A = D_data(1, col+1);
        B = D_data(1, col+1);

       for row = 1:sample:s1-sample+1

        %Method: Want to look for the minimum point
        %between everevery 5 samples. Will need to calculate the
sampling
        %time because this in effect re-samples the sensor signal
data.
```

```
        %METHOD VALUES ARE GOING TO BE CALCUATED: Starting from the
given
        %initial point, the min value is going to be set as the 5th
        %point, and the remaining middle 3 points are going to be
estimated
        %using a smoothing cubic spline with a smoothing parameter p
of
        %0.9.
        if row+sample > s1-sample

           Q = s1 - row;
           temp = D_data(row:s1, col+1);
           A = min(temp);
           xi = [row s1];
           yi = [B A];

           pp = csaps(xi , yi, .5, row:s1 );
           data3(row:s1, col) = pp';

           yy = spline (xi, yi, row:s1);
           data4(row:s1, col) = yy';

           row = s1;

           % for q = 1:Q
           %   data3(row+sample + q, col) = data(row+sample+q,
col+1);
           %   data4(row+sample + q, col) = data(row+sample+q,
col+1);
           %end
        else

            temp = D_data(row:row+sample, col+1);  %temp is a
temporary vector that will contain the 5 consecutive
            %points from the sensor signal data set.
            A = min(temp);

             xi = [row row+sample];
             yi = [B A];

             %Cubic smoothing spline using csaps function
             pp = csaps(xi , yi, .9, row:row+sample);
             data3(row:row+sample, col) = pp';


             %Cubic spline data interpolation using spline function
             yy = spline (xi, yi, row:row+sample);
             data4(row:row+sample, col) = yy';

             B = A;
             %A = 0;
```

```
            %This will fill in the remaining points that are not
interpolated
            %at the the end of time series.

       end

       end
end

%NEW METHOD OF LOOKING FOR THE MINIMUM VALUES!!! and ORDERING THE
DATA
%POSSIBLY LOOKING FOR THE MINIMUM VALUE BETWEEN EVERY 3 to 10 POINTS
AND
%EXTRAPOLATING THE MINS TOGEHTER USING INTERP1!!!!

%DATA5: vector that will contain the new data set that has been re-
sampled to
%contain the baseline.

%OBTAIN USER DEFINED SAMPLING VALUE AFTER DISPLAYING STEM PLOT of
the DATA
%(includes a default value)


for (col = 1:s2-1)

        A = D_data(1, col+1);
        x = zeros (ceil(s1/sample), 1);
        Y = zeros (ceil(s1/sample), 1);
        x_extrap = [1:s1-sample+1];
        count = 1;
        for row = 1:sample:s1-sample+1

        %Method: Want to look for the minimum point
        %between every 5 samples. Will need to calculated the
sampling
        %time because this in effect re-samples the sensor signal
data.

        %METHOD VALUES ARE GOING TO BE CALCUATED: Starting from the
given
        %initial point, the min value is going to be set as the 5th
        %point, and the remaining middle 3 points are going to be
estimated
        %using a smoothing cubic spline with a smoothing parameter p
of
        %0.9.

            %Need to check temp:  What if the minimum value is from
a severe drop due to an
            %electronic artifact. ---> This needs to be checked for
and
            %correct
```

```
            %Need to check for the type of spike to see if the spike
is
            %negative (spike drops below the baseline) but is not
severe.
            %This type of spike needs to be removed from the time
series.

            if row + sample*3 <=s1
                temp = D_data(row:row+sample, col+1);  %temp is a
temporary vector that will contain the 5 consecutive
                 %points from the sensor signal data set.

                temp2 = temp;
                temp3 = D_data(row:row+sample*3, col+1);

                avg_temp3 = mean(temp3);
                stdev_temp3 = std(temp3);
                index = 0;
                for j = 1:sample

                    if temp3(j) <= (avg_temp3 - stdev_temp3)
                        temp2(j-index) = [];
                        index = index+1;
                    end
                end
             x(count) = row;
             Y(count) = min(temp2);

            elseif row + sample*2 <= s1
                temp = D_data(row:row+sample*2, col+1);  %temp is a
temporary vector that will contain the 5 consecutive
                 %points from the sensor signal data set.

                 temp2 = temp;
                 temp3 = D_data(row:row+sample*2, col+1);
                 avg_temp3 = mean(temp3);
                 stdev_temp3 = std(temp3);
                for j = 1:sample*2

                    if temp3(j) <= (avg_temp3 - stdev_temp3)
                     temp2(j) = [];
                    end
               end

              x(count) = row;
              Y(count) = min(temp2);


            else
                x(count) = row;
                temp = D_data(row:s1, col + 1);
                temp2 = temp;
```

```
                index = 0;
                for j = 1:length(temp)

                    if temp(j) <= (avg(2) - 2.5*stdev(2))

                     temp2(j - index) = [];
                     index = index+1;

                end
            end

            Y(count) = min(temp2);
        end
        count = count+1;

        end

end

data5 = interp1(x, Y, x_extrap, 'linear');
data6 = interp1(x, Y, x_extrap, 'pchip');
data7 = interp1(x, Y, x_extrap, 'nearest');
data8 = interp1(x, Y, x_extrap, 'spline');
data9 = medfilt1(data2, sample); % Non-linear Median filtering
(smoothing) to the incoming time-signal.

%The following plotting code is only good for incoming data sets
that have
%only 2 columns of data (time, 1 signal). The code needs to be
adjusted for
%data that contains multiple serieses.

%Calculates the moving average based of a 4 point window

sig2 = filter([1/4 1/4 1/4 1/4], 1, data2);
sig4 = filter([1/4 1/4 1/4 1/4], 1, data4);
sig5 = filter([1/4 1/4 1/4 1/4], 1, data5)';
sig6 = filter([1/4 1/4 1/4 1/4], 1, data6)';
sig7 = filter([1/4 1/4 1/4 1/4], 1, data7)';
sig8 = filter([1/4 1/4 1/4 1/4], 1, data8)';
sig9 = data9;

sig2 = sig2(4:end);
sig4 = sig4(4:end);
sig5 = sig5(4:end);
sig6 = sig6(4:end);
sig7 = sig7(4:end);
sig8 = sig8(4:end);

%Detrends the data be calculating a straight-line fit for the signal
% d_sig2 = detrend(sig2);
% d_sig4 = detrend(sig4);
% d_sig5 = detrend(sig5);
```

```
%
%
% sig2 = d_sig2(4:end, :);
% sig4 = d_sig4(4:end, :);
% sig5 = d_sig5(4:end, :);

close(figure(3));
close(figure(4));
close(figure(5));

figure(1)
plot(D_data(4:end, 2:s2))
hold
plot(sig2,  'm')
title (['Filter using ROC thresholds, pos ', num2str(pos_Thresh), ',
neg ', num2str(neg_Thresh)])
hold off

% figure
% plot(D_data(:, 2:s2))
% hold
% plot(data3, '*')
% title (['Filter using ', num2str(sample), ' point re-sampling for
the minimum and using INTERP1 - CSAPS'])
% hold

% figure
% plot(D_data(:, 2:s2))
% hold
% plot(sig4, '*')
% title ('Filter using re-sampling for the minimum and using
SPLINE')
% hold


figure(2)
plot(D_data(8:end, 2:s2))
hold
plot(sig5, 'm')
title (['Filter using ', num2str(sample), ' point re-sampling for
the minimum and using INTERP1 - Linear'])
hold off


figure(3)
plot(D_data(8:end, 2:s2))
hold
plot(sig6,  'm')
title (['Filter using ', num2str(sample), ' point re-sampling for
the minimum and using INTERP1 - PCHIP'])
hold off

figure(4)
```

```
plot(D_data(8:end, 2:s2))
hold
plot(sig7, 'm')
title (['Filter using ', num2str(sample), ' point re-sampling for
the minimum and using INTERP1 - Nearest '])
hold off

figure(5)
plot(D_data(8:end, 2:s2))
hold
plot(sig8,  'm')
title (['Filter using ', num2str(sample), ' point re-sampling for
the minimum and using INTERP1 - Spline'])
hold off

figure(6)
plot(D_data(:, 2:s2))
hold
plot(sig9,  'm')
title (['Median Filtering using ', num2str(sample), ' order
filter'])
hold off

sig9;
```

## Power spectral analysis: psd_est.m

```
%Compares the FFT-baseds, AR, and Eigenanalysis Frequency Estimation
%(MUSIC) method od power spectral estimation.

function  psd_est(sig, fs)
%Input the signal and sampling frequency in Hz.

%Determine the nfft = N/8
len = length(sig);
N = 2;
i = 1;
if len > 256
    while (N<len)
        N = power(2, i);
        i = i +1;
    end
else
    N = 256;

end
wind = round(len/8);

%RULES FOR CHOOSING NFFT and N:
%N is the next power of 2 equal to or greater than the length of the
data
%signal. The NFFT is signal segment length, and according to the
default settings
```

```
%for Welch estimation, there are 8 segments such that NFFT = N/8.
The n-overlap,
%is chosen to be the maximum amount of overlap, nfft -1.

close(figure(1));

%AR Modified Covariance

n_order = 5;
while (n_order ~= 1)
    figure(1)
    n = n_order;
    [P, f] = periodogram(sig,[],[],fs);
    plot(f, db(P), 'b');
    hold;
    [P, f] = pwelch(sig, hanning(wind), wind -1, N, fs, 'onesided');
    plot(f, db(P), 'm');
    [P, f] = pmcov(sig, n, N, fs);
    plot(f, db(P), 'g');
    [P, f] = pyulear(sig, n, N, fs);
    plot(f, db(P), 'k');
    title(['Power Spectral Estimation with Model Order '
num2str(n)]);
    xlabel('Frequency (Hz)');
    ylabel('Power/Frequency (db/Hz)');
    legend('Periodogram', 'Welch', 'Mod Cov', 'Yule-Walker');
    hold off
    n_order = input('If the AR model order is good, enter 1, else
enter a new order: ');
    if isempty(n_order)
        n_order = 15; %Default value is an nth order of 15.
    end

end


 %MUSIC Spectrum, signal space p
 p_order = 2;
 [X, R] = corrmtx(sig, 20);
 [U, D, V] = svd(R, 0);
 eigen = diag(D);
 figure(1); subplot(1, 2, 1); grid; plot(eigen(1:20));
 title('Singular Values')
 while (p_order ~= 1)
    figure(1);
    subplot(1, 2, 2);
    p = p_order;
    [P, f] = periodogram(sig,[],[],fs);
    plot(f, db(P), 'r');
    hold;
    [P, f] = pwelch(sig, N/8, N/8 -1, N, fs, 'onesided');
    plot(f, db(P), 'm');
    [P, f] = pmusic(sig, p, N, fs);
    plot(f, db(P), 'g');
```

```
    xlim([f(1) f(end)]);
    title(['Power Spectral Estimation with SS ' num2str(p)]);
    xlabel('Frequency (Hz)');
    ylabel('Power/Frequency (dB/Hz)');
    legend('Periodogram', 'Welch', 'MUSIC');
    hold off
    p_order = input('If the SS value is good, enter 1, else enter a
new SS value: ');
    if isempty(p_order)
        p_order = 4; %Default singular subspace value is 4.
    end
end

close(figure(1));

%Fourer Transform Spectrum via WELCH method
figure(1);
subplot(2,2, 1);
pwelch(sig, N/8, N/8 -1, N, fs, 'onesided');

%AR Modified Covariance Spectrum
 subplot(2, 2, 2);
 [P, f] = pmcov(sig, n, N, fs);
 plot(f, db(P), 'g');
 hold
 [P, f] = pyulear(sig, n, N, fs);
 plot(f, db(P), 'b');
 grid;
 xlim([f(1) f(end)]);
 hold off;
 xlabel('Frequency (Hz)');
 ylabel('Power/Frequency (db/Hz)');
 legend('AR Mod Cov', 'Yule-Walker');
 title(['Parametric Spectral Estimation with AR model order '
num2str(n)]);

 %MUSIC Spectrum
 subplot(2, 2, 3);
 pmusic(sig, p, N, fs);
 title(['Eigenanalysis Spectral Estimation using MUSIC with SS value
' num2str(p)]);

 %Plot of Singular Values
 subplot(2, 2, 4);
 plot(eigen(1:20));
 grid;
 title( 'Singular Values');
 xlabel( 'Number');
 ylabel( 'Singular Values');

    close (figure(2));
    figure(2)

    hold
```

```
    [P, f] = periodogram(sig,[],[],fs);
    plot(f, db(P), 'b');
    [P, f] = pwelch(sig, N/8, N/8 -1, N, fs, 'onesided');
    plot(f, db(P), 'm');
    [P, f] = pmcov(sig, n, N, fs);
    plot(f, db(P), 'g');
    [P, f] = pyulear(sig, n, N, fs);
    plot(f, db(P), 'k');
    [P, f] = pmusic(sig, p, N, fs);
    plot(f, db(P), 'r');
    legend('Periodogram', 'Welch', ['Mod Cov n= ' num2str(n)],
'Yule-Walker', ['Music p= ' num2str(p)]);
    title('Power Spectral Estimation');
    xlim([f(1) f(end)]);
    xlabel('Frequency (Hz)');
    ylabel('Power/Frequency (dB/Hz)');
    hold off

    A_scal = 32;
    a_scal = 32;
    while (a_scal ~= 1)
        A_scal = a_scal;
        samp = 1/fs; %Sampling period
        A = 1:.5:A_scal;
        C = cwt(sig, A, 'morl');
        F = scal2frq(A, 'morl', samp);

        subplot(2, 1, 2);
        figure
        imagesc(1:len,F, abs(C));
        colormap(jet);
        colorbar;
        xlabel(['Time ( x' num2str(samp) ' /sample) ']);
        ylabel('Frequency (Hz)');
        title(['Continuous Wavelet Transform Scale Scale = 1 2 3...
' num2str(A_scal)]);
        a_scal = input('Enter the scale order for the wavelet
transform, if it is good, enter 1: ');


        if isempty(a_scal)
            a_scal = 64; %Default value is an nth order of 15.
        end
    end

    n = max(max(abs(C)));
    C = C./n;
    figure
    imagesc(1:len,F, abs(C));
        colormap(gray);
        colorbar;
        xlabel(['Time ( x' num2str(samp) ' sec/sample) ']);
        ylabel('Frequency (Hz)');
```

```
        title(['Continuous Wavelet Transform Scale Scale = 1 2 3...
' num2str(A_scal)]);
   figure
    subplot(3, 1, 1)
    plot(sig)
    xlabel(['Time ( x' num2str(samp) ' sec sampling period) ']);
    ylabel('Signal Magnitude');
    title('Oxygen Sensor Signal Response');

    subplot(3, 1, 2)
     imagesc(1:len,F, abs(C));
        colormap(gray);
        colorbar;
        xlabel(['Time ( x' num2str(samp) ' sec/sample) ']);
        ylabel('Frequency (Hz)');
        title(['Continuous Wavelet Transform Scale Scale = 1 2 3...
' num2str(A_scal)]);

    subplot(3, 1, 3)
     mesh(1:len,F, abs(C));
        colormap(gray);
        colorbar;
        xlabel(['Time ( x' num2str(samp) ' sec/sample) ']);
        ylabel('Frequency (Hz)');
        title(['Continuous Wavelet Transform Scale Scale = 1 2 3...
' num2str(A_scal)]);
```

## Correlation Analysis: corr_sig.m

```
function [P] = corr_sig(data1, data2, data3, data4, data5, data6,
data7)

% Assuming that the incoming sensor time series are all columns, the
same
% length, and that there are less than 7 incoming series.

if nargin > 1
    for i = 1:nargin
        temp = ['data' int2str(i)];
        data_sets(:, i) = eval(temp);
    end
end

% data_set is a matrix containing the incoming time serieses.

sets = size(data_sets, 2);

%Data1 through Data7 --> taking in as many processes time series and
%calculating the cross-correlations between them.

% The is a post processing function - the signal series has been
processed
```

```
% and filterd by baselinev5. The de-meaned, de-trended, and filtered
signal
% is now being analyzed.

% The first part of the analyzation is do determine the inherent
information
% from the lagged scatterplot and autocorrelation.


% The cross-correlationwill be determined elsewhere because the
input is
% only a signal signal.

% NOTE: data is the output from baselinev5.m

% Lagged Scatterplot: Let time series of length N be xi, i =
1,...,N. The
% lagged scatterplot for lag k is a scatterplot of the last N-k
observations
% against the first N-k observations.

% Random scattering of points in the lagged scatterplot indicates a
lack of
% autocorrelation - series is Random.  Alignment from lower left to
the
% upper right in the lagged scatterplot indicates a positive
% autocorrelation. Alignment from the upper left to the lower right
% indicates a negative autocorrelation. Attributes of the the lagged
% autocorrelation is that it can display autocorrelation regardless
of the
% form of dependence on its past values, and can show if the
% autocorrelation is driven by one or more outliers in the data.
(This
% would not be evident from ACF.)


s1 = length(data1); %Assuming that the length of the time series is
longer than 20 samples.

% Lagged Scatterplot: Scatterplot of the time series against itself
offset
% by one to several time samples.
% Check about correlation coefficients and %95% significance level
(stdev = 2)
% Confidence Bands =  +/- 2*sqrt(N), s = std, N = number of samples,
%
close all;
for i = 1:sets
    temp = 1;
    while (temp == 1)

    Lag = input('Enter the Lag k for the lagged scatterplot: ');
    if isempty(Lag)
```

```
        figure

        Lag = 1;
        subplot( 3, 2, 1);

        %X-axis : Xi
        %Y-axis: Xi-1
        scatter(data_sets(Lag:end, i), data_sets(1:end - Lag+1, i))
        title (['Lagged Scatterplot Series ' int2str(i), ' Lag k =
1'])
        xlabel('Yi');
        ylabel('Yi-1');
        grid


        Lag = 5;
        subplot(3, 2, 2);
        scatter(data_sets(Lag:end, i), data_sets(1:end - Lag+1, i))
        title (['Lagged Scatterplot Series ' int2str(i), ' Lag i =
5'])
         xlabel('Yi');
        ylabel('Yi-1');
        grid

        Lag = 10;
        subplot(3, 2, 3);
        scatter(data_sets(Lag:end, i), data_sets(1:end - Lag+1, i))
       title (['Lagged Scatterplot Series ' int2str(i), ' Lag i =
10'])
         xlabel('Yi');
        ylabel('Yi-1');
        grid

        Lag = 20;
        subplot(3, 2, 4);
        scatter(data_sets(Lag:end, i), data_sets(1: end - Lag+1, i))
       title (['Lagged Scatterplot Series ' int2str(i), ' Lag i =
20'])
         xlabel('Yi');
        ylabel('Yi-1');
        grid

        Lag = 50;
        subplot(3, 2, 5);
        scatter(data_sets(Lag:end, i), data_sets(1:end - Lag+1, i))
       title (['Lagged Scatterplot Series ' int2str(i), ' Lag i =
50'])
        xlabel('Yi');
        ylabel('Yi-1');
        grid

        Lag = 100;
```

```
        subplot(3, 2, 6);
        scatter(data_sets(Lag: end, i), data_sets(1:end - Lag+1, i))
       title (['Lagged Scatterplot Series ' int2str(i), ' Lag i =
100'])
         xlabel('Yi');
        ylabel('Yi-1');
        grid

        temp = 0;
    else
         close(figure(1));
        figure(1);
        scatter(data_sets(Lag:end, i), data_sets(1:end - Lag+1, i))
        title(['Time series ' num2str(i) ' Lagged Scatterplot, Lag i
= ', num2str(Lag)])
         xlabel('Yi');
        ylabel('Yi-1');
        temp = 1;
        grid


    end

    end
end

% Plot of the normalized autocorrelation, and indentification of any
% perodicities within the time seres.

% Autocorrelation plots: Measure the correlation between
obersvations
% at difference times. Tool for checking randomness in data sets.

%Contains the correlational lags and coefficients for the incoming
signals.
corr_A_lags = zeros(sets+1, s1);

figure
for i=1:sets

    [A, lags] = xcorr(data_sets(:, i), 'coeff');

    %Lags and A, cut in half, because autocorrelation is symmetric
so only
    %going to show the positive half.
    A = A(ceil(length(A)/2):end);
    lags = lags(ceil(length(lags))/2:end);
    corr_A_lags(i+1, :) = A;
    subplot(sets, 1, i)
    plot(lags, A, '*')
    title({['Normalized Autocorrelation of Time Series '
int2str(i)]; ['95% Confidence Bands']})
    xlabel('Sample Number')
```

```
    ylabel('Normalized Correlation Coefficient')
    hold
    grid
    %Confidence Bands: Testing for Randomness
    CI(1:s1) = 2/(s1.^0.5);
    plot(CI(3:end))
    plot(-1*CI(3:end))
    hold

    %Locate the roots in the stem plot: Assumed to indicate
perodicities in the
    %time series

    a = 1;
    for j =  1:length(A)-1
        if or(and (A(j)>0, A(j+1)<0), and(A(j)<0, A(j + 1)>0))
            roots(a, i) = j;
            a = a +1;
        end
    end

end
corr_A_lags(1, :) = lags;

n = ['Signal 1'];
N = cellstr(n);
figure
hold
for i = 2:sets+1
    plot(corr_A_lags(1, :), corr_A_lags(i, :))
    N(i-1) = cellstr(['Signal ' int2str(i-1)]);
end
grid
title ('Normalized Autocorrelation of the Time Signal 1 - 4 with 95%
Confidence Bands')
xlabel('Sample Number')
ylabel('Normalized Correlation Coefficient')
CI(1:s1) = 2/(s1.^0.5);
plot(CI(3:end))
plot(-1*CI(3:end))
legend(N)



%Not adjusted for data_sets (matrix of incoming time serieses)
%_____________________________________________________________________
% Large-Lag standard Error: Confidence Bands at 95% (std = 2)

% Successive values of the correlation r_k can be highly correlated
so that
% an individual r_k might be large simply because the value of the
next
% lower lag, r_k-1, is large. This interdependence makes it
diffucult to
```

```
% assess just how many lags the autocorrelation is significant.  THe
% large-lag standard error adjusts for the interdependence.

% var(r_k) = 1/N * (1 + 2 sum(r_k)^2))
%CI = +/-2 /(sqrt(var(r_k)) --> 95% confidence bands.

% var_r = zeros(length(A), 1);
% for k = 1:length(A)
%     var_r(k) = 1/s1 * ( 1 + 2*sum((A(1:k).^2)));
% end
%
%
% CI = 2/var_r.^0.5;
%_____________________________________________________________________



%CROSS_CORRELATION CODE!!!
n_plots = factorial(sets)/(factorial(2)*(factorial(sets-2)));
%Compute the number of permutations to
xcorr_A_lags = zeros(n_plots+1, s1);
%determine how many subplots are necessary;

xcorr_name = [];

temp = 1;
count = 1;
figure
for i=1:sets
    temp = 1;
    for j=2:sets
        temp = 1;
       while ((i ~= j) & (i < j) & (temp == 1))
             subplot( n_plots, 1, count);
             hold
             [A, lags] = xcorr(data_sets(:, i), data_sets(:, j),
'coeff');
             A = A(ceil(length(A)/2):end);
             lags = lags(ceil(length(lags))/2:end);
             xcorr_A_lags(count+1, :) = A;
             plot(lags, A, '*')
             grid
             title(['Normalized Cross-correlation of Time Signal 1 -
4 and 95% Confidence Bands ' int2str(i) ' and ' int2str(j)])
             xcorr_name(count, 1) = i;
             xcorr_name(count, 2) = j;
             count = count +1;
             temp = 0;
              %Confidence Bands: Testing for Randomness
             CI(1:s1) = 2/(s1.^0.5);
             plot(CI(3:end))
             plot(-1*CI(3:end))
             hold
        end
```

```
    end
end

xcorr_A_lags(1, :) = lags;

figure
hold
for i = 2:n_plots+1
    plot(xcorr_A_lags(1, :), xcorr_A_lags(i, :))
end
grid
title ('Normalized Cross-correlations of the Time Signals 1 - 4 with
95% Confidence Bands')
xlabel('Sample Number')
ylabel('Normalized Correlation Coefficient')
CI(1:s1) = 2/(s1.^0.5);
plot(CI(3:end))
plot(-1*CI(3:end))
hold
m = ['Signal 1'];
M = cellstr(m);
for(k = 1:count-1)
    M(k) = cellstr(['Signal ' int2str(xcorr_name(k, 1)) ' and '
int2str(xcorr_name(k, 2))]);
end
legend(M)

P = roots; %Contains roots of the autocorrelation of the sensor
signal series.
```

## Wavelet Analysis: wav_est.m

```
function  wavelet_est(sig, fs)
%Input the signal and sampling frequency in Hz.

%Determine the nfft = N/8
len = length(sig);

    A_scal = 32;
    a_scal = 32;
    while (a_scal ~= 1)
        A_scal = a_scal;
        samp = 1/fs; %Sampling period
        A = 1:A_scal;
        C = cwt(sig, A, 'morl');
        F = scal2frq(A, 'morl', samp);

        imagesc(1:len,F, abs(C));
```

```
        colormap(jet);

        colorbar;
        xlabel(['Time ( x' num2str(samp) ' /sample) ']);
        ylabel('Frequency (Hz)');
        title(['Continuous Wavelet Transform Scale Scale = 1 2 3...
' num2str(A_scal)]);
        a_scal = input('Enter the scale order for the wavelet
transform, if it is good, enter 1: ');

        if isempty(a_scal)
            a_scal = 64; %Default value is an nth order of 15.
        end
    end

    n = max(max(abs(C)));
    C_norm = abs(C./n);

    figure(1);
    subplot(3, 1, 1)
    plot(sig)
    xlabel(['Time ( x' num2str(samp) ' sec sampling period) ']);
    ylabel('Signal Magnitude');
    title('Oxygen Sensor Signal Response');

    subplot(3, 1, 2)
     imagesc(1:len,F, C_norm);
        colormap(gray);
        colorbar;
        xlabel(['Time ( x' num2str(samp) ' sec/sample) ']);
        ylabel('Frequency (Hz)');
        title(['Continuous Wavelet Transform Scale Scale = 1 2 3...
' num2str(A_scal)]);

    subplot(3, 1, 3)
     mesh(1:len,F, abs(C_norm));
        colormap(gray);
        colorbar;
        xlabel(['Time ( x' num2str(samp) ' sec/sample) ']);
        ylabel('Frequency (Hz)');
        zlabel('Wavelet Coefficient');
        title(['Continuous Wavelet Transform Scale Scale = 1 2 3...
' num2str(A_scal)]);
```

## Calculation of the AR model Coefficients, and Residual Error Validation: ar_test.m

```
function [m, y_est] = ar_test(sig, approach)
% Possible approach methods to solving for the AR parameters:
'burg', 'gl',
% 'ls', 'yw', 'fb' (default).
```

```
% Determine the autoregressive (ar) model for a time series of
sensor signal data
% The input SIG is vector containing the time series to be modeled,
Q is the order of the
% autoregressive model, and APPROACH contains the method used to
determine
% the ar parameter coefficients.
% The output is M, an idpoly that contains the ar model information,
and Y_EST contains that predicted signal.
% STATIONARY PROCESS: Property in which the mean, variance, and the
% autocorrelation structure don't change over time. I.E. A flat
looking series
% without trend, a constanct variance, and an constanct
autocorrelation
% structure with no periodic fluctions.
% Need to comvert the incoming time series signal to be statioanary.
% 1. Difference the data Y(i) = Z(i) - Z(i-1)
% 2. Detrend ( fit the series to sometype of curve) and model the
residuals
% from that fit.
% 3. For non-constant variance, taking the logarithm of square root
of the
% series to stabilize the varice.
% ARMA or AR Model validation: 1. Run squence plot, 2. Lag Plot, 3.
Histogram, 4.
% Normal probability plot.
% This is assuming that the sig, and ar model order are entered!!!!
if nargin < 3
approach = 'fb';
end
% y = iddata(sig);
% Piecewise detrending, will need the user's input to segment the
series.
% Plot of the time series will be shown, and use the data curser,
indices
% for the segments will be entered.
% Plot of the Autocorrelation to determine if there is any periodic
% fluctuations - seasonality.
figure
subplot(2, 2, 1)
[N, lags] = xcorr(sig, 'coeff');
stem(lags, N)
title('Normalized Autocorrelation of Time Series')
subplot(2, 2, 2)
hold
plot(sig)
title ('Time Series')
xlabel('Indices')
ylabel('Voltage')
% Piecewise detrending the signal to make the time series
stationary.
bp = input('Enter the segment index for the piecewise detrending: ',
's');
if isempty(bp)
bp = length(sig);
```

```
else
bp = str2num([bp]);
end
sig_detrend = detrend(sig, 'linear', bp);
y = iddata(sig_detrend);
plot(sig_detrend, 'r')
legend('Original Signal', 'Detrended Signal')
hold
subplot(2,2, 3)
[N, lags] = xcorr(sig_detrend, 'coeff');
stem(lags, N)
title ('Normalized Autocorrelation of Detrended Signal')
% Differenceing the time series to make in stationary: y(t) = x(t) =
x(t-1)
diff = input('Does the signal series need to be differenced? [Y/N]:
', 's');
if isempty(diff)
diff = 'Y';
end
if diff == 'Y'
for i = 2:length(sig)
sig_diff(i) = sig_detrend(i) - sig_detrend(i-1);
end
[N, lags] = xcorr(sig_diff, 'coeff');
subplot(2, 2, 3)
stem(lags, N)
title ('Normalized Autocorrelation of Detrended & Differenced
Signal')
y = iddata(sig_diff');
end
% Use partial autocorrelation as a tool to determin the order of the
AR
% model now that the time series is stationary.
subplot(2, 2, 4)
parcorr(y.y, [], 2);
q = input('Please enter the AR model order: ');
if isempty(q)
q = 3;
end
% y = iddata(sig); In order use the ar matlab function, the series
must
% be an iddata object.
m = ar(y, q, approach);
% Determining the AR model
A = m.A(2:q+1);
% A vector containing the ar parameter coefficients
A = A';
L = length (y.y);
% y_est is the AR estimated model for the stationary series
(de_trended and differenced).
y_est = zeros(L, 1);
y_est(1:q+2) = y.y(1:q+2);
% x_est is the AR estimated model for the de_trended series.
if diff == 'Y'
x_est = zeros(L, 1);
```

```
x_est(1:q+2) = sig_detrend(1:q+2);
end
r = zeros(L, 1);
% AR model: A(q)y(t) = e(t)
% y(t) + a(1)y(t-1) + ... + a(n)y(t-n) = e(t)
for i = q+2:L
temp_y = 0;
temp_x = 0;
for j= 1:q
temp_y = -1*A(j)*y.y(i - j) + temp_y;
% y_est(i) = -1*A(j)*y.y(i - j) + y_est(i);
% 10-21-08 y_est(i) = -1*A(j)*y.y(i - j) + y_est(i);
% Need to adjust back to the pre-differenced time series, x(t),
% and the AR estimated model x_est(t):
% x_est(i) = x_est(i-1) + -1*A(j)*(x_est(i-j) - x_est(i - j -1)) +
x_est(i);
if diff == 'Y'
temp_x = sig_detrend(i-1) + -1*A(j)*(sig_detrend(i-j) -
sig_detrend(i - j - 1)) + temp_x;
end
end
y_est(i) = temp_y;
x_est(i) = temp_x;
%Determining the residuals: residuals(t) = estimated_y(t) -
original_y(t)
if diff == 'Y'
r(i) = (y.y(i) - x_est(i));
else
r(i) = (y.y(i) - y_est(i));
end
end
figure
title('AR Model Validation')
subplot(3, 2, 1)
plot(sig_detrend)
hold
plot(x_est, 'r')
legend('Piecewise Detrended Signal', 'AR Model')
hold
% Checking the model - are the estimated coefficients significantly
% different from zero? For example, ar AR(2) model for which the
% second-order coefficients is not significantlt different form zero
might
% better be fit with at AR(1) model.
% std(coeff) = sqrt((1 - coeff^2)/N).
% Confidence Iinterval = coeff +/- 2*(std(coeff))
% 95 confidence interval (std = 2) around estimated autoregressive
coefficent,
% normally distributed. Check to see if coefficients are
statistically
% significant --> if the confidence band does not include zero,
thant the
% coefficient is (typically) significant.
for a = 2: q+1
std(a) = sqrt((1- (m.A(a))^2))/L;
```

```
CI(a, 1) = m.A(a) - 2*std(a);
%Assuming data has had the mean removed!!!!!
CI(a, 2) = m.A(a) + 2*std(a);
end
cout = '95% Confidence Interval for the AR model coefficients:'
CI
[N, lags] = xcorr(r,'coeff');
subplot(3, 2, 2)
stem(lags, N)
title('Normalzied Autocorrelation Plot of Residuals')
% AR Model Validation: The primary tool for model diagnostic
checkdsing is
% residual analysis.
% 4-plot a conveniet graphical technique for the model validation in
% that it test the assumptiosn for the residuals on a singal graph.
% A. Run Sequence Plot - shows that the residuals do not violate the
% assumption of constant location and scale.
% B. Lag Plot - indicates that the residuals are not autocorrelatied
at lag
% of 1. Checks whether a data set or time series is random or not
random.
% Non-random structure in the lag plot indicates that the underlying
data
% are not random. (A linear pattern suggest a non-randomness and
that the
% autoregressive model might be appropriate.
% C & D. Histogram and Normal probaility plot indiate that the
normal
% distrubutio provides an adequate fit for the model.
%Run Sequence Plot
subplot(3, 2, 3);
plot(r)
title('Run Sequence Plot of Residuals')
%Lag Plot
subplot(3, 2, 4);
plot(r(1:end-1), r(2:end), '.')
title('Lag Plot -1 of Residuals')
%Histogram
subplot(3, 2, 5);
hist(r)
title('Histogram of Residuals')
%Normal Probability Plot
subplot(3, 2, 6);
normplot(r)
```

# Chapter IX: References


**1.** Makale, M.T., J.T. Lin, R.E. Calou, A.G. Tsai, P.C. Chen, and D.A. Gough, Tissue window chamber system for validation of implanted oxygen sensors. Am J Physiol Heart Circ, 2003. 284: H2288–H2294. 289: H57–H65

**2.** Makale, M.T., P.C. Chen, and D.A. Gough, Variants of the tissue-sensor array window chamber. Am J Physiol Heart Circ, 2005.

**3.** Makale M.T., M.C. Jablecki, and D.A. Gough**,** Mass transfer and gas-phase calibration of implanted oxygen sensors. Anal Chem, 2004. 76: 1773–1776.

**4.** Gough, D.A., and J.D Andrade, Enzyme Electrodes. Science, 1973. 180(4084): p. 380-4.

**5.** Leypoldt, J.K. and Gough, D.A., Model of a two-substrate enzyme electrode for glucose. Anal Chem, 1984. 56 Suppl 14: p. 2896-904.

**6.** Gough, D.A. and Leypoldt, J.K., Membrane-covered, rotated disk electrode. Anal Chem, 1979. 51 Suppl 3: p. 439-44.h

**7.** Gough, D.A., Lucisano, J.Y., and Tse, P., Two-dimensional enzyme electrode sensor for glucose. Anal Chem, 1985. 57:2351-2357.

**8.** Lucsiano, J.Y. and D.A. Gough, Transient response of the two-dimensional glucose sensor. Anal Chem, 1988. 60:1272-1281

**9.** Wilkin, J.K. Poiseuille, periodicity, and perfusion: rhythmic oscillatory vasomotion in the skin. J Invest Dermatol, 1989. 93 Suppl 2: p. 113S-118S.

**10.** Nilsson, H and C. Aalkjaer,, Vasomotion: mechanisms and physiological importance. MI, 2003. 3 Suppl 2: p. 79-89.

**11.** Meyer J.U., L. Lindbom, and M. Intaglietta, Coordinated diameter oscillations at arteriolar bifurcations in skeletal muscle. Am J Physiol, 1987. 253:H568-H573.

**12.** Colantuoni, A., S. Bertuglia and M. Intaglietta, Quantification of rhythmic diameter changes in arterial microcirculation. Am. J. Physiol, 1984. 246:H508-H517.

**13.** Breit, G.A., Dissertation: theoretical and experimental evidence for the control of arteriolar vasomotion by independent local oscillators. University of California, San Diego, 1991.

**14.** Walley K.R., Heterogeneity of oxygen delivery impairs oxygen extraction by peripheral tissues: theory. J Appl Physiol, 1996. 81:885-894.

**15.** Tsai, A.G., P. Cabrales, R.M. Winslow, and M. Intaglietta, Microvascular oxygen distribution in awake hamster window chamber model during hyperoxia. Am J Physiol Heart Circ Physiol, 2003. 285: H1537-H1545.

**16.** Tsai, A.G., P.C. Johnson, and M. Intaglietta, Oxygen gradients in the microcirculation. Physiol Rev, 2003. 83: 933-963.

**17.** Intaglietta, M., P.C. Johnson, and R.M. Winslow, Microvascular and tissue oxygen distribution. Cardio Res, 1996. 32: 632-643.

**18.** Secomb, T.W., Theoretical model for regulation of blood flow. Microcirculation, 2008. 15:765-775.

**19.** Pries, A.R. and T.W. Secomb, Control of blood vessel structure: insights from theoretical model. J Physiol Heart Circ Physiol, 2005. 288:H1010-H1015

**20.** Bertuglia, S., A. Colantuoni, G. Coppini, and M. Intaglietta, Hypoxia- or hyperoxia-induced changes in arteriolar vasomotion in skeletal muscle microcirculation. Am J Physiol Heart Circ Physiol, 1991. 260: H362-H372.

**21.** Tsai, A.G., B. Friesenecker, M.C. Mazzoni, H. Kerger, D.G. Buerk, P.C. Johnson, and M. Intaglietta, Microvascular and tissue oxygen gradients in the rat mesentery. Proc Natl Acad Sci USA, 1998. 95 Suppl 12: p. 6590–6595.

**22.** Semmlow, J.L., Biosignal and biomedical image processing: Matlab-based application. CRC Press, 2004.

**23.** Bronzino, J.D., Biomedical engineering handbook. Springer-Verlag Berlin and Heidelberg GmbH & Co. K, 1996.

**24.** Torrence, C. and G.P. Compo, A practical guide to wavelet analysis. American Meteorological Society, 1998. 79 Supple : p. 61–78.

**25.** Morlet, D., F. Peyrin, P. Desseigne, P. Touboul, and P. Rubel, Wavelet analysis of high-resolution signal-averaged ECGs in postinfarction patients *Journal of Electrocardiology*, 1993. 26 Supple 4: p. 311-320

**26.** Matlab 7 ® Mathworks.

**27.** Shumway, R.H. and D.S. Stoffer, Time series analysis and its applications. Springer, 2005.

**28.** Hamilton, J.D., Time series analysis. Princeton University Press, 1994.

**29.** Colantuoni A., S. Bertuglia, and M. Intaglietta, Variations of rhythmical diameter changes at the arterial microvascular bifurcations. Pflügers Arch 1985; 403: 289-95.

**30.** Meyer J.U., L. Lindbom, and M. Intaglietta, Coordinated diameter oscillations at arteriolar bifurcations in skeletal muscle. Am J Physiol 1987; 253: H568-73.